HUNGARIAN UNIVERSITY OF AGRICULTURE AND LIFE SCIENCES

DOCTORAL (PhD) DISSERTATION

MOSTAFA AHMED ABDALMAGEED

Keszthely

2026

HUNGARIAN UNIVERSITY OF AGRICULTURE AND LIFE SCIENCES

Insights on Physiological and Transcriptomic Evaluation of Zinc Oxide Nanoparticle-Mediated Salinity Stress Tolerance in *Solanum lycopersicum* L. and *Zea mays* L.

DOCTORAL (PhD) DISSERTATION

By:

MOSTAFA AHMED ABDALMAGEED

Georgikon Campus

Keszthely

2026

The Doctoral School

Name: DOCTORAL SCHOOL OF NATURAL SCIENCES

Discipline: ENVIRONMENTAL SCIENCES

Specialization: AGRICULTURAL SCIENCES (AGRICULTURAL BIOCHEMISTRY)

Head:

Dr. ERIKA CSÁKINÉ MICHÉLI

University Professor, Institute Director, Head of Department, Szent István Campus, Gödöllő

Full member of the Hungarian Academy of Sciences

Doctoral School of Natural Sciences

Supervisors:

Dr. ZOLTÁN TÓTH

Associate Professor, PhD

Institute of Agronomy, Doctoral School of Food and Agriculture Sciences, Georgikon Campus, Keszthely

Dr. KINCSŐ DECSI

Associate Professor, PhD

Institute of Agronomy, Doctoral School of Food and Agriculture Sciences, Georgikon Campus, Keszthely

....

Approval of the Head of Doctoral School Approval of the Supervisor (1)

.....

Approval of the Supervisor (2)

Table of Contents

1. INTRODUCTION

A global scarcity of water resources, pollution, and an increase in soil and water salinization mark the beginning of the twenty-first century. A rise in human population and a decline in land available for cultivation threaten agricultural sustainability (Ingrao et al., 2023). High winds, harsh temperatures, soil salinity, drought, and flooding are only some of the environmental challenges affecting agricultural crop productivity and cultivation (Shrivastava & Kumar, 2015). Regarding the quality and quantity of crops produced, soil salinity is among the worst ecological pressures (Ingrao et al., 2023). A saline soil is defined as having an electrical conductivity (EC) of the saturation extract (ECe) at the root zone of more than 4 dS m^{-1} (about 40 mM NaCl) at 25°C and an exchangeable salt content of 15% (Grigore et al., 2017). Most crop plants have a decreased yield at this ECe, even though many crops exhibit yield losses at lower ECes (Shrivastava & Kumar, 2015). Based on estimations, high salinity has impacted around 33% of irrigated agricultural fields and 20% of the total farmed land globally (Negacz et al., 2022). Furthermore, the expansion of salinized lands at a rate of 10% per year (Nachshon, 2018) can be attributed to various factors, including insufficient precipitation, excessive surface evaporation, irrigation with salinized water, and suboptimal cultural practices. According to projections, the global proportion of arable land affected by salinization is anticipated to surpass 50% by 2050 (Butcher et al., 2016).

Crop plants' physiological and biochemical pathways are adversely affected by soil salinity through a complex mechanism (Nabati et al., 2011). When there is too much Na^+ in the cell, cytosolic K^+ and Ca^{2+} leave the cell. This upsets the balance of their homeostasis, which leads to nutritional deficiencies, oxidative stress, slowed growth, and cell death (Ahanger et al., 2015). Several stomatal restrictions, such as stomatal closure (Munns & Tester, 2008) and non-stomatal limitations like chlorophyll dysfunction (Jiang et al., 2017), deprivation of enzymatic proteins and membranes of the photosynthetic apparatus (Mittal et al., 2012), and chloroplast ultrastructure destruction (Gengmao et al., 2015), have been reported to have a significant negative impact on plant photosynthesis at high salinization levels, salt-affected soils demonstrate higher Na^+/K^+ and Na^+/Ca^{2+} ratios due to the increased presence of Na^+ in the soil solution. Consequently, a reduction in the uptake of potassium ions (K^+) and calcium ions (Ca^{2+}) might hinder cellular functioning, resulting in the destabilization of cell membranes and the impairment of enzymatic activity, which is facilitated by the enzymes (Quintero et al., 2007).

The production of too many reactive oxygen substances/species (ROS) in the cytosol, chloroplast, and mitochondria is influenced by osmotic pressure and ionic toxicity, leading to oxidative damage (Abbasi et al., 2015; Munns & Tester, 2008). These reactive oxygen species can damage plant tissues, alter the double-helical DNA, disrupt the phospholipid bilayer (Noctor & Foyer, 1998), degrade the active biomolecules like lipids and proteins, and destroy photoreceptors like phytochromes A and B (Pitzschke et al., 2006).

In a significant proportion of farmed plant species, the productivity starts to decline even when exposed to relatively moderate levels of salinity in irrigation water (electrical conductivity of water, ECw > 0.8 dS/m) or soil (electrical conductivity of saturated soil extracts, ECse > 1 dS/m) (Grigore et al., 2017). The impact of soil salinity on the productivity of several vital crops, including *Zea mays* L., *Solanum tuberosum* L., *Lycopersicon esculentum* Mill., and *Oryza sativa* L., has been shown to result in significant yield reductions. These reductions have been reported as 19.0% for *Zea mays* L., 12.0% for *Solanum tuberosum* L., 9.9% for *Lycopersicon esculentum* Mill., and 12% for *Oryza sativa* L. (Maas, 1990).

On a global scale, both fresh and processed tomatoes (*Solanum lycopersicum* L.) are consumed in significant quantities. Therefore, a widely consumed functional food can be ingested by individuals worldwide, either in its uncooked or cooked state, or as a primary ingredient that undergoes processing to create various products such as tomato powder, juice, puree, sauces, ketchup, and paste (Chabi et al., 2024; Li et al., 2021). These tomato fruits contain a higher concentration of bioactive compounds and nutrients than other fruits (Ali et al., 2021; De Sio et al., 2021) that are good for the skin and body and may help treat or prevent several chronic degenerative disorders in people (Ali et al., 2021).

Every year, a multitude of factors can impact the nutritional quality and quantity of tomatoes (Inculet et al., 2019). Agricultural crop productivity and cultivation are impacted by a variety of environmental difficulties, including strong winds, extreme temperatures, soil salinity, drought, and flooding (Shrivastava & Kumar, 2015). One of the harshest ecological stresses on crop quality and yield is salinity in the soil (Ahmed et al., 2024a; Ingrao et al., 2023). Tomatoes have a moderate sensitivity to soil salinity compared to other vegetable crops. The greatest threshold of soil sodicity for yield loss in tomatoes is 2.5 dS m^{-1}. The abundance of diverse germplasm, including a wide range of wild species, is valuable for incorporating characteristics that confer resistance to various diseases, as well as tolerance to soil salinity and drought (Tester & Langridge, 2010).

The tomato variety employed in the study, Kecskeméti 549, is a medieval cultivar known for its determinate growth. Tomato berries mature uniformly in a single hue, possess a somewhat elongated and cylindrical shape, and may be effortlessly detached from the stem by pinching. The typical weight of their berries ranges from 50 to 60 g (Norbert, 2023). Salt stress can cause a variety of problems at multiple levels, including molecular, morphological, and biochemical (metabolic) disruptions. Several regulatory elements are responsible for reducing the negative consequences of abiotic stress in plants (Ahmed et al., 2023a).

Maize, scientifically known as *Zea mays* L., is a versatile crop that can thrive in various agro-climatic conditions. It is cultivated in various regions worldwide, reaching elevations up to 3000 m above sea level (Sah et al., 2020). Farmers like this crop because it has the largest grain production potential among cereals (Pandit et al., 2016; Sah et al., 2020). It can be used for both grain and fodder (Chaudhary et al., 2016; Sah et al., 2016), and is also grown as a cash crop for specialized corn varieties such as green ear, baby corn, sweet corn, and popcorn (Manigopa & Sah, 2012). Additionally, it serves as a raw material for various industries. Maize is categorized as an industrial rather than a food crop since only a small fraction (12–13%) of its worldwide output is used for human consumption. The three primary staple cereals in the world, wheat, rice, and maize, make up a significant portion of the human diet. Approximately 42% of the world's caloric intake and 37% of its protein come from them (FAOStat, 2021). Maize is cultivated in regions with precipitation levels ranging from 300 to 500 mm, close to or below the crucial threshold for achieving a satisfactory yield (Ren et al., 2008).

The farm industry is one of developed countries' most important economic foundations. With an increasing global population comes a growing demand for food and agricultural products. Several factors, including plant diseases, increased environmental pollution, diminishing soil and water supplies, and climate change, make agriculture and producing enough nutrient-dense food difficult (Dresselhaus & Hückelhoven, 2018; Foley et al., 2011; Raza et al., 2019; Tuomisto et al., 2017). Over the past decade, nanotechnology has emerged as a crucial instrument for increasing agricultural productivity. Generally, nanotechnology has the potential to significantly contribute to the industry's rising prosperity by maximizing the use of agricultural inputs, including water, fertilizer, and pesticides, while lowering effluents and pollution (Sekhon, 2014). Since plants are sessile organisms, they have various coping mechanisms that allow them to adapt to changes in their growing settings and display essential flexibility in responding to environmental challenges without impairing cellular, physiological, or developmental processes (Yang et al., 2018).

Metallic nanoparticles (MNPs), including Zn^{2+}, $Fe^{2+/3+}$, Ti^{3+}, Ag^{+}, and Cu^{2+} NPs, have garnered significant attention due to their potential application in agriculture without causing adverse environmental effects (Rai et al., 2018). They have lately been used to test a variety of plants for stress tolerance, plant development, and germinating seeds (Abdel Latef et al., 2017; Taran et al., 2017). It has been observed that zinc oxide nanoparticles (ZnO-NPs) have important and essential functions in promoting plant growth and enhancing plant resistance to salt stress in several plant species (Gaafar, et al., 2020). Zinc (Zn^{2+}) is a crucial micronutrient that is necessary for the proper functioning of living organisms' metabolism (Natasha et al., 2022). It carries out vital duties by participating in the activities of many enzymes (Cuajungco et al., 2021) and serves as a regulatory cofactor in protein synthesis. Moreover, a lack of Zn^{2+} results in the decrease of multiple metabolic processes, including growth, ultimately affecting crop yields (Khan et al., 2022).

The application of ZnO-NPs is widely utilized in several fields, including agriculture, solar cells, lotions, paints, rubber, concrete, cosmetics, and medicine (Raha & Ahmaruzzaman, 2022). A study has shown that the use of ZnO-NPs improves growth by controlling photosynthetic processes and the production of active oxygen species such as superoxide and hydroxide anion (Mandal et al., 2022). Furthermore, a separate study showed that ZnO-NPs increased the concentration of chlorophyll, carotenoids, protein, and the activity of antioxidative enzymes in cotton plants (Perumal et al., 2016). Additionally, metal/metal oxide nanoparticles have diverse applications, notably in the food business (Smaoui et al., 2023). Applications in the food industry may involve the creation of novel biodegradable packaging materials that possess antibacterial qualities, as well as the development of protective coatings for work surfaces, specifically in the context of meat processing (Burmistrov et al., 2022; Gudkov et al., 2023, 2024).

It is critical to note that the mode of action of ZnO-NPs is highly influenced by various factors. At the nanoscale, smaller nanoparticles exhibit higher chemical reactivity and catalytic activity (Plaksenkova et al., 2020). The production and stability of ROS are highly affected by nanoparticle morphology, as larger nanoparticles may aggregate, leading to reduced effectiveness due to sedimentation or a smaller surface area (Mendes et al., 2025). On the other hand, sheet-shaped nanoparticles exhibit stronger surface interactions (Mendes et al., 2025). The dissolution of ZnO-NPs is pivotal in shifting from biostimulation to toxicity, so ZnO-NPs usually enhance nutrient absorption and antioxidant defenses at low concentrations, but excessive dissolution can lead to detrimental ion concentrations in plant tissues (Shen et al., 2022).

A revolution in biology has been brought about by next-generation sequencing, sometimes known as NGS. The production of libraries is necessary for next-generation sequencing (NGS), which involves fusing DNA or RNA molecules as fragments with adapters. A technology known as high-throughput complementary DNA sequencing (RNA-Seq) is an efficient method for analyzing the entire transcriptome (Parkhomchuk et al., 2009). This approach indicates the level of transcript expression, the quality of synthesis, and comprehends how the functionality of differentially expressed genes is crucial for elucidating complex biological processes. Pathway analysis is a valuable approach for understanding the interactions between genes in biological pathways. But the scarcity of annotation data, primarily derived from model organisms or frequently studied species, complicates the situation (Parkhomchuk et al., 2009; Sun et al., 2020).

A transcriptomic study of tomato and maize leaves stressed by salt and treated with ZnO-NPs showed that these nanoparticles help plants tolerate salt stress by altering the expression of genes that control stress responses and nutrient use. ZnO-NPs were shown to increase the activity of genes involved in nutrient transport, carbon (C) and nitrogen (N) assimilation, and secondary metabolism. This increased the levels of antioxidants, sugar, and amino acids in the leaves (Ahmed et al., 2025; Gupta et al., 2024; L. Sun et al., 2020).

This dissertation aimed to provide a comprehensive evaluation of the biological impact of chemically synthesized ZnO-NPs in mitigating salinity stress in *Solanum lycopersicum* L. and *Zea mays* L. This study relied on the dual-protection hypothesis and sought to quantify the impacts of ZnO-NPs across multiple levels of biological organization, ranging from field and greenhouse-scale agronomic assessments to *in silico* molecular docking analyses. This hypothesis suggested that ZnO-NPs served an extensive function in complex agricultural environments, acting simultaneously as physiological enhancers of abiotic salt tolerance and as molecular initiators of biotic plant defense.

This study primarily focused on the plant-morphological, physiological, biochemical, and transcriptomic adaptations required for survival under 150 mM NaCl. Nevertheless, the study intentionally integrated antimicrobial and molecular docking analyses to illustrate the crop's bioactive potential. It also examined cross-tolerance in field and greenhouse situations by demonstrating how ZnO-NPs enhance plant vitality and simultaneously increase the chemical efficacy of secondary metabolites. The transcriptome data, indicating significant regulation of pathways such as proline and thiamine synthesis, functioned as the genetic framework for our study.

The subsequent antimicrobial testing and molecular docking served as validation and functional tools to verify these genetic modifications. These investigations examined not only computational tasks independently but also the correlation between certain bioactive ligands, such as rutin, and their biological efficacy against infections. This comprehensive approach finally illustrated that tolerance must be evaluated not only by biomass preservation but also by the enhancement of the plant's nutritional and therapeutic properties, transforming salt-stressed leaves into significant sources of potent antimicrobial extracts.

THE OBJECTIVES OF THE STUDY IN POINTS

The objective of the present study was to investigate the effects of applying salinity stress and foliar application of chemically synthesized zinc oxide nanoparticles (ZnO-NPs) to the *Solanum lycopersicum* L. (tomato) and *Zea mays* L. (maize) under greenhouse and open field conditions. The greenhouse and open-field experiments were carried out to investigate the following:

1. Chemical synthesis and characterization of ZnO-NPs with different analytical techniques
2. The effects of applying the characterized chemically synthesized ZnO-NPs to the leaves of tomato and maize on the biochemical markers and different morphological attributes
3. Formation of phenolic compounds and fatty acids in the leaves of tomato and maize
4. The production levels of the antioxidative enzymes in tomato and maize leaves
5. Near-infrared (NIR) measurements of the tomato and maize harvested parts
6. Utilizing the RNA sequencing (RNASeq) to elucidate the expression of genes in tomato and maize leaves subjected to ZnO-NPs with/without salinity stress
7. Conducting the gene ontology (GO), plant reactome, and Kyoto Encyclopedia of Genes and Genomes (KEGG) enrichment analyses on the sequenced-RNA extracted from tomato and maize leaves to elucidate the functions of differentially expressed genes (DEGs) and their interactions within regulatory pathways
8. The antimicrobial activity of the aqueous and diethyl ether extracts from tomato and maize leaves
9. Molecular docking of the HPLC-detected compounds from tomato and maize, utilizing their functions as antibacterial and antifungal molecules

2. REVIEW OF LITERATURE

2.1. Salinity-induced reductions in plant productivity

When the growth requirements of crop plants are appropriately met, including effective management practices throughout the growing season, as well as proper management of nutrients, water, light, and temperature to align with their optimal growth conditions, these plants are capable of yielding high quantities of high-quality grain, fiber, and substances with high sugar, oil, or protein content. In the context of plant development, it has been observed that abiotic stressors, such as salt or drought, show an inverse correlation with yield-related traits (Goharrizi et al., 2020). If salt stress inhibits plant growth during the early stages of development, it can significantly reduce yield and negatively affect the quality and quantity of plant products (Hussain, Cao, et al., 2018). While the visible effects of salt may not always be immediately apparent, it is crucial to remember that salinity can reduce agricultural production. A specific crop's salt tolerance and sensitivity are determined by its ability to extract water and nutrients from saline soils and its capacity to prevent the accumulation of salt ions in its tissues (Ahmad et al., 2011; Munns et al., 2006).

Elevated levels of sodium ions (Na^+) and chloride ions (Cl^-) can be detrimental to plants, especially when they accumulate in the cytoplasm (Tavakkoli et al., 2010). Despite the significance of the topic, there remains a limited understanding of the specific cytosolic processes negatively affected by elevated salt levels, and the potentially harmful effects of chloride in the cytosol remain uncertain (Geilfus et al., 2017). Additionally, the accumulation of deleterious ions in photosynthetically active tissues can accelerate the aging process of transpiring leaves while reducing the availability of essential nutrients required for optimal health (Ma et al., 2020). The plant's capacity to acquire nutrients and energy through photosynthesis or to metabolically utilize them is limited at any given time (Munns & Gilliham, 2015).

The energy expenditure is necessary for stress mitigation, growth, and maintenance (Amthor, 2000). The relative proportions of plant constituents vary based on the plant's developmental stage and susceptibility to salt stress. An increase in salinity levels can lead to a decrease in the rate of photosynthesis due to induced stomatal closure, reduction of gas exchange (CO_2 input decreased), reduction of the size and frequency of stomata (after prolonged exposure), degradation of the chlorophylls, damaging the chloroplast ultrastructure, and inhibition of photophosphorylation and carbon reactions (enzyme reactions).

As a consequence, there will be a reduction in the total energy acquired. To effectively cope with the elevated salt content in the soil, the plant must allocate additional resources toward various processes (Shrivastava & Kumar, 2015). These include incurring higher energy investment for ion exclusion or compartmentalization, maintaining ion homeostasis, and detoxifying ROS. Plant growth is impeded by high salinity due to the equilibrium between the losses incurred by the plant and the energy acquired by the plant (Zhao et al., 2021).

The occurrence of tissue senescence is attributed to an imbalance between plant composition and demolishing processes, whereby the latter surpasses the former (Childs et al., 2015). The reaction of a crop that exhibits both sensitivity and tolerance to elevated soil salt levels (Werf et al., 1988). Each type of crop has a different response to saltiness, which can be broken down into three stages (Katerji et al., 2001): homeostasis, which keeps the rate of growth healthy; eustress, which turns on defense genes; and distress, which slows down metabolism and eventually leads to death.

Plant species that exhibit both sensitivity and intolerance may possess the ability to flourish within a limited range of salinity tolerance (Al-shareef & Tester, 2019). In the context of safeguarding vulnerable crops, defensive mechanisms are thought to be triggered earlier and with reduced intensity (Richard et al., 2022). The result is that the defensive ability of tolerant/resistant plant species is better precisely because they react faster. They start producing protective compounds more quickly and keep the number of compounds higher. Susceptible plants respond later and produce protective compounds more slowly and for a shorter period of time (De-la-Cruz Chacón et al., 2013).

2.2. Negative effects of soil salinity on crops

Compared to other abiotic stresses that reduce agricultural productivity in dry and semi-arid regions, salinity stress stands out as a particularly challenging obstacle to overcome. This is mainly attributable to the natural conditions in these regions, which promote salinization due to insufficient precipitation to enable the leaching of salts. In other words, these factors cause salinization to occur (Dresselhaus & Hückelhoven, 2018). In the biphasic model of growth reduction caused by salinization, the bad effects of salt-affected soils are shown by a drop in osmosis and ion cytotoxicity in the first phase. This is followed by the production of ROS and programmed cell death (PCD) in the second phase (Kamran et al., 2019a). These effects are further compounded by the generation of reactive oxygen species (ROS) and disturbances in nutrient equilibrium. This aligns with the theoretical proposition that salt induces a decrease in osmosis during the initial stage and an increase in ion cytotoxicity during the subsequent stage (Munns, 1993).

2.2.1. Influence of salinity on agronomic traits and yield components

Several elements, including the amount of salt present, the amount of time that has passed, the plant species and variations, the photochemical quenching capabilities, the plant growth stages, the type of stress, gas exchange characteristics, and photosynthetic pigments, all contribute to the retardation of plant development that occurs under salt stress (Aghighi Shahverdi et al., 2018). In several studies on corn (*Zea mays* L.) (Shahrajabian et al., 2019), rice (*Oryza sativa* L.) seedlings (Lee et al., 2011), *Vigna unguiculata* L. (Ibrahim, 2016), and rapeseed (*Brassica campestris* L.) (Ashraf, 2001), it was discovered that increasing plant height with even a slight quantity of salinization was beneficial.

The observed increase in plant height can be attributed to fewer soluble salts in the growth control medium; in the beginning, the nutrient salts added to the medium act as eustress on the plant, with a stimulating effect. Conversely, the decrease in plant height can be attributed to the adverse effects of excessive salts on various physiological processes. These effects include a reduction in photosynthetic rate, decreased levels of carbohydrates and growth hormones, which inhibit growth, and decreased protein synthesis due to alterations in antioxidant enzyme activities (Qados, 2011).

Salinity levels up to 8 dS/m substantially influenced various plant parameters, including fresh and dry weight, leaf area, and leaf count (Ahmadi et al., 2018; Hajiboland et al., 2014; Mallahi et al., 2018). Numerous researchers have observed that the reduction in dry matter production and deceleration of plant growth in soils influenced by salinity can be attributed to the hindrance of cell elongation (Aghighi Shahverdi et al., 2018) through the direct suppression of the activities of transport proteins like proton (H^+)-ATPase (Shi et al., 2007). Salt stress has been found to have detrimental effects on photosynthesis, leading to constraints in both plant and leaf growth and reductions in chlorophyll levels, as the central core of chlorophyll contains magnesium (Hameed et al., 2021). The absorption or uptake of magnesium is inhibited by acidic pH (Netondo et al., 2004).

Earlier studies have shown evidence that an increased concentration of salt negatively affects nitrogen accumulation in plants due to the interplay between chloride ions (Cl^-) and nitrate ions (NO_3^-), as well as sodium ions (Na^+) and ammonium ions (NH_4^+). Consequently, this phenomenon results in a decrease in the quantity of plant growth and agricultural productivity (Rozeff, 1995). Research has shown evidence that salinity stress has a secondary impact on plant feeding, leading to a notable decline in nutrient absorption due to a fall in osmotic pressure (Cantabella et al., 2017).

2.2.2. Impact of salinity stress on key physiological processes

Recent research indicates that the physiological characteristics of cereal crops, including wheat (*Triticum aestivum* L.) and mung bean (*Vigna radiata* L.), are negatively impacted by soil salinity stress (Ahanger et al., 2015; Elkelish et al., 2019; Khan et al., 2014). Decreasing leaf photosynthetic capacity and concentration of carotenoids and other photosynthetically active pigments, as well as altered energy in the mechanisms of ion exclusion, osmotic adjustment, and nutritional imbalance, may all be contributing factors to the loss in plant growth and output caused by soil salinity (Munns, 2005). Crops are often impacted by salt-affected soils in one of three ways: oxidative damage, ion imbalance, or osmotic stress (Hussain et al., 2017). The harmful effects of sodium (Na^+) and chloride (Cl^-) ion buildup in plant tissues are the predominant reaction of salt-affected soils (Hussain et al., 2017; Hussain, Zhong, et al., 2018). It has been demonstrated that plants under salinity stress collect more Na^+ ions, disturb the ionic balance, modify plant metabolism, and increase oxidative damage. In contrast, the K^+ ion status in plant tissues aids in the development of soil salt tolerance in plants (Wang et al., 2003).

When rice (*Oryza sativa* L.) was cultivated in salt-affected soil, the K^+ ion concentration was only marginally changed; however, the Na^+ content in the leaves was dramatically increased, and the K^+/Na^+ ratio was significantly decreased (Hussain et al., 2017; Hussain, Zhong, et al., 2018). A notable decline in strawberry plant growth was noted (Zahedi et al., 2019). These growth delays may partly be explained by decreased photosynthetic activity brought on by lower levels of Chl a and Chl b under varying salinity conditions (Gururani et al., 2015). Ion imbalance in plants and soil is brought on by the entry of Na^+ and Cl^- ions, and this imbalance in the plant's ions may lead to severe physiological issues (James et al., 2011). The high salt content in the soil profile may result in physiological dryness as a result of decreased water uptake, salt accumulation in the root zone of the plant, a reduction in plant osmotic potential, and subsequent disruption of cell metabolic processes as a result of ion toxicity (Evelin et al., 2009; James et al., 2011). Excessive Na^+ in plants damages the cell membrane and organelles and impairs physiological processes that result in the death of plant cells (Hussain et al., 2019; Hussain, Zhong, et al., 2018; Singam et al., 2011). These physiological processes include the net photosynthetic rate (Pn), stomatal conductance (Gs), transpiration rate (Tr), intracellular carbon dioxide (Ci) concentration, and soil plant analysis development (SPAD) chlorophyll value.

The disturbance of the selective permeability of the cell membrane, which makes it difficult for the plant to detoxify the ROS in the cytoplasm, a decrease in the rate of

photosynthetic activity, and alterations in the antioxidant enzymes may also occur as a result of these physiological changes (Hussain et al., 2019). These oxidative systems can interfere with dynamic cellular operations in plants under abiotic stress -particularly soil salinity- by disrupting the normal functions of numerous plant cellular components such as proteins, DNA, and lipids (Demiral & Türkan, 2005). Additionally, plants grown in saline environments may impair chlorophyll production and alter the activities and structure of the pigment-protein complex (Levitt, 1985). The decreased activity of several enzymes, including porphyrinogen IX oxidase, porphobilinogen deaminase, coproporphyrinogen III oxidase, 5-aminolevulinic acid dehydratase, protochlorophyllide oxidoreductase, and magnesium (Mg)-chelatase, may be the cause of the inhibition of chlorophyll pigment synthesis under salt stress (Pattanayak & Tripathy, 2011). These enzymes, in turn, are in charge of either an increase in chlorophyllase activity (Santos et al., 2009) or a decrease in leaf water potential, N absorption, and, consequently, the reduced ability of plants to synthesize oxygen (Khan et al., 2014). Salinity-induced superoxide radicals and hydrogen peroxide (H_2O_2), which deteriorate the membranes of thylakoids and chloroplasts, may also be responsible for chlorophyll degradation (Subramanyam et al., 2019).

2.2.3. Variant effects of salinity on enzymatic and non-enzymatic antioxidants in plants

The effects of soil salinity stress, which inhibits plant growth and development, are accompanied by a significant accumulation of ROS. Their (O_2^-, O_2, H_2O_2, and OH^-) production under stressful conditions (biotic and abiotic) serves as a cellular stress indicator and acts as a secondary messenger. ROSs play roles in plant biological activities, ranging from gene expression and translocation to enzymatic chemistry (Foyer and Noctor, 2003; Kamran et al., 2019a). ROS may eventually disrupt the average plant metabolism because of lipids, proteins, and nucleic acid structure changes (Adly, 2010). According to some reports, soil salinity-stimulated oxidative stress, driven by increased H_2O_2 levels, may cause DNA breakage, chromatin condensation, apoptosis, and cell shrinkage (Houot et al., 2001). Higher levels of ROS production during salinity stress may cause the thylakoid membranes to produce more malondialdehyde (MDA). Calculating the lipid peroxidation of plant cells involves using MDA concentration, which is recognized to be a reliable indication of lipid peroxidation (Farmer & Mueller, 2013). The degree of collateral damage to these molecules involved in plant metabolism is determined by the balance between ROS generation and their removal by the antioxidative defense mechanism (Asada, 1994).

Additionally, soil salinization results in acute oxidative damage to plant tissues. As a result, plants create their own sophisticated natural antioxidant defense mechanism to counteract the oxidative stress caused by salinity. The cell structural harm brought on by salinity-induced ROS is prevented by antioxidant enzymes (Ramachandra Reddy et al., 2004); these crop plants that have increasing tolerance to osmotic stress and efficient Na^+ and Cl^- exclusion are thought to be better at withstanding salt than other plant kinds because they have an effective antioxidant system. The varied effects of salinity stress on antioxidative enzymatic and non-enzymatic activities in *Tanacetum parthenium* L. (Mallahi et al., 2018), *Brassica napus* L. (Ahmadi et al., 2018), *Oryza sativa* L. (Li et al., 2014), and *Glycine max* L. (Farhangi-Abriz & Ghassemi-Golezani, 2018) have previously been documented by many studies. Carotenoids, ascorbic acid (vitamin C), α-tocopherol (vitamin E), flavonoids, and phenolics comprise most of the non-enzymatic antioxidant system.

In contrast, the enzymatic antioxidant system comprises peroxidase (POX), superoxide dismutase (SOD), ascorbate peroxidase (APX), glutathione reductase (GR), polyphenol oxidase (PPO), and other enzymes. The primary function of the enzymatic antioxidative system is to remove the harmful radicals generated during oxidative stress, aiding agricultural plants in withstanding abiotic stresses such as salinity (Kamran et al., 2019b). Nearly every component of the plant has some natural antioxidants. These natural antioxidants include vitamins, carotenoids, phenols, dietary glutathione, flavonoids, and endogenous metabolites (Krishnaiah et al., 2011). Plants' first line of defense against oxidative stress in soils influenced by salt is to synthesize and scavenge these antioxidants.

While the antioxidant responses is well-documented across species like *Brassica napus* L. and *Oryza sativa* L., there is a significant deficiency in research regarding using the metallic-oxide nanoparticles as regulators to optimize the efficiency. While, the conventional fertilizers address simple deficiencies, the potential for ZnO-NPs which have been used in the current study can act as a molecular signal that restores the antioxidant enzymes like SOD, CAT, and POX, etc, to manage the stress.

2.3. Different pathways of salt tolerance in plants

2.3.1. Osmotic adjustment

Salinity tolerance varies widely among plants, affecting their growth responses. Many salt-tolerant plants adjust mechanisms to counteract water stress (Figure 1) (Munns & Tester, 2008).

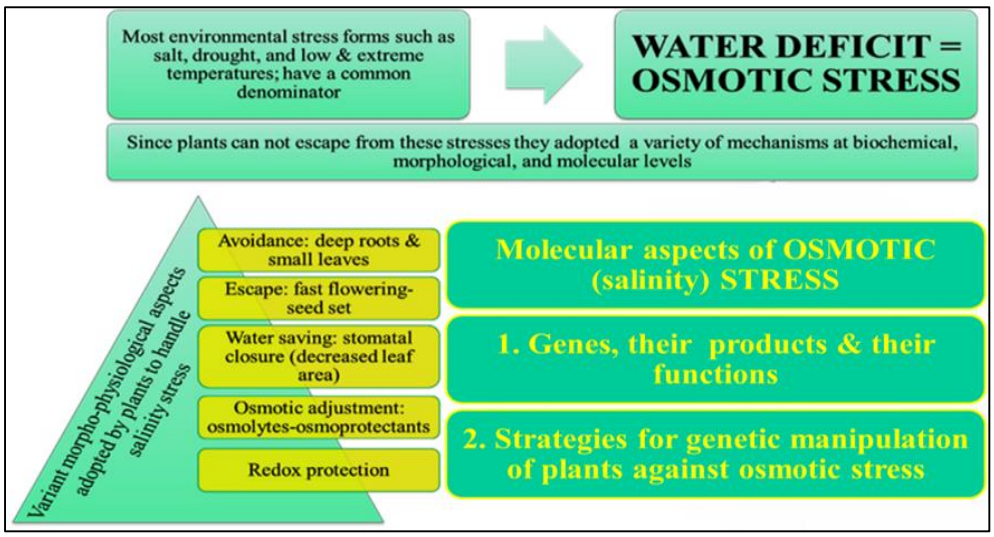

Figure 1. Illustration of different mechanisms that are adapted by the plants against salt stress (Ahmed et al., 2024a).

Plants may need osmotic adjustment to survive excessive salinity (Buchanan et al., 2015). The plant must maintain low cytosolic Na^+ concentrations, high K^+/Na^+ ratios, and cellular turgor at low osmotic potential to grow on salty soil. These properties support K^+-dependent metabolic processes through osmotic adjustment (Munns & Tester, 2008). Many appropriate solutes contain nitrogen. These N-containing compounds include glycine betaine, proline, and polyamines (Ashraf & Foolad, 2007; Mansour & Ali, 2017). Thus, nitrogen metabolism matters under stress.

2.3.2. Exclusion, redistribution, or inclusion/sequestration of salt-facing the ion toxicity

Some transporters work to prevent Na^+ from building up and to neutralize its harmful effects in the cytosol. In return for an H^+, the vacuolar Na^+/H^+ antiporter (NHXs) sequester a sodium ion into the vacuole (Balasubramaniam et al., 2023). Keeping cytosolic Na^+ levels low at the cellular level and reducing whole-plant Na+ concentrations are efficient ways for glycophytes to cope with salinity stress. In addition to these variables, K^+ uptake and maintenance were found to significantly affect plants' ability to withstand salt stress (Zhu et al., 1998). It has been strongly suggested that maintaining high cytosolic K^+/Na^+ ratios, particularly in shoots, is essential for glycophyte plants to be salt-tolerant (Hauser & Horie, 2010).

"Sodium exclusion" is frequently used interchangeably with "preventing its accumulation in the shoot." Na^+ extrusion from the root thus has an actual role. In animal cells, Na^+/K^+-ATPase releases three Na^+ ions in return for two K^+ ions (Galva et al., 2012).

While Na+ can be more easily extruded in lower plants by sodium ATPase (PpENA1), in higher plants, the Na^+/H^+ antiporter Salt Overly Sensitive 1 (SOS1) is still the only transporter that is known to keep Na^+ out of the cytosol and into the apoplast (Lunde et al., 2007). Wu et al. (2018) confirmed that 10- to 20-fold higher Na^+ extrusion ability was observed in their study on wheat (under the same considerations) in the root extension zone, with net Na^+ fluxes ranging from –284 ± 39 nmol m^{-2} s^{-1} to –1584 ± 237 nmol m^{-2} s^{-1}, compared with the study by Cuin et al. (2011) that reported mature root zone Na^+ efflux mostly ranged between –20 nmol m^{-2} s^{-1} and –70 nmol m^{-2} s^{-1}.

The mature root zone, which makes up most of the root and can lower the Na^+ load in the shoot, may provide the physiological explanation for the sequestration phenomena (Wu et al., 2018). It has been extensively shown that decreased Na^+ buildup in the shoot is associated with the high-affinity K^+ transporter (HKT)-mediated retrieval of Na^+ from the xylem (Byrt et al., 2007), and last, wheat's resistance to salt occurs (Munns et al., 2012). HKT transporters are constituents of the Trk/Ktr/HKT superfamily and are frequently denoted as monovalent cation transporters. Extensive research has been conducted on these entities across several plant species, revealing their vital role in enhancing salt tolerance. Their primary function involves preventing the infiltration of Na^+ ions into the vulnerable shoot tissues of plants (Jaime-Pérez et al., 2017). There isn't much physiological justification for intentionally loading Na^+ in the shot and retrieving it. By instantly depositing a salt load in the root cortex of the mature zone, this pointless cycle can be broken, and the same result can be obtained at a lesser cost (Wu et al., 2018). Notably, wheat's vacuolar fluorescence Na^+ signal has a notably higher intensity in the root elongation zone than in the mature zone, implying that Na^+ may be transferred from the mature root zone to the expanded zone (Wu et al., 2018).

2.3.3. Activation of redox responses

One of the critical mechanisms by which plants are damaged during adverse environmental conditions is the excess production of reactive oxygen species (ROS) (Figure 2)—the salt-induced ROS that most likely originate from the mitochondrial and chloroplast electron transport chains (Balasubramaniam et al., 2023). Eliminating harmful ROS species is the most crucial component of an effective acclimatization response in salt stress. Reduced stomatal conductance is how plants react to salt stress to prevent excessive water loss. Consequently, this lowers internal CO_2 concentrations (Ci) and slows down the Calvin cycle's elimination of CO_2 (Hsu & Kao, 2003), causing photorespiration, especially in C3 plants, which causes the peroxisome to produce more H_2O_2 (Ghannoum, 2009).

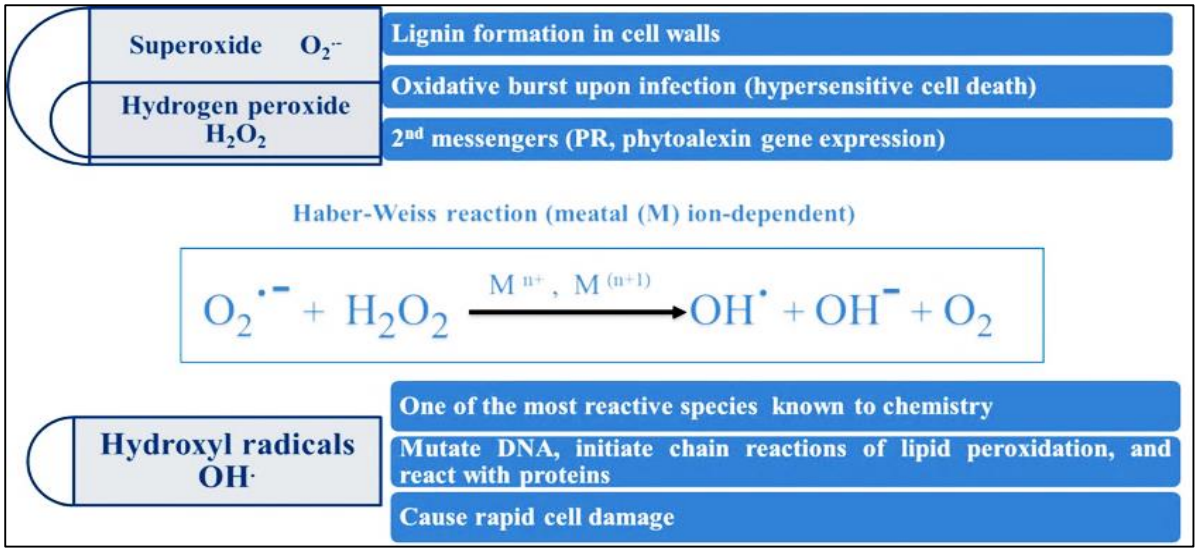

Figure 2. Formation of hazardous ROS under salt stress conditions (Ahmed, et al., 2024a).

Numerous findings suggest that various chemicals, pigments, and enzymes have defensive functions that reduce oxidative damage and improve plant tolerance to salt by eliminating hazardous ROS. The antioxidant enzymes are SOD, CAT, POX, and APX, while the nonenzymatic antioxidant compounds are glutathione (GSH), ascorbates (ASC), and carotenoids (Azeem et al., 2023). Some other types of antioxidants are called anthocyanins; they are flavonoids known to accumulate in plants subjected to salt stress (Balasubramaniam et al., 2023).

2.4. Classification of nanoparticles and their efficacy in abiotic stress mitigation

The exceptional characteristics of nanoparticles (NPs), which include their heightened reactivity, enhanced surface activity, and large surface-to-volume ratio, comprise both the nanoparticles' physical and chemical properties (Sukhanova et al., 2018). Typical classifications of nanoparticles (NPs) include many kinds that are typically divided according to concepts like the synthesis method and the compounds or elements used in the synthesis. Many studies on metal and metal oxide-based nanoparticles (NPs) have been conducted in agricultural settings over the past decade (Dziergowska & Michalak, 2022; Rastogi et al., 2017; Solaiman et al., 2020). These research studies have been carried out in several different countries with the goals of increasing crop output and enhancing plants' flexibility and resilience in the face of abiotic stresses (Ambrosone et al., 2012; Nguyen et al., 2015; Paramo et al., 2020; B. R. Singh et al., 2012). Researchers have shown a great interest in metal-based nanoparticles and the oxides that correspond to them.

These nanomaterials include a wide variety of metals, such as gold, silver, copper, aluminum, and iron; in addition, they form a variety of metal oxides, such as titanium dioxide (TiO_2; titanium has oxidation state "OS"= Ti^{4+}), cerium oxide (CeO_2; cerium has OS= Ce^{4+}), iron oxide (FeO; iron has OS= Fe^{2+}), aluminum oxide (Al_2O_3; aluminum has OS= Al^{3+}), and zinc oxide (ZnO; zinc has OS= Zn^{2+}) (Abdel Latef et al., 2017; Alabdallah & Alzahrani, 2020; Taran et al., 2017).

Scientists have employed the concentration-dependent impacts of magnetic nanoparticles (MNPs) on the growth and development of plants to illustrate their potential in helping plants endure abiotic challenges (Sarraf et al., 2022). Depending on the particular mechanism of action that MNPs possess, they can be applied to plants in various ways, including as a seed priming agent, soil treatments, or foliar applications. Several studies have shed light on the positive effects that specific ZnO-NPs have on certain plant species when those plants are subjected to various abiotic stresses. It has been discovered that zinc oxide nanoparticles (ZnO-NPs) can improve nutrient absorption, regulate the Na^+/K^+ ratio, maintain water balance, facilitate ion accumulation, and buffer the adverse effects of abiotic stressors. The elevation of flavonoid, anthocyanin, phenolic, and photosynthetic pigment levels and the overexpression of antioxidant enzymes are all responsible for these benefits. In addition, ZnO-NPs have been shown to reduce the expression of stress markers such as malondialdehyde (MDA) and hydrogen peroxide (H_2O_2) while also affecting transcriptional factors.

Foliar zinc can increase wheat yield in alkaline soils (Khattak et al., 2015). A study examined how foliar ZnO and its nanoparticle treatments affected safflower growth and yield under various watering regimens (Ghiyasi et al., 2023). ZnO foliar treatments increased safflower yield. The optimal spraying concentration was found to be 5-10 g L^{-1}. The authors discovered that applying ZnO increased crop productivity under various stress scenarios. Photosynthesis and dry matter accumulation increased biomass yield. ZnO foliar treatments increased the number of capitula per plant and the number of seeds.

Many of the previous research focuses on high concentrations (5–10 g L^{-1}), although there is limited understanding of nanoparticle behavior at lower, signaling-level levels (2 g/L and 75–150 mg/L). So, the current study was designed to examine how those low dosages of the synthesized ZnO-NPs can act in case of being sprayed on the leaves of tomato and maize leaves.

Nano-fertilizers improve product growth and performance while being environmentally friendly. Thus, molecular strategies using NPs can improve plant nutrition and stress resistance (Ghiyasi et al., 2023). Nano-fertilizers increase nutrient use efficiency, reduce chemical

fertilizer environmental impact, and minimize fertilization frequency (Aljutheri et al., 2020). The study found that safflower morphology and physiology have improved, especially in drought. Addressing Zn shortage developmental signals like seed oil content increases could explain this production increase (Rossi et al., 2019). The study revealed that nanomaterials applied by foliar spraying increased growth and yield. This relates to nanomaterial characteristics. After spraying nanoparticles on the plant, they assimilate quickly. Few researchers have examined how nanoparticles affect plant development or stress response, and the behavior of different NPs in plants is unknown (Rossi et al., 2019). The study discovered that 10 mg L^{-1} ZnO-NPs enhanced safflower growth, especially with extended irrigation intervals. This shows that safflower absorbs ZnO-NPs better than their conventional form. Because of their tiny size (1–100 nm), ZnO-NPs are more available to plants than regular ZnO (Rajput et al., 2018).

2.5. Modulation of stress-responsive gene expression and enzymatic activity by ZnO-NPs

The biological effects of ZnO-NPs are shaped by complex, integrated factors, as evidenced by differences in application technique and the physiological sensitivity of the crop under study. The inherent physical characteristics, such as nanoparticle morphology and size, strongly affect physiological and molecular outcomes (Seleiman, Ahmad, Battaglia, et al., 2023). The structural and configurational attributes determine the specific surface area available for biological interactions, and the ability of the nanoparticles to penetrate the target plant cells or leaves (Afzal et al., 2024). So, differences in nanoparticle structures lead to varied responses in the plant defense system (enzymatic and non-enzymatic), reducing ROS levels and alleviating the harmful morphological alterations induced by stress (Cao et al., 2025).

The delivery methods of nanoparticles, such as ZnO-NPs, also affect plant responses, including foliar application, seed priming, and hydroponic applications, which in turn influence nanoparticles' translocation, biodegradability, and sedimentation patterns (Balusamy et al., 2023). The plant species and genotype are also determining the response to the nanoparticles, for example the foliar application emphasizes nutrient absorption and accumulating osmoprotectants in soyabean (Dola & Mannan, 2022), in case it is regulating the chilling-induced genes expression levels and antioxidant enzymes activities in sugarcane (Elsheery et al., 2020).

Zinc oxide nanoparticles (ZnO-NPs) and some other nanoparticles significantly impact numerous plant types as stimulators to the antioxidative defensive mechanisms (Figure 3) and assimilate into the soil around the plant. In contrast, others enter the leaf of the plant and accumulate in the edible sections (Munir et al., 2021).

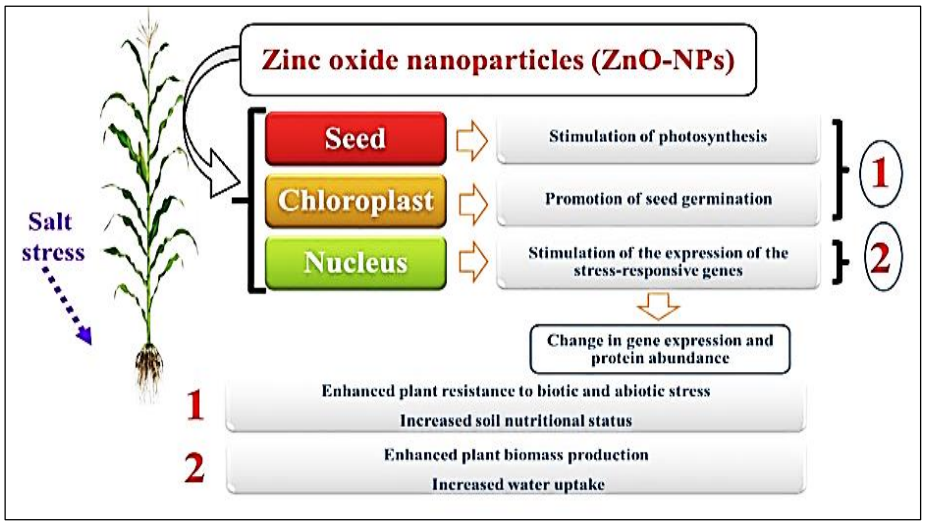

Figure 3. Illustration of proposed know-how of NPs in boosting the antioxidant enzymes to enhance the salt-stressed plants overcoming the harmful effects of ROS (Ahmed, et al., 2024a).
***NPs**= nanoparticles, **OH**˙ = hydroxyl radical, **H_2O**= water molecule, **O_2**= oxygen molecule, and **H_2O_2**= hydrogen peroxide.*

Among these genes, certain ones were shown to be associated with oxidative stress and metal responses, such as the vacuolar proton exchanger, superoxide dismutase (SOD), cytochrome P450-dependent oxidase, and peroxidase. In addition to identifying genes associated with plant defense, the study also revealed the presence of around 81 genes that exhibited downregulation. Some genes involved in regulating auxin, the ethylene signaling system, and systemic acquired resistance (SAR) were identified as responsible for conferring improved and often enduring protection against various illnesses in the plant kingdom. Identifying proteins that exhibit a reaction to silver nanoparticles has revealed their association with several metabolic processes, such as transcription, protein degradation, the oxidative stress response system, and the calcium signaling pathway (Mirzajani et al., 2014).

After treatment with zinc oxide nanoparticles, 660 up- and 826 down-regulated genes were found in *Arabidopsis thaliana* L. Tomato germination rate and seed germination were enhanced by treatment with multi-walled carbon nanotubes, which increase the expression of genes that respond to stress (Khodakovskaya et al., 2009). The effect of synthesized ZnO-NPs on plant characteristics is presented in Figure 4 and Table 1.

Although previous literature comprehensively detailed the physiological and antioxidant benefits of ZnO-NPs in improving crop tolerance to salinity, the current study primarily focused on descriptive analyses, emphasizing growth-attreibutional results like yield and restoring the growth characterstics (chlorophyll, plant height, leaf area, and stem width).

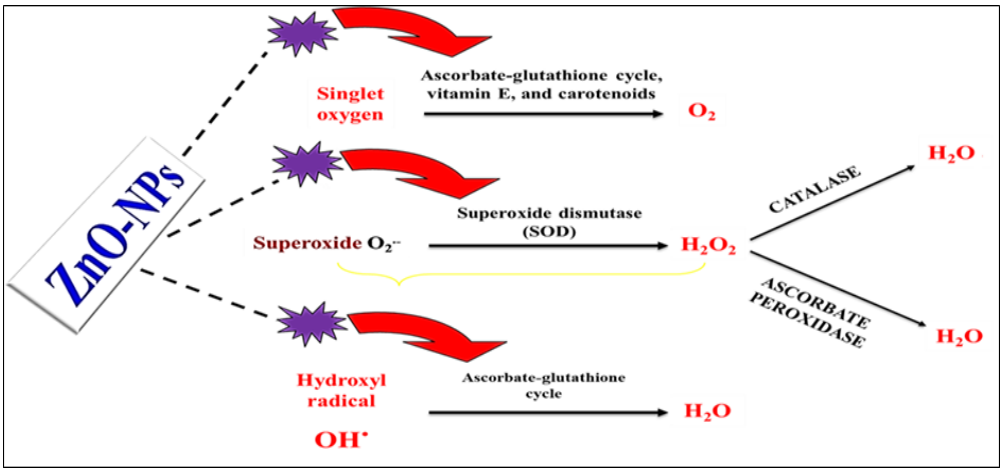

Figure 4. How engineered nanoparticles modify ecophysiological and molecular responses in salt-stressed plants. The image of the maize crop is just an example (Ahmed et al., 2024a).

Table 1. Investigating the adaptability of certain plant species to salt stress by utilizing zinc oxide nanoparticles (ZnO-NPs) (Ahmed et al., 2023a).

	Characters (Size ~nm)	Plant	Mode of application	Morphophysio-logical responses	References
Zinc oxide nanoparticles (ZnO-NPs)	Spherical and hexagonal (~20 nm), Spherical (80), Spherical (30), or Hexagonal, square, and spherical (2–64) (El-Badri et al., 2021; Ghani et al., 2022; Hassan et al., 2018; Song et al., 2021; Venkatachalam et al., 2017).	*Sorghum bicolor* L.	Hydroponics, silica sand, foliar fertilization, seed treatment (priming), and foliar spray (El-Badri et al., 2021; Ghani et al., 2022; Hassan et al., 2018; Song et al., 2021; Venkatachalam et al., 2017).	Reduction in ROS accumulation and lipid peroxidation, improved antioxidant defense system, nutrient absorption, and osmolytes accumulation, seedling development through the biosynthesis of pigments, osmotic protection, reduction of ROS accumulation, adjustment of antioxidant enzymes, and improvement of the nutrient absorption, upregulation of the chilling induced gene expression of the antioxidant system and chilling response transcription factors, or Reduced MDA content and the elevated level of antioxidant enzyme activities.	(Rakgotho et al., 2022)
		Tomato (variety PKM-1)			(Faizan et al., 2021)
		Soybean (cv. Giza111)			(Soliman et al., 2020)
		Glycine max L.			(Gaafar, et al., 2020)
		Rapeseed (Okapi cultivar)			(Akhavan et al., 2020)
		Brassica napus L.			(Hezaveh et al., 2019)
		Triticum aestivum L.			(Lalarukh et al., 2022)
		Zea mays L.			(Fathi et al., 2017)

And since an exhaustive review of the previous results revealed a significant gap in our comprehension of the precise "reconfiguration" of the transcriptome that governs these systemic defenses, particularly at lower dosages that activate signals, and the high-resolution transcriptomic analysis is also missing, so that gap in how energy diversion is regulated at the gene expression level in commercial crops such as tomato and maize under stress had to be addressed. So, the current study used RNA-seq to identify the genetic switches that ZnO-NPs activate to minimize the undesired metabolic changes induced by salt stress.

2.6. The effect of Zinc oxide nanoparticles on the pathogens

The pathogens have developed resistance to metronidazole, and the disease has many distressing side effects, including allergy, nausea, vomiting, increased susceptibility to cervical cancer, poor pregnancy outcomes, infertility, and a role in human immunodeficiency virus (HIV) transmission. Novel and effective therapeutic agents are needed (Tam et al., 2021). Tomato plants (*Lycopersicon esculentum* Mill.) synthesize the glycoalkaloids dehydrotomatine and alpha-tomatine, possibly as a defense against bacteria, fungi, viruses, and insects (Kozukue et al., 2004). ZnO-NPs, owing to their biodegradable and antibacterial properties in nanostructured form, are a feasible tool for controlling diseases in agriculture (Orfei et al., 2025; Rehman et al., 2024). They have been successfully tested as antibacterial agents, with high activity against various bacteria, fungi, and viruses (Siddiqi et al., 2018). ZnO-NPs have been found to protect *Nicotiana benthamiana* L. and tomato plants from the tobacco mosaic virus (TMV) (Cai et al., 2019; Sofy et al., 2021).

Additionally, metal/metal oxide nanoparticles have diverse applications, notably in the food business (Smaoui et al., 2023). Applications in the food industry may involve the creation of novel biodegradable packaging materials that possess antibacterial qualities, as well as the development of protective coatings for work surfaces, specifically in the context of meat processing (Burmistrov et al., 2022; Gudkov et al., 2023, 2024). A liquid-phase nanocomposite comprising ZnO nanoparticles (NPs) and fluoroplastic was created, which is suitable for application on several surfaces, including sputtering. When the mixture hardens, it creates a strong wall that stops the growth of important medical infectious Gram-positive bacteria (*Listeria monocytogenes* and *Staphylococcus aureus*) and Gram-negative bacteria (*Pseudomonas aeruginosa* and *Staphylococcus typhimurium*) (Gudkov et al., 2023; Serov et al., 2022). Furthermore, cultures of eukaryotic cells do not experience any harmful effects from the produced composite (Gudkov et al., 2023; Serov, Baimler, et al., 2022). The food industry has used a similar nanomaterial to treat cutting boards in meat processing facilities (Serov et al., 2022; Serov, Burmistrov, et al., 2022).

There is a notable lack of evidence linking nanoparticle-induced salt tolerance to the functional antimicrobial characteristics of the plant's secondary metabolites from the leaf extracts that usually used as agricultural wastes form both tomato and maize. This dissertation addresses these deficiencies by surpassing traditional observations to provide a framework between the ZnO-NPs-salt-stressed plants and the enhanced biopotency of leaf extracts in *Solanum lycopersicum* L. and *Zea mays* L. against some food-borne pathogenic bacteria and myctoxegenic fungi.

2.7. Molecular docking and the antimicrobial activities

In silico molecular docking has become an essential computational approach for elucidating the mechanisms underlying observed antimicrobial properties (Figure 5). The principal aim of molecular docking is to predict the binding affinity and orientation of plant-derived ligands within the active sites of designated microbial protein targets, such as DNA gyrase or protease enzymes (Kitchener, 2021; Nivatya et al., 2025).

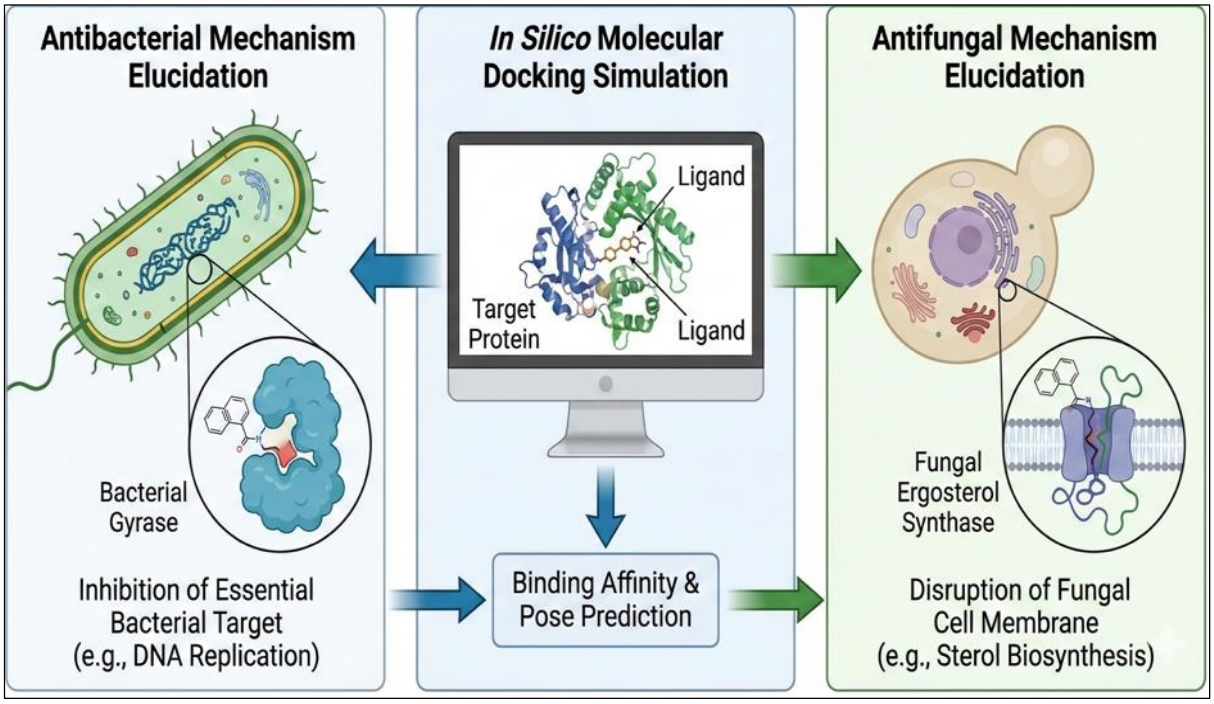

Figure 5. Computational insights into antimicrobial mechanism via molecular docking. Created with BioRender software (Version 1.0) https://biorender.com.

The application of *in silico* docking in natural product research has significantly enhanced the identification of bioactive scaffolds. Researchers can distinguish between non-specific interactions and robust inhibitory potential by simulating the thermodynamic stability of ligand-receptor complexes (Trombetta, 2022). This methodology is particularly crucial for plant extracts, which frequently comprise numerous distinct chemicals. Docking facilitates the "virtual isolation" of the most promising metabolites, enabling their prioritization before costly, time-intensive *in vitro* testing.

Computational microbiology often emphasizes DNA gyrase for its essential role in bacterial DNA replication and its structural differences from human topoisomerases. Docking studies frequently demonstrate interactions between plant-derived compounds, including some flavonoids and polyphenols, and the ATP-binding pocket of the GyrB subunit, thereby efficiently inhibiting the bacterial catalytic cycle (Gaikwad, 2023). In a similar vein, the

examination of microbial proteases uses docking techniques to quantitatively evaluate their binding affinity.

These scoring functions frequently exhibit a robust association with observed IC_{50} values. This elucidates why certain plant extracts are notably effective against perilous strains (Khan, 2021). Molecular docking transcends mere identification of molecules; it also enhances the structural integrity of plant-derived chemicals. By analyzing distinctive hydrogen-bonding configurations and hydrophobic interactions within the active site, researchers can predict how minor chemical modifications to a plant ligand may enhance its antibacterial efficacy (Pritchard & Du, 2023). This predictive capability converts conventional knowledge into a systematic, scientifically validated approach for medication discovery, thereby connecting old herbal remedies with contemporary pharmacology.

Nanoparticles (NPs) possess a significant surface-to-volume ratio and exhibit great reactivity. Over the past decade, metal-oxide nanoparticles have gained prominence due to their ability to enhance durability. Nevertheless, modern literature sometimes lacks a structural or computational justification for the improvement of plant quality by these nanoparticles. This dissertation goes beyond fundamental growth findings by employing molecular docking to clarify the binding interactions between ZnO-NPs-enriched metabolites, including various phenolic compounds detected, and targeted pathogen proteins, filling a notable gap in the previous studies on nano-agriculture.

3. MATERIALS AND METHODS

3.1. Design, preparations, and equipment for tomato planting

Tomato (*Solanum lycopersicum* L.) seeds of the variety Kecskemétii 549 (K-549) were used for the current experiment. Healthy tomato seeds were surface sterilized with 70% ethanol for 2 min and washed with deionized water three times. The seeds of the tomato cultivar were sown in a plastic tray (seedling tray) (29 May 2023), and after one month at the 3–4 true leaves stage (27 June 2023), the seedlings were transplanted in individual plastic pots. At 30 days after sowing (DAS), the plants were transferred into 28 cm diameter and 28 cm depth pots packed with soil and peat moss in a ratio of 1:1. Humidity and temperature inside the greenhouse were adjusted using a ventilation system and an automated window opening system at a range of day/night temperatures of 25/20 ± 5 °C and 60–65% relative humidity. Six treatments were applied, namely T1: control treatment (irrigation with distilled water "dw"), T2: irrigation with distilled water + foliar spray of ZnO-NPs (75 mg/L), T3: irrigation distilled water + foliar spray of ZnO-NPs (150 mg/L), T4: irrigation with saline solutions (150 mM NaCl), T5: irrigation with saline solutions (150 mM NaCl) + foliar spray of ZnO-NPs (75 mg/L), and T6: irrigation with saline solutions (150 mM NaCl) + foliar spray of ZnO-NPs (150 mg/L). Each pot contained two transplanted seedlings, and after two weeks, only one remained in the pot to continue growth. Each treatment had 4 pots (replicates).

The NaCl (150 mM) stress solution was applied in the soil on the 10^{th} day after transplanting (40 DAS) to provide salt stress. A foliar spray of ZnO-NPs was applied at different concentrations *viz.*, 75 or 150 mg/L three times at 10 days after salt stress (20, 34, and 48 DAT) (50, 64, and 78 DAS), and these specific times were chosen to include the vegetative and generative phases in the tomato plants. And, here is the BBCH scale:

- Salt stress application (150 mM NaCl): Establishment / Early elongation (from the end of leaf development to the start of stem elongation).
- First ZnO-NPs foliar spray: Inflorescence emergence (first flower cluster visible to flower buds enlarging).
- Second ZnO-NPs foliar spray: Full flowering (first inflorescence flowers open).
- Third ZnO-NPs foliar spray: Fruit development (first fruit cluster reaching typical size).

Control plants were treated with only distilled water. To unify soil electric conductivity (EC), EC water drainage was monitored daily for all treatments, and it was maintained equal to the EC irrigating solution.

That was done by allowing enough drainage from the root zone by the use of a corresponding saline solution until equilibrium between the EC of water drainage and irrigating solution. In that way, the EC root zone stabilized at the specified set point during the experiment. Consequently, the amount of water added at each time ranged between 1 and 1.5 Liters. It was adjusted based on the EC water drainage obtained at each time.

Plant height, stem diameter, leaf area, and chlorophyll content were measured first at 10 days after transplanting (DAT). Moreover, 2 kg of pre-washed and dried gravel was used to line the pot base and was covered by a plastic net. Three 8 mm holes were designed at the bottom of the pot using a hole-punched device for watering and aeration purposes. The remaining empty pot was filled with soil peat mixture (1:1 by weight): soil from "A" horizon of an Eutric cambisol soil, having a sandy clay loam texture, was collected from the research farm area of the Hungarian University of Agriculture and Life Sciences, Georgikon Campus, and Baltic peat (DURPETA FÖLD PH 5,5-6,5, profi mix 2B 250 L, 04789) was obtained from Latvia. Both soil and peat were sieved through a 4 mm sieve to obtain a finer and more favorable growth medium. Then, 4.5 kg of soil and 4.5 kg of peat were mixed using a cement mixer to obtain a homogenized mixture that was used as a growth medium in pots. The moisture content and water-holding capacity of the soil peat mixture were determined by the gravimetric method (Imakumbili et al., 2021) to quantify the amount of irrigation to be supplied to control and treated pots. The detailed protocols are presented in the appendix (A4-1 and A4-2).

3.2. Layout, scheduling, and implementation for growing maize plants

An experimental study employed a specific type of maize, FAO P0023 *Zea mays* L., on soil with a sandy loam texture. The soil used had the following physicochemical properties: water percentage at a field capacity of 30.28%, water percentage at the constant point of wilting of 24.4%, bulk density of 1.2 g cm^{-3}, pH of 7, with an organic matter content of 1.2%, and electric conductivity (EC) of 0.5 dS m^{-1} in the top 0.2 m of soil. The irrigation water quality employed for the experiment was satisfactory, with an electrical conductivity (EC) of 0.52 dS m^{-1} and a pH of 7.1. We conducted weekly monitoring of the soil's electrical conductivity (EC). The maize kernels were planted in rows within the plot, each measuring 3.0 m by 1.5 m. Each plot contained 45 seeded plants, which served as a copy, and it was replicated four times to fulfill the random distribution. The space between two consecutive plants in the same row was 20 cm, while the spacing between two neighboring rows was 75 cm. The treatment units were organized in a fully randomized fashion with four repetitions.

The plants were irrigated every 10 days. After sowing, the seeds, then seedlings, were left in the rainwater for the first 35 days to establish roots before the stress application. Salinity treatments were started 35 days after sowing (DAS), and ZnO-NPs were started at 60 DAS. The treatments were: M1: control treatment, irrigation only with tap water, M2: irrigation with saline solution (150 mM sodium chloride solution), M3: irrigation with 150 mM sodium chloride solution + 2 g/L ZnO-NPs, and M4: irrigation with tap water +2 g/L ZnO-NPs. Foliar ZnO-NPs were applied using a handheld aerosol-propelled sprayer. The salinity treatment was devised by incorporating a suitable quantity of NaCl into the irrigation water. The cumulative amount of water given from the start of planting treatments till the harvest was determined from the FAO CROPWAT 0.8 and CLIMWAT 0.2 software, "https://www.fao.org/land-water/databases-and-software/cropwat/en/", accessed on 4 June 2023 (Food & Organization, 1998). The Land and Water Development Division of FAO created CROPWAT is a decision-support tool that was used. The Land and Water Development Division of FAO designed this software application to calculate the water required for crops and irrigation. It uses data on soil, climate, and crop characteristics to make accurate calculations.

Furthermore, the application facilitates the creation of irrigation schedules tailored to various management situations, as well as the computation of water supply schemes for diverse crop patterns. Farmers can utilize CROPWAT 8.0 to assess their irrigation techniques and predict crop productivity in both rainfed and irrigated environments. The previous facts reinforced the section on materials and methods, validating the techniques employed. All calculation procedures used in CROPWAT 8.0 are based on the two FAO publications of the Irrigation and Drainage Series, namely "Crop Evapotranspiration—Guidelines for computing crop water requirements", No. 56 https://www.fao.org/docrep/X0490E/X0490E00.htm, accessed on 4 June 2023, and No. 33 titled "Yield response to water". The table demonstrates the volume of required water applied in liters, as the FAO CROPWAT and CLIMWAT software presented all the data in millimeters. The irrigation was applied in 9 sequential irrigations. The same water quantity as in the sixth irrigation was applied to the last three irrigations.

Plants were harvested 142 days after sowing. Post-harvest measurements were taken on two different plants from each replicate. The main purpose of that system of irrigation was to study the effect of compensating the irrigation water requirements of corn plants during the growing season by adding a sodium chloride solution (salt water), in a combined manner of rainwater and sodium chloride solution to irrigate the corn plants. By planting, extra mono-potassium phosphate was mixed into the soil.

The plants without stress were sprayed with the same amount of water. When planting began, all plots received the identical NPK fertilizers. Three instances of hand weeding occurred throughout the trial period. Five plants in one of the three rows were labeled to investigate various biochemical and growth properties at the appropriate stage; in the other three rows, the plants were cultivated to maturity to evaluate grain production. Four distinct times were selected to provide the ZnO-NPs treatment to the maize plants, taking into account their vegetative and generative phases:

- 1st time, in the vegetative phase (60 DAS).
- 2nd time, in the vegetative phase (71 DAS).
- 3rd time, in the reproductive development stages (87 DAS).
- 4th time, by the end of the generative phase (100 DAS).

And here is the BBCH scale of the treatments to provide the phonological description and the experimental milestone of the maize plants:

- Dry seed (sowing) — Start of experiment
- Germination and emergence — Establishment phase (rainwater)
- Leaf development (V-stages) — Root establishment
- Stem elongation (1st–2nd node detectable) — Commencement of salinity stress (M2 and M3)
- Late stem elongation/Near "V12" — 1st ZnO-NPs application (vegetative)
- Inflorescence emergence (tassel visible) — 2nd ZnO-NPs application (late vegetative)
- Flowering/Anthesis (pollen shedding & silking) — 3rd ZnO-NPs application (Reproductive)
- Fruit development/Milk to early dough stage — 4th ZnO-NPs application (generative end)
- Ripening (dough stage to fully ripe) — Maturation and dry down
- Senescence/Harvested product — Final harvest

3.3. Chemical synthesis of zinc oxide nanoparticles

ZnO nanoparticles were synthesized by the precipitation method using zinc nitrate hexahydrate "$Zn(NO_3)_2 \cdot 6H_2O$, thermos scientific A16282, LOT: 10242486" and sodium hydroxide "NaOH, 98.5–100.5%, pellets, AnalaR NORMAPUR® Reag. Ph. Eur. analytical reagent" as precursors. ZnO nanoparticles were produced by mixing aqueous solutions of zinc nitrate and sodium hydroxide.

ZnO nanoparticles were formed by the reaction between Zn^{2+} and hydroxide ions as shown by the following equations (Nejati et al., 2011); (1) $Zn(NO_3)_2 \rightarrow Zn^{2+} + 2NO^{3-}$ (2) $Zn^{2+} + 2OH^{-} \rightarrow Zn(OH)_2$ (3) $Zn(OH)_2 \rightarrow ZnO + H_2O$. The aqueous solution was prepared by mixing zinc nitrate hexahydrate and sodium hydroxide. The process involved dissolving 2.28 g of zinc nitrate hexahydrate in 75 mL of pure water, then adding 0.6 g of NaOH in 150 mL of pure water dropwise under magnetic stirring. The solution was centrifuged at 7871× *g* for 10 min at 25 °C, washed with pure water, dried at 60 °C for 24 h, and calcined at 200 °C for 2 h in an oven. Different concentrations of ZnO-NPs solution for foliar application were prepared by dissolving the obtained white crystals in distilled water using ultrasonic waves for 10 min.

Regarding the selected concentration of 2 g/L ZnO-NPs in *Zea mays* L. experiment. ZnO-NPs were used as a fertilizer source, not just a hormonal spray on the leaves. Some researchers used ZnO-NPs at concentrations of 1 and 1.25 g/L (Kumar et al., 2021). And, in another study by Ghiyasi et al. (2023), the authors used ZnO-NPs at a concentration of 10 g L^{-1}. They found that ZnO-NPs ameliorated the deleterious effects of water deficit in sunflowers. On the other hand, the selected ZnO-NPs (0.075 and 0.15 g/L) for *Solanum lycopersicum* L. were evaluated within the hormetic zone identified in the literature (Faizan et al., 2021). The concentrations were maintained below the phytotoxic threshold (Rajput, 2018; Venzhik, 2024), typically exceeding 500 mg/L for *Solanum lycopersicum* L. Foliar application was chosen to avoid soil-zinc immobilization, enabling direct nutrient absorption. Our data, which indicate an increase in biomass, confirm that these doses functioned as mitigators rather than additional stressors.

3.4. Characterization of chemically synthesized zinc oxide nanoparticles

The optical properties of ZnO-NPs were monitored by UV–VIS absorption spectroscopy by Genesys spectrophotometer (PG Instruments Ltd., T 80, UK) in the central lab of the Agronomy Department, Hungarian University of Agriculture and Life Sciences, Georgikon campus, Hungary, Keszthely. UV–VIS spectra were recorded in the wavelength range of 300–700 nm (Zak et al., 2011). The X-ray diffraction (XRD) measurements were carried out at the Micro Analytical Center, Cairo University, Faculty of Science, Giza, Egypt, using a Philips PW 3710-type instrument (CuKα radiation, $\lambda = 1.54056$ Å, 50 kV, 40 mA), in the 4°–15° 2θ range with a scanning speed of 0.02°/s and 1 s dwell time. The finely powdered samples were loaded into back-packed mounts to minimize preferential particle orientation. Calcined ZnO-NPs were applied as a reference sample for estimating the instrumental broadening for the average crystallite size calculation (Zak et al., 2011).

The Fourier-transform infrared (FTIR) spectra were recorded on a Bruker Vertex 70v instrument equipped with a Bruker Diamond ATR compartment, with a resolution of 2 cm^{-1}, using a DTGS detector at Nanolab, Pannon University, Veszprém, Hungary. The recorded spectra were the average of 512 individual scans (Zak et al., 2011).

Transmission electron microscope investigations were carried out at the Micro Analytical Center, Cairo University, Faculty of Science, Giza, Egypt, using a FEI Talos F200X type electron microscope Thermo Fisher Scientific Inc., with an X-FEG electron source, operated at 200 kV accelerator potential, in conventional transmission (TEM) and scanning modes (STEM). The composition of samples was analyzed using an energy-dispersive X-ray (EDAX) spectrometer attached to the transmission electron microscope. Both scanning and conventional TEM images were recorded. The samples were prepared from aqueous dispersion (MilliQ) by laying a droplet onto a lacy carbon-coated copper grid, which was dried at 60 °C before measurement (Solaiman et al., 2020).

The hydrodynamic size and zeta potential of ZnO-NPs in both water and full cell culture media were measured using dynamic light scattering (DLS) with the Nano-ZetaSizer-HT device from Malvern Instruments Zetasizer Nano-ZS in the UK. DLS examines the velocity distribution of particle motion by quantifying dynamic variations in light scattering intensity resulting from the Brownian motion of the particle. This method produces a hydrodynamic radius or diameter, which can be determined using the Stokes–Einstein equation. It provides a comprehensive measurement of the particle's perpendicular dimension to the light source at that particular moment.

The Zetasizer Nano-ZS utilizes laser Doppler velocimetry (LDV) as its measurement technique to determine the Zeta potential of particles in a solution. This method employs a laser that is directed into the sample to determine the speed of the particles under the influence of a known electric field, referred to as electrophoretic mobility. The device utilizes a 4 mW He-Ne 633 nm laser to analyze the samples, in addition to an electric field generator specifically designed for LDV measurements. The ZnO-NPs were diluted in deionized water and mixed vigorously for 5 min to create a uniform solution. Then, 1 mL of the solution was transferred to a Malvern Clear Zeta Potential cell for LDV measurements. The majority of solutions were prepared at a concentration of 25 µg/mL (Murdock et al., 2008).

3.5. Determination of the macro and microelements in tomato and maize leaves

The leaf samples were dried in an oven at 70 °C for 24 h. Approximately 0.2 g of the dried leaf and bark samples, respectively, were treated individually with 8 mL HNO_3 (65% Merck) and 10 mL H_2O_2 (30% Merck).

Then, they were mineralized using a microwave digestion system for 40 min. After 40 min of digestion, the samples were cooled for 30 min, and the clear solutions were filtered and brought at 50 mL with distilled deionized water. Metals concentrations in the final solutions were analyzed by Flame Atomic Absorption Spectrometry (FAAS; iCE 3000 Series, Thermo Fisher Scientific Inc., Waltham, MA, US). The concentration of the primary standards of Na, K, Mg, Zn, Cu, and Mn elements was 1000 ppm (1000 mg/L), and the matrixes were 2% HNO_3 (Barbes et al., 2014).

3.6. Determination of chlorophyll and growth attributes

In the current study, the previous recordings were collected in 4 different stages. Chlorophyll content per unit area was determined using Soil Plant Analysis Development (SPAD) 502 Plus, Konica Minolta.

The readings of tomato were recorded in SPAD units. SPAD values were recorded according to the biggest leaf on all its leaflets. The readings were recorded every 10 days starting at 10 DAT. The values of maize were measured at the apical, middle, and basal regions of the most giant leaf, where the leaf collar was visible. The leaf blade was included as the surface measurement area, but the leaf vein and mid-rib were excluded. The measurements were documented at intervals of 10 days, commencing from 35 days after sowing (DAS).

The area of tomato leaf (cm^2) was determined according to (Carmassi et al., 2010). It was recorded using the following equation: S= L.W. K. The maximum width (W) and length (L) of each sampled leaf were measured with a ruler. In tomato, the length was measured as the distance between the insertions of the first leaflet on the rachis to the distal end, whereas the width was measured on the widest leaflet. S: leaf surface area of the plant (cm^2). L: maximum leaf length (cm). W: maximum leaf width (cm). The correction coefficient (K) for the tomato surface was 0.5. The leaf's area (cm^2) of maize was measured using the method described by Sakalova (1979) (Sakalova, 1979). The data were obtained by applying the following equation: $S = L \times W \times N \times K$, representing the leaf surface area of the plant, measured in square centimeters (cm^2). L represents the maximum length of a leaf, measured in centimeters. W represents the greatest width of a leaf, measured in centimeters. N represents the number of leaves in the plant at the estimation time. The correction coefficient for the maize surface was 0.75, according to Musa et al. (2016) (Musa & Hassan, 2016).

Tomato plant height was measured in centimeters at each plant from the soil surface using the ruler that was placed on the ground next to the stem and measured to the height of the tallest stem (ignoring the leaves).

The stem thickness of each tomato plant was measured in centimeters using a caliper. From the ground level to the very top of the arch of the topmost leaf, with its pointed tip pointing downward, the height of each maize plant was measured in cm. The diameter of each maize plant's stem was measured in centimeters employing a caliper.

3.7. Determination of proline and protein contents

Fresh 500 mg leaf samples were extracted with sulfosalicylic acid. The extraction also used equal amounts of glacial acetic acid and acidic ninhydrin. After heating at 100 °C, 4 mL of toluene was added to the samples. A Genesys (PG Instruments Ltd., T 80, Lutterworth, UK) spectrophotometer evaluated the aspirated layer's absorbance at 520 nm. Proline concentration was measured in micrograms per gram FW (Bates et al., 1973). To determine the protein content, a homogenized 1 g of newly generated leaves was added into a protein extraction buffer. The buffer contained 10 mM tris-HCl (pH = 8.1), 5 mM β-mercaptoethanol, 0.57 mM PMSF, and 10 mM pH 8 EDTA. The mixture was then centrifuged for 10 min at 17,709× *g*. After gathering the liquid, Bradford reagent was used to induce the color. A Genesys (PG Instruments Ltd., T 80, UK) spectrophotometer measured the color intensity at 595 nm, and the protein concentration was presented in micrograms per gram FW (Bradford, 1976).

3.8. Determination of total free amino acids

The fresh leaves were pulverized into a fine powder using a mortar and pestle. The resulting powder was then mixed with 10 mL of phosphate buffer solution, which had a concentration of 0.05 M. The pulverized leaves were centrifuged at 12,298× *g* for 10 min at 4 °C. The reaction mixture in a test tube contained 0.5 mL of the extract, 0.5 mL of 4% ninhydrin, and 0.5 mL of 2% pyridine. The test tubes were vigorously vortexed and heated at 100 °C for 30 min in a water bath. The optical density at 570 nm was measured using a spectrophotometer (Genesys PG Instruments Ltd., T 80, UK) (Zafar et al., 2022).

3.9. Determination of total hydrolyzable sugars

The total soluble sugars were extracted and estimated using a significantly modified method. Dry tissue was immersed in 5 mL of 2.5 N HCl in a boiling water bath for 3 h with agitation to extract soluble sugars. Finally, the samples were centrifuged at 3075× *g*. The extracts were boiled for 10 min with 3.0 mL of freshly prepared anthrone and chilled to quantify total soluble sugars. The spectrophotometer (Genesys PG Instruments Ltd., T 80, UK) measured the green color intensity at 630 nm absorbance (Prud'homme et al., 1992).

3.10. Determination of lipid peroxidation

A slightly modified method used malondialdehyde (MDA) concentration to quantify lipid peroxidation. During this process, 100 mg of fresh plant leaves were well mixed in 1 mL of 0.1% TCA. After vigorous mixing, the tubes were centrifuged at 20,784× *g* at 4 °C for 10 min. In a Falcon tube, 800 microliters of centrifuged liquid were mixed with 2 milliliters of 0.5% TBA solution. A water bath heated the mixture to 80 °C for 25 min. After incubation, the tubes were chilled on ice for 5 min and centrifuged at 20,784× *g* at 4 °C for 10 min to separate and collect any remaining TBA. Using a Genesys (PG Instruments Ltd., T 80, UK) spectrophotometer at 532 and 600 nm, optical density was determined (Heath & Packer, 1968).

3.11. Determination of hydrogen peroxide (H_2O_2)

The fresh leaves, weighing approximately 0.5 g, were crushed in 5 mL of a solution containing 0.1% (*w*/*w*) trichloroacetic acid. The resulting mixture was centrifuged at 17,709× *g* for 15 min. Phosphate buffer with a pH of 7.2 and a concentration of 100 mM, and potassium iodide were added into a 0.5 mL solution of the reaction mixture. The achieved color was measured using a UV-visible spectrophotometer (Genesys PG Instruments Ltd., T 80, UK), which measured the absorbance of the mixture at a wavelength of 390 nm (Alexieva et al., 2001).

3.12. Determination of total flavonoid compounds (TFCs)

The flavonoid levels in tomato and maize aqueous extracts were assessed using the aluminum chloride colorimetric technique. Test tubes filled with tomato leaf extract were mixed with 5% sodium nitrite, 10% aluminum chloride, and 1 M sodium hydroxide. The tubes were incubated for 15 min, and the absorbance of the pink color was measured using a spectrophotometer (Genesys PG Instruments Ltd., T 80, UK) at 510 nm. Quercetin was used as a standard substance, and the total flavonoid content was quantified as the amount of Quercetin equivalent in micrograms per gram of dry extract (Ahmed et al., 2023b).

3.13. Determination of total phenolic compounds (TPCs)

The phenolic content of tomato and maize leaves was quantified using the Folin–Ciocalteu reagent method. The extract was adjusted to 2500 µg/mL and added to a solution of 1 N Folin–Ciocalteu reagent and 20% sodium carbonate. The mixture was kept in a dark environment for 90 min. The blue color was measured at 650 nm using a spectrophotometer (Genesys PG Instruments Ltd., T 80, UK), and the total phenolic content was determined by calculating the equivalent amount of Gallic acid in micrograms per gram of dry extract (Ahmed et al., 2023c).

3.14. Determination of phenolic compounds; high-performance liquid chromatography (HPLC) analysis

The powder sample was dissolved in 2 M sodium hydroxide, flushed with N_2, and stopped. The pH was adjusted to 2 with 6 M hydrochloric acid. The resulting supernatant was collected, and phenolic compounds were extracted twice with 50 mL of ethyl ether and ethyl acetate. The organic phase was separated, and the solvent evaporated at 45 °C. The residues were re-dissolved in methanol and analyzed using HPLC. The analysis was conducted at the National Research Centre, Dokki, Cairo, Egypt (Kim et al., 2006). The analytical column used was an Eclipse XDB-C18 with a C18 guard column (Phenomenex, Torrance, CA), and the mobile phase was acetonitrile and 2% acetic acid in water. The flow rate was maintained at 0.8 mL/min for 60 min, with a gradient program from 100% B to 85% B in 30 min, from 85% B to 50% B in 20 min, from 50% B to 0% B in 5 min, and from 0% B to 100% B in 5 min. The injection volume was 50 µL, and peaks were monitored at 280, 320, and 360 nm for benzoic acid, cinnamic acid derivatives, and flavonoids. All samples were filtered through a 0.45 µm Acrodisc syringe filter (Gelman Laboratory, MI) before injection. Peaks were identified by matching retention times and UV spectra to those of the standards.

3.15. NIRS™ DS 2500 FOSS-based analysis of foliar and seed biochemical composition

The Fresh Grass Silage measuring program is offered for the FOSS NIRS^{TM} DS 2500 device (FOSS Analytical A/S Co., Ltd., Whitworth Court, Manor Park, Runcorn, Cheshire, UK). It was initially designed for immediate nutrient testing after sampling corn silages, but later, it was also recommended for testing fresh samples of other silage grasses. The five parameters mentioned (dry matter content, crude protein, ash content, NDF, and ADF) were based on the water content of the plant sample sensing. The calibrations have been stabilized for sample temperatures between 10–30 °C/50–86 °F. The sample temperature was as close to the ambient temperature as possible for optimum performance. Analyzing at a temperature higher or lower than the environment temperature increases the risk for moisture condensation or evaporation from the sample and temperature drift during the analysis. NDF and ADF were determined with heat-stable amylase according to Van Soest et al. (1991) (Van Soest et al., 1991). The dry matter was estimated according to the Association of Official Agricultural Chemists (A.O.A.C.); A.O.A.C. 930.15; for the crude protein in leaves, A.O.A.C. 990.03 was used, and ash was analyzed according to A.O.A.C. 923.03 (A.O.A.C., 2019). Crude fat, ash, and protein contents in the grains were estimated according to Van Soest et al. (1991) as well (Van Soest et al., 1991).

3.16. Fatty acid profile; gas liquid chromatography (GLC) analysis

3.16.1. Gas liquid chromatography analysis for maize grains

The process of extracting fat was carried out utilizing the “cold” approach by Cequier-Sánchez et al. (2008. The samples were pulverized and subjected to extraction using a combination of dichloromethane and methanol in a ratio of 2:1 (*v/v*). Subsequently, the substance underwent filtration and was transferred to a fresh test tube. An aqueous potassium chloride solution (0.88%) was introduced. Subsequently, the samples were centrifuged at a speed of 1500 rpm, and the rotary evaporator was used to evaporate the bottom layer. The standard referred to EN ISO 12966-1:2014/AC:2015; Guidelines on Modern Gas Chromatography of Fatty Acid Methyl Esters. Polish Committee for Standardization: Warsaw, Poland, 2015. It was followed for the sample preparation of fatty acid composition determination (Stępień et al., 2024). To accomplish the above objective, 100 mg of lipids was placed into a test tube and heated on a heating block. Subsequently, the boiling mixture was supplemented with the following reagents; the substances mentioned include 2 M sodium hydroxide, boron trifluoride complex, isooctane, and a 1% sodium chloride solution. After the operation concluded, the upper layer of isooctane was transferred to a vial and subjected to analysis. Gas chromatography was employed to analyze fatty acid esters using a TRACE 2000 gas chromatograph (Thermo Scientific, Waltham, MA, USA). Fatty acids were identified using 37 standards.

3.16.2. Gas liquid chromatography analysis for tomato leaves

According to Christie (1993), the entire lipid was transesterified using 2% sulfuric acid in methanol to produce fatty acid methyl esters (FAMEs). A gas chromatography system (Perkin Elmer Auto System XL) with a flame ionization detector and a DB5 silica capillary column (60 m × 0.32 mm i.d.) was used to analyze the fatty acids. The oven was preheated to 45°C and then set to rise to 60°C at 1°C per minute. After that, it was scheduled to rise from 60°C to 240°C at a rate of 3°C per minute. The carrier gas, helium, was introduced at a rate of 1 mL every 60 minutes. We set the injector temperature to 230°C and the detector temperature to 250°C (Christie, 1993).

3.17. Estimation of enzyme activities

3.17.1. Extraction of the enzymes

0.5 grams leaf tissue (500 mg) was blended in a 50 mM phosphate buffer of monobasic $NaH_2PO_4.2H_2O$ (Mwt: 156) and dibasic $Na_2HPO_4.2H_2O$ (Mwt: 178) (pH 7.0) containing one mM polyethyleneglycol (PEG), one mM phenylmethylsulfonyl fluoride (PMSF), 8% (*w/v*) polyvinylpyrolydone (PVP), 0.01 % (*v/v*) Triton X-100.

These mixtures were centrifuged at 11,500 rpm for 10 minutes at 4°C, the resultant supernatant was employed to assess enzyme activity (Venisse et al., 2001).

3.17.2. Estimation of peroxidase's activity

A peroxidase's enzyme unit will form 1.0 mg of purpurogallin ($C_{11}H_8O_5$) from pyrogallol ($C_6H_3(OH)_3$) in 20 seconds at pH 6.0 at 20 °C, equivalent to ~18 µM units per minute at 25°C. The absorbance's change was observed every 20 seconds for 2 minutes at 420 nm (Chance & Maehly, 1955). The reaction involved 0.05 mL of leaf extract + 2 mL of reaction mix. The reacted combination contained 100 mM phosphate buffer of monobasic $NaH_2PO_4.2H_2O$ (Mwt: 156) and dibasic $Na_2HPO_4.2H_2O$ (Mwt: 178) (pH 6), 5% (*w/v*) pyrrogallol, and 0.5% (*v/v*) hydrogen peroxide (H_2O_2).

3.17.3. Estimation of glutathione reductase's activity

A UV–Visible spectrophotometer (Genesys, PG Instruments Ltd., T 80, UK) was employed to quantify the rate of nicotinamide adenine dinucleotide phosphate (NADPH) oxidation at 340 nm to assess the activity of glutathione reductase (GR) (Venisse et al., 2001). 0.1 mL of the extract was reacted with 2 mL of an assay mixture of 0.1 M Tris buffer, 2 mM ethylene diamine tetra acetic acid (EDTA) (Mwt: 292.24), 50 µM NADPH (Mwt: 833), and 0.5 mM oxidized glutathione (GSSG) (Mwt: 612.7). The enzymatic activity was recorded using the extinction coefficient of the ß-NADPH (6.2 mM^{-1} cm^{-1}) and expressed as unit/mg protein.

3.17.4. Estimation of glutathione-s-transferase's activity

The reaction involved 0.05 mL of leaf extract + 1 mL of reaction mix. The reaction mixture consisted of 6 mM reduced glutathione (GSH), 1 mM 1-chloro-2,4-dinitrobenzene (CDNB) (Mwt: 202.55) (Sigma-Aldrich, Darmstadt, Germany) and phosphate buffer of monobasic (KH_2PO_4) (Mwt: 136.086) and dibasic (K_2HPO_4) (Mwt: 174.2). The enzyme produced one nmol of conjugated product in 1 minute for a total of 1 unit. Genesys (PG Instruments Ltd., T80, UK) was employed to spectrophotometrically measure the absorbance and the extinction coefficient of CDNB (ε340) at 340 nm was 9.6 mmol L^{-1} cm^{-1} (Habig et al., 1974).

3.17.5. Estimation of superoxide dismutase's activity

The reacted combination contained 50 mM phosphate buffer of monobasic ($NaH_2PO_4.2H_2O$) and dibasic ($Na_2HPO_4.2H_2O$) (pH = 7.8), 20 µM vitamin B2 (riboflavin), 75 mM nitro blue tetrazolium chloride (NBT) ($C_{40}H_{30}Cl_2N_{10}O_6$), 13 mM amino acid methionine, and 0.1 mM ethylene diamine tetra acetic acid (EDTA) (Mwt: 292.24) (EDTA). The absorbed bluish color was observed and measured at 560 nm with a UV–Visible spectrophotometer (Genesys, PG Instruments Ltd., T 80, UK).

A SOD's enzyme unit activity was defined as the concentration that induced half-maximal inhibition of NBT reduction. The units in which values were measured are units mg^{-1} fresh weight (FW) (Beauchamp & Fridovich, 1971).

3.17.6. Estimation of catalase's activity

Catalase catalyzes the decomposition of hydrogen peroxide (H_2O_2) into $H_2O + O_2$. The enzyme assay depends on estimating residual H_2O_2 by titration with potassium permanganate ($KMnO_4$). 0.1 M H_2O_2 solution, 10% sulfuric acid (H_2SO_4) solution, and 0.05 N $KMnO_4$ (Eq.wt: 31.6) solution were prepared to be used in the titration (Bonnichsen et al., 1947; Maehly, 1954).

3.18. Transcriptomic analysis

Leaf tissue samples weighing approximately 40-50 mg were collected from each plant in the experimental treatments. Four biological replicates were collected, and the specimens were immersed in one mL of RNALater solution and kept at −20°C until further procedures were performed.

We used paramagnetic NEXTFLEX® Poly(A) Beads 2.0 to obtain messenger RNA (mRNA) from leaf tissue specimens. Only samples with an RNA integrity number (RIN) of 7 or above were good enough for further study. The NEXTFLEX® Rapid Directional RNA-Sequence Kit 2.0 facilitates the creation of strand-specific and directional RNA libraries suitable for sequencing with Illumina® sequencers. The Illumina NovaSeq 6000 technology was used for genome sequencing to sequence the completed library pools. Illumina NovaSeq is a platform for next-generation genome sequencing (https://bioconductor.org/packages/release/bioc/html/NOISeq.html) (accessed May 14 and June 7, 2025) using a deep sequencing technique (2x150 bp PE reads; average paired-end read count 50 million/sample) (van Dijk et al., 2014). The sequencing service provider employed FastQC software https://timkahlke.github.io/LongRead_tutorials/QC_F.html (accessed May 14 and June 7, 2025) (Andrews et al., 2010) to evaluate and adjust essential quality parameters. To remove bases of inferior quality, secondary pre-filtration of the raw readings was performed using the Trimmomatic tool http://www.usadellab.org/cms/index.php?page=trimmomatic (accessed May 14 and June 7, 2025) (Bolger et al., 2014).

In this study, we used the cleaned, filtered SRA datasets from our treatments, which were deposited in the NCBI bankit (Ahmed et al., 2025), to construct the *de novo* transcriptome. In the applied method, previous information of the raw reads, especially the genome that will be used as a reference, is unnecessary for processing. The objective is to generate longer contigs from the intermediate reads, improving their interpretability.

Quantifying the transcript level is a method for determining the extent of transcripts' biological expression (Li & Dewey, 2011). To examine the genes and determine the individual expression levels of them, will be identified later, firstly a count table derived from the *de novo* transcriptome was generated. When numerous treatments are administered, the transcripts expression levels within each treatment are evaluated. Consequently, it will be possible to accurately measure the differences in levels of gene expression among treatments. The abundance of transcripts was quantified (count table).

Differentially expressed genes (DEGs) between each treatment became visible from this. Gene enrichment analysis was then used to identify which contigs were overexpressed in each treatment. Pairwise differential expression gene analyses (DEG) were performed to narrow the ratio of up- and down-regulated genes. The pairwise analysis was performed in 7 combinations in case of tomato experiment: (1) between the datasets of non-treated (control) and salinity-stressed plants, (2) between the datasets of non-treated (control) and sprayed plants with 75 mg/L ZnO-NPs, (3) between the datasets of non-treated (control) and sprayed plants with 150 mg/L ZnO-NPs, (4) between the datasets of non-treated (control)and salinity-stressed but sprayed plants with 75 mg/L ZnO-NPs, (5) between the datasets of non-treated (control) and salinity-stressed but sprayed plants with 150 mg/L ZnO-NPs, (6) between the datasets of salinity-stressed and salinity-stressed + sprayed plants with 75 mg/L ZnO-NPs, and finally (7) between the datasets of salinity-stressed and salinity-stressed + sprayed plants with 150 mg/L ZnO-NPs. The comparisons can be summarized as: 1)- T1 × T4. 2)- T1 × T2. 3)- T1 × T3. 4)- T1 × T5. 5)- T1 × T6. 6)- T4 × T5. 7)- T4 × T6.

And for the maize experiment, the pairwise analysis was performed in 4 combinations: (1) between the datasets of non-treated (control) and salinity-stressed plants, (2) between the datasets of non-treated (control) and salinity-stressed but sprayed plants with 2 g/L ZnO-NPs, (3) between the datasets of non-treated (control) and sprayed plants with 2 g/L ZnO-NPs, (4) between the datasets of salinity-stressed and salinity-stressed + sprayed plants with 2 g/L ZnO-NPs, The comparisons can be summarized as: 1)- M1 × M2. 2)- M1 × M3. 3)- M1 × M4. 4)- M2 × M3. The completed pooled libraries were sequenced on the Illumina NovaSeq 6000 genome sequencing platform, from which we obtained an average of 22-25 million bp single-end reads per sample, which were 63 bp in length. In the next step, functional analysis was applied to the dataset to identify transcriptomic contigs generated during the *de novo* assembly. The unidentified contigs were transformed into a defined, mapped, and annotated dataset, with each contig accompanied by relevant metadata.

The results showed what the biological role of the sequence was and how it was involved in a number of metabolic processes. This work utilized OmicsBox Biobam software to generate an annotation table through the analysis of Gene Ontology (GO) https://www.biobam.com/omicsbox/ (accessed May 14, 2025) (OmicsBox, 2019). In the final step, each of the previously identified genes -differentially expressed between treatments- was subjected to combined pathway analysis, determining which biochemical pathways they were involved in.

3.19. Determination of the antimicrobial activity

3.19.1. Examined microorganisms

Two Gram-positive bacteria, *Bacillus cereus* EMCC 1080 and *Staphylococcus aureus* ATCC 13565, and four Gram-negative bacteria, *Pseudomonas aeruginosa* NRRL B-272, *Salmonella typhi* ATCC 25566, *Escherichia coli* O157:H7 ATCC 51659, and *Listeria monocytogenes* LMD 7726, were obtained from the holding company for biological products and vaccines; VACSERA, Egypt, and they were used with all tomato and maize eztracts. We grew stock cultures on nutrient agar slants at 37 °C for 1 day and then stored them in the refrigerator until needed. For the antifungal assay, *Fusarium proliferatum* MPVP 328, *Fusarium verticilloides* ITEM 10027, *Aspergillus niger* SSWT 2999, *Aspergillus carbonarius* ITAL 204, *Aspergillus ochraceus* ITAL 14, and *Aspergillus flavus* NRRL 3357, were used with the tomato extracts, but in the case of maize extracts, the *Aspergillus carbonarius* strain was replaced with *Penicillium verrucosum* BFE 500. The Cranfield University Applied Mycology Department provided the fungal isolates. We grew stock cultures on nutrient agar slants at 25°C for 5 days and then stored them in the refrigerator for later use.

3.19.2. Investigational microbiological medium

The nutritional agar medium (Fluka, BioChemika, Spain) contained 1 g meat extract, 2 g yeast extract, 5 g peptone, 5 g sodium chloride, and 15 g agar in 1000 mL distilled water. For the bacterial disc diffusion experiment, the pH was measured to 7.4±0.2 at 37˚C (A.T.C.C., 1984). Tryptic soya broth (TSB) (BD, Sparks, USA,) contained 17g pancreatic digest of casein, 3 g papain digest of soybean, 2.5 g dextrose, 5 g sodium chloride, and 2.5 g dipotassium phosphate in 1000 mL distilled water. To determine minimal inhibitory concentration, the pH was measured to 7.3±0.2 at 25˚C (A.T.C.C., 1984). Potato dextrose agar medium (PDA) contained 200 g potato, 15 g glucose, and 20 g agar in 1000 mL distilled water. For minimal inhibitory concentration, pH was adjusted at 7.0 (A.T.C.C., 1984). The fungal disc diffusion assay uses 20 g yeast extract, 150 g sucrose, and 20 g agar in 1000 mL distilled water (Tsubouchi et al., 1987).

3.19.3. Disc diffusion method

A tube with 4–5 mL of tryptic soy broth was inoculated with a loop full of each bacterial species from the 24-hour incubated nutrient agar slant. The broth culture is incubated at 35ºC for 2-6 hours until it reaches the 0.5 McFarland $BaSO_4$ standard turbidity. To make a 0.5 McFarland barium sulfate ($BaSO_4$) standard, 0.5 mL of 1.175% (*w/v*) $BaCl_2 \cdot 2H_2O$ solution was mixed with 99.5 mL of 1% (*v/v*) sulfuric acid solution, stirring continuously to guarantee suspension. The density of the turbidity standard was measured at 625 nm using a spectrophotometer. The 0.5 McFarland standard requires 0.008–0.1 absorbance at 625 nm. Before each use, stir the $BaSO_4$ turbidity standard with a mechanical vortex mixer and check for a murky look.

The Kirby-Bauer disc diffusion method was used to investigate the sensitivity of tomato extracts with various bacterial cultures (Ahmed et al., 2023a; Ahmed et al., 2023b; Bauer et al., 1996). With cotton swabs, bacterial cultures were uniformly injected from tryptic soy broth into 20 mL nutritional agar petri dishes. To reach 5 mg mL^{-1} extract concentration, each extract and fraction was solubilized in 1 mL of dimethyl sulfoxide (DMSO). Extract-impregnated 6 mm Whatman No. 1 filter paper discs were dried sterilely. The discs were placed on inoculation plates using sterile forceps. DMSO was the negative control, and tetracycline (500 µg mL^{-1}) was the positive control. Next, infected plates were incubated at 37°C for 24 hours. After incubation, inhibitory zones were quantified as the apparent zone diameter, including the paper disc diameter.

Fungi were inoculated onto potato dextrose agar (PDA) and incubated at 25°C for five days. Each fungus's spore suspension was in 0.01% Tween 80. Turbidity of the fungal suspension was measured against the 0.5 McFarland standard, suggesting approximately 2×10^8 cfu mL^{-1}. Sterilized filter paper discs (6 mm) were impregnated with extracts and dried, similar to the antibacterial assay. To infect YES medium petri dishes, 50 µL of each fungal culture was equally spread with a sterile L-glass rod. Removed loaded discs were placed on seeded plates with sterilized forceps. DMSO was used as a negative control and Nystatin (1000 Units mL^{-1}) as a positive control. Inoculation plates were incubated at 25°C for 24–48 hours. At the end, the zone of inhibition (mm) against the fungus was measured to determine antifungal efficacy (Medeiros et al., 2011). All treatments had three replicates, and experimental averages were determined.

3.19.4. Determination of minimum inhibitory concentration (MIC)

The tube dilution method was used to determine the MIC (Wiegand et al., 2008). To achieve inocula of 10^8 cfu mL^{-1}, a 24-hour culture of the bacterial species was diluted in 10 mL of tryptic soy broth (TSB) using the 0.5 McFarland standard Each extract was added to culture tubes at 5.0, 2.5, 1.75, 1.5, 1.0, 0.75, 0.50, 0.25, 0.1, and 0.05 mg mL^{-1} in DMSO. Each tube received 100 µL of bacterial cell suspension and was incubated at 37°C for 24 hours. Turbidity indicates inoculum proliferation in broth, and the extract's minimum inhibitory concentration (MIC) is the lowest concentration that inhibited test organism growth.

The technique by Perrucci et al. (2004) was used to determine the fungus's minimum inhibitory concentration (MIC). Crude extracts at different concentrations were diluted in 0.5 mL of 0.1% Tween 80 (Merck, Darmstadt, Germany), mixed with 9.5 mL of molten PDA at 45°C, and deposited on 6 cm Petri dishes. The middle of the plates was infected with 3 µL of fungal solution (108 cfu mL^{-1}; 0.5 McFarland standard). Plates were incubated at 25°C for 24–48 hours. The minimal inhibitory concentration (MIC) was determined after incubation (Perrucci et al., 2004).

3.20. The docking of molecules characterization

A molecular docking study was conducted using the Molecular Operating Environment software (version 2014.09) to evaluate the antibacterial activity of tomato and maize leaf extracts and corroborate the *in vitro* findings. For tomato, the Topoisomerase II ATPase enzyme (DNA Gyrase) (PDB Id: 3TTZ) served as an antibacterial target, while the sterol 14-alpha demethylase (CYP51) protein (PDB Id: 5FSA) was utilized as an antifungal target. For maize, the Topoisomerase II ATPase enzyme (DNA Gyrase) (PDB Id: 6F86) served as an antibacterial target, and the alpha-L-fucosidase (PDB Id: 9LXL) was utilized as as an antifungal target. The 17 compounds discovered by HPLC in our current study -for both plants- were evaluated within the active site of both targets. Two-dimensional structures of all tested compounds were generated using MOE using SMILES codes received from the National Library of Medicine (https://pubchem.ncbi.nlm.nih.gov/). Following a ligand preparation process that involved protonating the 3D structure, assigning partial charges, and performing energy minimization, the compounds were saved as MOE files.

The Protein Data Bank website (https://www.rcsb.org/) was utilized to get crystal structures of the antifungal target with posaconazole (X2N) (Sharma & Singh, 2023) and NAG (Korban et al., 2025) and the antibacterial targets with 07N (Shaker et al., 2022) and CWW (Narramore et al., 2019) as inhibitors.

Likewise, the two antimicrobial targets were prepared for the docking run by removing chains not involved in the interaction, as well as water, solvent molecules, and non-binding ligands. The 3D structure was protonated using the default settings, and the docking sites were delineated. A re-docking procedure was subsequently conducted to verify the docking configuration utilizing the proteins and their original co-crystallized ligand molecules. The interactions and binding modalities between the examined compounds and the enzymes' active site were subsequently predicted utilizing the validated configuration.

The docking configuration employed the triangle matcher for placement, utilized London dG for rescoring, and applied the forcefield technique for refinement. Subsequent to docking, the extent of the compounds' binding to the enzymes was evaluated based on internal energy scores (S), bond interactions, and lengths (Å), constrained to 3.5 for hydrogen bonds and 4.0 for ionic interactions (Marrez et al., 2024; Mashat et al., 2019). Two-dimensional and three-dimensional docked images depicting the optimal binding locations (ligand-to-protein) were preserved for a clear illustration of the results.

3.21. Statistical analysis

The experimental techniques in this study consisted of performing all assessments four times, and the resulting values were reported as the means ± standard error. The statistical analysis was performed utilizing the Web Agri Stat Package (WASP) (Ahmed, et al., 2023b) and JASP (Berkhout et al., 2024; Hoffmann et al., 2022) software. After Shapiro–Wilk and Levene tests, the data met normal distribution and homogeneity criteria, the study used a one-way analysis of variance (ANOVA) to investigate differences between groups. The Tukey test was employed using significance thresholds of 5%.

4. RESULTS AND DISCUSSION

4.1. Characterization of chemically synthesized ZnO-NPs

Figure 6 displayed the spectrum of a distinct ZnO absorption peak at 370 nm, corresponding to the intrinsic band-gap absorption. This absorption is caused by electron transitions from the valence band to the conduction band ($O_{2p} \rightarrow Zn_{3d}$).

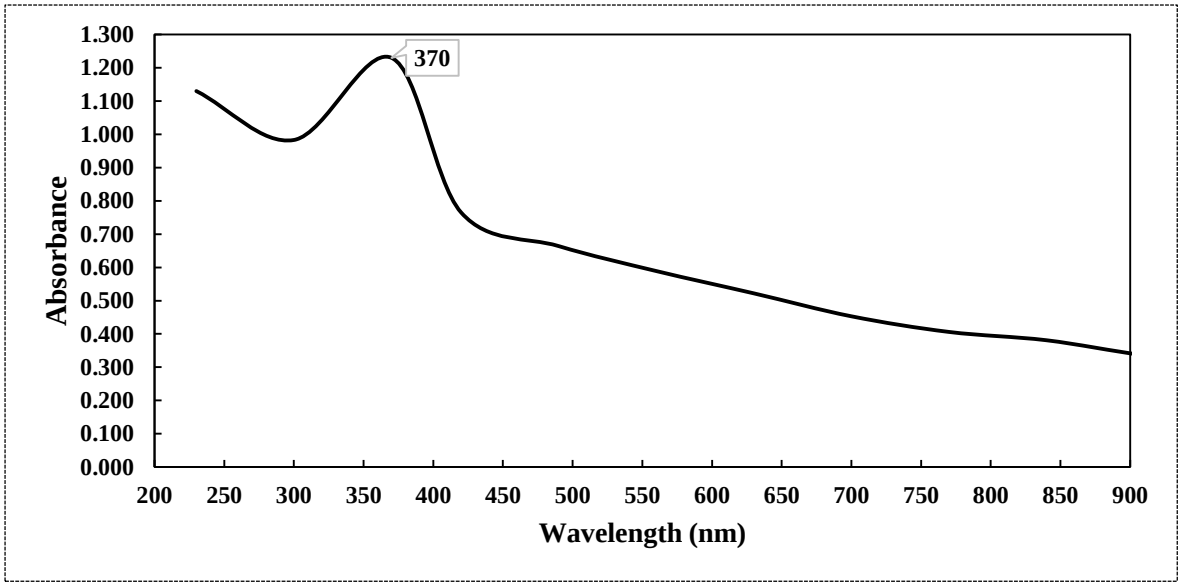

Figure 6. UV.VIS spectrum of chemically synthesized ZnO-NPs.

Figures 7–9 and Table 2 displayed the transmission electron microscopy (TEM), scanning electron microscopy (SEM), energy-dispersive X-ray spectroscopy (EDAX), and size distribution of the zinc oxide nanoparticles (ZnO-NPs) that were synthesized using the precipitation method. The transmission electron microscopy (TEM) image (Figure 7) revealed that the ZnO nanoparticles (NPs) have developed in a nearly hexagonal morphology, indicating the high quality of the ZnO-NPs. Figure 8 displayed scanning electron microscope (SEM) images of the ZnO-NPs, revealing uniform particle shape and size. Furthermore, the presence of ZnO-NPs in the powder form is evident. Figure 9 confirmed that the primary constituents of the ZnO sample consist of zinc (Zn) and oxygen (O), which were evenly distributed across the surface of the ZnO nanoparticles. The size distribution of the ZnO-NPs produced using the precipitation method at a calcination temperature of 200 °C for 2 h was monomodal with a half-width of approximately 41.166 nm.

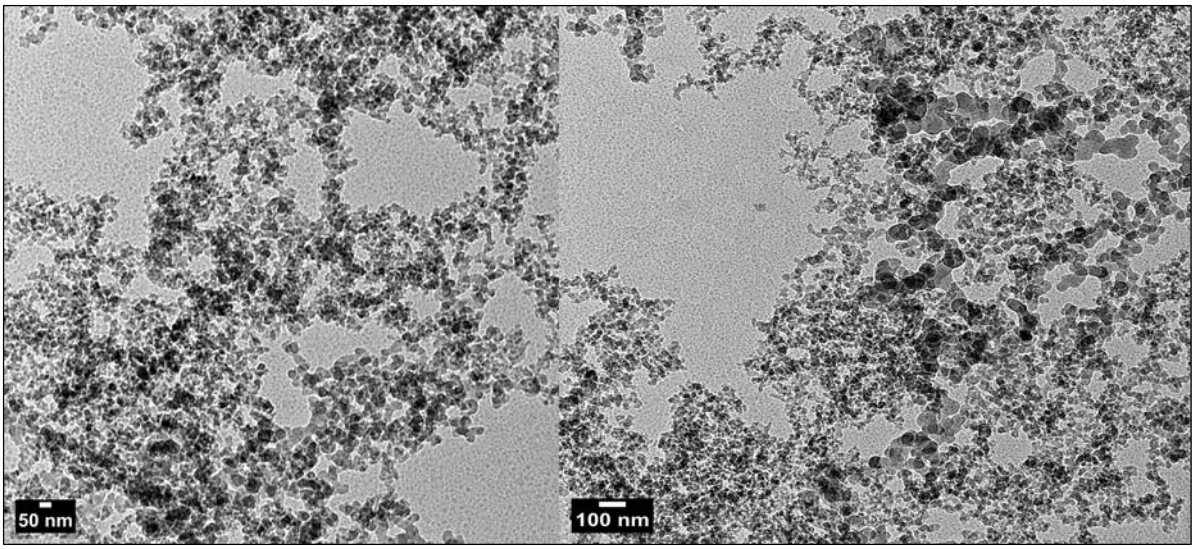

Figure 7. Electron micrographs (TEM) of chemically synthesized ZnO-NPs on 50 and 100 nm.

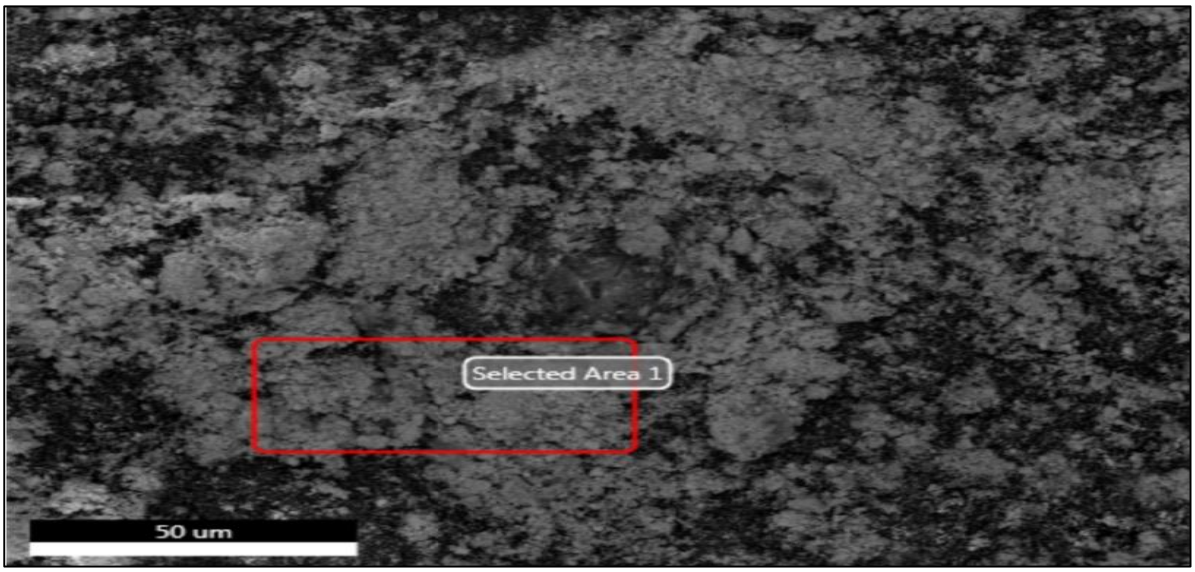

Figure 8. Electron micrographs (STEM) of chemically synthesized ZnO-NPs on 50 microns.

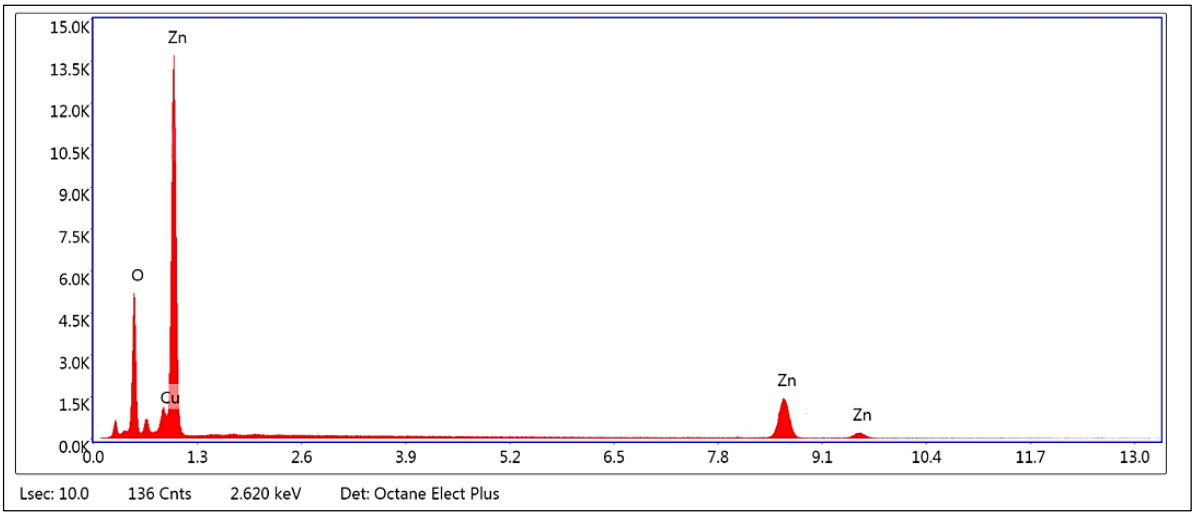

Figure 9. EDAX spectrum of chemically synthesized ZnO-NPs.

Table 2. eZAF Smart Quant results and oxide results.

Element	Weight %	Atomic %
ZnK	67.55	42.95
OxygenK	32.02	56.81
CuK	0.43	0.23

Figure 10 displayed the FTIR spectrum of chemically produced zinc oxide nanoparticles, obtained within the wavelength range from 3900 to 300 cm^{-1}. The spectrum of zinc oxide nanoparticles exhibited peaks corresponding to six functional groups at 3150, 1631.48, 1425.14, 1078.98, 447.404, and 370.23 cm^{-1}.

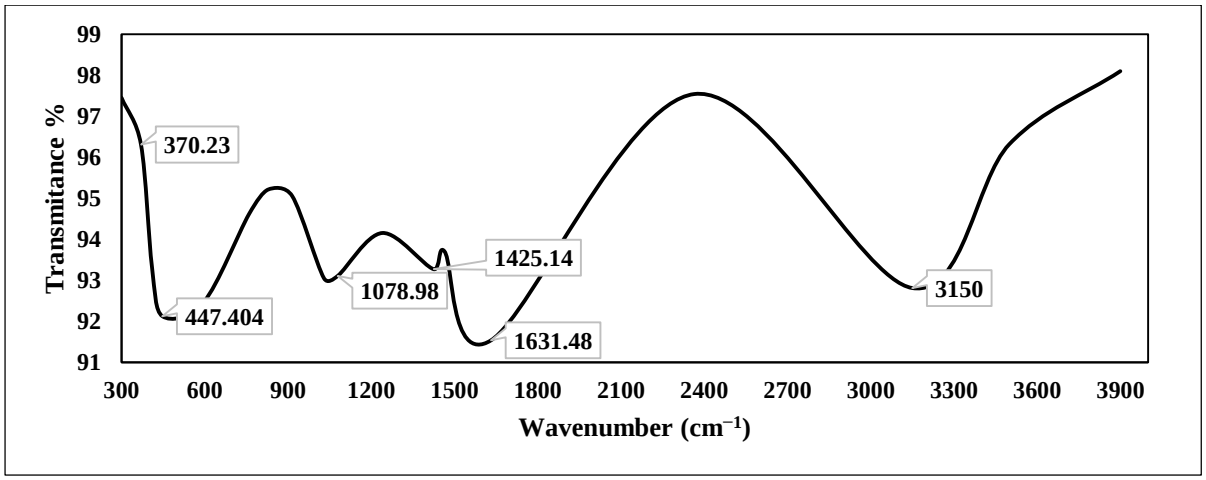

Figure 10. FTIR spectrum of chemically synthesized ZnO-NPs.

Figure 11 displayed the X-ray diffraction (XRD) pattern of chemically generated zinc oxide (ZnO) nanoparticles, both chemically and green. The diffraction peaks were seen at the following angles (2θ): 31.73°, 34.38°, 36.23°, 47.58°, 56.58°, 62.88°, and 76.92°.

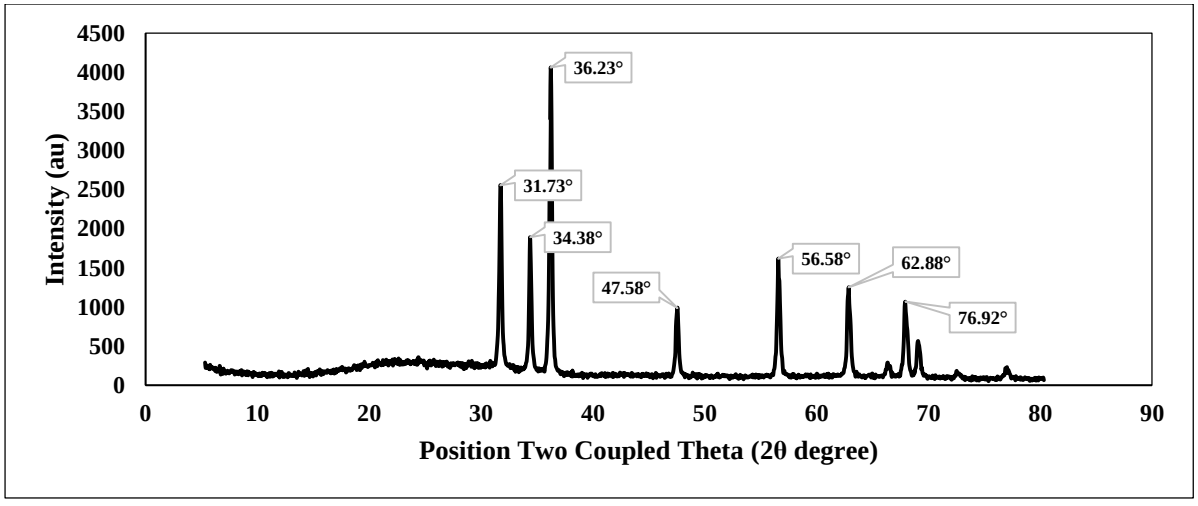

Figure 11. XRD pattern of chemically synthesized ZnO-NPs.

Zeta potential analysis was conducted to identify the surface charges accumulated by zinc oxide nanoparticles, providing additional information on the stability of the resulting colloidal zinc oxide nanoparticles. The magnitude of zeta potential indicates the possible stability of colloids. The nanoparticles produced in that study were highly stable, as evidenced by a zeta potential value of −30.214 mV. The zeta potential of the chemically produced zinc oxide nanoparticles was measured in water, using it as a dispersant. The measured zeta potential was determined to be −30.214 mV, as illustrated in Figure 12.

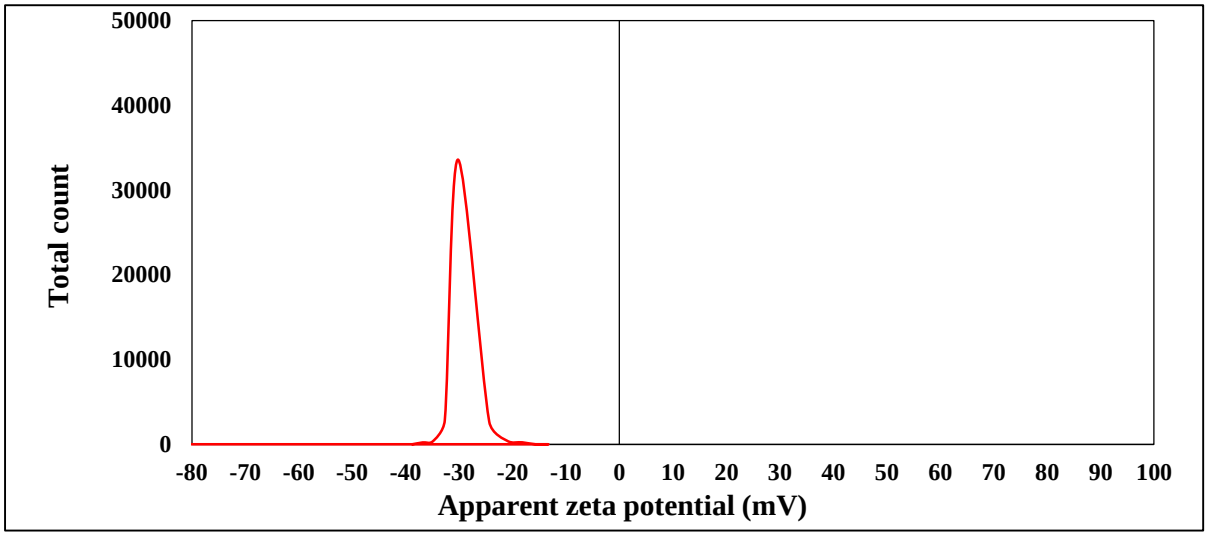

Figure 12. Zeta potential of chemically synthesized ZnO-NPs measuring the charge.

The UV-visible absorption spectrum was primarily employed to analyze the optical characteristics of nanoparticles (Rasha et al., 2021). This optical property aligns with the optical activity of ZnO-NPs that were synthesized using a solvothermal technique (Zak, Razali, et al., 2011). Furthermore, this distinct peak indicated that the particles were of nanoscale dimensions, and the distribution of particle sizes was highly concentrated. The shape, size, and elemental distribution of the obtained chemically synthesized ZnO-NPs were characterized using the STEM, TEM, EDAX, and DLS techniques.

The results from Figures 6–8 and Table 2 confirmed that ZnO-NPs generated using the precipitation process employing sodium hydroxide and zinc nitrate hexahydrate have a nearly hexagonal morphology, and limited size distribution of 41.166 nm, distinguishing them from other results previously documented in other research, compared to some of the other results (Zak, Abrishami, et al., 2011; Zak, Majid, et al., 2011; Zak, Razali, et al., 2011).

This size range is significant as it facilitates the movement of the stomata breadth of tomato and maize leaves, which typically measure 10-12 and 3-12 µm in width, respectively (Lucas & Dupree, 2023.; Xue et al., 2021). This elucidates the rapid biostimulatory effects observed in our investigations. However, the ZnO-NPs were 41 nm according to DLS measurements, and the STEM image showed aggregation; the obtained results showed that ZnO-NPs could penetrate the stomatal channels. This led to a sufficient amount of the sprayed nanoparticles reaching the mesophyll and triggering the antioxidant response. This reveals a surface-to-volume ratio due to polydispersity.

This alteration also results in a sustained-release profile of Zn^{2+} ions. Smaller particles initiate "molecular priming," while larger aggregates serve as reservoirs, providing prolonged biostimulatory effects during both vegetative and generative phases. The plant classification was associated with its "safety valve" function. The current arguments indicates that ZnO-NPs may mitigate phytotoxicity by aggregation. This would avoid a fast, excessive influx of reactive Zn into the cytoplasm, enabling the plant to gradually elevate SOD and CAT levels without ion-induced stress.

To obtain additional insight into the topographies of ZnO-NPs, the EDAX analysis of the sample was performed from the same area as shown in Figure 9. The EDAX examination confirmed the presence of zinc and oxygen in a percentage of 67.55 and 32.02%. The detection of copper in the EDAX analysis is attributed to the use of the lacy carbon-coated copper grid, which enhances the quality of the SEM pictures (Yedurkar et al., 2016). The 370 nm peak detected by the UV-VIS spectrophotometer is linked to the EDAX spectrum, as the high chemical purity of the ZnO-NPs confirm that the observed plant responses are related to the nanoparticles not to contaminants.

Using Fourier transform infrared spectroscopy, the sample showed six functional groups detected at 3150, 1631.48, 1425.14, 1078.98, 447.404, and 370.23 cm^{-1} (Figure 10), and these groups are expanded to interpret the chemical bonds on the ZnO-NPs surface, which determined their stability and interactions with the leaf cuticles of both studied plants. The intense and wide peak observed at 3150 cm^{-1} in the upper region was a result of the stretching vibration of hydroxyl (OH) groups (Jayarambabu, 2014; Zafar et al., 2021). The peak observed at 1631.48 cm^{-1} was a result of the presence of the C=O amide I and amide II functional groups. The bending vibration band of the C-H bond occurred at a frequency of 1425.14 cm^{-1}. The C–O stretching vibration band occurred at a frequency of 1078.98 cm^{-1}. The frequencies of 447.404 and 370.23 cm^{-1} corresponded to the stretching vibration of Zn–O bonds, providing evidence for the synthesis of the product.

FTIR analysis was conducted to determine the potential biomolecules accountable for the bioreduction of zinc oxide nanoparticles. The prior results are consistent with the findings reported in other papers (Mahalakshmi & Vijaya, 2020; Yedurkar et al., 2016; Zak et al., 2011; Zak et al., 2011; Zak et al., 2011).

The XRD is a rapid test providing information on crystal size and structure (Modena et al., 2019). In Figure 11, the XRD analysis confirmed that the diffraction peak planes of the precipitated ZnO-NPs were matched well with the quartzite ZnO reported in the joint committee on powder diffraction standards (JCPDS) data (Salih et al., 2021). They represent the reflection resulting from the crystal planes of the hexagonal wurtzite structure of ZnO nanoparticles. Zinc oxide exists in two primary crystalline structures: hexagonal wurtzite and cubic zincblende. The wurtzite structure is the most stable and prevalent under normal conditions. The presence of strong peaks suggests that the ZnO nanoparticles exhibited a high degree of crystallinity. The XRD patterns did not exhibit diffraction peaks associated with the contaminant, thereby validating the excellent purity of the produced nanoparticles. The observed results are supported by the findings of other authors who have examined the produced zinc oxide nanoparticles using the XRD diffractometer (Antony Lilly Grace et al., 2023; Mahalakshmi & Vijaya, 2020).

When the particles in a suspension possess significant negative or positive zeta potential values (Figure 12), they will exhibit repulsive forces toward one other, preventing the aggregation of nanoparticles. Conversely, when particles possess low zeta potential levels, no opposing force hinders their aggregation and subsequent coming together. zeta potential values exceeding +30 mV or falling below −30 mV are typically associated with the formation of stable suspensions (García et al., 1997). The zeta potential of the chemically produced zinc oxide nanoparticles was measured in water using it as a dispersant. The measured zeta potential was determined to be −30.214 mV, as illustrated in Figure 12. The zeta potential is directly related to the stability of the nanoparticles while they are in a solution. The nanoparticles produced in this work were highly stable (Jain et al., 2020).

4.2. Distribution of micro and macro elements in of tomato and maize leaves

In the current study, three macro and three other microelements were determined as shown in Tables 3 and 4 in the leaves of tomato and maize. **In case of tomato (Table 3)**, under severe salt stress (150 mM NaCl), the highest sodium (Na) contents were measured from the fourth stressed treatment (T4) in a concentration of 26.48 ± 0.21, followed by the T5 and T6 treatments in concentrations of 13.51 ± 0.06 and 13.27 ± 0.23 µg/g, respectively. Without any noticeable significant difference between the ZnO-NPs foliar sprayed treatments (T5 and T6).

The highest potassium (K) contents were obtained from T1–T3 treatments, and they varied between 29.20 ± 0.22 and 29.02 ± 0.02 µg/g. The highest zinc (Zn) contents were obtained from the ZnO-NPs foliar sprayed T2, T3, T5, and T6 treatments, and the copper (Cu) content was noticed to be a little bit higher in the stressed treatments than the non-stressed treatments. In addition, the magnesium (Mg) and manganese (Mn) contents were obtained from the six different treatments without any significant differences.

Table 4 shows the influence of salinity stress (150 mM NaCl) with/without the application of ZnO-NPs foliar spray (2 g L^{-1}) on the ion homeostasis for **maize plants**. The maize plants of the second treatment (M2) showed a significant increase in the concentrations of sodium, potassium, and magnesium compared to the control plants (M1). The elevation in sodium levels was around 5.8 mg g^{-1} in the second treatment (M2); however, this elevation was significantly reduced to 1.9 mg g^{-1} when ZnO-NPs were applied in the third treatment (M3). A similar moderating effect was observed for potassium: ZnO-NPs supplementation during salt stress (M3) resulted in a significant reduction in potassium accumulation to the salt-only treatment (M2).

The foliar spray of ZnO-NPs led to an increase in the levels of zinc in the third and fourth treatments (M3 and M4). The Zn content was around 0.6 mg g^{-1} in both M3 and M4 treatments. In contrast, NaCl reduced the Cu levels in the salinity-stressed treatments, whether they were sprayed with ZnOnps or not. Concentrations of Mn were relatively stable in the control and salt-stressed groups (M1–M3), whereas a significant increase was observed in the M4 treatment (tap water + ZnO-NPs), suggesting a synergistic or additive effect of the nanoparticles on Mn absorption in the absence of salt stress. Thus, the evidence demonstrates that ZnO-NPs are essential for maintaining ion homeostasis, particularly by mitigating the excessive accumulation of Na^+ and Mg^{2+} induced by salinity.

Table 3. Determination of some macro and microelements in the leaves of tomato.

Treatments	Concentrations (µg/g)					
	Na	K	Mg	Zn	Cu	Mn
T1 Control (dw)	1.47 ± 0.13 ^{c}	29.20 ± 0.22 ^{a}	5.57 ± 0.02 ^{ns}	0.48 ± 0.11 ^{c}	0.01 ± 0.04 ^{c}	0.22 ± 0.01 ^{ns}
T2 (dw+ZnO-NPs 75 mg/L)	1.31 ± 0.10 ^{c}	29.02 ± 0.02 ^{a}	5.56 ± 0.02 ^{ns}	2.72 ± 0.37 ^{b}	0.02 ± 0.03 ^{c}	0.22 ± 0.00 ^{ns}
T3 (dw+ZnO-NPs 150 mg/L)	1.49 ± 0.06 ^{c}	29.10 ± 0.23 ^{a}	5.59 ± 0.02 ^{ns}	3.06 ± 0.58 ^{ab}	0.01 ± 0.01 ^{c}	0.21 ± 0.01 ^{ns}
T4 NaCl (150 mM)	26.48 ± 0.21 ^{a}	13.56 ± 0.38 ^{c}	5.63 ± 0.03 ^{ns}	0.47 ± 0.08 ^{c}	0.02 ± 0.03 ^{b}	0.63 ± 0.00 ^{ns}
T5 (150 mM NaCl+ZnO-NPs 75 mg/L)	13.51 ± 0.06 ^{b}	26.66 ± 0.40 ^{b}	5.63 ± 0.01 ^{ns}	2.44 ± 0.18 ^{b}	0.004 ± 0.09 ^{ab}	0.77 ± 0.00 ^{ns}

Table 3. *Continued*.

T6 (150 mM NaCl+ZnO-NPs 150 mg/L)	13.27 ± 0.23 ^{b}	26.34 ± 0.42 ^{b}	5.62 ± 0.01 ^{ns}	4.13 ± 0.38 ^{a}	0.012 ± 0.05 ^{a}	0.78 ± 0.00 ^{ns}

Each value represents the mean ± SE (n=4). Values with the same letter are not significantly different at ($p \leq 0.05$), and the comparison is done according to different treatments in the same column.

Table 4. Determination of some macro and microelements in the leaves of maize.

Treatments	**Concentrations (mg/g)**					
	Na	**K**	**Mg**	**Zn**	**Cu**	**Mn**
M1 Control (dw)	0.87 ± 0.00 ^{c}	5.83 ± 0.08 ^{c}	1.53 ± 0.25 ^{c}	0.04 ± 0.04 ^{b}	0.10 ± 0.00 ^{a}	0.07 ± 0.02 ^{b}
M2 (NaCl 150 mM)	5.75 ± 0.14 ^{a}	17.54 ± 0.10 ^{a}	5.06 ± 0.01 ^{a}	0.15 ± 0.04 ^{b}	0.02 ± 0.00 ^{c}	0.10 ± 0.01 ^{b}
M3 (NaCl 150 mM + ZnO-NPs 2 g/L)	1.84 ± 0.05 ^{b}	9.73 ± 0.18 ^{b}	0.56 ± 0.01 ^{d}	0.58 ± 0.08 ^{a}	0.02 ± 0.00 ^{c}	0.09 ± 0.00 ^{b}
M4 (dw + ZnO-NPs 2 g/L)	0.87 ± 0.03 ^{c}	5.25 ± 0.12 ^{d}	1.95 ± 0.01 ^{b}	0.61 ± 0.08 ^{a}	0.07 ± 0.00 ^{b}	0.33 ± 0.01 ^{a}

Each value represents the mean ± SE (n=4). Values with the same letter are not significantly different at ($p \leq 0.05$), and the comparison is done according to different treatments in the same column.

It is possible for plant pores to more easily access and absorb nanosized nutrients, which ultimately results in higher efficiency (Shebl et al., 2019). Zn^{2+} is a cofactor for several enzymes, and the size of its particles makes it possible for it to be soluble and to enter the leaf surface, where it can then release Zn^{2+} ions via the cuticle (Bihmidine et al., 2013). Zinc oxide nanoparticles (ZnO-NPs) have been found to enhance nutritional absorption, regulate the ratio of sodium to potassium ions (Na^{+}/K^{+}), maintain water balance, enable ion accumulation, and mitigate the negative impacts of abiotic stressors like salinity stress (Ahmed, et al., 2024c).

K^{+} and Na^{+} ions act as antagonists: when a plant absorbs a large amount of Na^{+}, it displaces K^{+} ions from the available Donnan binding sites, resulting in a relative deficit of K^{+} in the plant (Kinraide, 1999). Insufficient potassium results in the withering of plants, loss of moisture, and impaired water equilibrium (Lefoulon, 2021). Plants exhibit stunted growth and display dead white or brown patches as a result of cellular shrinkage and tissue collapse, and potassium is the element that is needed in the second highest amount, as plants take it in the form of K^{+} ions (Pardo & Rubio, 2011).

Potassium stimulates about 40 enzymes, influences hydration, and has a crucial function in signal transmission, and adequate provision of potassium is essential for numerous metabolic and physiological processes (Johnson et al., 2022). K^+ enhances the production of complex carbohydrates and improves crop resilience, hence mitigating crop damage caused by factors such as wind, water scarcity, cold, and pathogens. To protect against wind damage, the plant activates a process called enhanced high-molecule carbohydrate biosynthesis, which leads to the build-up of cellulose that increases the fiber content of the plant's tissues, making them stronger (Hasanuzzaman et al., 2018). Potassium enhances protein synthesis by facilitating the interaction between mRNAs and the ribosome (Rozov et al., 2019). It exerts a beneficial influence on the process of photosynthesis and the movement of materials within the plant, enhances the water utilization efficiency of plants, and plays a crucial part in the process of plant evaporation and respiration as it decreases the magnitude of evaporation (Sardans & Peñuelas, 2021).

In case of tomato, the current study showed a significant decrease in potassium content in the fourth stressed treatment that was not sprayed with ZnO-NPs. However, the exogenous application of ZnO-NPs improved the element concentration in tomato plants of the stressed treatments that were sprayed with ZnO-NPs (T5 and T6) (Table 3). ZnO-NPs were effective in the nutrient balance in plants and the survival of the plant under NaCl stress, as the contents of the mineral Na were decreased in the foliar sprayed stressed treatments (T5 and T6) compared to the non-sprayed stressed treatment (T4). Copper is predominantly concentrated in chloroplasts, accounting for 70% of its presence. It is an integral part of plastocyanins, which are proteins that contain copper. It has a function in the electron transport chain during photosynthesis. The individual was responsible for the development of a highly significant antioxidant enzyme, known as superoxide dismutase, in conjunction with the element zinc (Cohu et al., 2009).

The Cu^{2+} content showed a significant difference between the stressed treatments and the non-stressed treatments (Uresti-Porras et al., 2021). On the other side, there was not any significant difference between the stressed and non-stressed treatments in the concentrations of the two elements Mg and Mn, even if they were sprayed with ZnO-NPs or not, and these results were reinforced by a previous research article on *Ginkgo biloba* (Wang et al., 2023). The previous findings could be attributed to the impact of ZnO-NPs on minerals in plants, which is contingent upon the concentration.

It was confirmed that a noteworthy rise in the levels of zinc ions (Zn^{2+}) in the leaves and seeds when 40 ppm of ZnO-NPs was applied to the foliage (Salama et al., 2019). In a recent study, it has been shown that ZnO-NPs stimulated the uptake of K^+, Zn^{2+}, and Cu^{2+} in faba bean (Mogazy & Hanafy, 2022) and rapeseed (El-Badri et al., 2021) under salinity stress and substituting the Na^+ with the previous minerals, thus decreasing the phytotoxicity by Na^+.

In case of maize, salinity stress is a major abiotic factor that disrupts ionic equilibrium, often leading to the toxic accumulation of sodium (Na^+) and the subsequent inhibition of essential nutrient uptake (Ahmed et al., 2026). The significant elevation of Na^+, K^+, and Mg^{2+} observed under the 150 mM NaCl treatment (M2) is a typical physiological response to osmotic and ionic stress (Ahmed, et al., 2024a). The accumulation of Na^+ results directly from salt exposure, whereas the concurrent increase in K^+ and Mg^{2+} may indicate a compensatory mechanism for osmotic correction, which could lead to metabolic imbalances if not adequately regulated (Ahmed, et al., 2024b).

Despite the salinity is responsible for reducing the potassium concentration (K^+) as a response for the elevation of Na^+ concentration according to the antagonistic effect, the current study found that there was a simultaneous increase in the concentrations of Na^+, K^+, and Mg^{2+} in maize leaves under salt stress. That deviation from the normal trend may be attributed to the cultivar P0023 adaptive mechanism or the high cytosolic K^+ levels, that phenomena was sometimes found in salt-tolerant genotypes (Almeida et al., 2017; Gao et al., 2016). On the other side, Mg^{2+} elevations may be recognized as potential compensatory mechanism to maintain the dynamic equilibrium of the osmosis and the functional enzymes in saline conditions (Tang et al., 2022).

Significantly, the incorporation of 2 g L^{-1} ZnO-NPs (M3) successfully inhibited the excessive buildup of these ions. Declining the sodium concentration in the third treatment plants (M3) that were stressed but sprayed with ZnO-NPs indicated that ZnO-NPs may enhanced the proton-ATPase to exclude the sodium, which reinforced the ion selectivity (Faizan, 2020). The observed increase in Zn^{2+} levels in the M3 and M4 treatments confirms effective nanoparticle absorption and bioaccumulation. Although ZnO-NPs appear to freshen Cu^{2+} levels in the absence of salt (M4), they fail to alleviate the salt-induced reduction of Cu^{2+} in the M3 group. This observation indicates that NaCl's inhibitory effect on Cu^{2+} transport is significant, and ZnO-NPs cannot mitigate it.

The significant increase in Mn^{2+} in the M4 treatment suggests a synergistic interaction in which ZnO-NPs may facilitate Mn^{2+} absorption or translocation, without salinity limitations (Rossi, 2019). By alleviating excessive buildup of Na^{+} and Mg^{2+} under stress, ZnO-NPs help maintain the structural and functional integrity of biological systems (Sturikova, 2018). That proved regulatory role by ZnO-NPs is considered a critical element in many physiological interactions inside the plants including the dark and light reaction in the photosynthetic system and activating the enzymes for the defensive systems (Gaafar, et al., 2020).

4.3. Assessment of the growth and chlorophyll attributes in different treatments of tomato and maize

The chlorophyll content (soil plant analysis development, SPAD units) in the different **tomato** treatments was determined as shown in Table 5. It was examined in four stages to determine how it would be influenced by NaCl stress and foliar spraying with chemically synthesized zinc oxide nanoparticles. It was observed that the readings of the SPAD measuring the chlorophyll content in the different treatments were not significantly different in the first two stages, but the chlorophyll content decreased in a time manner for the stressed treatments in the third stage even if they were sprayed by ZnO-NPs. On the other side, the chlorophyll content increased in the non-stressed treatments (T1–T3). It was observed that the non-stressed treatments (T1–T3) had higher chlorophyll content than the stressed treatments (T4–T6) in the third stage, but chlorophyll content began to rise again in the fifth and sixth stressed treatments sprayed with ZnO-NPs in the fourth stage. However, in the fourth treatment, which was not sprayed with ZnO-NPs, chlorophyll content did not significantly increase. It was clear that there was a manner of increasing the chlorophyll content in the stressed treatments when they were sprayed with ZnO-NPs.

Table 5. Determination of chlorophyll content (SPAD-units) in the leaves of tomato.

Treatments	Readings of Chlorophyll Content in Different Stages			
	5 July 2023	19 July 2023	28 July 2023	11 August 2023
T1 Control (dw)	48.50 ± 1.89 ^{ns}	51.9 8± 2.82 ^{ns}	60.4 3± 1.24 ^{ab}	63.1 3± 1.97 ^{a}
T2 (dw+ZnO-NPs 75 mg/L)	46.05 ± 0.42 ^{ns}	57.7 8± 1.65 ^{ns}	60.1 3± 2.55 ^{b}	61.25 ± 2.25 ^{ab}
T3 (dw+ZnO-NPs 150 mg/L)	44.6 0± 1.06 ^{ns}	56.8 3± 1.05 ^{ns}	62.75 ± 2.09 ^{a}	63.75 ± 2.43 ^{a}
T4 NaCl (150 mM)	46.9 3± 0.93 ^{ns}	54.8 8± 1.14 ^{ns}	52.65 ± 0.44 ^{cd}	55.25 ± 0.85 ^{c}
T5 (150 mM NaCl+ZnO-NPs 75 mg/L)	49.2 0± 0.71 ^{ns}	55.7 8± 1.05 ^{ns}	53.1 8± 2.22 ^{c}	60.75 ± 1.11 ^{abc}
T6 (150 mM NaCl+ZnO-NPs 150 mg/L)	48.6 8± 1.08 ^{ns}	54.6 8± 2.75 ^{ns}	52.4 8± 1.26 ^{d}	61.6 8± 2.47 ^{ab}

Each value represents the mean ± SE (n=4). Values with the same letter are not significantly different at ($p \leq 0.05$), and the comparison is done according to different treatments in the same column.

The **tomato plant height** (cm) in the different treatments was determined as shown in Table 6. Like the chlorophyll content, it was determined in four different stages as an indication of how growth and morphological attributes would be influenced along the experiment. It was observed that the tomato plant heights in the different treatments were not significantly different in the first two stages. The tomato plants showed an increase in height according to the six different treatments, but it was observed that the rate of increase in the non-stressed treatments (T1–T3) was higher than in the stressed treatments (T4–T6). In the third stage, the increasing rate of tomato plants' height for the fifth and sixth stressed treatments (T5 and T6) was close to the rate of elongation in the non-stressed treatments (T1–T3), as they were sprayed by ZnO-NPs. On the other side, the increasing rate of tomato plants' height for the fourth stressed treatment (T4) was lower than in the other stressed treatments (T5 and T6).

Table 6. Determination of growth attributes (plant height) in tomato.

Treatments	**Readings of Plant Height (cm) in Different Stages**			
	5 July 2023	**19 July 2023**	**28 July 2023**	**11 August 2023**
T1 Control (dw)	24.80 ± 2.16 ^{ns}	47.50 ± 1.19 ^{ns}	57.75 ± 1.93 ^{b}	60.75 ± 2.01 ^{c}
T2 (dw+ZnO-NPs 75 mg/L)	28.38 ± 2.51 ^{ns}	50.75 ± 0.85 ^{ns}	63.50 ± 2.72 ^{a}	67.00 ± 2.16 ^{b}
T3 (dw+ZnO-NPs 150 mg/L)	28.38 ± 2.50 ^{ns}	50.75 ± 3.48 ^{ns}	63.50 ± 1.80 ^{a}	75.25 ± 2.10 ^{a}
T4 NaCl (150 mM)	25.50 ± 2.25 ^{ns}	47.00 ± 0.71 ^{ns}	54.75 ± 2.25 ^{c}	57.00 ± 2.42 ^{d}
T5 (150 mM NaCl+ZnO-NPs 75 mg/L)	25.75 ± 1.65 ^{ns}	49.50 ± 1.19 ^{ns}	57.75 ± 2.98 ^{b}	60.00 ± 1.68 ^{cd}
T6 (150 mM NaCl+ZnO-NPs 150 mg/L)	24.13 ± 1.68 ^{ns}	47.00 ± 0.58 ^{ns}	57.25 ± 2.75 ^{bc}	61.13 ± 2.09 ^{bc}

Each value represents the mean ± SE (n=4). Values with the same letter are not significantly different at ($p \leq 0.05$), and the comparison is done according to different treatments in the same column.

The **tomato stem width** (cm) in the different treatments was determined as shown in Table 7. Like the previous growth and morphological attribute (plant height), stem width was determined in four different stages. It was observed that the tomato plants' stem width in the different treatments was not significantly different in the first stage. The tomato plants showed an increase in stem width according to the six different treatments. By the second stage, it was observed that the rate of increase in the non-stressed treatments (T1–T3) was higher than in the stressed treatments (T4–T6). In the third stage, the increasing rate of tomato stem width for the stressed treatments (T5-T6) was lower than the rate of elongation in the non-stressed treatments (T1–T3), but the fifth and sixth treatments (T5 and T6) were sprayed with different concentrations of ZnO-NPs three times, so they showed a little bit of increase compared to the fourth treatment (T4).

Table 7. Determination of growth attributes (stem width) in tomato.

Treatments	Readings of Stem Width (cm) in Different Stages			
	5 July 2023	19 July 2023	28 July 2023	11 August 2023
T1 Control (dw)	0.48 ± 0.03 ^{ns}	0.73 ± 0.73 ^{abc}	0.95 ± 0.03 ^{b}	1.13 ± 0.01 ^{ab}
T2 (dw+ZnO-NPs 75 mg/L)	0.50 ± 0.00 ^{ns}	0.86 ± 0.00 ^{a}	1.09 ± 0.08 ^{a}	1.20 ± 0.02 ^{a}
T3 (dw+ZnO-NPs 150 mg/L)	0.50 ± 0.03 ^{ns}	0.86 ± 0.05 ^{ab}	1.08 ± 0.03 ^{ab}	1.16 ± 0.04 ^{ab}
T4 NaCl (150 mM)	0.50 ± 0.00 ^{ns}	0.64 ± 0.02 ^{bc}	0.75 ± 0.04 ^{d}	0.78 ± 0.03 ^{d}
T5 (150 mM NaCl+ZnO-NPs 75 mg/L)	0.48 ± 0.03 ^{ns}	0.59 ± 0.01 ^{c}	0.81 ± 0.02 ^{c}	0.90 ± 0.02 ^{c}
T6 (150 mM NaCl+ZnO-NPs 150 mg/L)	0.46 ± 0.02 ^{ns}	0.66 ± 0.02 ^{bc}	0.94 ± 0.04 ^{b}	1.09 ± 0.05 ^{b}

Each value represents the mean ± SE (n=4). Values with the same letter are not significantly different at ($p \leq 0.05$), and the comparison is done according to different treatments in the same column.

The tomato leaf area (cm^2) in the different treatments was determined as shown in Table 8. The leaf area was determined in four different stages as an indication of the influence of NaCl stress and foliar spraying of chemically synthesized zinc oxide nanoparticles. It was observed that the readings in the different treatments were not significantly different. There was an increasing manner in the leaf area within the different stages, and there was an obvious increase in the leaf area of the non-stressed treatments (T1–T3) during the study compared to the stressed treatments (T4–T6).

Table 8. Determination of growth attributes (leaf area) in tomato.

Treatments	Readings of Leaf Area (cm^2) in Different Stages			
	5 July 2023	19 July 2023	28 July 2023	11 August 2023
T1 Control (dw)	119.56 ± 3.94 ^{c}	448.15 ± 15.85 ^{a}	510.75 ± 0.75 ^{b}	596.10 ± 15.90 ^{ab}
T2 (dw+ZnO-NPs 75 mg/L)	182.63 ± 1.38 ^{a}	434.73 ± 0.78 ^{a}	482.13 ± 3.63 ^{bc}	638.10 ± 5.40 ^{a}
T3 (dw+ZnO-NPs 150 mg/L)	136.38 ± 1.38 ^{bc}	414.63 ± 5.13 ^{a}	594.00 ± 16.50 ^{a}	632.15 ± 17.15 ^{a}
T4 NaCl (150 mM)	154.875 ± 18.38 ^{ab}	351.50 ± 26.50 ^{b}	392.25 ± 20.25 ^{d}	452.75 ± 40.25 ^{c}
T5 (150 mM NaCl+ZnO-NPs 75 mg/L)	131.63 ± 1.63 ^{bc}	360.88 ± 3.13 ^{b}	442.25 ± 7.25 ^{cd}	510.80 ± 58.20 ^{bc}
T6 (150 mM NaCl+ZnO-NPs 150 mg/L)	136.13 ± 16.13 ^{bc}	435.19 ± 14.81 ^{a}	479.75 ± 31.75 ^{bc}	484.50 ± 34.50 ^{bc}

Each value represents the mean ± SE (n=4). Values with the same letter are not significantly different at ($p \leq 0.05$), and the comparison is done according to different treatments in the same column.

The chlorophyll levels in the various treatments in **maize plants** were measured using soil plant analysis development (SPAD) units, as indicated in Table 9. A four-stage examination assessed the impact of NaCl stress and foliar spraying of ZnO-NPs. During the initial stage, there was no significant difference in the chlorophyll levels across the various treatments. However, the chlorophyll content dropped over time, specifically in the stressed treatment that did not receive ZnO-NPs spray (T2).

Table 9. Quantification of chlorophyll levels (measured in SPAD units) in maize.

Treatments	Chlorophyll Levels at Various Growth Phases			
	20 June 2023	**3 July 2023**	**15 July 2023**	**1 August 2023**
M1 Control (tap water)	56.58 ± 0.27 ^{ns}	60.54 ± 2.26 ^{a}	64.00 ± 0.72 ^{a}	63.62 ± 0.87 ^{a}
M2 (NaCl 150 mM)	53.76 ± 0.20 ^{ns}	49.11 ± 1.30 ^{c}	50.66 ± 0.15 ^{b}	50.58 ± 0.15 ^{b}
M3 (NaCl 150 mM + ZnO-NPs 2 g/L)	56.26 ± 0.37 ^{ns}	55.40 ± 0.64 ^{b}	55.24 ± 1.53 ^{b}	63.96 ± 1.05 ^{a}
M4 (tap water + ZnO-NPs 2 g/L)	55.44 ± 1.97 ^{ns}	58.40 ± 1.92 ^{ab}	61.21 ± 2.39 ^{a}	64.08 ± 0.90 ^{a}

Each value represents the mean ± SE (n=4). Values with the same letter are not significantly different at ($p \leq 0.05$), and the comparison is done according to different treatments in the same column. "ns": non-significant.

Conversely, the chlorophyll levels increased in the non-first and fourth treatments (M1 and M4) and the stressed treatment that received a spray of ZnO-NPs (M3). In the fourth stage, it was observed that the stressed treatment sprayed with ZnO-VPS (M3) had the same chlorophyll content as the non-stressed treatments (control "tap water" and "tap water + ZnO-NPs 2 g/L") (M1 and M4). The results demonstrated that spraying ZnO-NPs substantially increased chlorophyll levels in the third treatment (M3).

The height of the maize plants (measured in centimeters) under each treatment was determined and recorded in Table 10. Four stages were identified to assess the impact of chlorophyll concentration on growth and morphological characteristics during the experiment. Significant differences in maize plant heights were observed among the different treatments at all stages. The maize plants exhibited height increases in response to the four treatments, except for the second treatment (M2), where height growth ceased after the third stage. It was noted that the growth rate in the non-stressed treatments (M1 and M4) and the stressed treatment treated with ZnO-NPs, was more significant than in the stressed treatments (M2). At the fourth stage, the growth rate of maize plants' height in the third treatment (M3) approached the elongation rate observed in the first and fourth treatments (M1 and M4) when ZnO-NPs were applied through spraying. In contrast, the rate of growth in height of maize plants was higher for the fourth treatment (M4), where no stress was applied and the plants were sprayed, compared to the control treatment (M1).

Table 10. Measurement of plant height in maize plants.

Treatments	Plant Height (cm) at Various Growth Phases			
	20 June 2023	**3 July 2023**	**15 July 2023**	**1 August 2023**
M1 Control (tap water)	93.20 ± 0.41 ^{b}	186.10 ± 2.76 ^{b}	233.50 ± 1.87 ^{b}	233.50 ± 1.87 ^{b}
M2 (NaCl 150 mM)	80.23 ± 2.37 ^{d}	162.64 ± 3.85 ^{c}	208.43 ± 5.93 ^{c}	209.71 ± 6.56 ^{c}
M3 (NaCl 150 mM + ZnO-NPs 2 g/L)	86.00 ± 0.84 ^{c}	191.60 ± 1.89 ^{ab}	238.40 ± 1.44 ^{ab}	238.80 ± 1.24 ^{ab}
M4 (tap water + ZnO-NPs 2 g/L)	97.80 ± 1.55 ^{a}	199.00 ± 1.52 ^{a}	246.80 ± 1.36 ^{a}	246.80 ± 1.36 ^{a}

Each value represents the mean ± SE (n=4). Values with the same letter are not significantly different at ($p \leq 0.05$), and the comparison is done according to different treatments in the same column.

The thickness (in centimeters) of the maize stem was measured for each treatment, as indicated in Table 11. Like the previous measurement of growth and morphological characteristics (namely plant height), stem width was assessed in four phases. Significant differences in stem width of maize plants were detected across all stages in the other treatments. Until the third stage, it was noted that the growth rate in the first and fourth treatments (M1 and M4) was similar to the control treatment and more significant than the second treatment (M2). During the fourth stage, the rate of maize stem width growth was higher for the non-stressed and sprayed treatment (M4) compared to the control treatment (M1) and the third one (M3). Treatment M4 showed a slight rise in comparison to treatments M1 and M2.

Table 11. Measurement of stem diameter in maize plants.

Treatments	Stem Width (cm) at Various Growth Phases			
	20 June 2023	**3 July 2023**	**15 July 2023**	**1 August 2023**
M1 Control (tap water)	2.57 ± 0.07 [a]	2.86 ± 0.09 [a]	2.86 ± 0.09 [a]	2.88 ± 0.08 [bc]
M2 (NaCl 150 mM)	2.26 ± 0.05 [b]	2.44 ± 0.12 [b]	2.64 ± 0.09 [b]	2.76 ± 0.02 [c]
M3 (NaCl 150 mM + ZnO-NPs 2 g/L)	2.60 ± 0.03 [a]	2.77 ± 0.05 [a]	2.90 ± 0.00 [a]	2.92 ± 0.02 [b]
M4 (tap water + ZnO-NPs 2 g/L)	2.69 ± 0.07 [a]	2.98 ± 0.00 [a]	3.02 ± 0.04 [a]	3.05 ± 0.03 [a]

Each value represents the mean ± SE (n=4). Values with the same letter are not significantly different at ($p \leq 0.05$), and the comparison is done according to different treatments in the same column.

The leaf area of maize (measured in cm^2) in each treatment was determined and is presented in Table 12. The leaf area was assessed in four stages to evaluate the impact of NaCl stress and foliar application of chemically produced zinc oxide nanoparticles. The growth rate in the first and fourth treatments (M1 and M4) was similar to the control treatment and more significant than the second treatment (M2). During the fourth stage, it was noticed that the rate of maize leaf area growth was higher in the non-stressed and sprayed treatment (M4) compared to the control treatment (M1) and the treatment sprayed with ZnO-NPs (M3). This indicates that the leaf area increased faster in MT4 than in M1 and M3.

Table 12. Measuring the leaf area in maize plants.

Treatments	Area of Leaves (cm^2) at Various Growth Phases			
	20 June 2023	**3 July 2023**	**15 July 2023**	**1 August 2023**
M1 Control (tap water)	7271.28 ± 243.49 [a]	9800.28 ± 201.28 [b]	12,130.32 ±275.13 [a]	13,646.61 ±309.52 [a]
M2 (NaCl 150 mM)	5378.72 ± 135.50 [c]	7389.00 ± 175.33 [c]	10,296.00 ±293.78 [b]	11,668.80 ±309.87 [b]
M3 (NaCl 150 mM + ZnO-NPs 2 g/L)	6320.505 ± 205.30 [b]	9441.18 ± 66.56 [b]	12,348.33 ±168.74 [a]	13,963.05 ±168.59 [a]
M4 (tap water + ZnO-NPs 2 g/L)	6789.675 ± 58.62 [ab]	10,447.215 ± 153.33 [a]	12,411.6 ±149.86 [a]	14,495.22 ±321.29 [a]

Each value represents the mean ± SE (n=4). Values with the same letter are not significantly different at ($p \leq 0.05$), and the comparison is done according to different treatments in the same column.

Salinity results in significant economic losses in agricultural output due to crop yield and quality reductions. The prevailing consensus is that a significant portion of cultivable agricultural land will become inoperable in the future because of salt. Hence, this study aimed to examine the impact of zinc oxide nanoparticle influence on tomato and maize plants in the presence of salt conditions.

In the current study, the effect of severe salt stress (150 mM NaCl) on the chlorophyll content, **tomato** plant height, stem width, and leaf area was detrimental to tomato plants depending on the different concentrations used to spray the plants with ZnO-NPs (75 and 150 mg/L). A decrease was observed in the chlorophyll content, plant height, stem width, and leaf area at the severe concentration of NaCl (150 mM) (Yildirim et al., 2023); however, for this inhibitory effect of salt stress on chlorophyll content, and the growth attributes—plant height, stem width, and leaf area in tomato plants—it was noticed that harmful effect was less when ZnO-NPs foliar spray was applied.

SPAD value is an indicator of chlorophyll content, which displays the functions of photosynthetic apparatus (Mahawar et al., 2024). The current study confirmed that the chlorophyll content exhibited a considerable drop in correlation with the severe salt concentration, with the most pronounced reduction found in plants cultivated under 150 mM NaCl (Table 3). Shin et al. (2020) found that the levels of chlorophyll a and chlorophyll b in tomatoes reduced in proportion to high salt concentrations. Additionally, salt stress adversely affects the SPAD value in cucumber plants (Sarwar et al., 2021). In the present study, it was found that the content of chlorophyll began to rise again in the fifth and sixth stressed treatments that were sprayed with ZnO-NPs (75 and 150 mg/L) in the fourth stage of collecting the readings, but in the fourth stressed treatment that was not sprayed with ZnO-NPs (T4), the chlorophyll content did not significantly rise. It was clear that there was a manner of increasing the chlorophyll content in the stressed treatments when they were sprayed with ZnO-NPs. In a study by Mahawar et al. (2024), it was primarily observed the combined impact of NaCl and zinc oxide nanoparticles on the photochemistry of the photosystems (PSII and PSI) at a higher salt concentration of 300 mM.

Generally, applying metal oxide nanoparticles to plant leaves and subjecting them to higher NaCl treatment enhanced the plant's ability to convert sunlight into energy by speeding up the flow of electrons from active reaction centers to the quinone pool. This resulted in an increase in the efficiency of photosystem II, a decrease in the amount of light that is not used for photosynthesis, and a reduction in the stress placed on the cytochrome complex (Mahawar et al., 2024).

Foliar zinc oxide nanoparticles (ZnO-NPs) have been observed to be more efficient in improving the effectiveness of photosystem II (PSII) photochemistry. Zinc is a crucial element that is recognized for its ability to enhance photosynthetic activities in plants under stress (Umair Hassan et al., 2020). The replacement of zinc ions in the soil is not possible, making it crucial to restore them through foliage (Montalvo et al., 2016). The zinc ion, an essential nutrient, greatly influences the synthesis of auxin, metabolic processes related to nitrogen, and the proliferation of root cell tissue. This is because zinc enhances the biosynthesis of tryptophan (Ahmed, et al., 2024a; Chen et al., 2017). Indole-based auxins are produced from tryptophan; therefore, the zinc nanoparticles will have an indirect impact on the elongation growth (Hamzah Saleem et al., 2022). This is because it functions as a cofactor for a range of enzymes, including oxidases, dehydrogenases, and anhydrases, such as peroxidases. Zinc enhances the cation-exchange capacity of the root, facilitating the absorption of vital nutrients, such as nitrogen. Consequently, this leads to an increase in the overall quantity of protein. In addition, zinc plays a crucial role in the metabolism by facilitating the breakdown of carbohydrates and proteins (Ahmed, et al., 2024a; Fageria, 2001). The presence of zinc oxide nanoparticles can modify the photosynthetic systems when plants are exposed to NaCl stress. This modification occurs by stimulating the enzymes responsible for the photosynthetic electron transport and water-splitting processes (Chanu Thounaojam et al., 2021).

The foliar spray of ZnO-NPs had a substantial impact on the plant height, stem width, and leaf area of the tomato Kecskeméti 549 variety, as indicated by the data presented in Tables 6–8. That positive impact of the ZnO-NPs was thought to be because of increasing the tryptophan amino acid that increased the production of the indole-based auxins (Hamzah Saleem et al., 2022).

The tomato plant reached its maximum height of 75.25 ± 2.10 cm at the fourth stage of the experiment, namely in the third treatment (T3), where a concentration of 150 mg/L of ZnO-NPs was used (Table 4). This height was greater than that seen in the control group. The fourth treatment (T4), with a concentration of 150 mM NaCl, resulted in the lowest plant height, measuring 57.00 ± 2.42 cm. The utilization of zinc oxide nanoparticles may enhance plant growth, particularly in terms of plant height, by facilitating the release of essential nutrients for crop development (Khanm et al., 2018). In their study, Sun et al. (2020) found that applying a solution of 100 mg/L ZnO-NPs through foliar spraying resulted in the highest number of tomato plants. The tomato plants that were treated with a concentration of 50 parts per million (ppm) of zinc oxide nanoparticles (ZnO-NPs) showed the greatest increase in shoot length, with a growth increment of 30.1% compared to the control group (Faizan & Hayat, 2019).

The tomato plant reached its maximum stem width of 1.20 ± 0.02 cm at the fourth stage of the experiment, namely in the second treatment (T2), where a concentration of 75 mg/L of ZnO-NPs was applied (Table 5). This width was a little greater than that seen in the control group. The fourth treatment (T4), with a concentration of 150 mM NaCl, resulted in the lowest plant stem width, measuring 0.78 ± 0.03 cm. In the case of leaf area (Table 6), the increased leaf area (638.10 ± 5.140 cm^2) was obtained from the plant receiving 75 mg/L ZnO nanoparticles (T2) followed by the plant receiving 150 mg/L ZnO-NPs (T3) with 632.15 ± 17.15. The lowest result (452.75 ± 40.25 cm^2) was in the fourth treatment (T4), which was severely stressed with 150 mM NaCl and did not receive any foliar spray with zinc oxide nanoparticles.

Exposure to salt stress severely reduced the growth and morphological traits of **maize plants**, including stem width, leaf area, chlorophyll levels, and plant height (150 mM NaCl) to compensate for the irrigation requirements in this study in the second treatment (M2) compared to the other treatments in all stages that the measurements were recorded in. However, spraying ZnO-NPs, particularly on the third and fourth treatments (M3 and M4), greatly enhanced the previously mentioned growth metrics by ameliorating the saline-stress-mediated decline in T3 or the positively stimulated non-saline-stressed (M4) as shown in Tables 9–12.

The regulation of the apoplastic and symplastic pathways is crucial in alleviating the harmful effects of high salinity on the entry of Na^+ and Cl^- into the transpiration stream, thus preventing ionic poisoning in the top sections of the plant (Badawy et al., 2021; Gerona et al., 2019). Exceeding a specific threshold, the presence of Na^+ and Cl^- ions hampers the process of protein synthesis, restricts metabolic function, impairs cellular structures, and ultimately leads to cell death (Ahmad et al., 2023; Z. Yang et al., 2020). Moreover, it stimulates the generation of reactive oxygen species (ROS), which, when they build up, cause oxidative damage to nucleic acids and the denaturation of the plasma membrane. This, in turn, impacts osmotic pressure, cellular elongation, and cell division (Ahmad et al., 2023; Badawy et al., 2021).

The observed improvement in the performance of the third treatment plants was attributed to utilizing ZnO-NPs. ZnO-NPs treatment improves plant growth by increasing resilience to abiotic stress (Seleiman et al., 2023a). Using ZnO nanoparticles in plants significantly facilitates the production of plant hormones, such as indole acetic acid (IAA) and gibberellic acid (GA3), leading to increased synthesis.

Consequently, this process enhances plant growth by increasing dividing cells and expansion, maintaining intact membranes, and activating enzymes. It enables plants to withstand abiotic stresses, such as salinity (Cakmak, 2008). Zinc (Zn) nanoparticles alleviated the adverse impacts of saltwater stress by regulating metabolic activities in plant cells under stress and promoting the proper synthesis of pigments for photosynthesis. (El-Badri et al., 2021) observed a notable enhancement in the length of shoots in *Brassica napus* L. when subjected to 150 mM NaCl stress after being treated with ZnO-NPs seed priming, as compared to the control group.

ZnO-NPs are highly efficient in providing Zn^{2+} since they play a crucial role in supporting several aspects of plant growth and development, such as glucose and protein metabolism. Zinc ions participate in the formation of enzyme-substrate complexes, and bind NAD to the surface of the apoenzyme in the plants (Bahr et al., 2023). Additionally, they aid in auxin synthesis, which eventually promotes the development of plant cell walls and cell differentiation (Ahmed, et al., 2023a). The decreased reduction of tomato and maize stem under salinity can be related to the excessive accumulation of Na^+ and Cl^- ions in many cellular compartments of both the root and aerial plant organs (Gerona et al., 2019; A. Singh, 2021).

The accumulation of these ions to harmful levels disrupts the process of genetic expression, protein synthesis, enzyme activity, energy consumption, and cell division. It also harms the cellular ultrastructure and can finally lead to cell death (Ahmed et al., 2024b; A. Singh, 2022). Salinity not only leads to ionic toxicity but also disrupts osmotic balance, denatures cell membranes, causes leakage of osmolytes, and disrupts nutritional balance. As a result, it affects turgor pressure, cell elongation, and the morphological characteristics of plants under stress (Shahzad et al., 2021; Singh, 2021).

While many plants can regulate their osmotic balance by producing suitable organic electrolytes through biosynthesis, this process can require up to 10 times more energy. This energy expenditure is further exacerbated when plants are continuously exposed to hypertonic solutions (Seleiman et al., 2023b). Seleiman et al. (2023b) demonstrated that applying ZnO-NPs to the leaves, particularly at a concentration of 100 mg/L, effectively improved the negative effects of salt on growth metrics. Zinc, supplied by ZnO-NPs, stimulates the production of endogenous plant regulators and growth promoters including indole-3-acetic acid (IAA) and gibberellic acid (GA3). These substances have a role in metabolic activity, cell elongation, and cell division, ultimately leading to improved plant growth (Cakmak, 2008; Zulfiqar & Ashraf, 2021).

4.4. Identifying particular post-harvest attributes in tomato and maize following diverse treatments

Table 13 presents the post-harvest measurements **in tomato**, indicating that the plants treated with NaCl solution exhibited the lowest values across various examined post-harvest variables, including fruit number and weight. Conversely, the plants treated with foliar-sprayed ZnO-NPs, regardless of stress levels, exhibited higher values compared to those subjected to salty-water irrigation (T4). For the weight of the moist dried leaves, the plants that were not stressed, but sprayed with 75 mg/L ZnO-NPs showed the highest values compared to those that were sprayed with 150 mg/L , and also higher values than the stressed and sprayed plants (T5 and T6).

Table 13. Measurements taken after harvest from various tomato treatments.

Treatments	No. of the fruits	Weight of the fruits (g)	Weight of the fresh leaves (g)	Weight of the dried leaves (g)
T1	17.50 ± 0.65 ^{b}	963.13 ± 33.83 ^{b}	280.71 ± 19.78 ^{a}	37.33 ± 3.15 ^{ab}
T2	20.50 ± 0.65 ^{ab}	1042.31 ± 36.72 b	293.24 ± 16.14 ^{a}	40.36 ± 2.68 ^{a}
T3	22.50 ± 0.65 ^{a}	1304.60 ± 62.83 ^{a}	274.32 ± 26.54 ^{a}	37.35 ± 4.46 ^{ab}
T4	5.25 ± 0.25 ^{d}	283.29 ± 28.72 ^{e}	261.91 ± 12.86 ^{a}	32.48 ± 2.28 ^{b}
T5	12.00 ± 0.91 ^{c}	489.94 ± 25.26 ^{d}	216.00 ± 12.61 ^{b}	28.31 ± 1.25 ^{b}
T6	17.25 ± 0.48 ^{bc}	508.78 ± 55.48 ^{d}	246.65 ± 41.13 ^{a}	32.11 ± 5.20 ^{ab}

Each value represents the mean ± SE (n=4). Values with the same letter are not significantly different at ($p \leq 0.05$), and the comparison is done according to different treatments in the same column.
***T1**: Control (non-treated) (dw). **T2**: (dw + ZnO-NPs 75 mg/L). **T3**: (dw + ZnO-NPs 150 mg/L). **T4**: NaCl (150 mM). **T5**: (150 mM NaCl + ZnO-NPs 75 mg/L). **T6**: (150 mM NaCl + ZnO-NPs 150 mg/L).*

Table 14 shows the results of post-harvest measurements in **maize**; the salty water-treated plants showed the lowest values of the different examined post-harvest parameters such as weight of the humid and dried, weight of the humid and dried stalk, weight of the humid cob, weight of humid and dried 100 seeds, weight of humid and dried all seeds in the cob, the moisture content in the corn seeds, and even the number of the rows and seeds per the cob. On the other hand, the foliar-sprayed plants with ZnO-NPs, even if they were stressed or not, showed higher values than in the salty-water irrigated treatments, sometimes the values were also higher than were in the control treatment.

Table 14. Post-harvest measurements from different treatments of maize.

Treatments	Weight of the humid leaves (g)	Weight of the dried leaves (g)	Weight of the humid stalk (g)	Weight of the dried stalk (g)	Weight of the humid Cob (g)	Weight of humid 100 seeds (g)	Weight of dried 100 seeds (g)
M1	36.83 ± 1.17 ^{a}	32.25 ± 0.81 ^{b}	197.42 ± 8.38 ^{bc}	73.22 ± 1.71 ^{b}	314.98 ± 25.16 ^{a}	40.00 ± 1.16 ^{ab}	34.09 ± 1.20 ^{bc}
M2	27.10 ± 0.78 ^{b}	23.27 ± 1.02 ^{c}	150.78 ± 14.58 ^{c}	59.98 ± 1.86 ^{b}	211.98 ± 13.75 ^{b}	36.03 ± 2.53 ^{b}	31.12 ± 1.32 ^{c}
M3	39.58 ± 1.28 ^{a}	35.23 ± 0.59 ^{a}	247.33 ± 21.53 ^{ab}	115.88 ± 11.54 ^{a}	301.57 ± 2.09 ^{a}	43.58 ± 1.72 ^{a}	38.46 ± 1.91 ^{ab}
M4	41.15 ± 1.20 ^{a}	36.27 ± 0.95 ^{a}	265.45 ± 29.18 ^{a}	128.10 ± 8.44 ^{a}	307.53 ± 3.50 ^{a}	45.75 ± 2.63 ^{a}	41.07 ± 1.48 ^{a}

Each value represents the mean ± SE (n=4). Values with the same letter are not significantly different at ($p \leq 0.05$), and the comparison is done according to different treatments in the same column. ***M1****: Control (tap water);* ***M2****: (NaCl 150 mM);* ***M3****: (NaCl 150 mM + ZnO-NPs 2 g/L); and* ***M4****: (tap water + ZnO-NPs 2 g/L).*

Table 14. *Continued.*

Treatments	Weight of humid all seeds (g)	Weight of dried all seeds (g)	Moisture in corn seeds (g)	No. of rows/cob	No. of seeds/row
M1	239.85 ± 12.28 ^{a}	204.20 ± 8.99 ^{a}	0.15 ± 0.01 ^{ns}	16 ± 0.33 ^{ns}	40 ± 0.33 ^{a}
M2	184.15 ± 11.78 ^{b}	159.12 ± 5.64 ^{b}	0.13 ± 0.02 ^{ns}	16 ± 1.15 ^{ns}	36 ± 1.86 ^{b}
M3	241.98 ± 11.44 ^{a}	213.57 ± 12.16 ^{a}	0.12 ± 0.01 ^{ns}	16 ± 1.15 ^{ns}	41 ± 1.33 ^{a}
M4	254.02 ± 1.06 ^{a}	228.63 ± 5.92 ^{a}	0.10 ± 0.02 ^{ns}	15 ± 0.67 ^{ns}	43 ± 0.33 ^{a}

Each value represents the mean ± SE (n=4). Values with the same letter are not significantly different at ($p \leq 0.05$), and the comparison is done according to different treatments in the same column. ***M1****: Control (tap water);* ***M2****: (NaCl 150 mM);* ***M3****: (NaCl 150 mM + ZnO-NPs 2 g/L); and* ***M4****: (tap water + ZnO-NPs 2 g/L).*

In **tomato** fruits, salt stress can increase lycopene concentration by two to three times, facilitating the accumulation of carbohydrates, sugars, and amino acids (Sun et al., 2024; Tang et al., 2020). T3 is the superior treatment, yielding the most quantity of fruits (22.50) and the heaviest fruits (1304.60). Conversely, T4 performed the poorest in all domains, exhibiting values significantly inferior to those of all other treatments. T1, T2, T3, T4, and T6 for moist leaves exhibited no significant differences among them. Treatment T5 resulted in a drastically reduced weight of 216. Most treatments yielded comparable results for dried biomass; however, T2 exhibited the highest weight (40.36), significantly surpassing T4 and T5. Quddus et al. (2024) showed that using foliar ZnONPs has significantly enhanced the growth and development, yield, quality, and absorption of the nutrients by tomato plants. Their experiment revealed that the application of 0.01 ppt of ZnONPs yielded optimal results for critical growing and productivity parameters (Quddus et al., 2024).

Sun et al. (2024) proved that by applying variant levels of salinity stress to the potted tomatoes, the plant growth was adversely affected. Plants subjected to salinity stress experienced a reduction of 25.23% and 51.39% in their aboveground fresh weight relative to the control group, which received fresh water. Under 300 mg salt/1000 g and 600 mg salt/1000 g soil conditions, the weight of an individual tomato fruit was reduced by 14.28% and 38.17%, respectively, compared to the non-salinated soil treatment.

In case of maize plants, zinc oxide nanoparticles significantly enhanced the weight (humid/dried) of cob and seeds in foliar-treated plants as compared to stressed (without spraying) and control plants. They recorded maximum cob and all seeds humid weight at 307.53 ± 3.50 g and 254.02 ± 1.06 g in 2 g/L of ZnO-NPs sprayed fourth treatment (M4) compared to salt-stressed second treatment (M2) at 211.98 ± 13.75 g, and 184.15 ± 11.78 g, respectively. Nano foliar application (2 g/L) also enhanced the weight (humid/dried) of cob and seeds in foliar-treated stressed plants (M3) compared to salt-stressed non-sprayed second treatment (M2). The number of seeds/row was also noted. In foliar-treated plants, even if they were stressed (M3) or non-stressed (M4), the maximum number of seeds/row was 43 seeds, and 41 seeds/row compared to the salt-stressed treatment that was not sprayed with ZnO-NPs and control as they recorded 36 and 40 seeds/row, respectively.

Raddy et al. (2018) examined the impact of applying zinc oxide nanoparticles to the leaves of maize plants on their development and productivity. The researchers observed an increase in both the length and weight of the cobs in plants treated with nanoparticles, compared to those treated with zinc oxide in a bulky form and the control group.

Tondey et al. (2021) observed improved maize yielding characteristics with seed priming with zinc oxide nanoparticles. Satdev et al. (2020) reported that using zinc nanoparticles as a priming ingredient and foliar spray increased the length, girth, and number of cobs per plant. The likely cause could be attributed to the high absorption and efficient movement of nano zinc oxide. The correlation may be attributed to the heightened chlorophyll levels and photosynthetic activity observed in maize plants treated with ZnO-NPs (Zhou et al., 2011).

Zhou et al. (2011) further elucidated that ZnO nanoparticles (NPs) exhibit a high affinity for physical surfaces and strongly interact with biological proteins owing to their elevated specific surface reactivity. Consequently, this leads to enhanced absorption on the cellular surface. According to Lin and Xing (2008), ZnO-NPs were primarily penetrated to the cell surface and rapidly removed. The enhancement observed in plants treated with foliar application may be attributed to the swift transportation and incorporation of Zn nanoparticles, which subsequently stimulates the production of enzyme activity that accelerates growth and the metabolism of auxin in plants.

4.5. Phenolic profile of tomato and maize leaves

The HPLC analysis of **tomato and maize leaves'** extracts for determining their phenolic compounds was performed as shown in Tables 15 and 16. The tables showed 20 examined compounds. Three compounds out of those twenty were not found in any of the examined tomato extracts from the different treatments. These three compounds were genetisic acid, rosmarinic acid, and kampferol. It was noticed that the obtained phenolic compounds from the tomato stressed treatments (T4–T6) were higher in concentration with totals of 937.62, 1223.78, and 1309.78 µg/g in T4–T6 treatments, respectively. The concentrations of the compounds obtained from the non-stressed treatments (T1–T3) were 562.02, 753.02, and 937.62 µg/g, respectively. It was also noticed that the obtained phenolic compounds from the maize stressed treatments (M2 and M3) were higher in concentration with totals of 1030.12 and 1099.81 µg/g, respectively. The concentrations of the compounds obtained from the non-stressed treatments (M1 and M4) were 917.37 and 966.99 µg/g, respectively. Tables 15 and 16 showed the presence of gallic acid, protocatechuic acid, *p*-hydroxybenzoic acid, catechin, chlorogenic acid, caffeic acid, syringic acid, vanillic acid, ferulic acid, sinapic acid, rutin, *p*-coumaric acid, apigenin-7-glucoside, cinnamic acid, quercetin, apigenin, and chrysin.

Table 15. HPLC analysis of phenolic compounds in the leaves from different treatments of tomato.

Compounds to be detected	RT (min)	Concentration (µg/g)/Treatment					
		T1	T2	T3	T4	T5	T6
Gallic acid	3.7	122.91	149.63	141.73	206.62	192.26	203.61
Protocatechuic acid	6.4	1.38	1.74	18.07	20.26	21.04	24.13
Gentisic acid	9.7	0.00	0.00	0.00	0.00	0.00	0.00
***p*-hydroxybenzoic acid**	9.8	10.19	12.96	15.21	19.03	22.25	25.36
Catechin	11.8	25.14	25.23	31.37	95.52	91.60	99.66
Chlorogenic acid	12.7	154.08	239.25	355.54	359.51	617.96	603.38
Caffeic acid	13.5	0.63	2.32	1.59	7.90	5.05	8.69
Syringic acid	14.6	8.10	4.66	44.27	49.33	46.87	46.72
Vanillic acid	16.0	4.36	4.49	4.79	7.74	10.47	9.20
Ferulic acid	20.6	37.35	41.80	44.71	58.35	67.70	80.53
Sinapic acid	21.5	18.88	25.99	36.12	27.67	65.09	60.21
Rutin	24.5	5.58	17.72	1.03	2.11	3.14	5.27
***p*-coumaric acid**	25.4	13.22	11.35	0.86	1.13	2.97	27.21
Apigenin-7-glucoside	27.5	5.69	15.31	36.98	52.80	39.21	69.89
Rosmarinic acid	29	0.00	0.00	0.00	0.00	0.00	0.00
Cinnamic acid	35.1	1.61	1.26	7.31	13.80	15.03	23.22
Quercetin	36.3	1.10	2.93	1.02	1.40	2.04	2.71
Apigenin	39.2	0.19	1.19	5.50	4.62	6.79	5.20
Kaempferol	40.8	0.00	0.00	0.00	0.00	0.00	0.00
Chrysin	51.5	4.00	4.19	6.92	9.83	14.31	14.79
Total		414.41	562.02	753.02	937.62	1223.78	1309.78

T1: *control (dw);* ***T2****: dw+ZnO-NPs 75 mg/L;* ***T3****: dw+ZnO-NPs 150 mg/L;* ***T4****: NaCl (150 mM);* ***T5****: 150 mM NaCl+ZnO-NPs 75 mg/L; and* ***T6****: 150 mM NaCl+ZnO-NPs 150 mg/L.*

Table 16. HPLC analysis of phenolic compounds in the leaves from different treatments of maize.

Compounds to be detected	RT (min)	Concentration (µg/g)/Treatment			
		M1	M2	M3	M4
Gallic acid	3.7	118.49	147.16	106.52	117.09
Protocatechuic acid	6.4	7.15	6.40	5.24	5.51
Gentisic acid	9.7	0	0	0	0
***p*-hydroxybenzoic acid**	9.8	2.92	3.20	6.09	7.94
Catechin	11.8	20.36	22.26	91.23	87.94
Chlorogenic acid	12.7	56.34	79.37	73.84	49.85
Caffeic acid	13.5	11.36	9.85	10.08	9.37
Syringic acid	14.6	6.27	7.08	8.40	9.30
Vanillic acid	16.0	19.87	16.85	18.08	17.03
Ferulic acid	20.6	381.53	401.97	400.13	339.25
Sinapic acid	21.5	243.4	283.08	324.17	278.09
Rutin	24.5	2.31	2.65	2.84	3.08
***p*-coumaric acid**	25.4	4.76	3.53	3.29	3.13
Apigenin-7-glucoside	27.5	4.46	5.30	4.12	3.28
Rosmarinic acid	29	0	0	0	0
Cinnamic acid	35.1	3.21	1.97	1.94	1.97
Quercetin	36.3	14.5	16.39	15.21	16.01
Apigenin	39.2	19.87	22.56	26.52	15.41
Kaempferol	40.8	0	0	0	0
Chrysin	51.5	0.57	0.50	2.11	2.74
Total		917.37	1030.12	1099.81	966.99

M1*: Control (tap water);* ***M2****: (NaCl 150 mM);* ***M3****: (NaCl 150 mM + ZnO-NPs 2 g/L); and* ***M4****: (tap water + ZnO-NPs 2 g/L).*

Cellular respiration is accelerated by stress, leading to a shift in biochemical pathways from glycolysis to the pentose phosphate pathway. The secondary metabolic pathways, such as the shikimic acid pathway and phenylpropanoid biosynthesis pathway that originate from this point experience an increase in speed. This acceleration leads to the production of secondary metabolites, such as phenolic compounds and antioxidants, which aid in the cellular-level regeneration processes of plants (Jethva et al., 2022; Zhang et al., 2020).

Phenolic compounds play a crucial role in neutralizing harmful free radicals through the process of detoxification (Ksouri et al., 2007)**,** and environmental stress can enhance the secretion of these scavenging molecules (Toscano et al., 2019). According to Stewart et al. (2000), the selection of a certain cultivar significantly influenced the overall quantity of phenolic compounds in tomatoes, even when they were cultivated in equal environmental conditions. Moreover, the presence of water can significantly impact the process of plant phenolic metabolism and the overall composition of fruit (Tomás-Barberán & Espín, 2001). Conflicting data on the impact of salinity on phenolic compounds in tomato fruits may be found in the literature, which leads to an uncertain increase (Krauss et al., 2006; Sgherri et al., 2007), decrease (Hernández-Fuentes et al., 2017), or perhaps maintenance at the same level (Kim et al., 2008).

Similarly, researchers have observed that tomato fruits grown in saline conditions have an elevated level of flavonoids, indicating an increase in the overall flavonoid content (Hernández-Fuentes et al., 2017)**,** and others confirming a decrease (Moles et al., 2019). Rutin, a flavonoid belonging to the category of phenolic chemicals, has a wide range of significant biological and pharmacological effects (Ihme et al., 1996). Growers must comprehend the delicate equilibrium between optimizing phytochemical content through irrigation regulation while ensuring product quality remains high. The study by Sánchez-Rodríguez et al. (2012) indicated that tomato drought-tolerant cv. Zarina-like rootstocks (ZarxJos) have a better-quality value and are a potential source of health-promoting chemicals due to their abundance of bioactive compounds, especially under water stress situations. ZnO-NPs have been found to enhance nutrient absorption, regulate the Na^+/K^+ ratio, maintain water balance, enable ion accumulation, and mitigate the negative impacts of abiotic stressors. The increase in flavonoid, anthocyanin, phenolic, and photosynthetic pigment levels, as well as the upregulation of antioxidant enzymes, are the factors that contribute to these advantages (Ahmed, et al., 2024a).

4.6. Gas Chromatographic (GC) analysis of fatty acids (FA) in tomato leaves and maize seeds (grains)

The fatty acid profile of the tomato leaves' extracted oil was determined, as shown in Table 17. Nine fatty acids were expressed. One of those detected fatty acids is medium chain (lauric acid), and the other eight fatty acids were long chain. The lauric fatty acid was not detected in the investigated tomato leaves' extracts, except in the leaves from the fifth treatment plants (T5) with a percentage of 1.81%. It was noticed that the highest obtained fatty acid was the palmitic (C16:0), and it was observed in all the leaves from different treatments with 67.24% in T6, 66.21% in T2, 58.04% in T1, 56.5% in T3, 56.44% in T5, and 56.33% in T4. The lowest fatty acid was lauric acid, with 1.81% in T5, and it was not detected in the other treatments. The lauric acid was ascendingly followed by the palmitoleic acid (C16:1n-7) with 2.9% in T3 and T4, 2.43% in T6, 2.31% in T1, 2.24% in T5, and 2.08% in T2. Myristic acid (C14:0) was not detected in T2, T3, and T4. And, arachidic acid (C20:0) was also not detected in T3 and T4.

Table 17. Gas chromatographic (GC) analysis of fatty acids in tomato leaves.

Compounds to be detected	Concentration (%)/Treatments					
	T1	**T2**	**T3**	**T4**	**T5**	**T6**
Lauric acid (C12:0)	0	0	0	0	1.81	0
Myristic acid (C14:0)	2.54	0	0	0	2.32	0
Palmitic acid (C16:0)	58.04	66.21	56.5	56.33	56.44	67.24
Palmitoleic acid (C16:1n-7)	2.31	2.08	2.9	2.91	2.24	2.43
Margaric acid (C17:0)	11.65	8.37	8.08	7.89	9.21	9.09
Stearic acid (C18:0)	8.18	6.22	7.43	9.01	9.81	8.31
Linoleic acid (C18:2)	5.1	4.11	10.24	9.58	4.42	6.67
γ- Linolenic acid (C18:3)	6.19	6.86	14.85	14.28	6.87	6.26
Arachidic acid (C20:0)	5.99	6.15	0	0	6.88	0

T1: *control (dw);* ***T2****: dw+ZnO-NPs 75 mg/L;* ***T3****: dw+ZnO-NPs 150 mg/L;* ***T4****: NaCl (150 mM);* ***T5****: 150 mM NaCl+ZnO-NPs 75 mg/L; and* ***T6****: 150 mM NaCl+ZnO-NPs 150 mg/L.*

The long-chain fatty acid (LCFA) profile of maize seeds' extracted oil was determined, as shown in Table 18. The prepared standards expressed 15 fatty acids. Three fatty acids were not detected in the investigated maize seeds' extracts. These fatty acids were Eicosapentaenoic acid (EPA), docosadienoic acid, and docosapentaenoic acid. It was noticed that the obtained fatty acids from the stressed treatment that was not sprayed with ZnO-NPs (M2) were higher in concentration, with totals of 97.56 mg/g, compared with the other three treatments that showed concentrations of 94.94, 96.00, and 95.78 mg/g in M1, M3, and M4, respectively. Table 18 shows the presence myristic acid, palmitic acid, palmitoleic acid, stearic acid, oleic acid, vaccenic acid, linoleic acid, γ-linolenic acid, α-linolenic acid, ecosenoic acid, arachidonic acid, and docosahexaenoic acid (DHA).

Table 18. Gas chromatographic **(**GC) analysis of long-chain fatty acids (LCFA) in maize grains.

Compounds to be detected	Concentrations (g/100 g)/Treatments			
	M1	**M2**	**M3**	**M4**
Myristic acid	0.04	0.07	0.06	0.06
Palmitic acid	13.32	13.66	12.9	13.3
Palmitoleic acid	0.05	0.05	0.05	0.04
Stearic acid	2.43	2.67	2.62	2.54
Oleic acid	27.09	27.84	27.76	27.53
Vaccenic acid	0.34	0.30	0.32	0.33
Linoleic acid	50.54	51.79	51.29	51.09
γ-linolenic acid	0.05	0.06	0.07	0.05
α-linolenic acid	0.93	0.95	0.95	0.7
Ecosenoic acid	0.10	0.13	0.11	0.10
Arachidonic acid	0.03	0.03	0.03	0.02
Eicosapentaenoic acid (EPA)	0	0	0	0
Docosadienoic acid	0	0	0	0
Docosapentaenoic acid	0	0	0	0
Docosahexaenoic acid (DHA)	0.02	0.01	0.02	0.02
Total	94.94	97.56	96.00	95.78

***M1**: Control (tap water); **M2**: (NaCl 150 mM); **M3**: (NaCl 150 mM + ZnO-NPs 2 g/L); and **M4**: (tap water + ZnO-NPs 2 g/L).*

Fatty acid profiling was conducted to evaluate the integrity and adaptive response of the plant's lipidome under oxidative stress induced by salinity. Fatty acids are essential components of the plasma membrane. Their saturation levels influence the fluidity of the membrane and the efficacy of membrane-bound proteins such as H^+-ATPase. It is crucial for maintaining ionic equilibrium during salt stress (Guo et al., 2019). Moreover, fatty acids such as linolenic acid (C18:3) serve as the primary precursors for the biosynthesis of jasmonic acid (JA), a crucial signaling molecule that initiates the production of secondary metabolites and defense proteins (Wasternack & Feussner, 2018).

This study showed a positive correlation between exposure to salt stress and secreting the fatty acids and the mitigatory influence of ZnO-NPs on limiting the production of those secreted fatty acids as a response to salinity stress in tomato and mazie. The examination of fatty acids in corn, triticum, groundnut, arabidopsis, and *Suaeda salsa* under salinity stress revealed that the concentrations of unsaturated FAs rose as a response to counteract the effects of salt stress (Gogna et al., 2020; D. Kumar et al., 2013). Oleic acid, linoleic acid, and linolenic acid are the primary unsaturated fatty acids that determine the level of unsaturation in most plants. An analysis of *Vitis vinifera* seeds using lipid profiling and GC–MS/MS demonstrated that particular unsaturated fatty acids serve as precursors for the synthesis of prostaglandins and jasmonates in response to environmental stresses (Gogna et al., 2020).

Salinity stress in sunflowers results in a significant decrease in linoleic acid and δ-tocopherol. At the same time, there was an increase in the levels of palmitic, stearic, linolenic acids, and α- and γ-tocopherols (Noreen & Ashraf, 2010). Recent research has demonstrated that exposure to high salt levels reduces the activity of certain enzymes called desaturases, namely the membrane-bound ω-3 and ω-6 desaturases in the olive mesocarp. As a result, this alters the ratio of oleic acid to linoleic acid (Di Caterina et al., 2007). Oleic acid serves as a critical stress-inducer in plants, as it stimulates phospholipase D enzyme (PLD) (Hong et al., 2016). Liu et al. (2019), in his research on plant lipid remodeling has demonstrated that palmitic and oleic acids concentrations exhibited an increase because of abiotic stress, which matches the findings of the current research. Research on lipid alteration in salt-sensitive and salt-tolerant barley roots reveals that the salt-sensitive type exhibits lower amounts of 18:2 and 18:3 lipids (Yu et al., 2020).

Trienoic fatty acids constitute a significant portion of the membrane lipids in higher plants. Some believe that specific fatty acids, particularly linolenic acid, are essential since they facilitate the production of a signaling molecule known as jasmonate, which aids the body in combating sickness (Nishiuchi & Iba, 1998). Dombrowski (2003) proved that the salt stress in tomato plants may increase the accumulation of linolenic acid, the precursor to jasmonic acid biosynthesis. As the increase in salt-induced signals in jasmonic acid levels may occur due to changes in membrane composition and structure, or the activation of fatty acid desaturases. In another study, the microsomal fraction from soybean was purified. It exhibited the most significant modifications in lipids compared to the plasma membrane fraction. The concentration of phospholipids and sterols decreased by 50%, although the level of saturated fatty acids increased. saturated fatty acids (16:0) and (18:0), which represent 49% of the total fatty acids in the plasma membrane, they increased by 56% under salt stress (Surjus & Durand, 1996).

In the present study, the level of oleic acid was upregulated by the exposure to salinity stress in **maize grains** of the second treatment (M2). Increasing the oleic acid (18:1) in salt-stressed grains indicated the tolerance to salinity. As the presence of salinity stress increases, the formation of oleic and linoleic acid increases, boosting the plasma membrane's activity. H^+-ATPases are responsible for regulating ion homeostasis in the roots of barley plants (Yu et al., 1999). The saline growing conditions were shown to be associated with a reduction in cis-vaccenic acid. In their study, Paulucci et al. (2011) found that there was a significant reduction in the proportion of cis-vaccenic acid and a corresponding rise in the case of saturated fatty acids in peanut nodulating rhizobia when exposed to high temperatures and salinity.

Gogna et al. (2020) found that the levels of cis-vaccenic acid in the 1,2-diacylglycerol fraction of the variety, which was salt sensitive, decreased significantly during salinity stress. It is worth noting that cis-vaccenic acid was not present in the salt-tolerant and semi-tolerant varieties. Therefore, cis-vaccenic acid can serve as an indicator or signal for salt-sensitive sunflower types experiencing salt stress. Eicosanoic acid levels were slightly elevated under salinity stress.

Thus, eicosanoic was considered to play a possible signaling role. Its elevated levels in salinity-stressed plants may affect membrane fluidity (Yu et al., 2020). Multiple studies have documented the role of fatty acids in regulating ion balance through voltage-gated ion channels (Elinder & Liin, 2017). The roots of both barley cultivars, sensitive and tolerant, experienced fast oxidation of membrane lipids during salinity stress. Differences in the oxidation pattern produced by salt are observed in both cultivars (Yu et al., 2020). Hence, it can be suggested that there may be an interaction between sodium, potassium, and calcium ions, and unsaturated fatty acids, including oleic, linoleic, linolenic, and eicosanoic acids, and distinctive fatty acids such as cis-vaccenic, in the roots and seeds of plants.

4.7. Determination of different biochemical and stress markers in the leaves from different treatments of tomato and maize

Table 19 showed the results of the biochemical parameters in tomato: as the salt concentrations increased in the tomato leaves, the total phenolics and flavonoids (TPCs and TFCs), total hydrolyzable sugars, total free amino acids, proline, hydrogen peroxide (H_2O_2), the malondialdehyde (MDA) contents also increased. The effects of treatments on plant contents of the previous stress and biochemical markers were found to be statistically significant. The fourth stressed treatment (T4) had the highest concentrations of the aforementioned parameters compared to the two other stressed treatments (T5 and T6) except with the protein content. Those treatments (T5 and T6) were sprayed with 75 and 150 mg/L zinc oxide nanoparticles solutions. So, the secretion of the above-mentioned compounds was controlled to be in a compatible manner with the non-stressed treatments (T1–T3).

Table 19. Determination of the different biochemical and stress markers in the leaves from different treatments of tomato.

Treatments	Concentrations							
	TPCs (µg/g)	TFCs (µg/g)	Total Hydrolazable Sugars (µg/g)	Total Free Amino Acids (µg/g)	Protein Content (µg/g)	Proline Content (µg/g)	H_2O_2 (µg/g)	MDA (mmols/mL)
T1 Control (dw)	2096 ± 0.10 ^{d}	401 ± 3.39 ^{b}	84.58 ± 4.10 ^{d}	163.73 ± 2.92 ^{f}	81.28 ± 1.16 ^{a}	15.23 ± 0.64 ^{f}	418.76 ± 1.78 ^{e}	1.56 ± 0.077 ^{e}
T2 (dw+ZnO-NPs 75 mg/L)	2829 ± 0.39 ^{bc}	356.56 ± 37.23 ^{b}	107.25 ± 3.43 ^{c}	265.09 ± 5.63 ^{e}	79.11 ± 0.50 ^{ab}	26.90 ± 0.42 ^{e}	571.14 ± 13.33 ^{d}	2.00 ± 0.75 ^{d}
T3 (dw+ZnO-NPs 150 mg/L)	3628 ± 0.50 ^{ab}	362.48 ± 25.98 ^{b}	121.78 ± 4.70 ^{b}	352.59 ± 2.84 ^{d}	78.61 ± 1.13 ^{b}	30.71 ± 1.99 ^{d}	744.00 ± 2.33 ^{b}	2.41 ± 0.094 ^{c}
T4 NaCl (150 mM)	4043 ± 0.44 ^{a}	1191.83 ± 16.66 ^{a}	155.97 ± 0.90 ^{a}	986.68 ± 8.61 ^{a}	26.11 ± 0.33 ^{d}	71.54 ± 2.60 ^{a}	1158.76 ± 11.40 ^{a}	11.77 ±0.24 ^{a}
T5 (150 mM NaCl+ZnO-NPs 75 mg/L)	3730 ± 0.32 ^{ab}	1222.39 ± 62.84 ^{a}	103.22 ± 4.04 ^{c}	694.18 ± 7.24 ^{b}	37.78 ± 0.41 ^{cd}	45.67 ± 1.55 ^{b}	682.57 ± 4.67 ^{c}	2.37 ± 0.08 ^{c}
T6 (150 mM NaCl+ZnO-NPs 150 mg/L)	2596 ± 0.11 ^{c}	1271.37 ± 79.35 ^{a}	121.83 ± 4.04 ^{b}	552.14 ± 3.35 ^{c}	38.89 ± 0.75 ^{c}	41.38 ± 1.91 ^{c}	558.76 ± 7.38 ^{d}	3.55 ± 0.06 ^{b}

Each value represents the mean ± SE (n=4). Values with the same letter are not significantly different at ($p \leq 0.05$), and the comparison is done according to different treatments in the same column.

The fourth treatment (stressed) (T4) had the highest values of the estimated parameters among the other stressed or non-stressed treatments (T1–T3, T5, and T6), and it showed concentrations of 4043 ± 0.44, 1191.83 ± 16.66, 155.97 ± 0.90, 986.68 ± 8.61, 71.54 ± 2.60, 1158.76 ± 11.40 µg/g, and 11.77 ± 0.24 mmols/mL for TPCs, TFCs, total hydrolyzable sugars, total free amino acids, proline, H_2O_2, and MDA contents, respectively.

However, for protein content, the first treatment (T1) had the highest value in a concentration of 81.28 ± 1.16 µg/g. The lowest concentrations of the previously estimated biochemical and stress markers were 2096 ± 0.10 µg/g of TPCs, 401 ± 3.39 µg/g of TFCs, 84.58 ± 4.10 µg/g of total hydrolyzable sugars estimated as glucose, 163.73 ± 2.92 µg/g of total free amino acids estimated as L-leucine, 15.23 ± 0.64 µg/g of proline, 418.76 ± 1.78 µg/g of H_2O_2, and 1.56 ± 0.07 mmols/mL of MDA in the first non-stressed treatment (T1), but 26.11 ± 0.33 µg/g of protein estimated as BSA in the fourth treatment (T4).

Table 20 showed the results of the biochemical parameters in maize leaves. The maize leaves' phenolics, flavonoids, hydrolyzable sugars, free amino acids, proline, hydrogen peroxide (H_2O_2), and malondialdehyde (MDA) contents all rose as the maize leaves were exposed to the salt. This study discovered that treatments' effects on plant contents of the prior stress and biochemical markers were statistically significant. Compared to the three previous treatments (M1, M3, and M4), the second treatment (M2) had the highest concentrations of the mentioned parameters. The only exception was the protein content, which declined to the lowest content among the various treatments in the second treatment (M2).

Table 20. Analysis of biochemical and stress indicators in variously treated maize leaves.

Treatments	Concentrations							
	TPCs (mg/g)	**TFCs (mg/g)**	**Total Hydrolazable Sugars (mg/g)**	**Total Free Amino Acids (mg/g)**	**Protein Content (mg/g)**	**Proline Content (mg/g)**	**H_2O_2 (mg/g)**	**MDA (mmols/mL)**
M1 Control (tap water)	19.99 ± 0.22 ^{c}	18.83 ± 0.07 ^{ab}	177.50 ± 5.60 ^{bc}	53.83 ± 1.23 ^{c}	1.56 ± 0.03 ^{b}	0.22 ± 0.00 ^{b}	1.02 ± 0.01 ^{d}	5.16 ± 0.46 ^{c}
M2 (NaCl 150 mM)	28.42 ± 0.47 ^{a}	19.919 ± 0.06 ^{a}	228.49 ± 2.17 ^{a}	74.35 ± 1.19 ^{a}	0.93 ± 0.01 ^{c}	0.32 ± 0.03 ^{a}	1.78 ± 0.02 ^{a}	13.06 ± 1.61 ^{a}
M3 (NaCl 150 mM + ZnO-NPs 2 g/L)	24.09 ± 0.20 $_{b}$	17.53 ± 0.63 ^{b}	186.31 ± 4.32 ^{b}	56.71 ± 0.72 ^{c}	0.98 ± 0.02 ^{c}	0.31 ± 0.00 ^{a}	1.35 ± 0.03 ^{b}	9.35 ± 0.56 ^{b}
M4 (tap water + ZnO-NPs 2 g/L)	18.61 ± 0.33 ^{d}	17.78 ± 0.11 ^{b}	170.76 ± 2.86 ^{c}	60.83 ± 1.28 ^{b}	2.39 ± 0.03 ^{a}	0.23 ± 0.00 ^{b}	1.19 ± 0.01 ^{c}	5.97 ±0.41 ^{c}

Each value represents the mean ± SE (n=4). Values with the same letter are not significantly different at ($p \leq 0.05$), and the comparison is done according to different treatments in the same column.

Spraying the treatments (M3 and M4) with a zinc oxide nanoparticle solution at a concentration of 2 g/L was employed. As was noted before, the secretion of the compounds was controlled to ensure that it was compatible with the initial therapy (control) (M1). The predicted parameter values for the second treatment (M2) were in the greatest range compared to those of the other treatments (M1, M3, and M4), regardless of whether they were stressed. It was observed that the concentrations of hydrolyzable sugars, total free amino acids, proline, H_2O_2, and MDA were as follows: 177.50 ± 5.60 mg/g, 53.83 ± 1.23, 1.56 ± 0.03, 0.22 ± 0.00 mg/g, 1.02 ± 0.01 mg/g, and 5.16 ± 0.46 mmols/mL, respectively.

The highest value for protein content was found in the fourth treatment, and the concentration of 2.39 ± 0.03 mg/g was the highest value reported for this treatment. The indicators that had been previously estimated to have the lowest concentrations were 170.76 ± 2.86 mg/g of hydrolyzable sugars estimated as glucose in M4, 53.83 ± 1.23 mg/g of free amino acids determined as L-leucine in M1, 0.22 ± 0.00 and 0.23 ± 0.00 mg/g of proline in M1 and M4, respectively, 1.02 ± 0.01 mg/g of H_2O_2 in M1, and 5.16 ± 0.46 and 5.97 ± 0.41 mmols/mL of MDA in M1 and M4, respectively, and 0.93 ± 0.01 and 0.98 ± 0.02 mg/g of protein estimated as bovine serum albumin (BSA) in M2 and M3, respectively.

The treatments had a considerable impact on the amount of TPCs and TFCs. It was found that the second stressed treatment (M2) had the highest concentrations in comparison to the other stressful treatment (M3) and the treatment that was sprayed with 2 g/L ZnO-NPs (M4). In order to bring the secretion of the TPs and TFs into alignment with the non-stressed treatments (M1 and M4), the latter were controlled. With concentrations of 0.02 ± 0.47 mg/g for total phenolics (TPCs) and 0.02 ± 0.06 mg/g DW for total flavonoids (TFCs), respectively, the second treatment (stressed) (M2) displayed the highest values of estimated total phenols (TPCs) and total flavonoids (TFCs) in comparison to the other treatments, which included both stressed and non-stressed treatments (M1, M3, and M4).

The increase in H_2O_2 (a reactive oxygen substance that increases due to stress and is highly destructive), MDA (a cytotoxin produced by the breakdown of lipid cell membranes due to ROS), proline (an amino acid that increases in reaction to stress and functions as an effective osmolyte), and total hydrolyzable sugar contents in tomato and maize were quite evident under salt stress (Anjum et al., 2022; Hasanuzzaman et al., 2020; Hayat et al., 2012) (Tables 19 and 20).

The tomato leaves reached their maximum content of total hydrolyzable sugars at the level of 155.97 ± 0.90 µg/g in the fourth treatment (T4), where a concentration of zero mg/L of ZnO-NPs was applied (Table 19). That value was higher than that seen in the control group (T1) and the other two non-stressed treatments (T2 and T3) in concentrations of 84.58 ± 4.10, 107.25 ± 3.43, and 121.78 ± 4.70 µg/g, respectively. Another increased content of sugars was observed in the fifth and sixth stressed treatments with 103.22 ± 4.04 and 121.83 ± 4.04 µg/g, respectively. Applying ZnO-NPs (75 and 150 mg/L) on the leaves of the fifth and sixth treatments (T5 and T6) decreased the sugar content against the severe NaCl concentration (150 mM). The same manner was observed in the proline, H_2O_2, and MDA contents.

The tomato leaves showed the highest contents of those stress markers in the fourth treatment with 71.54 ± 2.60 µg/g, 1158.76 ± 11.40 µg/g, and 11.77 ± 0.24 mmols/mL, respectively. The content was decreased in the fifth and sixth treatments after spraying with 75 and 150 mg/L ZnO-NPs to be 45.67 ± 1.55 and 41.38 ± 1.91 µg/g for proline, 682.57 ± 4.67 and 558.76 ± 7.38 for H_2O_2, and 2.36 ± 0.08 and 3.55 ± 0.06 mmols/mL for MDA, respectively. The contents of tomato leaves from proline, H_2O_2, and MDA in the non-stressed treatments (T1–T3) were less than in the stressed treatments (T4–T6) (Table 19). The reason for the increase in MDA and H_2O_2 in plants under salt stress is due to the increase of reactive oxygen species (ROS) and cell membrane damage with stress (Ahmed, et al., 2024a).

In a separate study on tomatoes, Li (2009) discovered that the salinity caused an increase in the levels of proline and MDA in tomato seedlings . Furthermore, the amount of NaCl had an impact on the soluble sugar content, as Shaba.Zahra et al. (2010) discovered that the levels of soluble sugars and proline in tomatoes rise in response to increased salt. The tomato leaves reached their maximum content of total free amino acids content in the fourth treatment (T4) at the level of 986.68 ± 8.61 µg/g (Table 19). That value was higher than that seen in the control group (T1) and the other two non-stressed treatments (T2 and T3) in concentrations of 163.73 ± 2.92 and 265.09 ± 5.63 and 352.59 ± 2.84 µg/g, respectively.

Another increased content of free amino acids was observed in the fifth and sixth stressed treatments compared to the control group (T1), but that increase was much less than in the fourth treatment when exposed to 150 mM and did not receive any spray of ZnO-NPs. The tomato leaves reached their maximum content of protein content in the first treatment (T1) at the level of 81.28 ± 1.16 µg/g (Table 17). That value was close to the contents of the second and third treatments (T2 and T3) that were sprayed with 75 and 150 mg/L ZnO-NPs, respectively.

The protein content in tomato leaves reached its lowest content in the fourth treatment, was stressed with 150 mM, and did not receive any spray of ZnO-NPs in a concentration of 26.11 ± 0.33 µg/g, but there was an evident increase in the contents of protein in the fifth and sixth treatments (T5 and T6) with concentrations of 37.78 ± 0.41 and 38.89 ± 0.75 µg/g, respectively. The study conducted by Faizan et al. (2021) found that tomato seedlings grown in soil containing NaCl showed a reduction in protein content. The decrease in cellular integrity and excessive formation of reactive oxygen species (ROS) was caused by the presence of NaCl (Tavallali et al., 2010).

The protein content significantly increased when ZnO-NPs (10, 50, or 100 mg/L) were applied to the leaves, regardless of the presence or absence of NaCl stress. This indicates that ZnO-NPs had a good effect in reducing the impact of NaCl stress. Tavallali et al. (2009) have previously reported similar findings, demonstrating that Zn^{2+} application can enhance protein content in pistachio plants subjected to NaCl stress. The increase in protein content following the injection of Zn^{2+} may be attributed to the reduction in ion leakage, which, in turn, improves the damage caused by NaCl stress (Cakmak, 2000).

The H_2O_2, MDA, proline, total free amino acids, and total hydrolyzable sugar levels significantly increased in response of **maize plants** to salt stress (Ahmed, et al., 2024c; Anjum et al., 2022) (Table 20). The maize leaves exhibited the most elevated levels of stress indicators in the second treatment, with 228.49 ± 2.17, 74.35 ± 1.19, 0.32 ± 0.03, 1.78 ± 0.02 mg/g, and 13.06 ± 1.61 mmols/mL, for sugars, free amino acids, proline, hydrogen peroxide, and malondialdehyde, respectively. After spraying with 2 g/L ZnO-NPs, the levels were decreased in the third and fourth treatments (M3 and M4). It was also noticed that the control treatments that were not stressed or sprayed with ZnO-NPs had the lowest values of those determined stress markers compared to the second stressed treatment, the sprayed stressed third treatment and even the fourth treatment that was not stressed at all but sprayed with zinc oxide NPs.

The amount of protein in maize leaves was minimal in the second treatment, which involved exposure to 150 mM NaCl and no application of ZnO-NPs, and the protein level measured 0.93 ± 0.01 mg/g. However, it was clear that the protein concentrations noticeably increased in the fourth treatment (M4) and gave 2.39 ± 0.03 mg/g. But, in the case of the third treatment (M3), it gave 0.98 ± 0.02 mg/g. It was found that the protein content in cluster beans and green peas was increased by applying ZnO-NPs. Furthermore, it is widely recognized that Zn is an essential element necessary for the optimal development and growth of plants. The roots' cation-exchange ability enhances nutritional absorption, particularly nitrogen, which leads to greater protein content (Naseer et al., 2023; Raliya & Tarafdar, 2013).

The elevation in MDA, H_2O_2, and other identified biomolecules in plants under salt stress can be linked to the heightened reactive oxygen species (ROS) and the consequential impairment of cell membranes. The current study demonstrated that applying zinc oxide nanoparticles to the leaves enhanced the plants' sensitivity to NaCl stress. The preceding report can be attributed to the fact that ZnO nanoparticles enhanced plant resilience to sodium chloride stress by mitigating the generation of ROS and oxidative harm, leading to mitigating the harmful effects of salinization. The decrease in ROS generation is linked to a decline in enzymatic and non-enzymatic antioxidant activity (Mahawar et al., 2024; Rai-Kalal & Jajoo, 2021). Another possible explanation is the impact of ZnO-NPs on the absorption of nutrients, which counteracts the deficit of micro and macronutrients caused by NaCl in plants (Tavanti et al., 2021). In some other studies and in line with the obtained results in the current experiment, evidence has demonstrated that zinc oxide NPs have increased the absorption of calcium, potassium, zinc, iron, and copper in faba bean (Mogazy & Hanafy, 2022) and rapeseed (El-Badri et al., 2021) when exposed to high salinity levels, these components replaced the Na ions, reducing the harmful consequences of Na^+ toxicity.

4.8. Analyzing the dry matter, protein, acid and neutral detergent fibers in tomato and maize leaves and the water content, protein, fat, and starch in maize grains (seeds)

Table 21 showed the changes in dry matter, crude protein, ash, ADF, and NDF values in **the leaves of tomato**. According to the dry matter, the non-stressed treatments (T1-T3) had higher values than the stressed treatments (T4-T6). For the crude protein content, the lowest value was observed with the fourth treatment, that was stressed with 150 mM NaCl and never sprayed with the ZnO-NPs, but the highest content of crude protein was observed in the third treatment, followed by the fifth and sixth treatments. No significant differences were observed between all the treatments according to the ash and the neutral detergent fiber contents. On the other hand, the second treatment, which was not stressed but sprayed with 75 mg/L ZnO-NPs, showed the highest content of the acid detergent fiber compared to the other treatments. The results demonstrated the positive effect of using the foliar spray of synthesized zinc oxide nanoparticles and the adverse effects of salinity stress on various parameters.

Table 21. Changes in dry matter, crude protein, Ash, ADF, and NDF values in tomato leaves.

Treatments	Concentrations (g/100 g dry weight)				
	Dry matter	**Crude protein**	**Ash**	**Acid detergent fiber (ADF)**	**Neutral detergent fiber (NDF)**
T1	70.61±0.49^{a}	4.56±0.87^{bc}	13.91±0.24^{a}	15.99±0.89^{b}	13.87±0.09^{a}
T2	71.14±0.32^{a}	6.54±0.70^{b}	13.033±0.49^{a}	19.46±1.19^{a}	13.63±0.19^{a}
T3	70.45±0.80^{a}	12.33±0.23^{a}	13.83±0.49^{a}	18.75±0.60^{ab}	13.63±0.10^{a}
T4	64.73±0.80^{b}	3.61±0.50^{c}	13.98±0.15^{a}	16.05±0.36^{ab}	14.98±0.65^{a}
T5	65.07±0.91^{b}	10.20±0.25^{a}	13.83±0.26^{a}	16.80±0.76^{ab}	13.74±0.25^{a}
T6	65.56±0.40^{b}	10.80±0.47^{a}	13.72±0.34^{a}	17.27±0.46^{ab}	13.79±0.28^{a}

Each value represents the mean ± SE (n=4). Values with the same letter are not significantly different at ($p \leq 0.05$), and the comparison is done according to different treatments in the same column. ***T1****: Control (non-treated) (dw).* ***T2****: (dw + ZnO-NPs 75 mg/L).* ***T3****: (dw + ZnO-NPs 150 mg/L).* ***T4****: NaCl (150 mM).* ***T5****: (150 mM NaCl + ZnO-NPs 75 mg/L).* ***T6****: (150 mM NaCl + ZnO-NPs 150 mg/L).*

Table 22 showed changes in dry matter, crude protein, ash, ADF, and NDF in maize leaves. No statistically significant differences were found in dry matter between the treatments. However, the fourth treatment (M4) showed the highest values for crude protein content, ash, and acid- and neutral-detergent fiber content compared with the other three treatments (M1, M2, and M3), indicating a positive effect of ZnO-NPs foliar application. The second treatment (M2) showed the lowest values, although sometimes the third treatment, which was stressed but sprayed with ZnO-NPs, showed values close to those of that treatment. The moisture, crude protein, crude fat, crude ash, and starch values of maize seeds were analyzed and are displayed in Table 23. Crude fat content did not show any statistically significant differences across the treatments. M4, which did not undergo stress but was sprayed with ZnO-NPs, exhibited the most significant ash values and crude protein content. M3, in contrast, had the highest moisture and starch content values among the treatments.

Table 22. Changes in dry matter, crude protein, ADF, and NDF values in the leaves of maize.

Treatments	Concentrations (g/100 g Dry Weight)			
	Dry Matter	**Crude Protein**	**Acid Detergent Fiber (ADF)**	**Neutral Detergent Fiber (NDF)**
M1 Control (tap water)	78.83 ± 0.41 ^{ns}	6.87 ± 0.00 ^{b}	21.17 ± 0.20 ^{a}	34.53 ± 0.49 ^{a}
M2 (NaCl 150 mM)	78.08 ± 0.70 ^{ns}	6.05 ± 0.23 ^{c}	19.82 ± 0.02 ^{b}	31.42 ± 0.11 ^{b}
M3 (NaCl 150 mM + ZnO-NPs 2 g/L)	78.56 ± 0.73 ^{ns}	7.26 ± 0.08 ^{a}	20.21 ± 0.33 ^{b}	32.53 ± 0.73 ^{b}
M4 (tap water + ZnO-NPs 2 g/L)	78.92 ± 1.01 ^{ns}	7.35 ± 0.02 ^{a}	21.57 ± 0.37 ^{a}	34.60 ± 0.48 ^{a}

Each value represents the mean ± SE (n=4). Values with the same letter are not significantly different at ($p \leq 0.05$), and the comparison is done according to different treatments in the same column.

Table 23. Changes in moisture, crude protein, crude fat, and starch values in the grains of maize.

Treatments	Concentrations (g/100 g Dry Weight)			
	Moisture	**Crude Protein**	**Crude Fat**	**Starch**
M1 Control (tap water)	5.58 ± 0.09 ^{d}	8.57 ± 0.15 ^{b}	3.60 ± 0.02 ^{ns}	68.84 ± 0.03 ^{b}
M2 (NaCl 150 mM)	6.77 ± 0.12 ^{b}	7.43 ± 0.06 ^{c}	3.64 ± 0.04 ^{ns}	68.21 ± 0.04 ^{c}
M3 (NaCl 150 mM + ZnO-NPs 2 g/L)	7.07 ± 0.05 ^{a}	7.79 ± 0.25 ^{c}	3.54 ± 0.01 ^{ns}	69.55 ± 0.12 ^{a}
M4 (tap water + ZnO-NPs 2 g/L)	6.40 ±0.07 ^{c}	9.20 ± 0.17 ^{a}	3.60 ± 0.02 ^{ns}	68.19 ± 0.02 ^{c}

Each value represents the mean ± SE (n=4). Values with the same letter are not significantly different at ($p \leq 0.05$), and the comparison is done according to different treatments in the same column.

The consumption and digestibility of fodder are significantly impacted by parameters such as the number of cell walls, the ratio of tissues with different biodegradability, the composition of the chemicals, the proportion of lignin, and other physicochemical factors that affect the digestibility of cell walls in the rumen (Vago et al., 2021). ADF and NDF data evaluate forage digestibility, total digestive nutrients, and energy and relative feed values. The relative feed value is an index that allocates forage for animal performance. The entire cellular structure, comprising ADF (acid detergent fiber) and hemicellulose, is classified as NDF (neutral detergent fiber). NDF values quantify the amount of forage an animal can consume. ADF stands for the cell walls of forage composed of cellulose and lignin. These variables impact the process of fodder digestion in animals. The assessment also includes an evaluation of prices and the management, harvest, and storage procedures for fodder (Beauchemin, 1996).

The current study showed that the non-stressed treatments (T1-T3) from **tomato** were significantly different from the stressed treatments (T4-T6) in the dry matter content in the different treatments from tomato. The crude protein determined using the NIRS matched the obtained results from the colorimetric technique used to determine the protein content in the leaves, as the protein values were decreased in the salt-stressed plants leaves from the fourth treatment (T4) compared with the plants that were sprayed with 75 and 150 mg/L ZnO-NPs in the fifth and sixth treatments (T5 and T6), respectively. The plants of the third treatment that was sprayed with 150 mg/L ZnO-NPs (T3) showed the highest crude protein content compared to the second treatment (T2) that was sprayed with less concentration of the ZnO-NPs (75 mg/L),and the control plants that were not sprayed at all (T1), as well. The current study showed that there were no significant differences between all the treatments from tomato plants in case of the ash and NDF values. While, the second treatment (T2) that was not stressed at all but sprayed with 75 mg/L ZnO-NPs had the highest value of the ADF compared to the other treatments that were not significantly different.

These alterations caused by salinity stress in plants may lead to the accumulation or degradation of certain metabolites, potentially disrupting the balance of a restricted set of cellular proteins. Following salt treatment, these proteins may exhibit increased or decreased abundance, appear, or vanish (Kong-Ngern et al., 2005). In their study on tomato, Amini et al. (2007) showed that salinity inhibited the formation of -at least- four leaf proteins. In the current study, it was found that the lowest value of protein content was observed in the fourth treatment (T4) which was salinity-stressed without any spraying with ZnO-NPs.

In a study by De Lima et al. (2014), the authors found that salt stress on *Coffea arabica* L. leaves led to alterations in cell wall polysaccharides, an increase in monolignol levels, and damage to mesophyll cells. Although tomato leaves are considered agricultural waste, they can be used as a high-value fodder for ruminants (Seoudi et al., 2013). So, the quality of fodder significantly influences the production of animal products. Furthermore, animals will encounter increased difficulty in digesting feed. Animals can consume inferior forages and digest them more rapidly to compensate for the diminished quality. Conversely, ruminants are unable to adjust their food intake to compensate for inferior-quality nourishment.

The lower the quality of the fodder, the longer it remains in the ruminant's digestive tract. This renders the animal less productive (Ahmed, et al., 2024a; Hoppe & Carlson, 2023; Vago et al., 2021). The acid detergent fiber (ADF) and neutral detergent fiber (NDF) metrics indicate the digestibility of fodder, its nutrient content, energy value, and feeding costs. These factors influence animal feed consumption (Beauchemin, 1996; Hoppe & Carlson, 2023). Grinding or pelleting forages may mitigate the adverse effects of low-quality forage, characterized by elevated neutral detergent fiber concentration, on dry matter intake. The present investigation revealed no substantial differences in NDF among the treatments. This suggests that tomato leaves are suitable for use as animal feed.

The current study also showed no significant differences in the dry matter content in the different treatments from **maize**. The crude protein determined using the NIRS matched the obtained results from the colorimetric technique used to determine the protein content in the leaves, as the protein values were decreased in the salt-stressed plants leaves from the second treatment (M2) compared with the plants that were sprayed with 2 g/L ZnO-NPs in the third treatment (M3), the control plants (M1), and the non-stressed plants that were only sprayed with 2 g/L ZnO-NPs (T4).

The current study showed that the crude protein values in the grains were decreased in the leaves of the salt-stressed plants, even they were not sprayed with 2 g/L ZnO-NPs as in M2 or were sprayed with 2 g/L ZnO-NPs as in M3, compared to the non-stressed plants that were only sprayed with 2 g/L ZnO-NPs (M4), followed by the control treatment (M1). The results showed the positive effect of spraying ZnO-NPs on increasing the crude protein values in maize grains. However, there were no noticeable differences observed across the treatments for the crude fat content. For starch content, the third treatment (M3) showed the highest content of starch compared to the non-stressed treatment that was sprayed (M4), and the stressed treatment that was not sprayed (M2). The moisture content in the salt-stressed treatment (M2) was higher than in the non-stressed sprayed treatment (M4), and the control treatment (M1). However, the stressed treatment sprayed with ZnO-NPs (M3) showed the highest moisture content.

The current study showed that the ADF and NDF values were decreased in the salt-stressed maize leaves in the second treatment (M2) compared with the salt-stressed plants from the third treatment that was sprayed ZnO-NPs (M3), the control plants (M1), and the non-stressed plants from the fourth treatment that were only sprayed with 2 g/L ZnO-NPs (M4). The results proved the effects of applying the foliar spray of ZnO-NPs on ADF- and NDF-enhanced values.

Previously, saline stress has been linked to decreases in NDF and ADF (Boga et al., 2014), for *Lotus corniculatus* shoots and leaves, and other legumes. Higher salt concentrations in water were found to be positively correlated to a decrease in NDF level and an increase in the level of soluble carbohydrates in *Lolium multiflorum*, Lam (Ben-Ghedalia et al., 2001). The composition must consist of oligo- and polysaccharides, low molecular weight and cell wall carbohydrates like pectins and highly soluble hemicelluloses. Previous studies have shown that carbohydrates, such as glucose, fructose, sucrose, and starch, tend to build up when exposed to stress caused by salt (de Lima et al., 2014; Kerepesi & Galiba, 2000; Khatkar & Kuhad, 2000; Vago et al., 2021).

Despite varying environmental conditions that can significantly impact the quality of maize grains (Sabagh et al., 2020). There is not enough investigation into the detrimental effects of salt stress on the quality of grains. While the impact of different salinity levels on the starch and protein content in maize grain yielded conflicting results, it is essential to maintain an appropriate equilibrium of salt levels in the irrigation water to control the quantity of each constituent.

Optimal moisture content in the grain is advantageous for storage reasons, as it inhibits the growth of fungal infections that can lead to mycotoxin contamination and a decline in the quality of maize grain (Weinberg et al., 2008). Li et al. (2019) observed no discernible variations in maize grain's oil, crude fiber, and ash compositions. On the other hand, as salinity increased, there was a drop in grain moisture and starch content. The highest values were when the total dissolved solids (TDS) reached 1, 2, and 3 g L^{-1}.

Conversely, protein content increased with higher salt levels, reaching maximum values over 12% when the TDS was 4 and 5 g L^{-1}. Nevertheless, the outcome did not match the findings of Kang and Wan (2005) who confirmed that there was no notable disparity in the moisture, starch, protein, and oil content of the kernel. The quality of maize grain is directly related to the concentration of starch and protein, with higher levels of these nutrients indicating better quality. According to Weinberg et al. (2008) storing maize with low grain moisture content is preferable since it reduces the likelihood of fungal infections and the risk of mycotoxin contamination in the kernels.

4.9. Assessment of the enzymatic activities in tomato and maize leaves

Figure 13 showed the released enzymes in tomato leaves: peroxidase (POX), glutathione reductase (GR), glutathione-S-transferase (GST), superoxide dismutase (SOD), and catalase (CAT) in tomato leaves. A trend was observed for all released enzymes, where the third non-stressed and sprayed with 75 mg/L ZnO-NPs (T3) had the highest concentration of produced antioxidant enzymes. The plants that were stressed with 150 mM NaCl and sprayed with ZnO-NPs in two different concentrations (T5 and T6); 0.075 and 150 mg/L ZnO-NPs had a higher concentration of produced GR, POX, GST, SOD, and CAT enzymes than the plants that were stressed with NaCl but were not sprayed with the zinc oxide nanoparticles (T4). It was also observed that the plants stressed with sodium chloride and not treated with ZnO-NPs (T4) had the lowest enzyme production values compared to all the other treatments. The second treatment (T2), which was not stressed but treated with ZnO-NPs, resulted in plants with higher values of the produced antioxidative enzymes compared to the control plants that were neither stressed nor sprayed with ZnO-NPs (T1). According to the comparison between the fifth treatment (T5), which was stressed with 150 mM NaCl and sprayed with 75 mg/L ZnO-NPs, and the second treatment, which was not stressed but sprayed, there was a significant difference in the production level of GR and GST, with higher values for the second treatment. On the other hand, the higher values were observed in the fifth treatment plants in the case of SOD. There was minimal variance among the aforementioned interventions in case of POX and CAT.

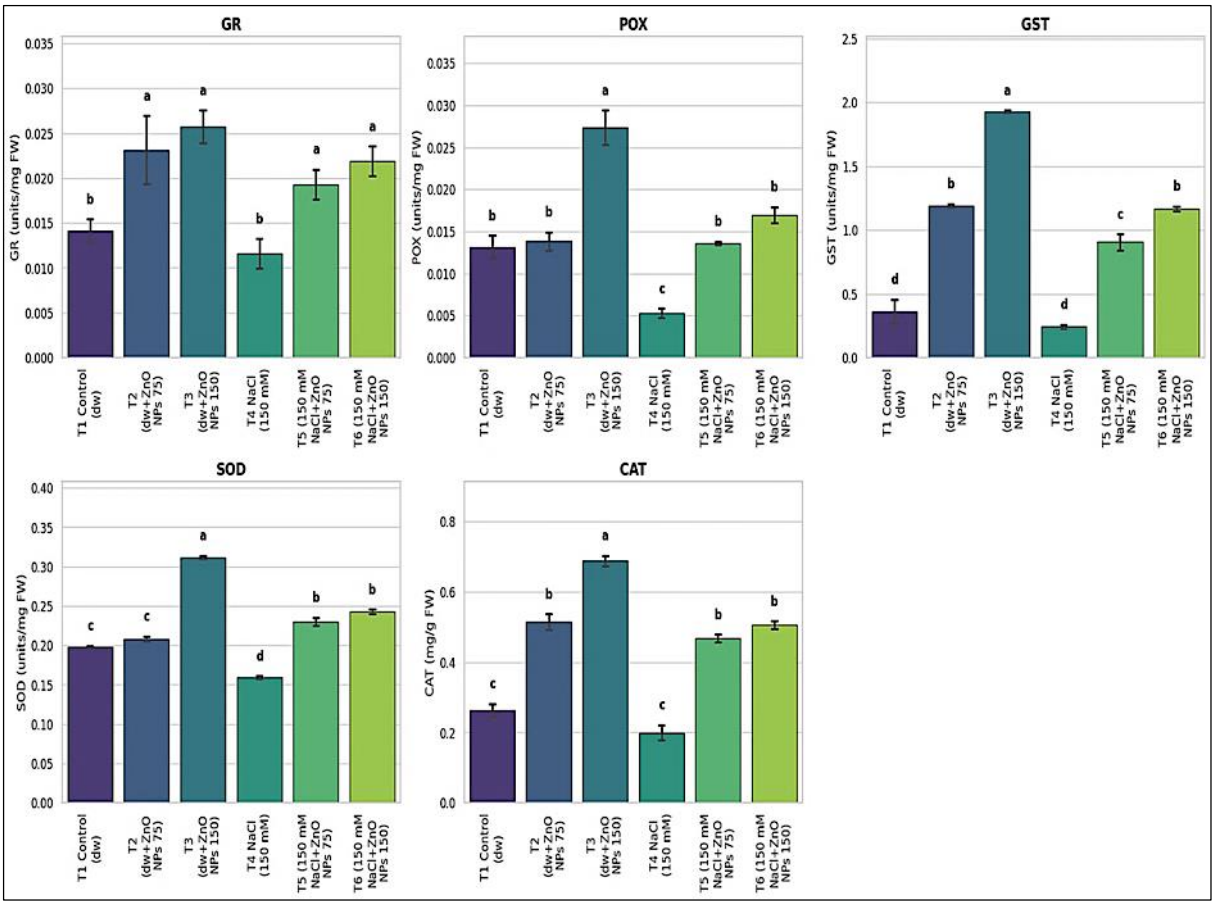

Figure 13. The effects of different treatments on the concentration of peroxidase (POX), glutathione reductase (GR), glutathione-S-transferase (GST), superoxide dismutase (SOD), and catalase (CAT) enzymes in tomato leaves.

Each value represents the mean ± SE (n=4). Values with the same letter are not significantly different at ($p \leq 0.05$), and the comparison is done according to different treatments in the same column.

Figure 14 showed the released enzymes in maize leaves: peroxidase (POX), glutathione reductase (GR), glutathione-S-transferase (GST), superoxide dismutase (SOD), and catalase (CAT) in maize leaves. A trend was observed for all released enzymes, where the second stressed and non-sprayed with ZnO-NPs (M2) had the highest concentration of produced antioxidant enzymes. The plants that were stressed with 150 mM NaCl and sprayed with 2 g/L ZnO-NPs (M3); had a higher concentration of produced GR, POX, GST, SOD, and CAT enzymes than the plants that were not stressed with NaCl (control plants) (M1) and also than the plants were not stressed but sprayed with the zinc oxide nanoparticles (M4). It was also observed that the plants were not stressed with sodium chloride and not treated with ZnO-NPs (control plants) (M1) had the lowest enzyme production values compared to all the other treatments. In case of determining the production level of SOD and CAT, there were not any significant differences between the enzymes production according to the plants were sprayed with 2 g /L, however they were stressed with NaCl or not.

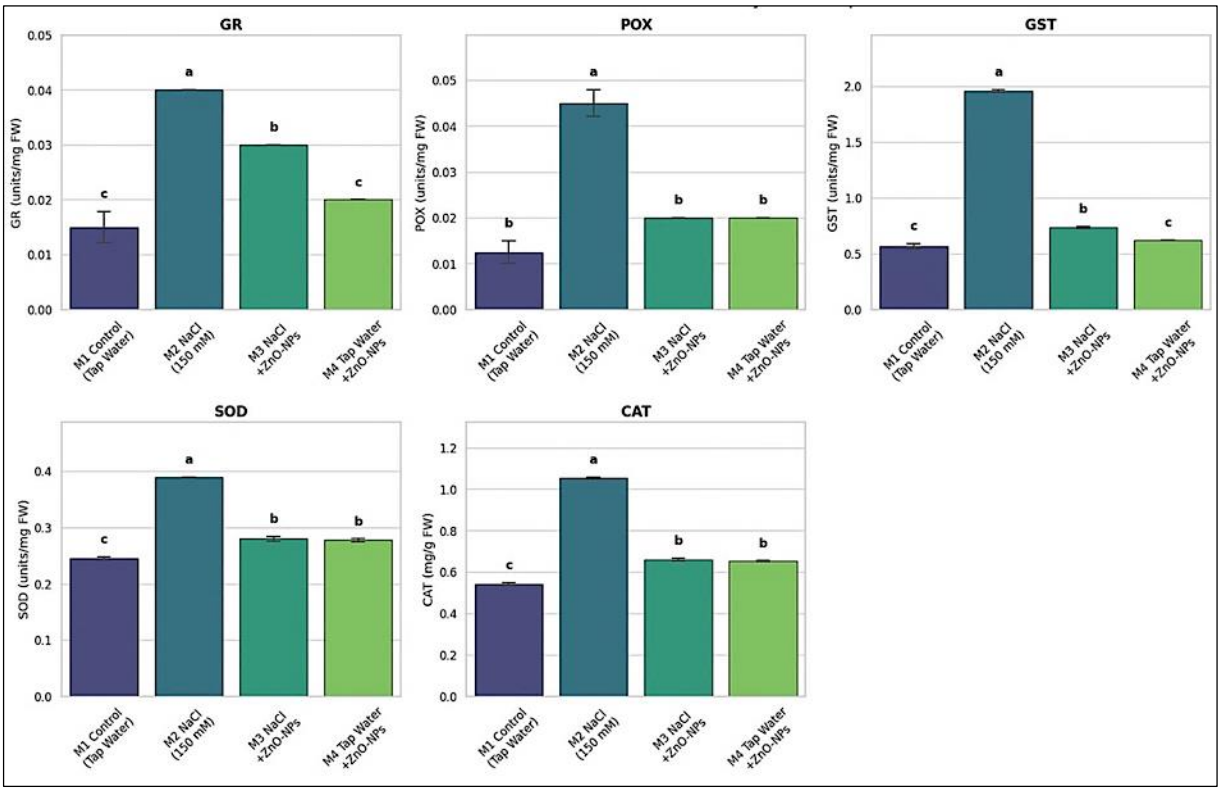

Figure 14. The effects of different treatments on the concentration of peroxidase (POX), glutathione reductase (GR), glutathione-S-transferase (GST), superoxide dismutase (SOD), and catalase (CAT) enzymes in maize leaves. *Each value represents the mean ± SE (n=4). Values with the same letter are not significantly different at ($p \leq 0.05$), and the comparison is done according to different treatments in the same column.*

In some investigations, heightened stress resulted in reduced enzyme activity. Ali et al. (2022) conducted a study demonstrating that NaCl stress significantly impacts the activity of antioxidant enzymes in broccoli, particularly superoxide dismutase, catalase, and ascorbate peroxidase (APX). Broccoli plants exhibited a significant reduction in APX activity under elevated NaCl stress (80 mM NaCl) compared to the control group. Salinity stress evidently diminishes the crude protein content in leaves, as our prior research indicated that **tomato plants** subjected to 150 mM NaCl stress had significantly reduced protein levels. Enzymes are organic protein molecules; thus, it is logical that their activity diminishes under significant stress. A significant finding from this study is that the foliar application of chemically synthesized ZnO NPs enhanced the activity of antioxidative enzymes, regardless of the presence or absence of NaCl.

On the other hand, **in maize plants**, the incorporation of sodium chloride resulted in a considerable increase in the activity of antioxidative enzymes. Plants that can withstand high amounts of salt stress typically contain antioxidant enzymes that function more effectively. When plants were subjected to salt stress, their responses varied depending on the amount of salt present in the soil. It is essential to keep this fact in mind.

When there was a significant amount of salt stress, antioxidant enzymes operated more effectively, as demonstrated by several earlier investigations (Abogadallah, 2010; Lu et al., 2023; Zhu et al., 2004). In plants, ROSs are neutralized by antioxidative enzymes, including superoxide dismutase (SOD), glutathione reductase/-s-transferase (GR/GST), peroxidase (POX), or catalase (CAT) (Mishra et al., 2023). Nonetheless, the presence of NaCl has markedly decreased the activity of antioxidative enzymes in our current study. Nevertheless, a significant finding from this study is that the foliar application of chemically synthesized ZnO-NPs enhanced the activity of antioxidative enzymes, regardless of the presence or absence of NaCl.

Recent research has revealed the significance of nanotechnology in enhancing the ability of many plant species to tolerate salt. The primary aim of this work was to clarify the function of ZnO-NPs in the modulation of salt (NaCl) stress tolerance in tomato and maize plants, and how the salt stress and foliar application may contribute to changes on the transcriptomic level. Plants exposed to NaCl stress accumulate ROS; however, maintaining a balance between ROS generation and degradation is crucial to prevent oxidative damage (Faizan et al., 2021; Meneguzzo et al., 1999). El-Zohri et al. (2021) demonstrated that, in response to foliar application of green ZnO-NPs, antioxidant enzymes such as SOD, CAT, and APX were increased in tomato plants, thereby reducing the negative effects of drought stress by mitigating oxidative stress.

Superoxide dismutase catalyzes the dismutation of superoxide free radicals into hydrogen peroxide (H_2O_2) and oxygen (O_2), serving as the first line of defense against oxygen free radicals in the cytosol, chloroplasts, and mitochondria (Demidchik, 2015; El-Zohri et al., 2021). Catalase (CAT) and other peroxidases serve as significant scavengers of excess H_2O_2, which is transformed into H_2O and O_2 (Smirnoff, 1998). CAT can effectively decompose elevated levels of hydrogen peroxide (H_2O_2) and mitigate the harm caused by hydroxyl radicals ($OH^{\bullet}$) generated, for example, in Fenton or Haber-Weiss-type reactions (Chawla et al., 2019). Faizan et al. (2021) investigated the activity of SOD, POX, and CAT enzymes in tomato plants exposed to varying concentrations of ZnO-NPs (10, 50, or 100 mg/L), either in the presence or absence of 150 mM NaCl. They found that those enzymes exhibited an upward trend when compared to the control group (plants not stressed or sprayed with ZnO-NPs). The highest enhancement in the activity of CAT (57%), SOD (44%), and POX (59%) was observed in plants treated with 50 mg/L of ZnO-NPs in conjunction with NaCl (Faizan et al., 2021).

Glutathione reductase (GR), or glutathione disulfide reductase (GSR), is a flavoprotein classified under the NADPH-dependent oxidoreductase family. It facilitates the conversion of oxidized glutathione (glutathione disulfide) (GSSG) to reduced glutathione (GSH), which is crucial for cellular defense against reactive oxygen species (ROS) (Vokkaliga et al., 2017). GSTs exhibiting GSH-dependent reductase activity, such as dehydroascorbate reductase (DHAR) and glutathione-s-transferase lambda class GSTL, may contribute to the preservation of reductants pools (including ascorbic acid, α-tocopherol, and anthocyanins), while other isoenzymes facilitate the detoxification of reactive metabolites (Csiszár et al., 2014; Dixon & Edwards, 2010).

The GST activity depletes GSH, which explains why the overproduction of GST competes with other antioxidant mechanisms. In tomatoes, salt reduces ascorbic acid and glutathione (GSH) levels and promotes lipid peroxidation (Mittova et al., 2004). Maintaining a high ratio of GSH/GSSG is crucial for the salt and drought tolerance of tomato, maize, and wheat (Csiszár et al., 2014; Shalata & Neumann, 2001). The previous results were in line with the current study's results.

At a concentration of 120 mM sodium chloride, Seleiman et al. (2023a) found that the antioxidant defense mechanisms of enzymes such as SOD, CAT, and APX **in maize plants** were considerably influenced by salt . When compared to the control plants, the antioxidant enzymatic activities of SOD, CAT, and APX increased by 77%, 95%, and 102%, respectively, in maize plants that were exposed to 120 mM NaCl over the experiment. Notably, the antioxidant defense systems functioned more effectively after the application of ZnO-NPs to the leaves at a dosage of 100 mg/L. The total amount of SOD, CAT, and APX all increased by 16%, 22%, and 26%, respectively, as a consequence of this. When it came to the antioxidant profile of maize plants, the interaction impacts of ZnO-NPs and salt were shown to be substantial. When 120 mM NaCl and 100 mg/L ZnO-NPs were combined, the highest antioxidant activity was 188.67 U/g FW for SOD, 66.33 U/g FW/min for CAT, and 41.67 µmol/g FW/min for APX.

Recent research indicates that ZnO-NPs enhance antioxidant defense systems, enzymatic activity, and glucose metabolism in plants, hence mitigating abiotic stresses (Adil et al., 2022; Adrees et al., 2021; Aqeel et al., 2022; Decsi, et al., 2025). Fertilization with ZnO-NPs at a concentration of 200 µg/mL in *Gossypium barbadense* significantly enhanced the plant's resistance to salinity by increasing its antioxidant activity (Hussein & Abou-Baker, 2018).

4.10. Genome-wide transcriptomic analyses

Total raw reads (post-sequencing) of the different treatments in tomato varied between 40,332,114 and 63,450,658. The raw reads measured 151 bp in length, the total count of contigs after *de novo* assembling was 87,567 (Table S1-1), and the mean length of the contigs was 1,176 bp (Ahmed et al., 2025). The comprehensive super transcriptome (Transcriptome Shotgun Assembly – TSA) serves as a depository of programmatically assembled transcript sequences obtained from primary sources of data, such as archived raw sequencing data (SRAs) and next-generation sequencing.

Overlapping reads from the entire transcriptome were computationally reconstructed into transcripts (*in silico*). The data underwent blasting, mapping, and annotation, subsequently followed by RNA sequencing read quantification to determine the level of expression of the *de novo* transcriptome contigs (Table S1-1). This was crucial since differential expression analysis requires the assessment of individual degrees of expression of the contigs.

The number of reads that were aligned in more than one way is shown in Figure 15. It was obtained from a total of six libraries that were processed. In the control (T1) set, it was 25,307,547; in the salinity-stressed treatment (T4) set, it was 21,684,741; in the salinity-stressed and sprayed with ZnO-NPs 75 mg/L treatment (T5) set, it was 23,858,687; in the salinity-stressed and sprayed with ZnO-NPs 150 mg/L treatment (T6) set, it was 35,338,131; in the sprayed with ZnO-NPs 75 mg/L treatment (T2) set, was 23,152,130; and in the sprayed with ZnO-NPs 150 mg/L treatment (T3) set, it was 22,740,011.

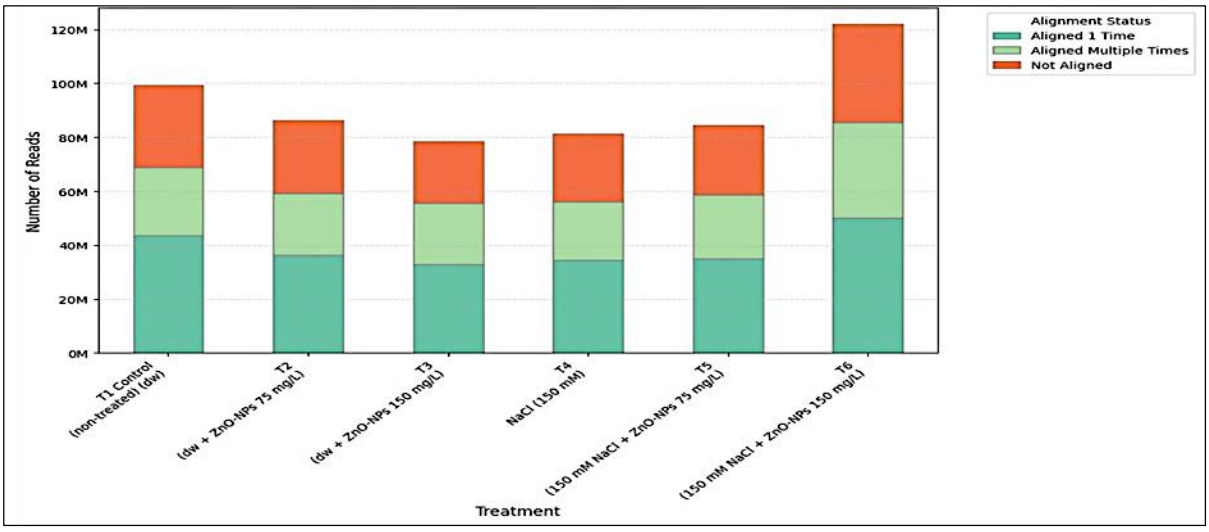

Figure 15. Transcript level quantification in tomato. The figure is obtained in its original form out of OmicsBox https://www.biobam.com/omicsbox/ (accessed: May 14, 2025).

The number of supertranscript contigs reconstructed from the sequences modulated by the treatments was 71,284 (Table S1-2). The pairwise differential between the datasets of control and salinity-stressed plants showed that the number of differentially expressed (DE) sequences (Probability > 0.9) was 2,740, with 1,021 up-regulated and 1,719 down-regulated (Table S2-1). In the case of the comparison between the datasets of control and sprayed plants with 75 mg/L ZnO-NPs, 1,609 differentially expressed (DE) sequences (Probability > 0.9) were obtained, with 495 up-regulated and 1,114 down-regulated (Table S2-2). The comparison between the datasets of control and sprayed plants with 150 mg/L ZnO-NPs resulted in 863 differentially expressed (DE) sequences (Probability > 0.9), with 441 up-regulated and 422 down-regulated (Table S2-3). In the comparison between the datasets of salinity-stressed and salinity-stressed + sprayed plants with 75 mg/L ZnO-NPs, 3,177 differentially expressed (DE) sequences (Probability > 0.9) were obtained, with 899 up-regulated and 2,278 down-regulated (Table S2-4).

The pairwise differential analysis between the datasets of salinity-stressed and salinity-stressed + sprayed plants with 150 mg/L ZnO-NPs resulted in 2,492 differentially expressed (DE) sequences (Probability > 0.9) with 971 up-regulated and 1,521 down-regulated (Table S2-5). However, the comparison between the datasets of salinity-stressed and salinity-stressed + sprayed plants with 75 mg/L ZnO-NPs showed 659 differentially expressed (DE) sequences (Probability > 0.9) with 299 up-regulated and 360 down-regulated (Table S2-6). Moreover, the comparison between the datasets of salinity-stressed and salinity-stressed + sprayed plants with 150 mg/L ZnO-NPs, 728 differentially expressed (DE) sequences (Probability > 0.9) were obtained, with 392 up-regulated and 336 down-regulated (Table S2-7).

In case of supertranscript analysis, blasting, mapping, and annotating the obtained contigs were done to find similar sequences, associating the blasted contigs with functional information (Gene ontology), and finally to determine the biological meanings of the sequences. We employed the plant reactome and KEGG for a deep pathway analysis to identify biochemical pathways that responded positively or negatively to the treatments (Fabregat et al., 2018; Kanehisa & Goto, 2000) to the super transcriptome (Tables S3-1, S3-2, S3-3, S3-4, S3-5, S3-6, S3-7). In all seven comparisons, we identified up- and down-regulated and over-expressed sequences (genes) through executing their blasting, mapping, and functional annotation, grounded in the data acquired from the combined analyses.

In the case of comparing T1 with T4, it was found that 1,019 sequences were up-regulated, and 445 were overexpressed. They could be linked to 129 biochemical pathways based on the KEGG database, with 109 sequences, while the plant reactome database found 313 pathways, with 383 linked sequences. On the other hand, for the same comparison, it was found that 1,715 sequences were down-regulated, while 1,217 were overexpressed. They were linked to 617 and 209 pathways based on the plant reactome and KEGG databases, with 770 and 331 sequences, respectively. In the case of comparing T1 with T2, it was found that 494 sequences were up-regulated, and 341 were overexpressed. They could be connected to 79 biochemical pathways based on the KEGG database, with 108 sequences, while the plant reactome database found 218 pathways, with 236 linked sequences. On the other hand, for the same comparison, it was found that 1,112 sequences were down-regulated, while 831 were overexpressed. They were linked to 480 and 151 pathways according to the plant reactome and KEGG databases, with 504 and 200 sequences, respectively.

By comparing T1 with T3, it was found that 439 sequences were up-regulated, and 285 were overexpressed. They could be connected to 74 pathways based on the KEGG database, with 46 sequences, and the plant reactome database found 212 pathways, with 196 linked sequences. On the other hand, for the same comparison, it was found that 421 sequences were down-regulated, while 308 were overexpressed. They could be connected to 101 pathways based on the KEGG database, with 46 sequences, and the plant reactome database identified 81 pathways, with 172 linked sequences. By comparing T1 with T5, it was found that 897 sequences were up-regulated, and 459 were overexpressed. They could be connected to 124 pathways based on the KEGG database, with 95 sequences, and the plant reactome database identified 297 pathways, with 333 linked sequences. On the other hand, for the same comparison, it was found that 2,271 sequences were down-regulated, while 1,843 were overexpressed. They could be connected to 240 pathways based on the KEGG database, with 550 sequences, and the plant reactome database found 897 pathways, with 950 linked sequences.

When T1 was compared to T6, it was found that 966 sequences were up-regulated, and 656 were overexpressed. They could be connected to 111 pathways based on the KEGG database, with 189 sequences, while the plant reactome database found 369 pathways, with 436 linked sequences.

On the other hand, for the same comparison, it was found that 1,517 sequences were down-regulated, while 1,217 were overexpressed. They could be linked to 190 biochemical pathways based on the KEGG database, with 346 sequences, and the plant reactome database found 731 pathways, with 680 linked sequences. Taking the salinity-stressed treatment (T4) into account as a references, T4 was compared to T5, and it was found that 299 sequences were up-regulated, and 190 were overexpressed. They could be linked to 43 biochemical pathways based on the KEGG database, with 35 sequences, and the plant reactome database identified 110 pathways, with 113 linked sequences. On the other hand, for the same comparison, it was found that 359 sequences were down-regulated, while 246 were overexpressed. They could be linked to 57 biochemical pathways based on the KEGG database, with 61 sequences, while the plant reactome database found 307 pathways, with 129 linked sequences.

On the other hand, T4 was compared to T6, so it was found that 391 sequences were up-regulated, and 287 were overexpressed. They could be connected to 55 pathways based on the KEGG database, with 52 sequences, and the plant reactome database identified 168 pathways, with 167 linked sequences. On the other hand, for the same comparison, it was found that 336 sequences were down-regulated, while 194 were overexpressed. They could be connected to 71 biochemical pathways based on the KEGG database, with 51 sequences, and the plant reactome database identified 133 pathways, with 125 linked sequences. In case of pairwise differential analysis of the top 50 contigs, blasting, mapping, and annotating the obtained contigs were done. In all seven comparisons, we identified top 50 up- down regulated sequences. The possible biochemical pathways and their linked sequences were studied based on the KEGG database, and the results are presented in Table 24 (Tables S4-1, S4-2, S4-3, S4-4, S4-5, S4-6, S4-7). Heat maps can be used to visualize the gene expression across samples. The top 50 up- and down-differentially expressed contigs (Tables S5-1, S5-2, S5-3, S5-4, S5-5, S5-6, S5-7) involved in the pairwise differential analysis between treatments were identified, as shown in the heat maps (Figures 16-22).

Table 24. Possible pathways of the top 50 up- and down-regulated sequences in tomato according to the KEGG database.

Comparison	Pathways linked to KEGG	No. of sequences linked to KEGG database
T1 vs T4	Fatty acid elongation, Biosynthesis of unsaturated fatty acids, Brassinosteroid and Phenylpropanoid biosynthesis, Steroids and steroid hormone biosynthesis, Metabolism of Phenylalanine, Ascorbate and aldarate, Purine, Glycerolipid, Inositol phosphate, Riboflavin, and Thiamine.	19
T1 vs T2	Metabolism of Purine, Glycerolipid, Riboflavin, and Thiamine. Steroid degradation, Terpenoid backbone biosynthesis, Steroid hormone biosynthesis, and Brassinosteroid biosynthesis.	10
T1 vs T3	Metabolism of Nicotinate and nicotinamide, Porphyrin, Glyoxylate and dicarboxylate, Phenylalanine, Ascorbate and aldarate, Purine and pyrimidine, Glycerolipid, Inositol phosphate, Riboflavin, Thiamine, and Pantothenate and CoA biosynthesis.	20
T1 vs T5	Metabolism of Purine & Pyrimidine, Ascorbate and aldarate, Methane, Nicotinate and nicotinamide, Inositol phosphate, Riboflavin, Drugs-other enzymes, Thiamine, Pyruvate, Starch and sucrose, Oxidative phosphorylation, Citrate cycle, Glycolysis, Pantothenate and CoA biosynthesis, Carbon fixation pathways in prokaryotes, Gluconeogenesis, and Carbon fixation in photosynthetic organisms.	26
T1 vs T6	Metabolism of Thiamine, Starch and sucrose, Galactose, Glycerolipid, and Riboflavin. Phenylpropanoid biosynthesis, Oxidative phosphorylation, and Photosynthesis,	10
T4 vs T5	Metabolism of xenobiotics by cytochrome P450, Thiamine, Drugs-other enzymes, Glutathione, Purine, and Amino sugar and nucleotide sugar. Tight junction, Longevity regulating pathway – worm, MAPK signaling pathway – yeast, Endocytosis, and Ubiquitin-mediated proteolysis.	11
T4 vs T6	Cysteine and methionine metabolism, Arachidonic acid, Linoleic acid, Tyrosine, Purine, Sulfur metabolism and Thiamine. Synthesis and secretion of cortisol, Prolactin signaling pathway, Steroid hormone biosynthesis, Ovarian steroidogenesis, Serotonergic synapse, Isoquinoline alkaloid biosynthesis, Inflammatory mediator regulation of TRP channels, Tight junction, Biosynthesis of various antibiotics, MAPK signaling pathway – yeast, Endocytosis, Monoterpenoid biosynthesis, Ubiquitin-mediated proteolysis, and Diterpenoid biosynthesis.	24

***T1**: Control (non-treated) (dw). **T2**: (dw + ZnO-NPs 75 mg/L). **T3**: (dw + ZnO-NPs 150 mg/L). **T4**: NaCl (150 mM). **T5**: (150 mM NaCl + ZnO-NPs 75 mg/L). **T6**: (150 mM NaCl + ZnO-NPs 150 mg/L).*

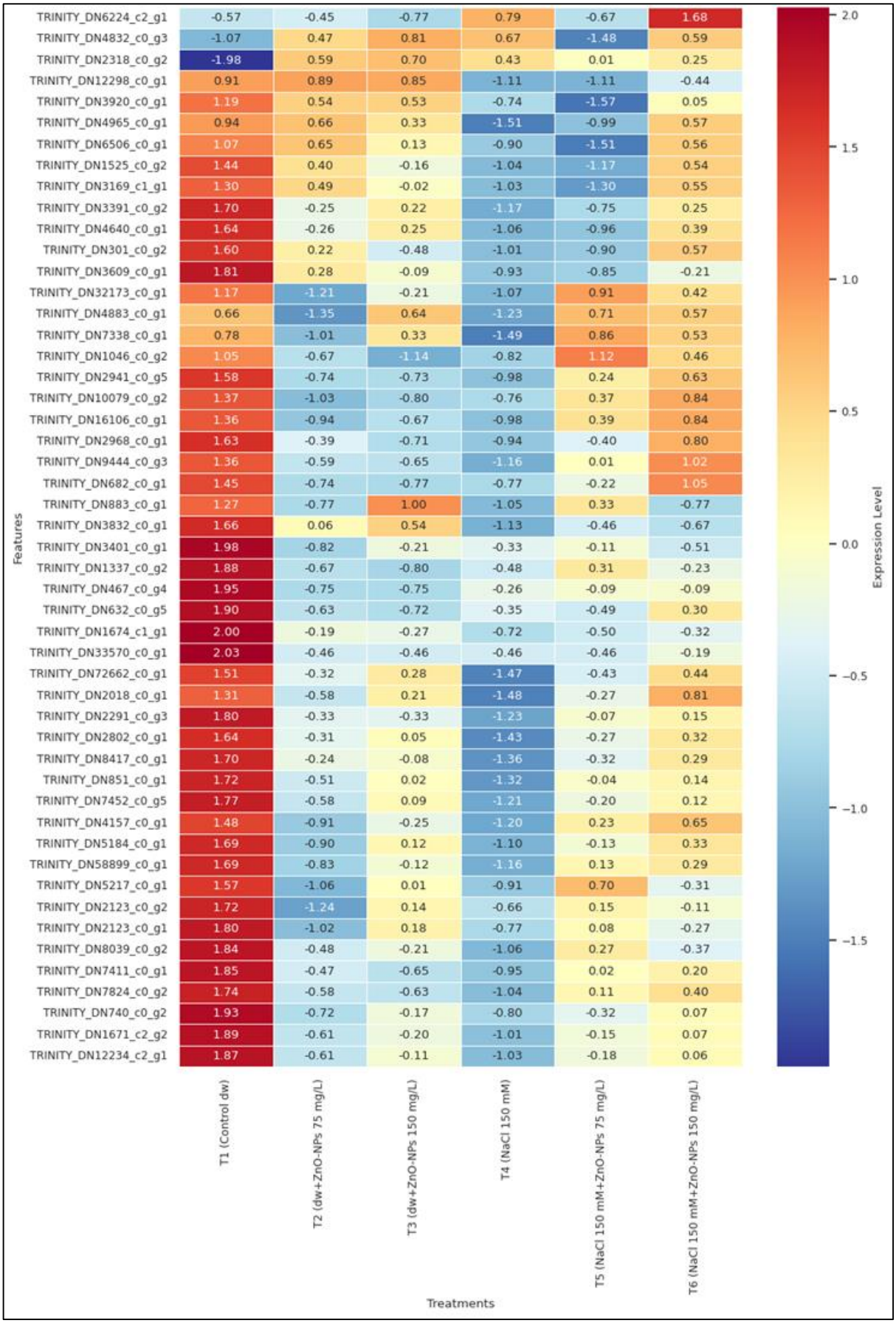

Figure 16. Comparative transcriptome analysis of control vs. salinity-stressed treatments. Up-regulated and down-regulated DEGs are observed in red and green, respectively.

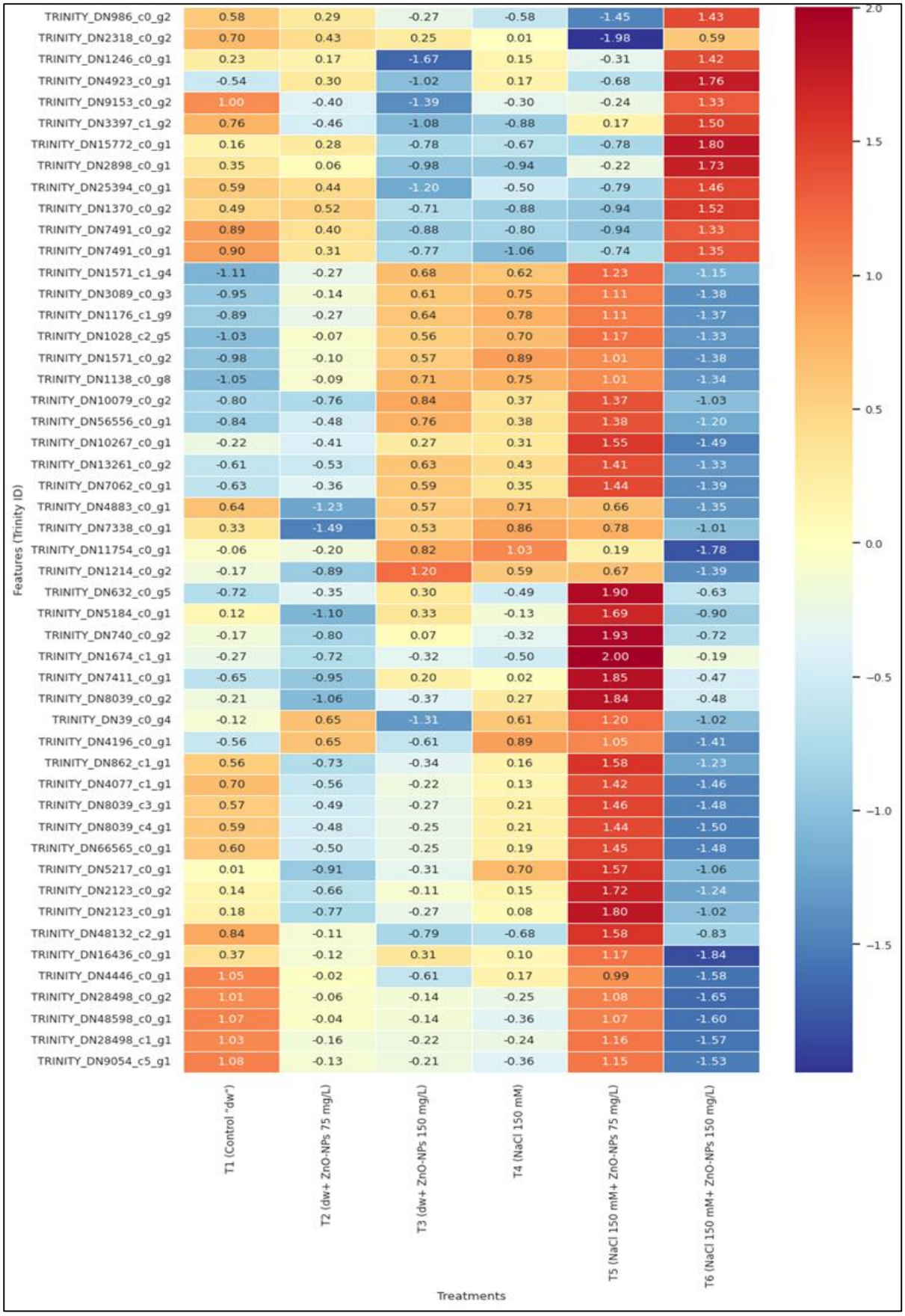

Figure 17. Comparative transcriptome analysis of control vs. 75 mg/L ZnO-NPs sprayed treatments. Up-regulated and down-regulated DEGs are observed in red and green, respectively.

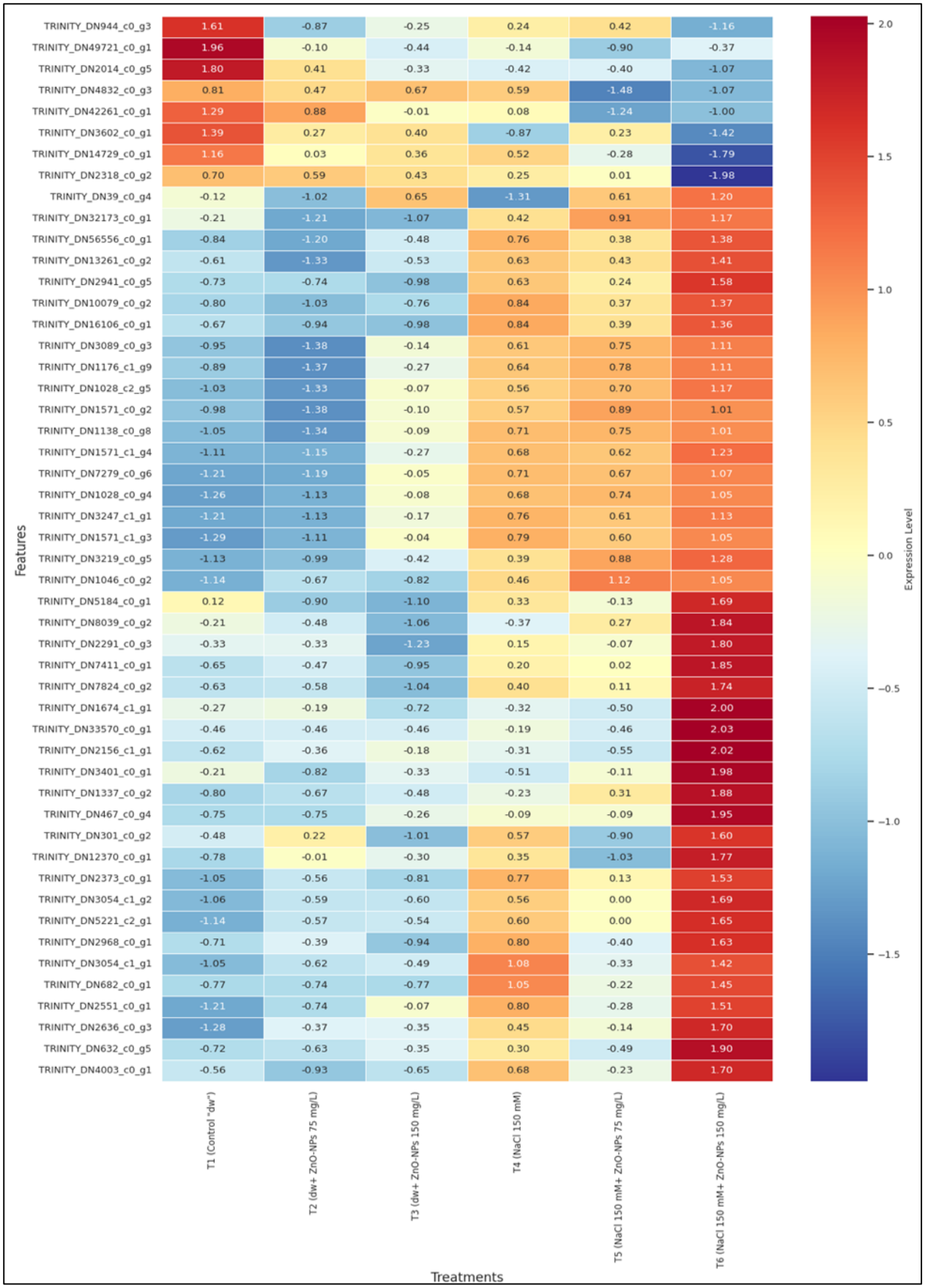

Figure 18. Comparative transcriptome analysis of control vs. 150 mg/L ZnO-NPs sprayed treatments. Up-regulated and down-regulated DEGs are observed in red and green, respectively.

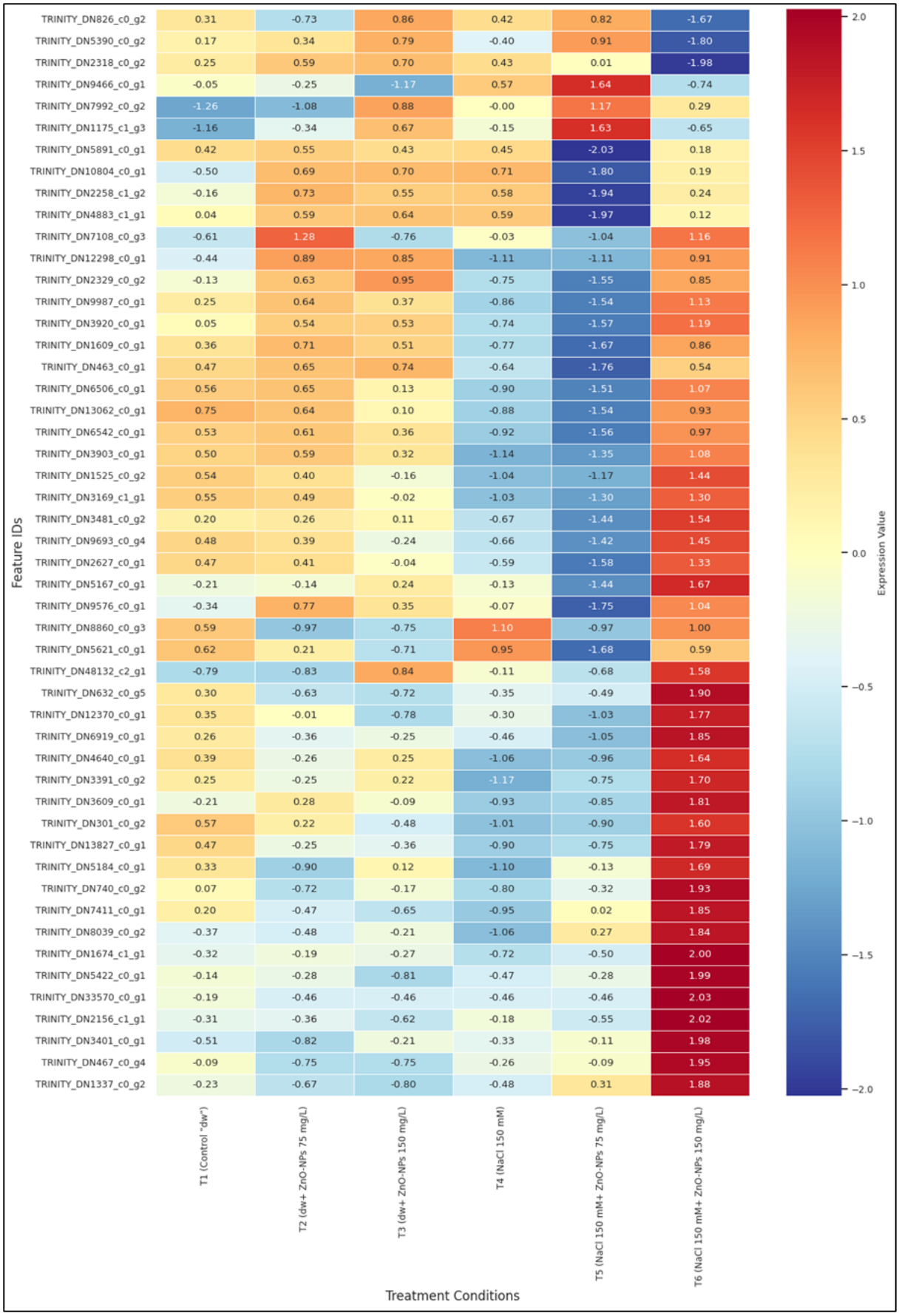

Figure 19. Comparative transcriptome analysis of control vs. salinity-stressed and 75 mg/L ZnO-NPs sprayed treatments. Up-regulated and down-regulated DEGs are observed in red and green, respectively.

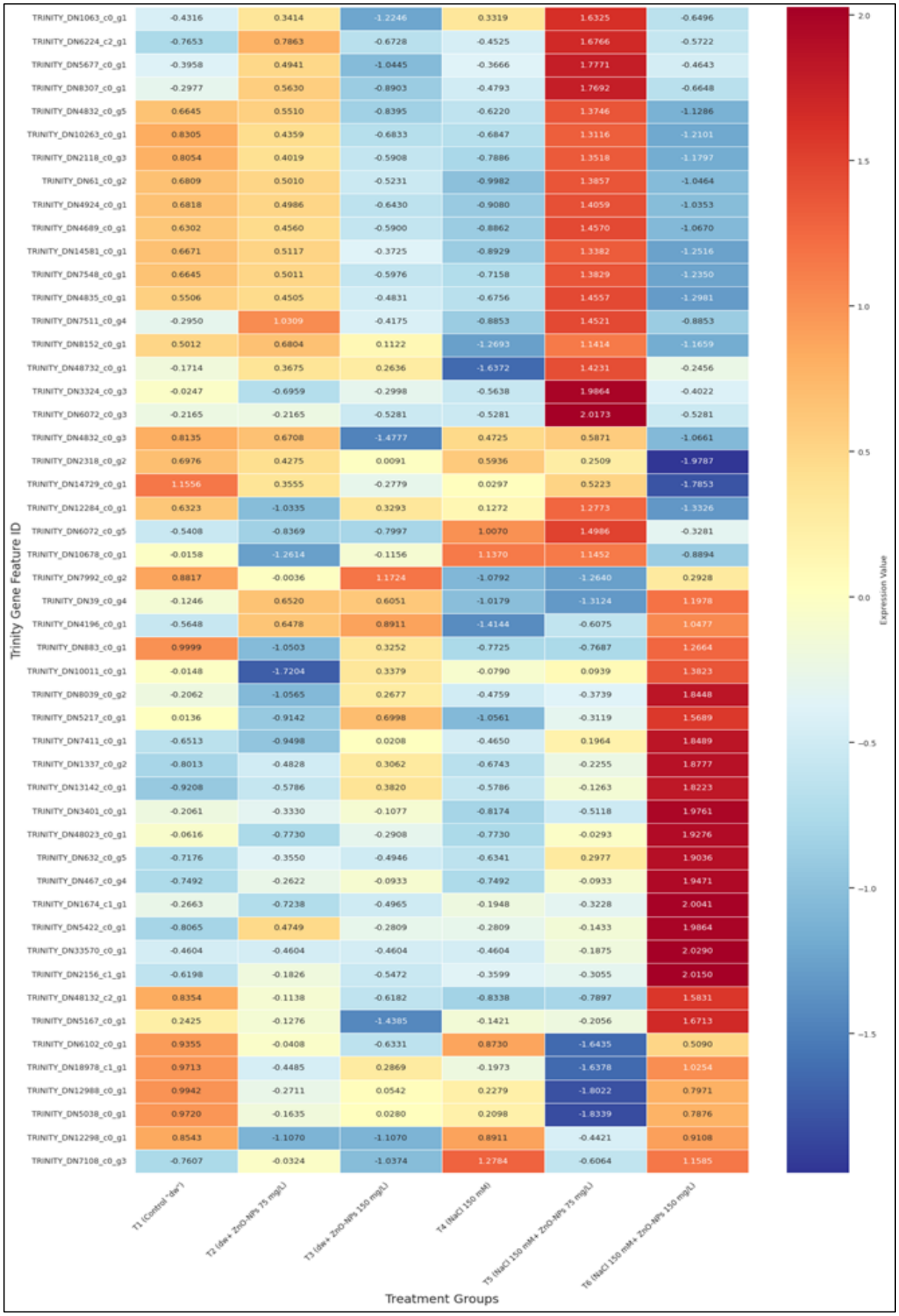

Figure 20. Comparative transcriptome analysis of control vs. salinity-stressed and 150 mg/L ZnO-NPs sprayed treatments. Up-regulated and down-regulated DEGs are observed in red and green, respectively.

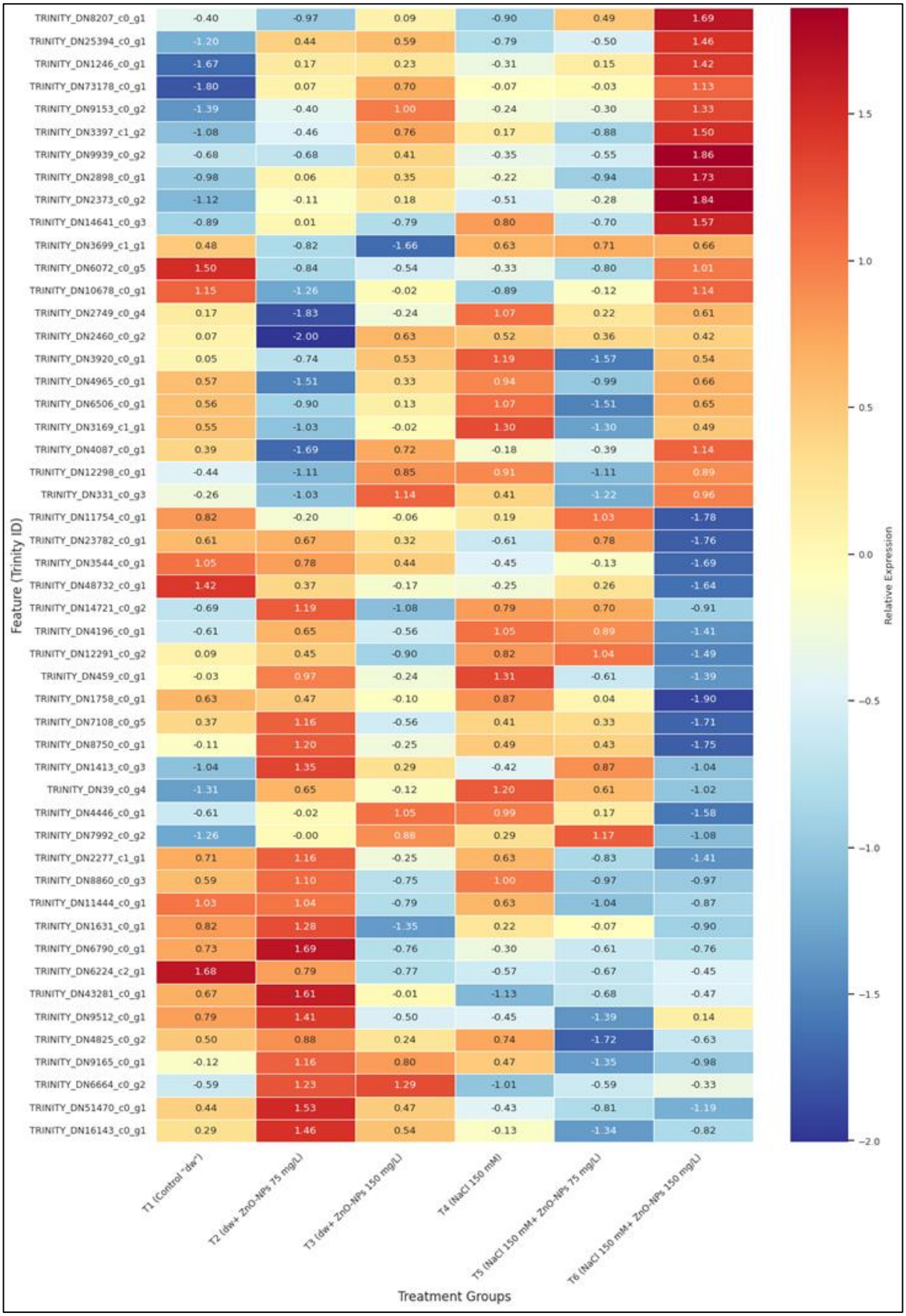

Figure 21. Comparative transcriptome analysis of salinity-stressed vs. salinity-stressed + 75 mg/L ZnO-NPs sprayed treatments. Up-regulated and down-regulated DEGs are observed in red and green, respectively.

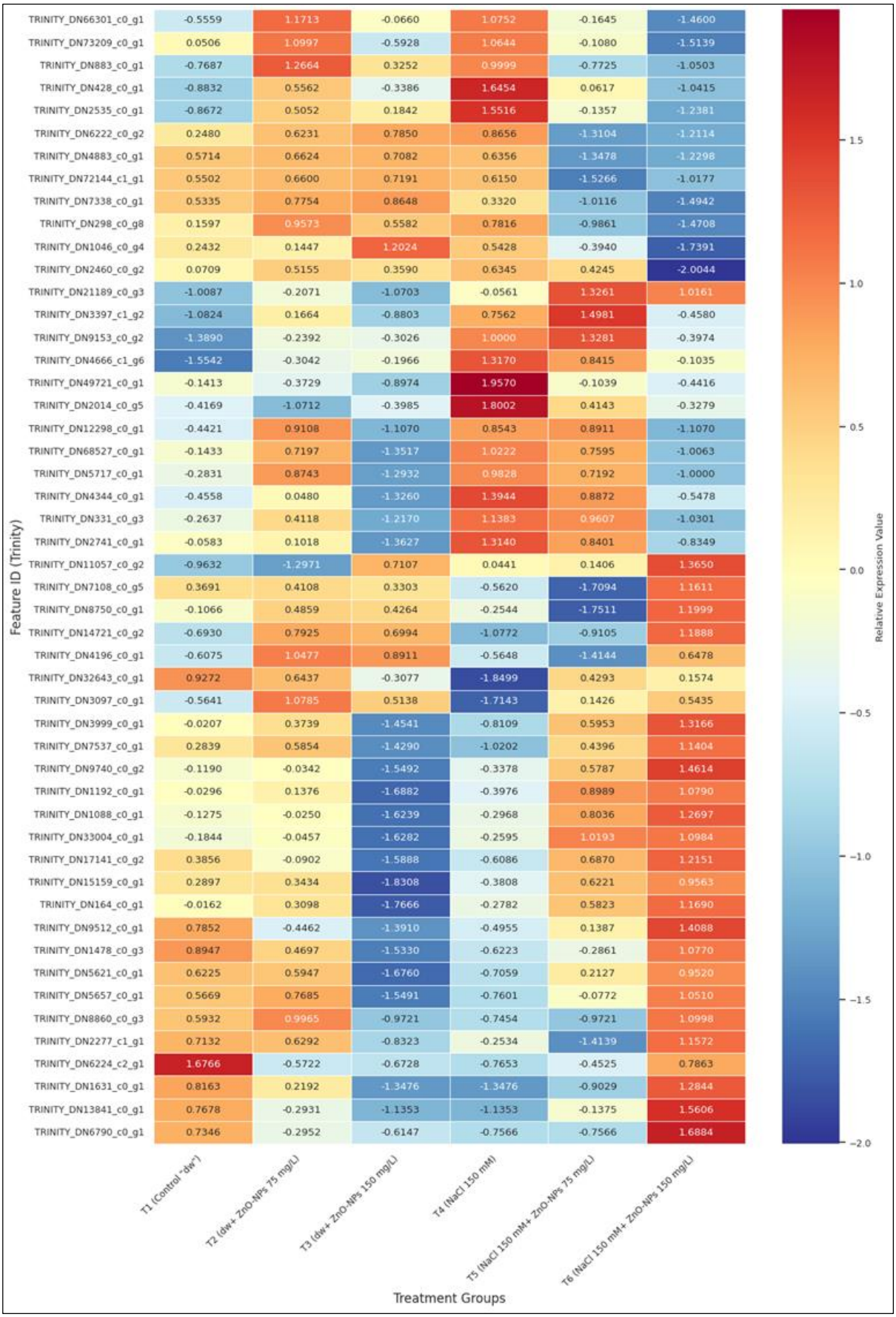

Figure 22. Comparative transcriptome analysis of salinity-stressed vs. salinity-stressed + 150 mg/L ZnO-NPs sprayed treatments. Up-regulated and down-regulated DEGs are observed in red and green, respectively.

The raw reads of maize measured 201 bp in length; the total count of contigs after *de novo* assembling was 22,108 **(**Table S8-1). The total assembled bases were varied between 6,174,394 and 7,623,144, and the mean length of the contigs was 348 bp. The comprehensive super transcriptome (Transcriptome Shotgun Assembly – TSA) serves as a depository of programmatically assembled transcript sequences obtained from primary sources of data, such as archived raw sequencing data (SRAs) and next-generation sequencing. Overlapping reads from the entire transcriptome were computationally reconstructed into transcripts (*in silico*) (Table S8-1). This was crucial since differential expression analysis requires the assessment of individual degrees of expression of the contigs.

The number of reads that were aligned in more than one way is shown in Figure 23. It was obtained from a total of six libraries that were processed. In the control (M1) set, it was 3,425,366; in the salinity-stressed treatment (M2) set, it was 4,473,091; in the salinity-stressed and sprayed with ZnO-NPs 2 g/L treatment (M3) set, it was 3,687,807; and in the sprayed with ZnO-NPs 2 g/L treatment (M4) set, it was 4,553,038.

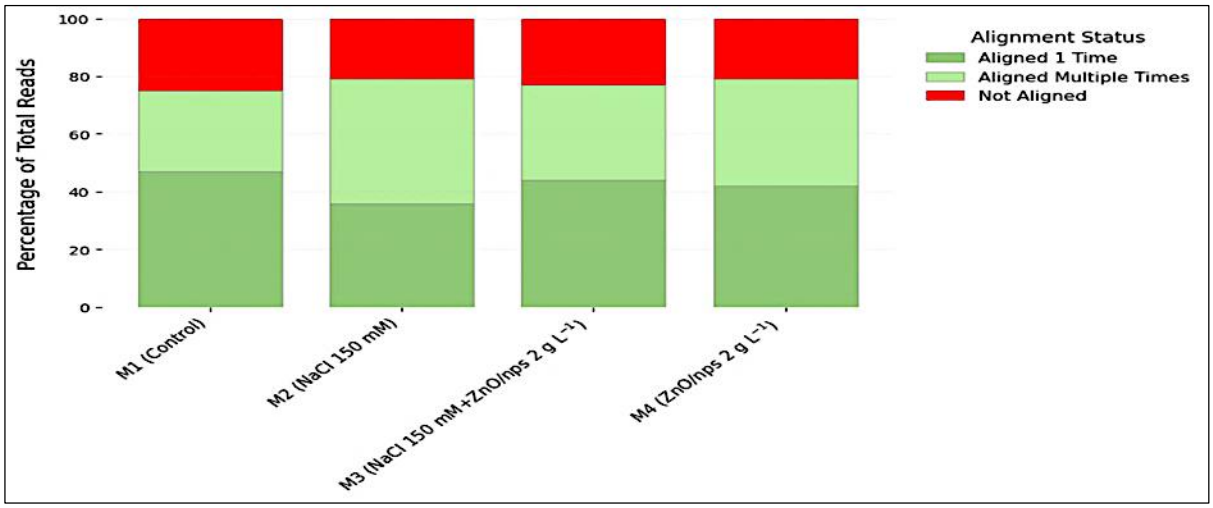

Figure 23. Transcript level quantification in maize. The figure is obtained in its original form out of OmicsBox https://www.biobam.com/omicsbox/ (accessed: June 7, 2025).

The number of supertranscript contigs reconstructed from the sequences modulated by the treatments was 18,893 (Table S8-2). The pairwise differential between the datasets of control and salinity-stressed plants showed that the number of differentially expressed (DE) sequences (Probability > 0.9) was 8,518, with 347 up-regulated and 8,171 down-regulated (Table S9-1). In the case of the comparison between the datasets of control and salinity-stressed but sprayed plants with 2 g/L ZnO-NPs, 3,507 differentially expressed (DE) sequences (Probability > 0.9) were obtained, with 632 up-regulated and 2,875 down-regulated (Table S9-2).

The comparison between the datasets of control and sprayed plants with 2 g/L ZnO-NPs resulted in 4,438 differentially expressed (DE) sequences (Probability > 0.9), with 509 up-regulated and 3,929 down-regulated (Table S9-3). In the comparison between the datasets of salinity-stressed and salinity-stressed + sprayed plants with 2 g/L ZnO-NPs, 3,301 differentially expressed (DE) sequences (Probability > 0.9) were obtained, with 2,642 up-regulated and 389 down-regulated (Table S9-4). Plant reactome and KEGG databases were employed for a deep pathway analysis to identify biochemical pathways to the super transcriptome (Tables S10-1, S10-2, S10-3, S10-4). In all four comparisons, we identified up- and down-regulated and over-expressed sequences (genes)

In the case of comparing M1 with M2, it was found that 347 sequences were up-regulated, and 114 were overexpressed. They could be linked to 55 biochemical pathways based on the KEGG database, with 24 sequences, while the plant reactome database found 53 pathways, with 38 linked sequences. On the other hand, for the same comparison, it was found that 8,171 sequences were down-regulated, while 2,909 were overexpressed. They were linked to 626 and 270 pathways based on the plant reactome and KEGG databases, with 639 and 837 sequences, respectively.

In the case of comparing M1 with M3, it was found that 632 sequences were up-regulated, and 299 were overexpressed. They could be connected to 109 biochemical pathways based on the KEGG database, with 90 sequences, while the plant reactome database found 98 pathways, with 86 linked sequences. On the other hand, for the same comparison, it was found that 3,875 sequences were down-regulated, while 842 were overexpressed. They were linked to 273 and 188 pathways according to the plant reactome and KEGG databases, with 247 and 236 sequences, respectively.

By comparing M1 with M4, it was found that 509 sequences were up-regulated, and 239 were overexpressed. They could be connected to 86 pathways based on the KEGG database, with 68 sequences, and the plant reactome database found 84 pathways, with 71 linked sequences. On the other hand, for the same comparison, it was found that 3,929 sequences were down-regulated, while 1235 were overexpressed. They could be connected to 206 pathways based on the KEGG database, with 376 sequences, and the plant reactome database identified 359 pathways, with 334 linked sequences.

By comparing M2 with M3, it was found that 2642 sequences were up-regulated, and 984 were overexpressed. They could be connected to 227 pathways based on the KEGG database, with 290 sequences, and the plant reactome database identified 268 pathways, with 226 linked sequences. On the other hand, for the same comparison, it was found that 389 sequences were down-regulated, while 76 were overexpressed. They could be connected to 36 pathways based on the KEGG database, with 18 sequences, and the plant reactome database found 28 pathways, with 22 linked sequences.

For the pairwise differential analysis of the top 50 contigs, blasting, mapping, and annotation of the obtained contigs were performed. In all four comparisons, we identified the top 50 up- and down-regulated sequences. The possible biochemical pathways and their linked sequences were studied based on the KEGG database, and the results are presented in Table 25 (Tables S11-1, S11-2, S11-3, S11-4).

Table 25. Possible pathways of the top 50 up- and down-regulated sequences in maize according to the KEGG database.

Comparison	Pathways linked to KEGG	No. of sequences linked to KEGG database
M1 vs M2	Thiamine metabolism, Benzoxazinoid biosynthesis, Biosynthesis of various plant secondary metabolites, Cysteine and methionine metabolism, Pyrimidine metabolism, One carbon pool by folate, Seleno compound metabolism, Purine metabolism, Pantothenate and CoA biosynthesis, Arginine and proline metabolism, beta-Alanine metabolism, and Riboflavin metabolism	17
M1 vs M3	Cysteine and methionine metabolism, Pyrimidine metabolism, Purine metabolism, Arginine and proline metabolism, Porphyrin metabolism, Riboflavin metabolism, beta-Alanine metabolism, Drug metabolism - cytochrome P450, Thiamine metabolism, Benzoxazinoid biosynthesis, Sulfur metabolism, Biosynthesis of various antibiotics, and Biosynthesis of various plant secondary metabolites	16
M1 vs M4	Cysteine and methionine metabolism, Pyrimidine metabolism, Purine metabolism, One carbon pool by folate, Selenocompound metabolism, Arginine and proline metabolism, Porphyrin metabolism, beta-Alanine metabolism, Drug metabolism - cytochrome P450, Riboflavin metabolism, Thiamine metabolism, Benzoxazinoid biosynthesis, and Biosynthesis of various plant secondary metabolites	18
M2 vs M3	Thiamine metabolism, Drug metabolism - other enzymes, Oxidative phosphorylation, Glutathione metabolism, Purine metabolism, Metabolism of xenobiotics by cytochrome P450, Riboflavin metabolism, Glycerophospholipid metabolism, and Drug metabolism - cytochrome P450	10

***M1**: Control (tap water); **M2**: (NaCl 150 mM); **M3**: (NaCl 150 mM + ZnO-NPs 2 g/L); and **M4**: (tap water + ZnO-NPs 2 g/L).*

Heat maps can be used to visualize the gene expression across samples. The top 50 up- and down-differentially expressed contigs (Tables S12-1, S12-2, S12-3, S12-4) involved in the pairwise differential analysis between treatments were identified, as shown in the heat maps (Figures 24-27).

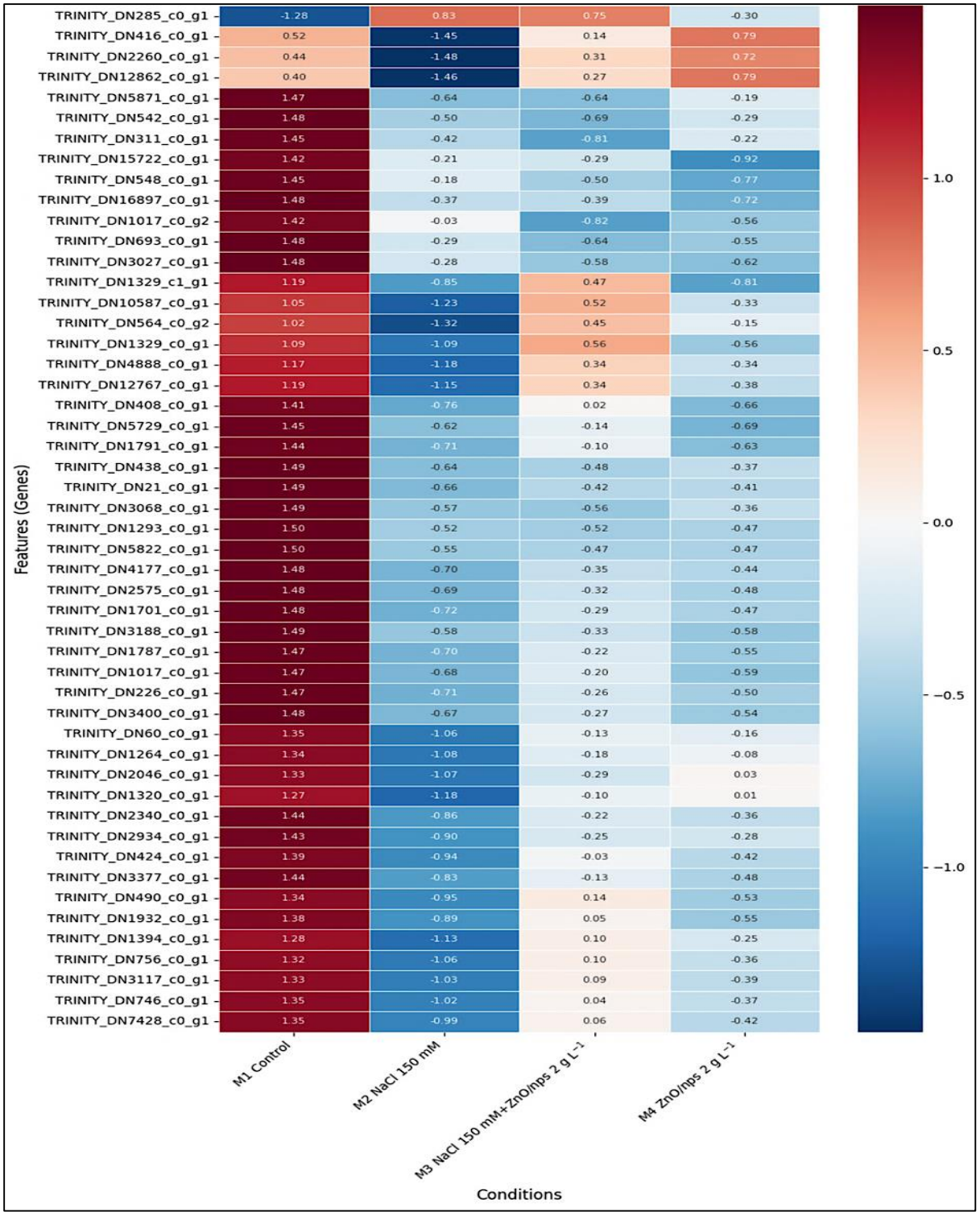

Figure 24. Comparative transcriptome analysis of control vs. salinity-stressed treatments. Up-regulated and down-regulated DEGs are observed in red and green, respectively.

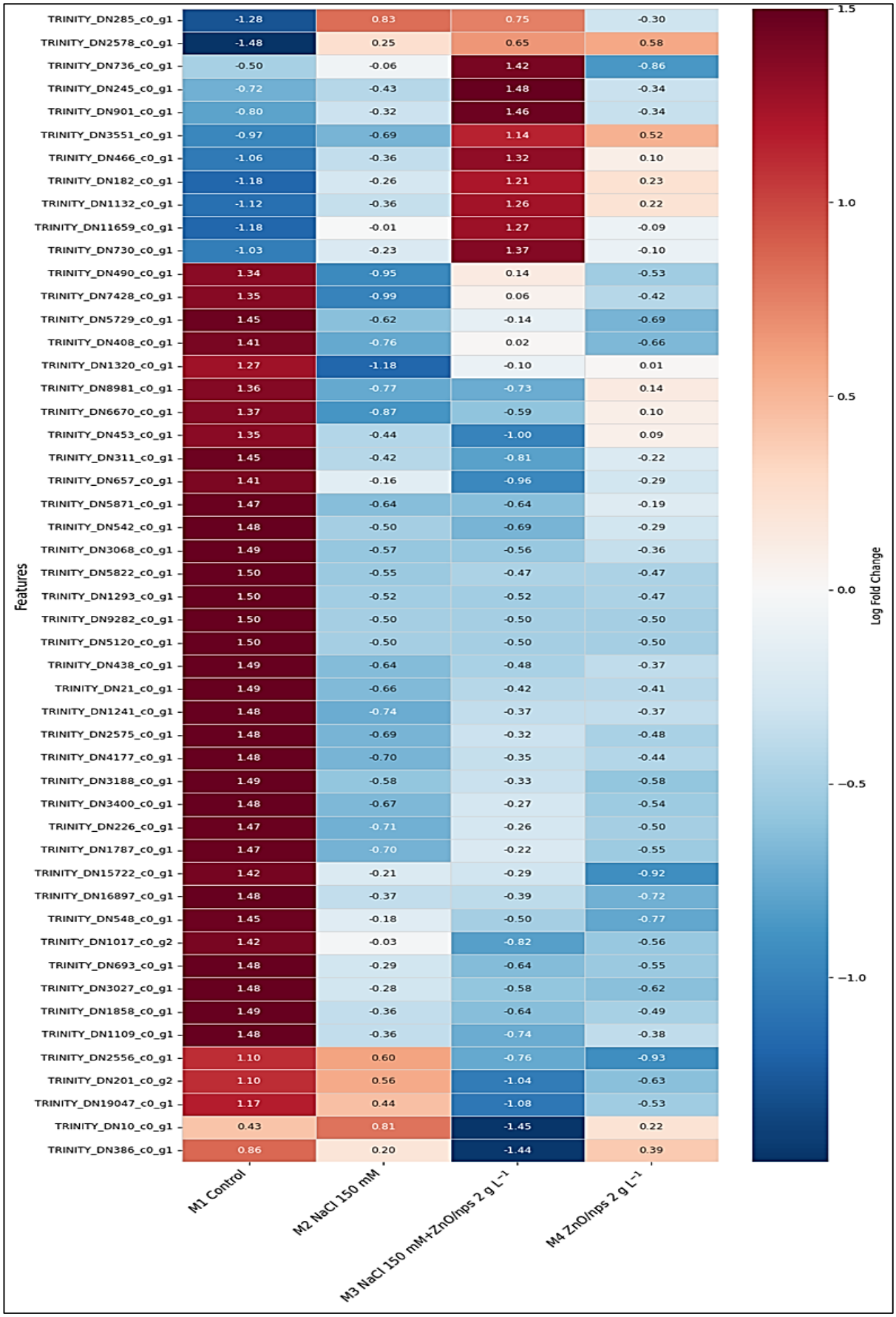

Figure 25. Comparative transcriptome analysis of control vs. salinity-stressed and 2 g/L ZnO-NPs sprayed treatments. Up-regulated and down-regulated DEGs are observed in red and green, respectively.

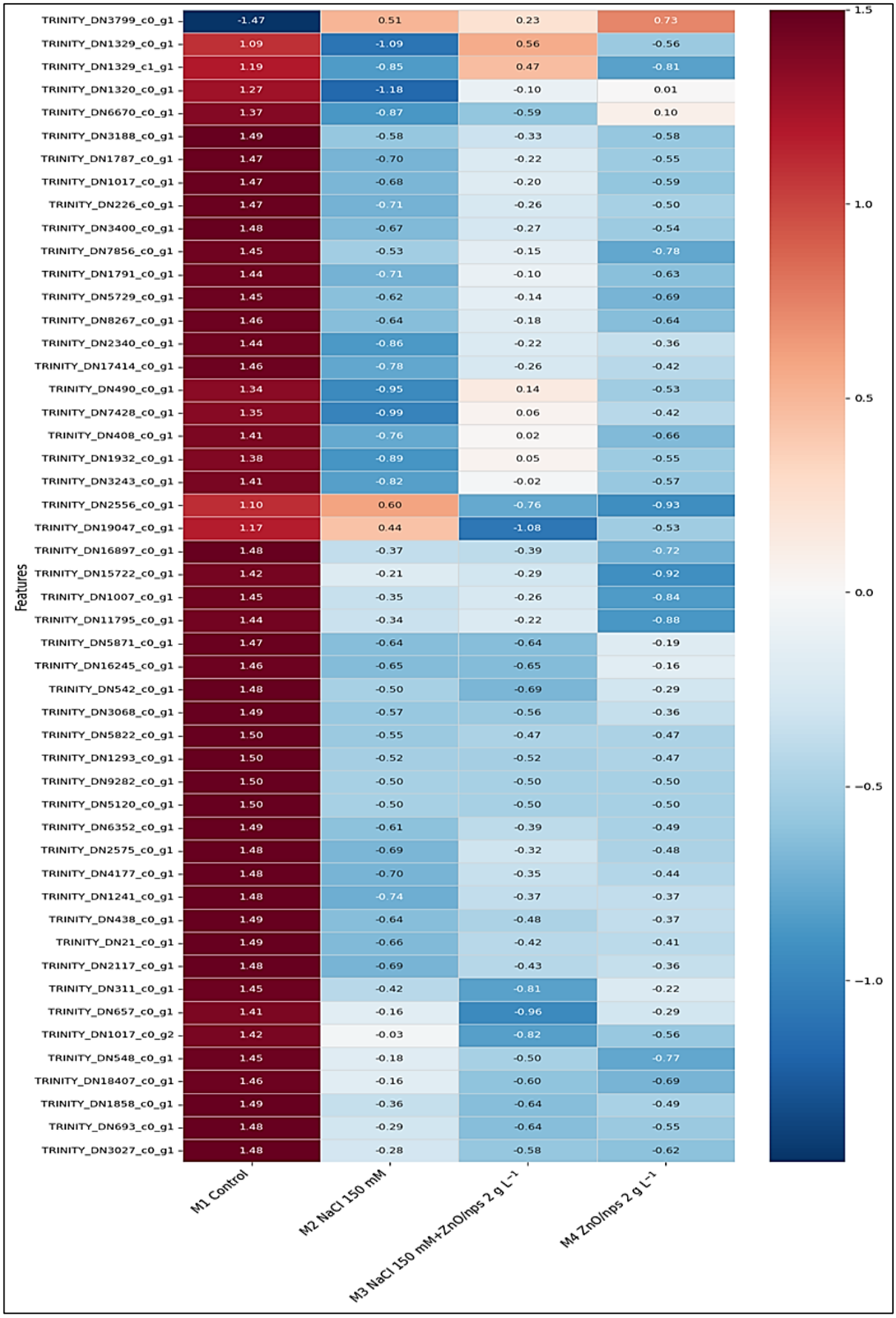

Figure 26. Comparative transcriptome analysis of control vs. 2 g/L ZnO-NPs sprayed treatments. Up-regulated and down-regulated DEGs are observed in red and green, respectively.

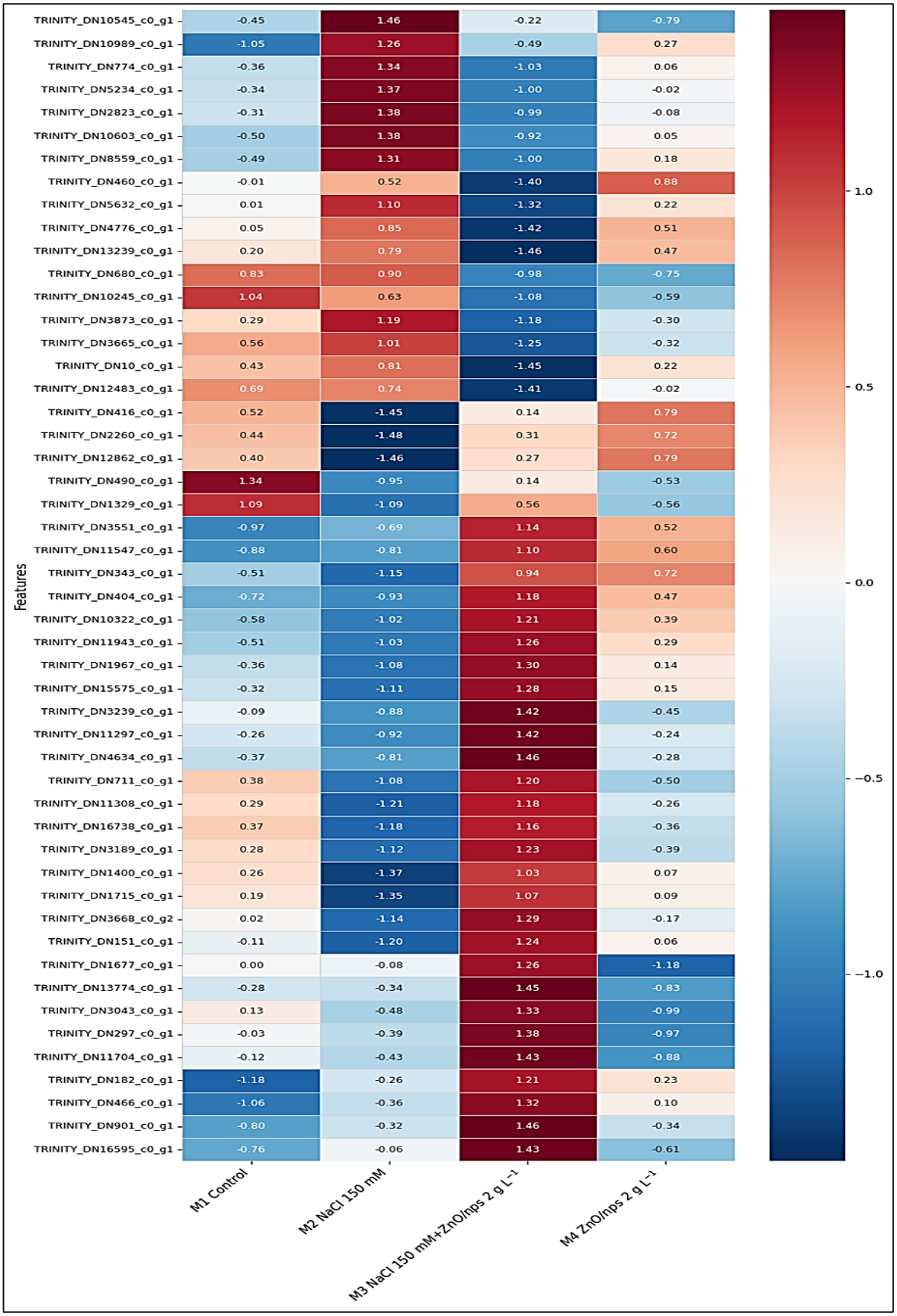

Figure 27. Comparative transcriptome analysis of salinity-stressed vs. salinity-stressed + 2 g/L ZnO-NPs sprayed treatments. Up-regulated and down-regulated DEGs are observed in red and green, respectively.

According to the sub-cellular analysis, we aimed to reproduce the workflow using transcriptome analysis, employing the OmicsBox tool, particularly the functional analysis and transcriptomics modules. This firstly involved obtaining sequencing data and performing a combined differential expression analysis of the whole transcriptome (supertranscript) by replicating the original data within OmicsBox, thereby establishing a solid foundation for further analysis and ensuring comparability with the up- and down-regulated sequences, so we can figure out the different biochemical pathways that the treatments may trigger and also find out the linked sequences to those pathways through the plant reactome and KEGG databases (databases of plant metabolic and regulatory pathways). Secondly, we examined the top 50 up- and down-regulated sequences to visualize gene expression across samples and their associated biochemical pathways, as per the KEGG database.

For the species *Solanum lycopersicum* L. in the plant reactome database in case of the comparison between T1 and T4, there were 112 sequences linked to different pathways, for example, arsenic uptake and detoxification (12 genes), cytosolic glycolysis (7 genes), TCA cycle (plant) (6 genes), Calvin cycle (5 genes) sucrose biosynthesis (4 genes), and regulation of seed germination and coleoptile growth under submergence, normal gravity environment (4 genes), choline biosynthesis I (3 genes), and short day regulated expression of florigens (3 genes) (Table S6-1). Moreover, for the same database, there were 322 down-regulated linked sequences (genes), for example, 14 genes for sterol biosynthesis, 11 for the regulation of seed germination and coleoptile growth under submergence and normal gravity environment, 10 for intracellular auxin transport, and 9 for recognition of fungal and bacterial pathogens and immunity response (Table S6-2).

In case of the comparison between T1 and T2, there were 102 sequences linked to different pathways in plant reactome database, for example, photorespiration (8 genes), cytosolic glycolysis (7 genes), starch biosynthesis (6 genes), and sucrose biosynthesis (6 genes) (Table S6-3). And for the same database, there were 221 linked down-regulated sequences (genes), for example, 16 genes sterol biosynthesis, 9 for the regulation of seed germination and coleoptile growth under submergence and normal gravity environment, 7 for mevalonate pathway, 5 for leucodelphinidin biosynthesis, and 9 for galactosylcyclitol biosynthesis (Table S6-4).

But, in case of the comparison between T1 and T3, there were 41 sequences linked to different pathways in plant reactome database, for example, regulation of seed germination and coleoptile growth under submergence and normal gravity environment with 7 genes and jasmonic acid signalling with 3 genes (Table S6-5). Moreover, for the same database, there were 85 down-regulated linked sequences (genes), for example, phenylpropanoid biosynthesis with 4 genes and and cellulose biosynthesis with 4 genes (Table S6-6).

Solanum lycopersicum L. in the plant reactome database when T1 compared to T5 showed 76 sequences linked to different pathways, for example, arsenic uptake and detoxification with 11 genes (Table S6-7). Moreover, for the same database, there were 471 down-regulated linked sequences (genes), for example, lysine biosynthesis II (18 genes), lysine biosynthesis I (18 genes), activation of pre-replication complex (16 genes), DNA replication initiation (16 genes), and sterol biosynthesis (16 genes) (Table S6-8). And on the other hand, it showed 176 sequences linked to different pathways in case T1 compared to T6 in plant reactome database, for example, photorespiration with 28 genes and cytosolic glycolysis with 19 genes (Table S6-9). Moreover, for the same database, there were 257 down-regulated linked sequences (genes), for example, sterol biosynthesis (16 genes) (Table S6-10).

By comparing T4 with T5, there were 26 sequences linked to different pathways in plant reactome database, for example, salicylic acid signaling with 2 genes (Table S6-11). Moreover, for the same database, there were 44 down-regulated linked sequences (genes), for example, DNA replication initiation (9 genes), activation of pre-replication complex (6 genes), and isoleucine biosynthesis from threonine (4 genes) (Table S6-12). And there were 66 sequences linked to different pathways in plant reactome database in case of comparing T4 with T6, for example, regulation of seed germination and coleoptile growth under submergence and normal gravity environment with 4 genes and cytokinins-O-glucoside biosynthesis with 3 genes (Table S6-13). Furthermore, for the same database, there were 61 down-regulated linked sequences (genes), for example, the ammonia assimilation cycle with 1 gene (Table S6-14). Figures 28 and 29 show the general biochemical pathways to which some of the DEGs could be assigned to.

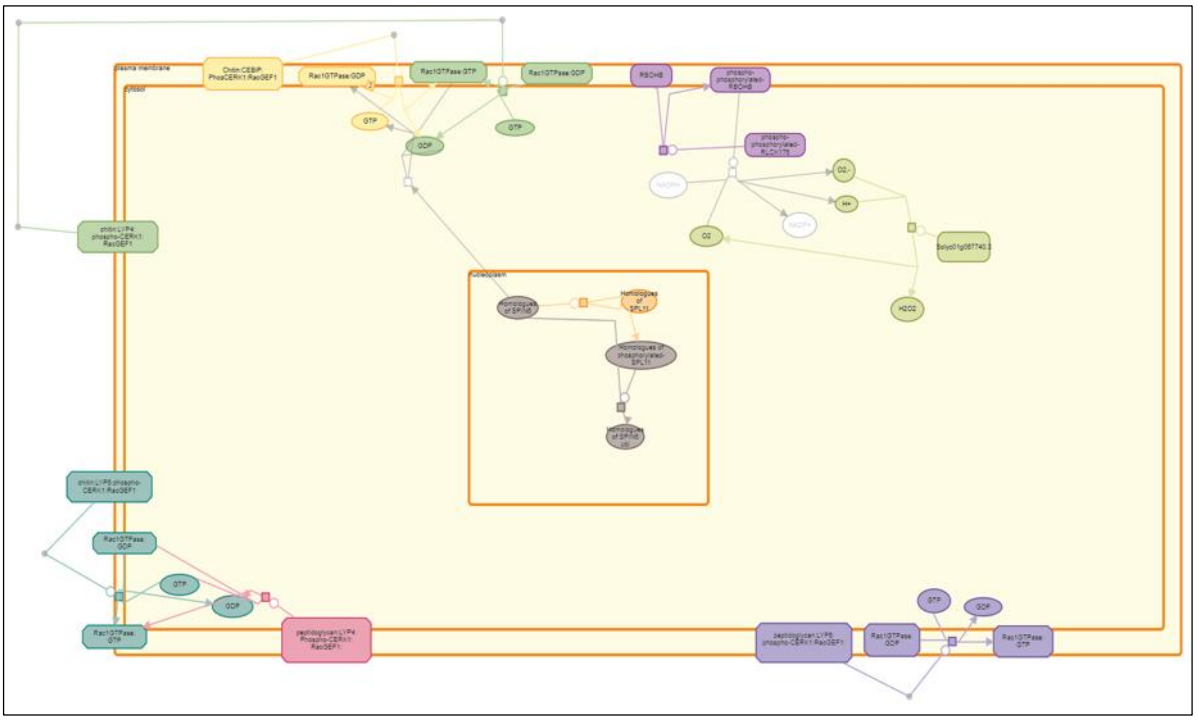

Figure 28. Recognition of fungal and bacterial pathogens and immunity response. The figure is obtained in its original form out of OmicsBox https://www.biobam.com/omicsbox/ (accessed: May 14, 2025). The figure illustrates the processes activated by the identified genes.
***GDP**: guanosine diphosphate. **GTP**: guanosine triphosphate. **RBOH**: respiratory burst oxidative homologs. **SP(L/IN)**: squamosa promoter binding protein. **LYP4**: lysin motif–containing proteins. **CERK1**: chitin elicitor receptor kinase 1. **RAC**: ras-related C3 botulinum toxin substrate 1. **RAC-GEF1**: rac guanine nucleotide exchange factor. **RLCK**: receptor like cytoplasmic kinases.*

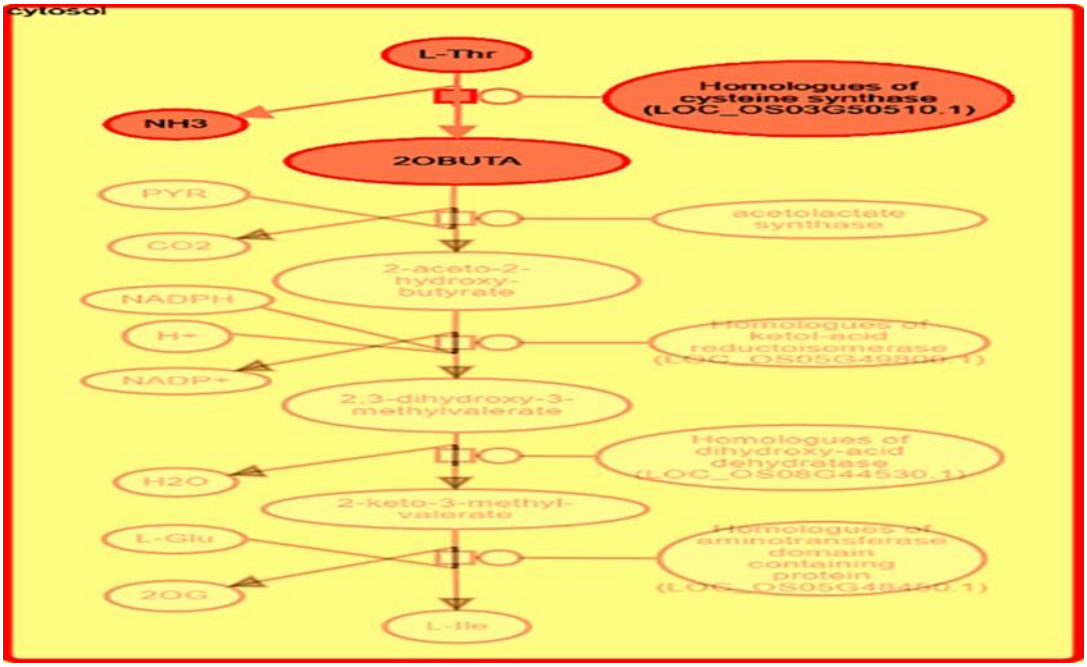

Figure 29. Biosynthesis of L-isoleucine amino acid (aa) from threonine (aa). The figure is obtained in its original form out of OmicsBox https://www.biobam.com/omicsbox/ (accessed: May 14, 2025). The figure illustrates the processes activated by the identified genes.
***L-Thr**: L-threonine. **2OBUTA**: 2-oxobutanoate. **L-Glu**: L-glutamate. **2OG**: 2-oxoglutarate (α-ketoglutarate). **L-Ile**: L-isoleucine.*

Table 26 shows the possible biochemical pathways linked to the up- and down-regulated sequences from the supertranscript according to the KEGG database according to tomato treatments. The values in front of each biochemical pathway refers to the number of up/down-regulated sequences connected to that pathway. In this work, ZnO nanoparticles were evaluated on salt-stressed and non-salt-stressed tomatoes under greenhouse conditions. Salinity stress significantly elevated the expression of genes involved in the metabolism of purine, thiamine, starch, sucrose, and other secondary metabolites in plants (Decsi et al., 2025). Salt stress increases and prolongs starch buildup in early fruit development (Yin et al., 2010).

Table 26. Selected possible pathways in the KEGG database for the highest and most common supertranscript up- and down-regulated sequences in tomato.

Comparison	**Pathways linked to the KEGG database and their responsible sequences**	
	Up-regulated sequences	**Down-regulated sequences**
T1 vs T4 (Table S7-1)	Metabolism of Purine 23 Metabolism of Thiamine 18 Carbon fixation by the Calvin cycle 15 Methane metabolism 13 Metabolism of Starch and sucrose 13	Metabolism of Purine 43 Metabolism of Thiamine 38 Metabolism of Starch and sucrose 25 Pentose and glucuronate interconversions 19 Phenylpropanoid biosynthesis 16
T1 vs T2 (Table S7-2)	Metabolism of Purine 24 Metabolism of Thiamine 22	Metabolism of Purine 21 Metabolism of Thiamine 20
T1 vs T3 (Table S7-3)	Metabolism of Thiamine 12 & Purine 10 Glyoxylate and dicarboxylate metabolism 6 Metabolism of Starch and sucrose 6	Metabolism of thiamine 12 & Purine 10 Glyoxylate & dicarboxylate metabolism 6 Metabolism of Starch and sucrose 6
T1 vs T5 (Table S7-4)	Metabolism of Purine 18 Metabolism of Thiamine 16 Metabolism of Starch and sucrose 10	Metabolism of Purine 108 Metabolism of Thiamine 95 Metabolism of Starch and sucrose 38
T1 vs T6 (Table S7-5)	Carbon fixation by Calvin cycle 41 Methane metabolism 37 Glycine, serine and threonine metabolism 35 Glyoxylate and dicarboxylate metabolism 32 Purine metabolism 31 Thiamine metabolism 30 Glycolysis / Gluconeogenesis 28 Fructose and mannose metabolism 23 Pentose phosphate pathway 21 Lipoic acid metabolism 19 Cysteine & methionine metabolism 15 Tryptophan metabolism 11 Pyruvate metabolism 11	Metabolism of Purine 63 Metabolism of Thiamine 59 Metabolism of Starch and sucrose 31 Phenylpropanoid biosynthesis 22 Pentose & glucuronate interconversions 18 Oxidative phosphorylation 17 Cyanoamino acid metabolism 16 Glycerophospholipid metabolism 15 Biosynthesis of various plant secondary metabolites 15 Degradation of flavonoids 14
T4 vs T5 (Table S7-6)	Metabolism of Purine 5 Metabolism of Thiamine 5 Phenylpropanoid biosynthesis 4	Metabolism of Purine 5 Metabolism of Thiamine 5 Phenylpropanoid biosynthesis 4

Table 26. *Continued*.			
T4 vs T6 (Table S7-7)	Metabolism of Purine	8	Phenylpropanoid biosynthesis 9
	Metabolism of Thiamine	8	Oxidative phosphorylation 6
	Pentose & glucuronate interconversions 6		Phenylalanine metabolism 6

***T1**: Control (non-treated) (dw). **T2**: (dw + ZnO-NPs 75 mg/L). **T3**: (dw + ZnO-NPs 150 mg/L). **T4**: NaCl (150 mM). **T5**: (150 mM NaCl + ZnO-NPs 75 mg/L). **T6**: (150 mM NaCl + ZnO-NPs 150 mg/L).*

In the studies by Balibrea et al. (1999) (1996), it was found that salt stress had negatively affected starch accumulation, and this occurred due to the complete breakdown of transiently generated starch into soluble sugars in mature tomato fruits. Yin et al. (2010) found that the increase of starch accumulation may increase sugar content in salt-stressed red tomato fruits. Balibrea et al. (2006) discovered that sucrose import during ripening enhanced sugar concentration in wild species under saline stress, suggesting various germplasm processes regulate sugar levels. Sun et al. (2020) discovered that foliar application of ZnO nanoparticles increased zinc in leaves while decreasing zinc in roots. The findings indicated that the increased Zn^{2+} in leaves negatively regulates Zn^{2+} transport to the roots.

In support of this hypothesis, two ZIP family such as: Zrt- and Irt-like protein (facilitates the transport of Zn^{2+}, Fe^{2+}, Mn^{2+}, and Cd^{2+} across cellular membranes) (ZIP3 and ZIP5), demonstrated reduced expression in ZnO-NPs-treated roots relative to untreated plants. The analysis of the transcriptome indicated that foliar application of ZnO-NPs stimulated the expression of various metal transporters, and two ZIP-like transporters, in iron-deficient tomato leaves treated with ZnO-NPs. In Table 36, it was observed that salinity stress significantly down-regulated the purine and thiamine metabolism genes in case of comparisons; T1 & T4, T1 & T5, and T1 & T6, as thiamine induces systemic acquired resistance (SAR) in plants, which is linked to plant immunity and defense (Li et al., 2022), so –sometimes- there is a need to decrease the metabolic rate and accumulate total thiamine and purine content.

Thiamine, vitamin B1, is necessary for several metabolic activities (Yusof, 2019). Active thiamine pyrophosphate (TPP) cofactors are critical for metabolic activities like glycolysis, the hexose monophosphate shunt, and the citric acid cycle in all living things (Goyer, 2010). According to Tunc-Ozdemir et al. (2009), TPP (the active form of thiamine) is a crucial stress response molecule that induces thiamine production in Arabidopsis in response to various abiotic stimuli (Tunc-Ozdemir et al., 2009). Arabidopsis seedlings exposed to cold, osmotic, and salt conditions showed a substantial increase in total thiamine content compared to control seedlings (Yusof, 2019). Thiamine content increased due to a significant rise in TPP.

Salinity stress dramatically increased transcript abundance of thiamine biosynthesis genes (THI4, THIC, TH1, and TPK). The transcript expressions are highest in leaves, supporting the assumption that thiamine production occurs in chloroplasts (Yusof, 2019). Increasing polyethylene glycol (PEG) and NaCl concentrations caused osmotic and salt stress, leading to a substantial rise in total thiamine content in maize seedlings. Higher thiamine levels were in turn linked to higher abscisic acid (ABA) levels (Tunc-Ozdemir et al., 2009). Additionally, drought and salinity stress conditions led to a slight increase in transketolase activity, a key TPP-dependent enzyme. The disruption of transketolase activity shows that thiamine metabolism plays a role in plant stress adaptation (Tunc-Ozdemir et al., 2009). The mechanism of how the thiamine metabolism is being regulated is presented in Figure 30.

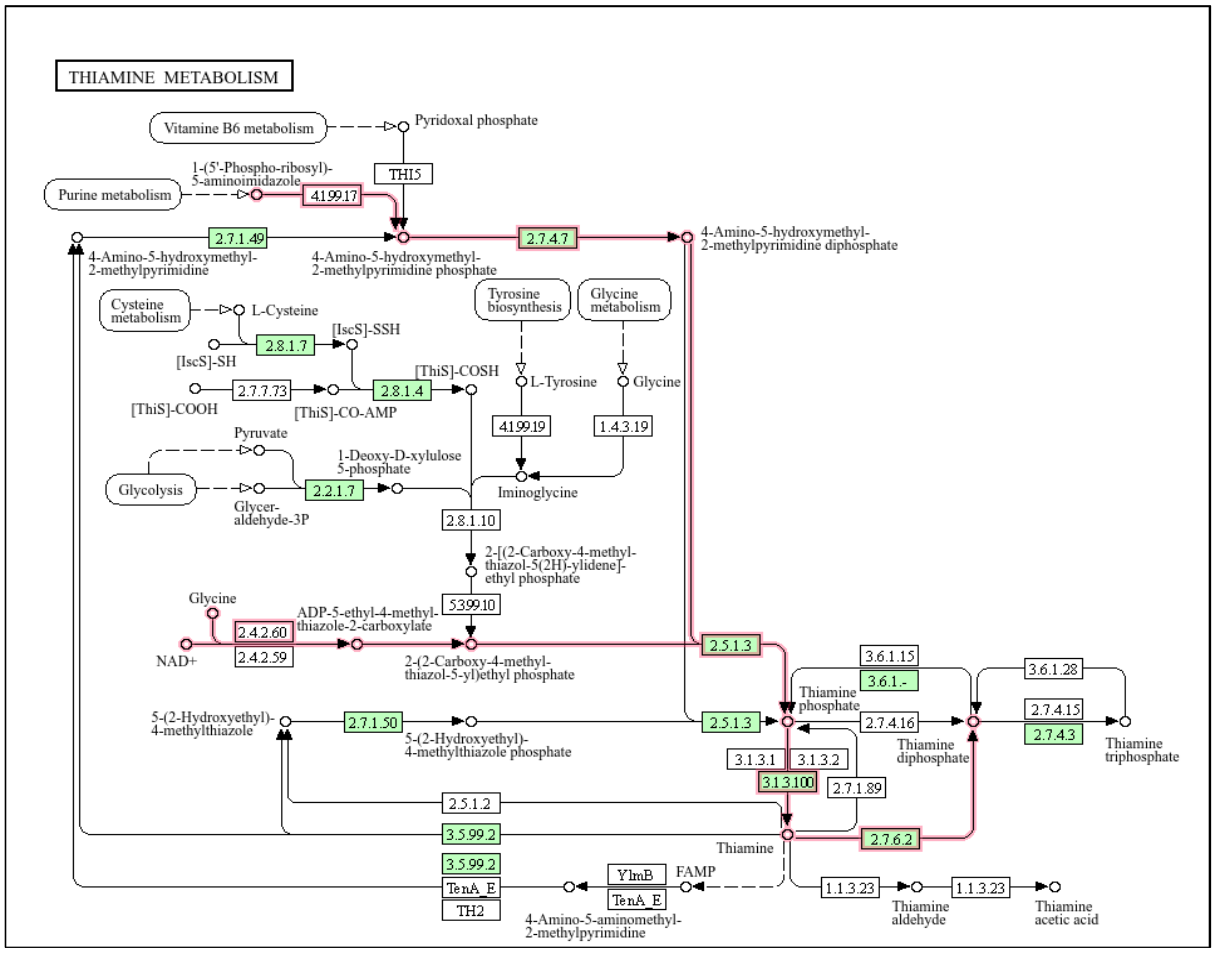

Figure 30. Induction of thimine metabolism activating enzymes during salinity stress. The figure is obtained in its original form out of OmicsBox software https://www.biobam.com/omicsbox/ (accessed: May 14, 2025) and is presented in its original form (it can also be found here https://www.kegg.jp/pathway/lmon00730). Genes start subprocesses, as shown in the picture. The letters stand for all the genes and enzymes (EC: code classification name) that are part of the biochemical pathway. The purple color show the pathway in the plants, and the green colors show the key enzymes.

Purine nucleotides serve as substrates for coenzymes such as nicotinamide adenine dinucleotide (NADH) and coenzyme A (CoA), which are essential for cellular metabolic activities, including stress signaling and the initiation of adaptive responses (Li et al., 2025;

Sun et al., 2019; Zrenner et al., 2006). Purine metabolism is essential for alleviating drought and salinity stress in plants. Initially, plant cells can modify osmotic pressure in reaction to drought/salinity stress by adjusting the concentration of purine molecules. Then, certain compounds originating from purines can affect hormone metabolism or regulate the equilibrium of ROS and antioxidants in drought/salinity conditions (Li et al., 2025; Sun et al., 2019; Watanabe et al., 2014; Werner & Witte, 2011). Finally, plants may modify adenosine triphosphate (ATP) levels to cope with drought stress (Li et al., 2025; Qiao et al., 2024).

Li et al. (2025) proved that the primary trend in the gene expression profile associated with metabolic pathways, secondary metabolite biosynthesis, plant hormone signal transduction, and carbon metabolism was enhanced following drought treatment in rice. Conversely, the down-regulated differentially expressed genes (DEGs) were predominantly associated with metabolic pathways and the manufacture of secondary metabolites. The findings of the current study revealed that under salinity stress, tomato leaves can respond to environmental changes by modulating the expression of genes associated with specific adaptive biological processes. Notably, analysis of the DEGs revealed that several genes associated with purine metabolism (Figure 31) exhibited responsiveness to salinity and ZnO-NPs, suggesting that this pathway is crucial for the adaptive response to salinity stress in tomato.

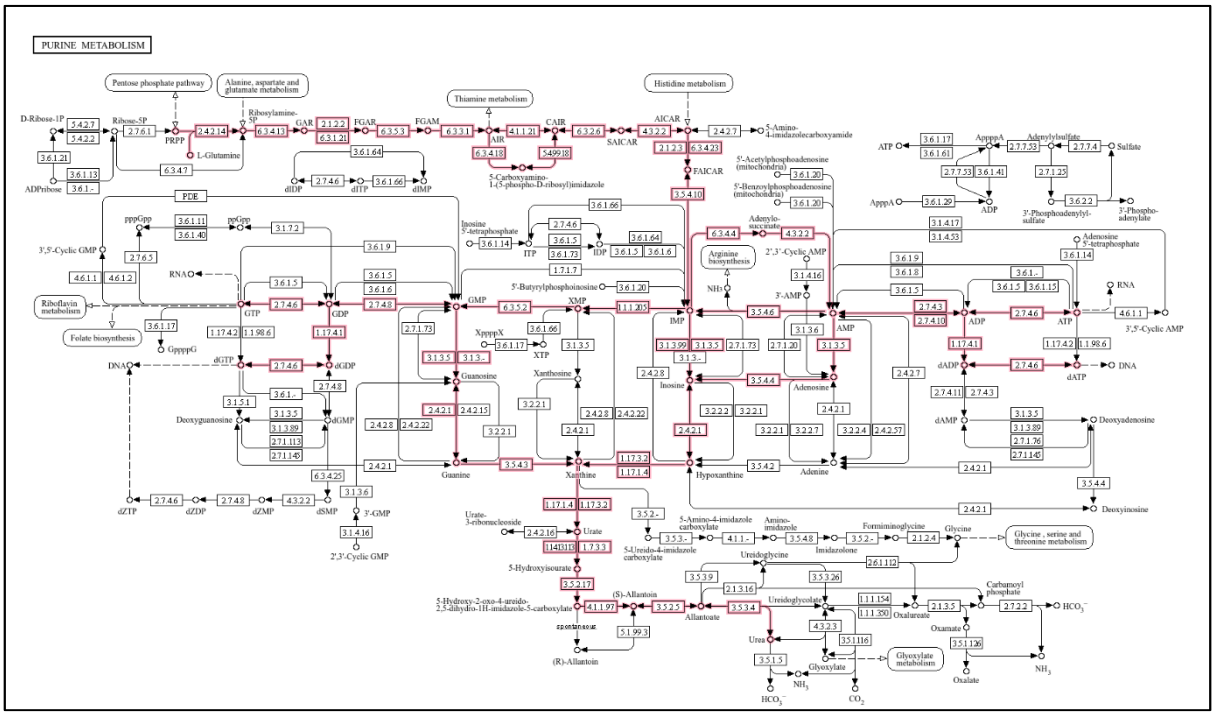

Figure 31. Induction of purine metabolism activating enzymes during salinity stress. The figure is obtained in its original form out of OmicsBox software https://www.biobam.com/omicsbox/ (accessed: May 14, 2025) and is presented in its original form (It can also be found here https://www.kegg.jp/pathway/map00230). Genes start subprocesses, as shown in the picture. The letters stand for all the genes and enzymes (EC: code classification name) that are part of the biochemical pathway. The purple color shows *de novo* purine biosynthesis, adenine ribonucleotide biosynthesis, guanine ribonucleotide biosynthesis, deoxyribonucleotide biosynthesis, adenine ribonucleotide degradation, guanine ribonucleotide degradation, and purine degradation.

In a study by Sun et al. (2020), they found that although foliar spraying with ZnO-NPs increased the Zn content in leaves, it decreased Zn accumulation in roots. Those results suggested that the elevated Zn content in leaves forms a negative feedback regulation of Zn uptake in roots. In support of the notion, two ZIP family Zn transporters, *ZIP3* (*Solyc02g081600.3*) and *ZIP5-like* (*Solyc07g043230.3*), exhibited lower expression in ZnO-NP-treated roots compared with untreated control plants. They also found that the transcriptome analysis revealed that foliar spraying with ZnO-NPs induced the expression of several metal transporters, including *VIT4-like* (*Solyc01g104780.3*), *Nramp2-like* (*Solyc04g078250.3*), *YSL7* (*Solyc03g031920.3*), and two ZIP-like transporters, *Solyc07g065380.4* and *Solyc01g087530.3*, in ZnO-NP-treated Fe-deficient tomato leaves.

For the species *Zea mays* L. in the plant reactome database in case of the comparison between M1 and M2, there were 21 sequences linked to different pathways, for example, abscisic acid (ABA) mediated signalling (2 genes), HSFA7/ HSFA6B-regulatory network-induced by drought and ABA (2 genes), polyisoprenoid biosynthesis (2 genes), TCA cycle (plant) (2 genes) and mevalonate pathway (2 genes) (Table S13-1). Moreover, for the same database, there were 303 down-regulated linked sequences (genes), for example, 16 genes for TCA cycle (plant), 12 for jasmonic acid signalling, 8 for cytosolic glycolysis, 8 for cellulose biosynthesis, and 17 for tryptophan biosynthesis (Figure 32) (Table S13-2).

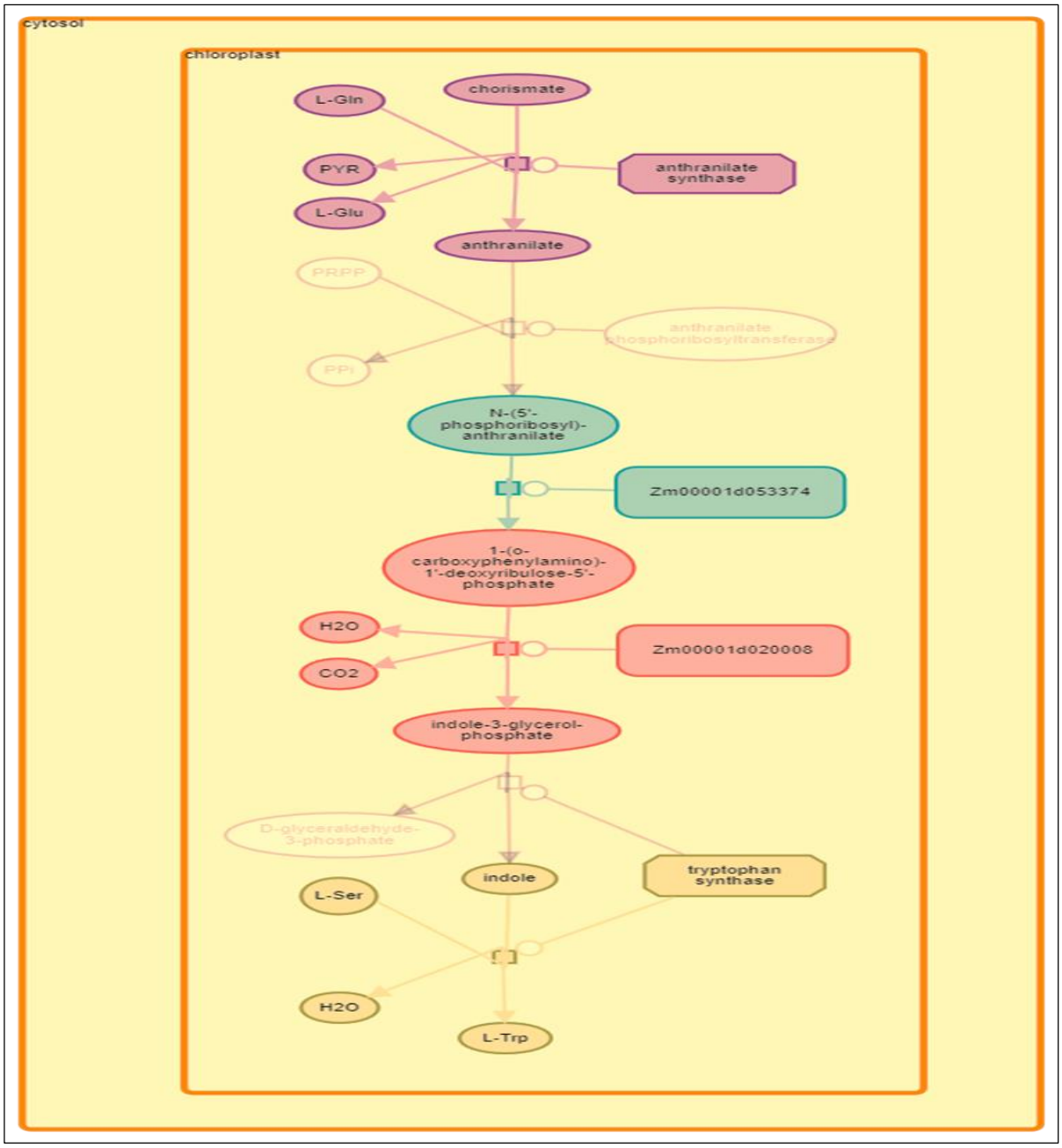

Figure 32. Biosynthesis of the amino acid L-tryptophan. The data utilized to generate the figure is sourced directly from OmicsBox **https://www.biobam.com/omicsbox/** (accessed on 4 June 2025). The graphic depicts the mechanisms activated by the identified genes.
L-Gln*: L-glutamine.* ***PYR****: Pyruvate.* ***L-Glu****: L-glutamate.* ***PRPP****: phosphoribosyl pyrophosphate.* ***PPi****: pyrophosphate.* ***L-Ser****: L-serine.* ***L-Trp****: L-tryptophan.* ***Zm00001d053374****: gene encodes for the phosphoribosylanthranilate isomerase enzyme.* ***Zm00001d020008****: gene encodes for the indole-3-glycerol-phosphate synthase enzyme.*

According to Ahemad and Kibret (2014), canola synthesis of IAA improved water use efficiency and nutritional availability to the plant. So, down-regulation of the tryptophan biosynthetic pathway is needed, as tryptophan plays an essential role in plant development and stress tolerance as a precursor to plant natural products. Plants produce essential protective metabolites like melatonin, camalexin and indole glucosinolates (IGs) through tryptophan metabolism (Lv et al., 2021; Wang et al., 2025; Xu et al., 2023). By forming a metabolic network through complex interactions, the wide variety of tryptophan metabolites controls plant health in response to biotic and abiotic stressors. For this reason, managing plant health in stressful environments requires knowledge of the regulatory processes underlying the tryptophan metabolic network.

In case of the comparison between M1 and M3 there were 50 sequences linked to different pathways in plant reactome database, for example, sucrose biosynthesis (3 genes), sulfate activation for sulfonation (3 genes), starch biosynthesis (3 genes), and cyanate degradation (3 genes) (Table S13-3). And for the same database, there were 130 linked down-regulated sequences (genes), for example, 2 genes for homoserine biosynthesis, 2 for long day regulated expression of florigens, 2 for recognition of fungal and bacterial pathogens and immunity response, and 2 for gibberellin signaling (Table S13-4).

But, in case of the comparison between M1 and M3, there were 28 sequences linked to different pathways in plant reactome database, for example, myo-inositol biosynthesis with 1 gene, polyisoprenoid biosynthesis with 1 gene, Calvin cycle, polar auxin transport with 1 gene, and trehalose biosynthesis I with 1 gene (Table S13-5). Moreover, for the same database, there were 207 down-regulated linked sequences (genes), for example, lysine biosynthesis VI with 5 genes and and arginine biosynthesis with 4 genes (Table S13-6).

Zea mays L. in the plant reactome database when M2 was compared to M3, showed 105 sequences linked to different pathways, for example, polyisoprenoid biosynthesis, valine degradation (Figure 33) with 2 genes, glutathione redox reactions II with 2 genes, nitrate assimilation with 2 genes, and vitamin E biosynthesis with 2 genes (Table S13-7). Moreover, for the same database, there were 5 down-regulated linked sequences (genes), for example, isoleucine biosynthesis from threonine, 13-LOX and 13-HPL pathway, jasmonic acid biosynthesis, valine biosynthesis (Figure 34), and trehalose biosynthesis I, with 1 gene for each possible pathway (Table S13-8).

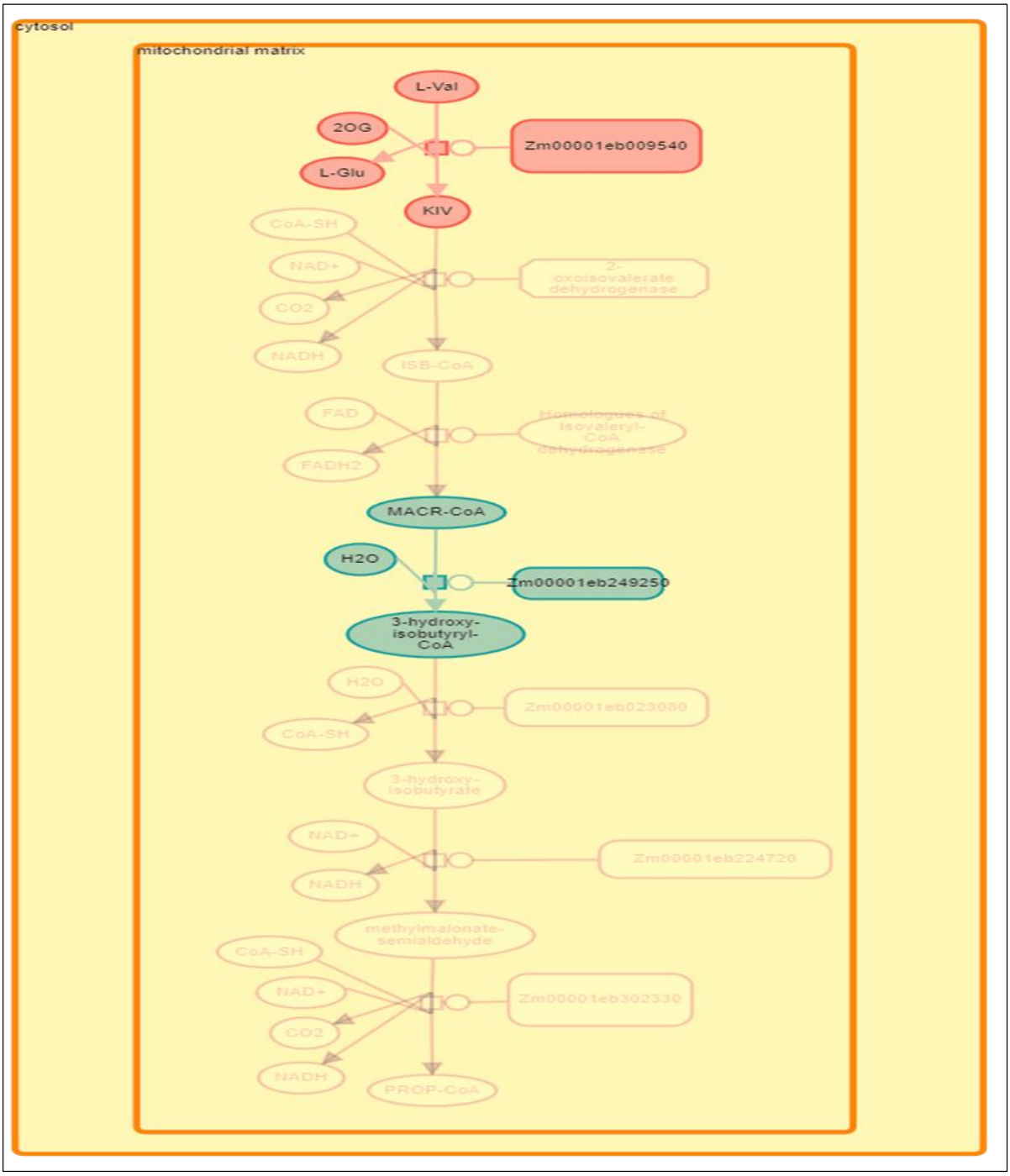

Figure 33. Degradation of the amino acid L-valine. The data utilized to generate the figure is sourced directly from OmicsBox **https://www.biobam.com/omicsbox/** (accessed on 4 June 2025). The graphic depicts the mechanisms activated by the identified genes.
***PYR**: Pyruvate. **[2]**: 2 molecules of pyruvate. **NADPH**: nicotinamide adenine dinucleotide phosphate (Reduced form). **NADP$^+$**: nicotinamide adenine dinucleotide phosphate (oxidized form). **KIV**: 2-ketoisolvalerate. **L-Glu**: L-glutamate. **2OG**: 2-oxoglutarate (α-ketoglutarate). **L-Val**: L-valine. **FAD**: flavin adenine dinucleotide. **FADH$_2$**: reduced flavin adenine dinucleotide. **CoA-SH**: Co enzyme A. **ISB Co-A**: Isobutyryl Co-A. **MACR Co-A**: metylacrylyl Co-A. **PROP Co-A**: Propionyl Co-A. **Zm00001eb009540**: gene encodes for the transaminase enzyme. **Zm00001eb249250**: gene encodes for the crotonase enzyme. **Zm00001eb023080**: gene encodes for the hydroxyisobutyryl-CoA hydrolase enzyme. **Zm00001eb224720**: gene encodes for the hydroxyisobutyric acid dehydrogenase enzyme. **Zm00001eb302330**: gene encodes for the methylmalonic semialdehyde dehydrogenase enzyme.*

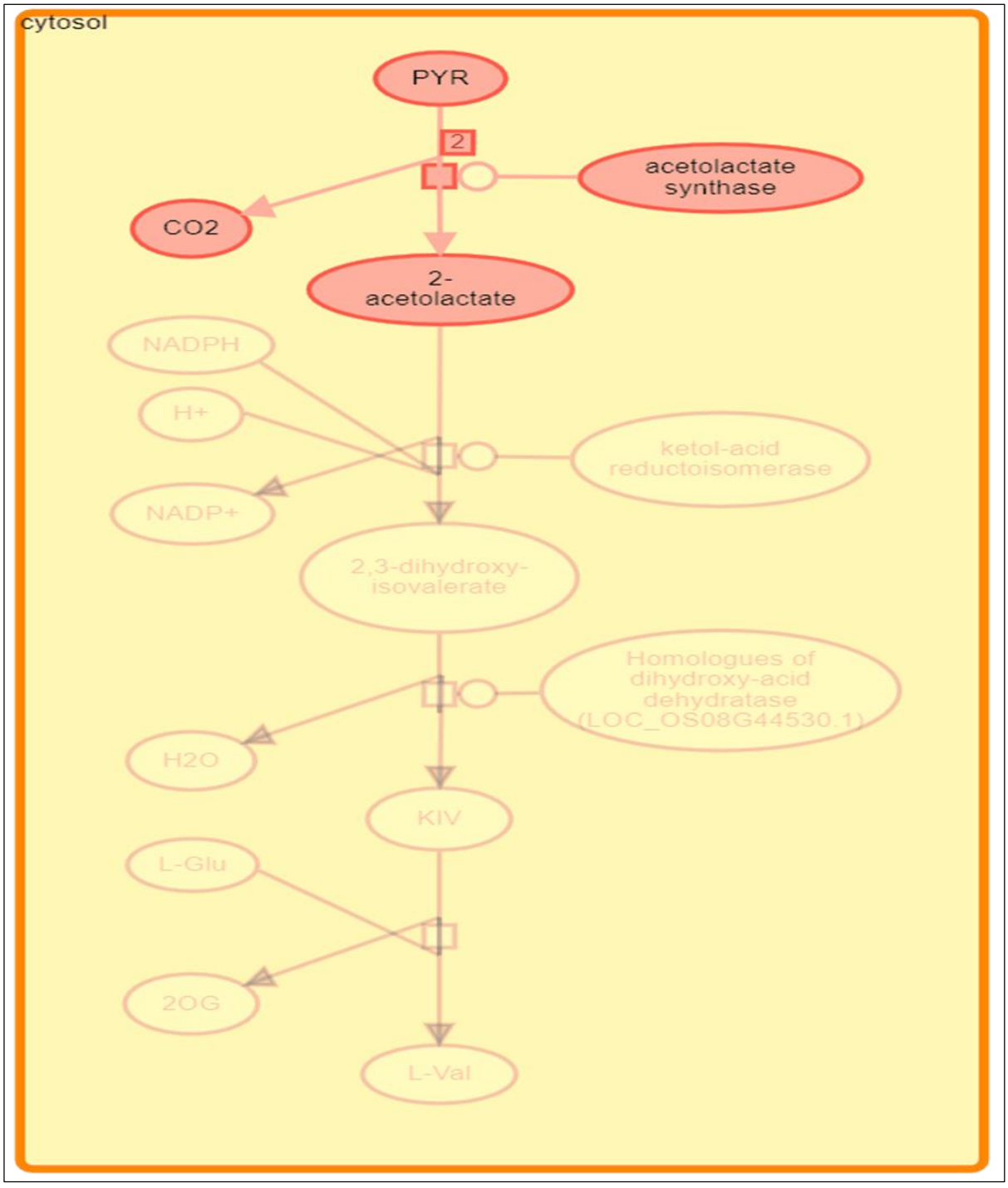

Figure 34. Biosynthesis of the amino acid L-valine. The data utilized to generate the figure is sourced directly from OmicsBox **https://www.biobam.com/omicsbox/** (accessed on 4 June 2025). The graphic depicts the mechanisms activated by the identified genes.
***PYR**: Pyruvate. **[2]**: 2 molecules of pyruvate. **NADPH**: nicotinamide adenine dinucleotide phosphate (Reduced form). **NADP**$^{+}$: nicotinamide adenine dinucleotide phosphate (oxidized form). **KIV**: 2-ketoisolvalerate. **L-Glu**: L-glutamate. **2OG**: 2-oxoglutarate (α-ketoglutarate). **L-Val**: L-valine.*

In Figure 32, since Zn is a critical cofactor for the enzymes that convert the tryptophan amino acid into indole acetic acid (IAA), auxin, which plays a vital role in plant elongation. This pathway provided the mechanistic basis for how ZnO-NPs application maintains hormonal balance and promotes cell elongation, directly supporting our morphological results. In Figures 33 and 34, the branched-chain amino acid (BCAA) pathways are critical for osmotic adjustment and metabolic reprogramming during salinity stress. These pathways illustrated how the plant regulated nitrogen metabolism and energy production when chlorophyll, critical for photosynthesis, was inhibited by salt stress. These figures served as the molecular map for the discussion on how ZnO-NPs act as metabolic elicitors.

An elevation in valine production safeguards cells against oxidative stress by diminishing reactive oxygen species (ROS) and enhancing mitochondrial activity; valine metabolism is a crucial regulator of photosynthesis and respiration. A study demonstrated that valine enhances the expression of genes related to mitochondrial function, such as peroxisome proliferator-activated receptor-γ coactivator 1α (PGC-1α), which supports cellular energy production during oxidative stress induced by H_2O_2 (Sharma et al., 2023). There is strong evidence that proteins with valine-glutamine (VQ) motifs are essential for plant development, growth, and stress responses. These proteins have a core sequence that is very conserved and reads F(aa)(aa)(hydrophobic aa)VQ(aa)(hydrophobic aa)TG, as aa refers to amino acid (Shan et al., 2021). Through their interactions with other proteins, notably WRKY transcription factors, some VQ proteins contribute to stress tolerance (Yuan et al., 2021).

Among plant transcriptional regulators, the WRKY family is by far the largest. Binding to the conserved V and Q residues of the VQ proteins, they regulate biological processes in plants and react to various biotic and abiotic stresses (Lai et al., 2011). In a previous study, six motifs were identified in maize (Song et al., 2016). Song et al. (2016 showed that similar to VQ genes in Arabidopsis and rice, a significant proportion of *ZmVQ* genes (67.21%) demonstrated expression that was responsive to drought and osmotic stress. Biotic and abiotic stresses induced the expression of 22 out of 39 VQ genes in rice (Kim et al., 2013). Analogous to *ZmVQ* genes which encode maize VQ proteins (*ZmVQ21*, *ZmVQ13*, and *ZmVQ1*), *OsVQ* genes which encode rice VQ proteins such as; *OsVQ2*, *OsVQ16*, and *OsVQ20*, they were significantly upregulated by drought (Kim et al., 2013; Song et al., 2016).

The authors of the previous study conducted a comprehensive genome-wide analysis of the gene structure and tissue specificity of VQ domain-containing genes in maize. The expression study of these VQ genes under drought and sodium chloride treatments revealed that certain VQ genes participate in abiotic stress responses.

A strong co-expression correlation between VQ genes and WRKY genes indicates that numerous VQ and WRKY genes are probably functionally interconnected (Song et al., 2016). The previous investigations explained the crucial role of the valine regulation in response to stress in plants.

Salinity stress dramatically increased transcript abundance of thiamine biosynthesis genes (THI4, THIC, TH1, and TPK). The transcript expressions are highest in leaves, supporting the assumption that thiamine production occurs in chloroplasts (Yusof, 2019). Increasing polyethylene glycol (PEG) and NaCl concentrations caused osmotic and salt stress, leading to a substantial rise in total thiamine content in maize seedlings. In maize seedlings, higher thiamine levels were linked to higher abscisic acid (ABA) levels (Tunc-Ozdemir et al., 2009). Additionally, drought and salinity stress conditions led to a slight increase in transketolase activity, a key TPP-dependent enzyme. The disruption of transketolase activity shows that thiamine metabolism plays a role in plant stress adaptation (Tunc-Ozdemir et al., 2009).

4.11. Determination of the antimicrobial activities of the aqueous and diethyl ether extracts from tomato and maize leaves

The antimicrobial activity was determined against foodborne pathogenic bacteria (antibacterial) and mycotoxigenic fungi (antifungal activity). According to the aqueous extract from **tomato leaves**, it was reported in Figure 35 that T1, T3, and T4 extracts had the highest antibacterial activity against *B. cereus*, followed by T2, T5, and T6 extracts. For *E. coli* and *Staph. aureus*, there was no significant difference between the six treatments' extracts (T1-T6) except the positive control (tetracycline), which had the highest effect. For *L. monocytogenes*, *S. typhi*, and *P. aeruginosa*, T1 extract had the highest activity. On the other hand, the diethyl ether extract from tomato leaves showed no significant differences between the six different treatments extracts (T1-T6) with *L. monocytogenes* and *P. aeruginosa* (Figure 36). However, T1 extract had the highest activity against *E. coli* and *S. typhi*. T6 extract had the highest activity against *B. cereus*, and T2 extract had the highest activity against *Staph. aureus*.

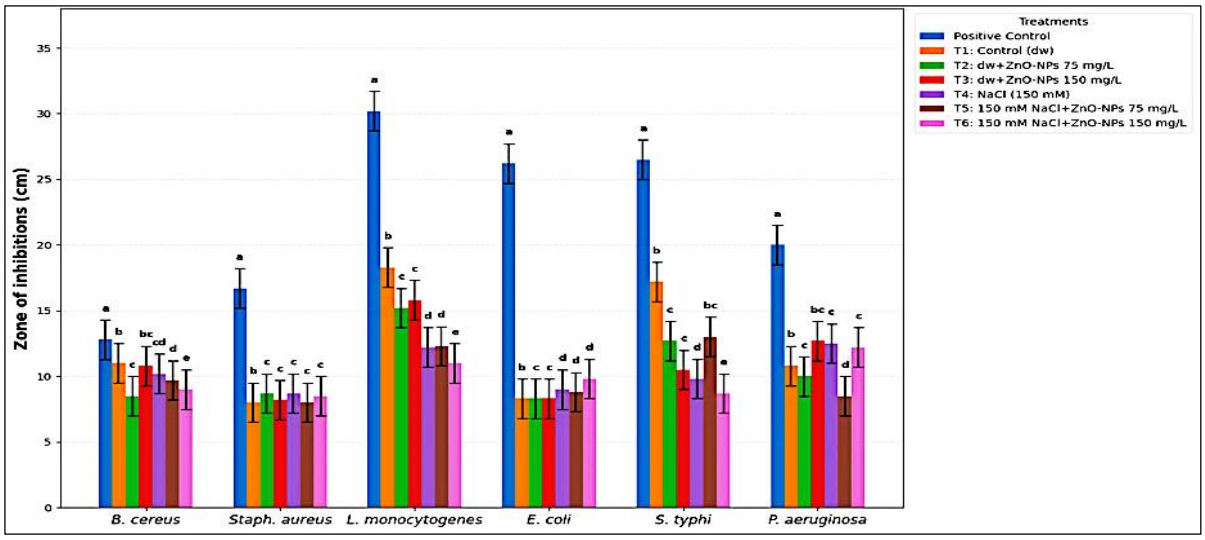

Figure 35. Antibacterial activity of tomato aqueous extract against different bacterial strains by disc diffusion method. *+Ve Ctrl: tetracycline. Each value represents the mean ± SE. The lower-case letters above the values (bars) indicate the significance level. The same letter over values denotes that they are not significantly different at ($p \leq 0.05$), and comparison is performed according to each strain with all samples (confidence intervals corrected using Tukey method).*

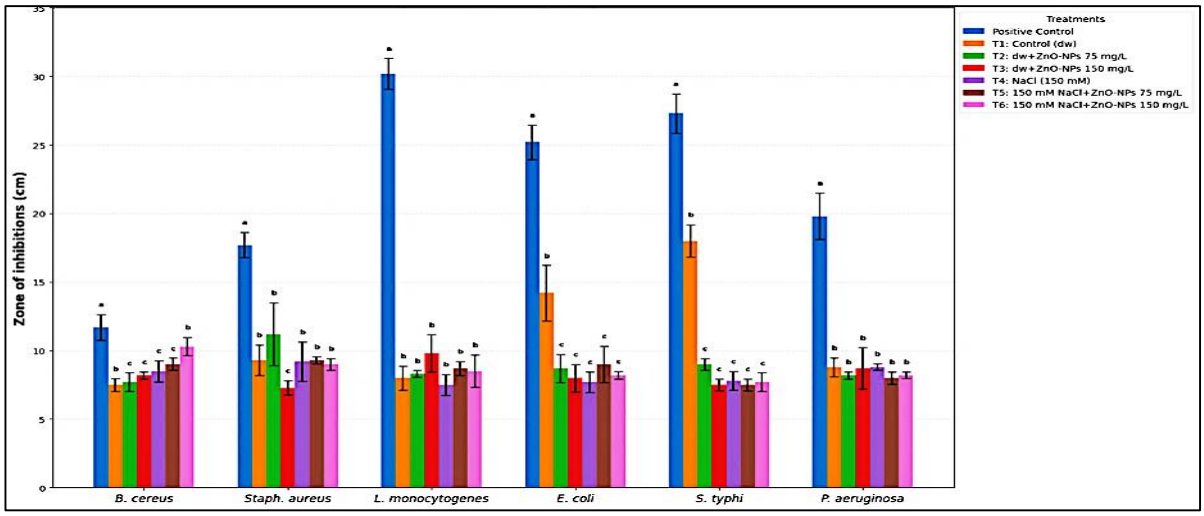

Figure 36. Antibacterial activity of tomato diethyl ether extract against different bacterial strains by disc diffusion method. *+Ve Ctrl: tetracycline. Each value represents the mean ± SE. The lower-case letters above the values (bars) indicate the significance level. The same letter over values denotes that they are not significantly different at ($p \leq 0.05$), and comparison is performed according to each strain with all samples (confidence intervals corrected using Tukey method).*

Following the antifungal activity, the aqueous extract from the tomato leaves showed varying results against the fungi (Figure 37), depending on the examined treatment extracts. There was a trend that the aqueous extract from T1 plants showed the highest activity against all the tested mycotoxigenic fungi; *A. flavus*, *A. niger*, *A. carbonarius*, *A. ochraceus*, *F. verticilioides*, and *F. proliferatium*, followed by the extract from T2 plants that were not stressed but sprayed with 75 mg/L ZnO-NPs. For the diethyl ether extract, there was no significant difference between the different extracts from all the treatments against the fungi (Figure 38); *A. carbonarius*, *A. ochraceus*, and *A. flavus*. But, T1 extract showed the highest activity against *F. verticilioides* and *F. proliferatium*. T2 and T4 extract showed the highest activity against *A. niger*.

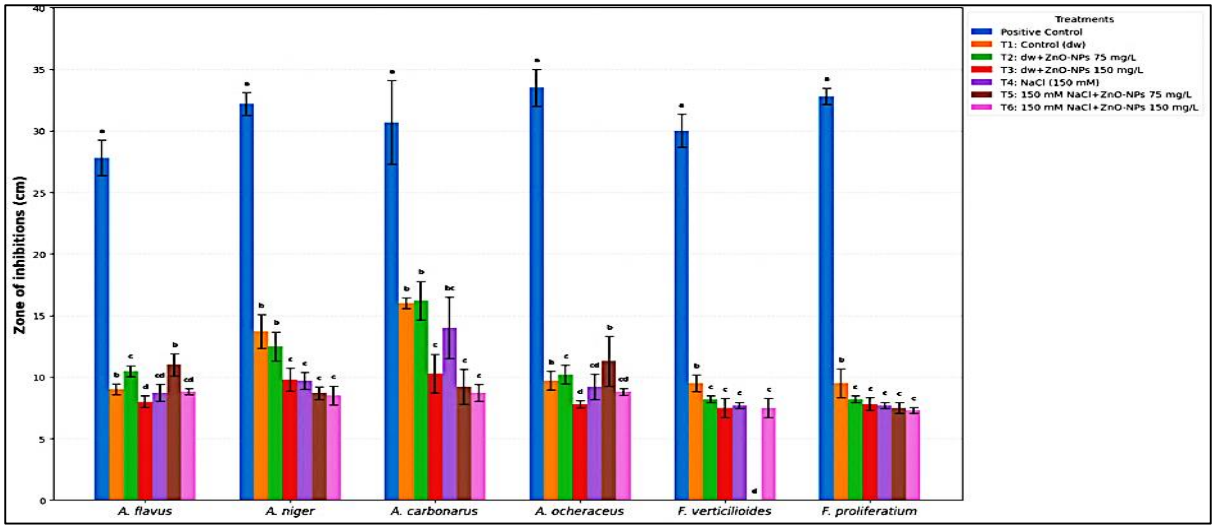

Figure 37. Antifungal activity of tomato diethyl ether extract against different fungal strains by disc diffusion method. *+Ve Ctrl: nystatin. Each value represents the mean ± SE. The lower-case letters above the values (bars) indicate the significance level. The same letter over values denotes that they are not significantly different at ($p \leq 0.05$), and comparison is performed according to each strain with all samples (confidence intervals corrected using Tukey method).*

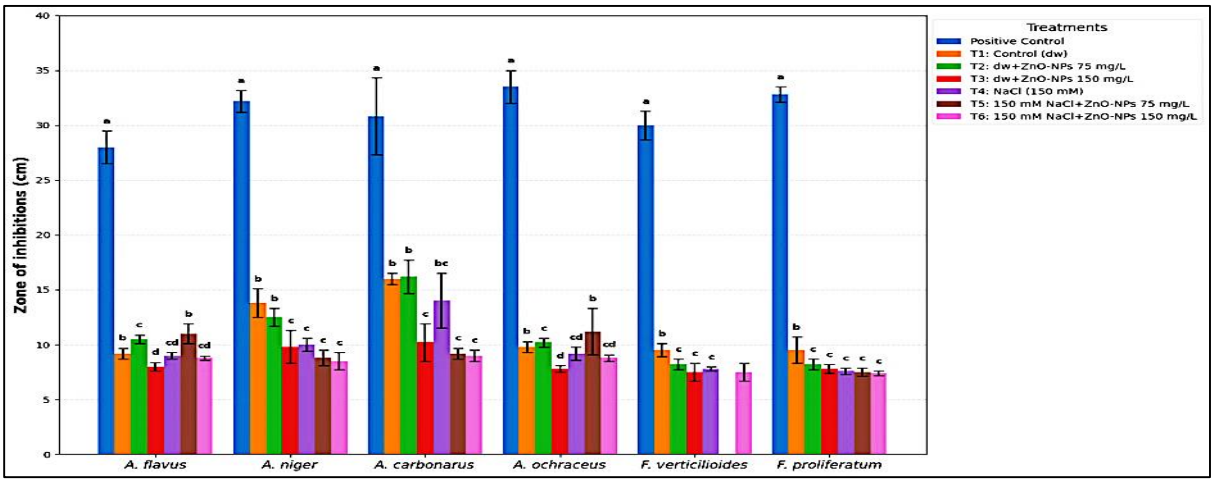

Figure 38. Antifungal activity of tomato aqueous extract against different fungal strains by disc diffusion method. *+Ve Ctrl: nystatin. Each value represents the mean ± SE. The lower-case letters above the values (bars) indicate the significance level. The same letter over values denotes that they are not significantly different at ($p \leq 0.05$), and comparison is performed according to each strain with all samples (confidence intervals corrected using Tukey method).*

As illustrated in Table 27, the aqueous extract of different treatments exhibited minimum inhibitory concentration (MIC) values within the range of 1.08 to 0.42 mg/mL against *Staph. aureus*, and the most potent activity with the lowest MIC value of 0.42 mg/mL resulted from T6 aqueous extract. No notable distinction was observed among various treatments concerning the following pathogenic bacteria: *B. cereus*, *E. coli*, and *L. monocytogenes.* The lowest MIC values against *S. typhi* resulted from T1, T2, and T5 aqueous extracts with 0.15, 0.2, and 0.2 mg/mL, respectively. While T3 aqueous extract had the highest activity (lowest MIC) against *P. aeruginosa*.

Table 27. Minimum inhibitory concentration (mg/mL) of tomato leaf aqueous extracts against pathogenic bacteria.

Bacteria	T1	T2	T3	T4	T5	T6
B. cereus	0.15 ± 0.08^{a}	0.33 ± 0.12^{a}	0.07 ± 0.08^{a}	0.28 ± 0.18^{a}	0.42 ± 0.13^{a}	0.33 ± 0.12^{a}
Staph. aureus	0.67 ± 0.12^{ab}	0.75 ± 0.22^{ab}	1.08 ± 0.12^{a}	0.67 ± 0.12^{ab}	0.83 ± 0.25^{ab}	0.42 ± 0.25^{b}
L. monocytogenes	0.1 ± 0.00^{a}	0.15 ± 0.0^{a}	0.2 ± 0.08^{a}	0.28 ± 0.20^{a}	0.37 ± 0.23^{a}	0.2 ± 0.08^{a}
E. coli	0.58 ± 0.12^{a}	0.83 ± 0.12^{a}	0.58 ± 0.34^{a}	0.42 ± 0.12^{a}	0.33 ± 0.12^{a}	0.42 ± 0.12^{a}
S. typhi	0.15 ± 0.08^{b}	0.2 ± 0.08^{b}	0.42 ± 0.12^{ab}	0.5 ± 0.22^{ab}	0.2 ± 0.08^{b}	0.67 ± 0.12^{a}
P. aeruginosa	0.42 ± 0.12^{ab}	0.58 ± 0.12^{ab}	0.33 ± 0.12^{b}	0.42 ± 0.12^{ab}	0.83 ± 0.12^{a}	0.5 ± 0.22^{ab}

Each value represents the mean ± SE (n=4). Values with the same letter are not significantly different at ($p \leq 0.05$), and the comparison is done according to different treatments in the same column. ***T1****: Control (non-treated) (dw).* ***T2****: (dw + ZnO-NPs 75 mg/L).* ***T3****: (dw + ZnO-NPs 150 mg/L).* ***T4****: NaCl (150 mM).* ***T5****: (150 mM NaCl + ZnO-NPs 75 mg/L).* ***T6****: (150 mM NaCl + ZnO-NPs 150 mg/L).*

Table 28 shows the MIC results of the diethyl ether extracts from different treatments against the food-borne pathogenic bacteria. In case of *B. cereus*, the diethyl ether extract from T6 showed the highest effect with 0.41 mg/mL. *Staph. aureus* was highly affected by the diethyl ether extract from T2, followed by T1 with 0.2 and 0.33 mg/L. T3 extract showed the lowest MIC value against *L. monocytogenes* with 0.33 mg/mL, while T1 extract had the highest effect against *E. coli* with 0.2 mg/mL. For *S. typhi* and *P. aeruginosa*, they were highly affected by the extracts of T1 with 0.15 and 0.58 mg/mL, compared to the other treatment extracts.

Table 28. Minimum inhibitory concentration (mg/mL) of tomato leaf diethyl ether extracts against pathogenic bacteria.

Bacteria	T1	T2	T3	T4	T5	T6
B. cereus	1.0 ± 0.22^{a}	0.92 ± 0.12^{ab}	0.83 ± 0.12^{ab}	0.67 ± 0.12^{ab}	0.58 ± 0.08^{ab}	0.41 ± 0.05^{b}
Staph. aureus	0.33 ± 0.12^{b}	0.2 ± 0.08^{b}	0.92 ± 0.12^{a}	0.58 ± 0.25^{ab}	0.5 ± 0.22^{ab}	0.58 ± 0.12^{ab}
L. monocytogenes	0.83 ± 0.12^{ab}	0.58 ± 0.12^{ab}	0.33 ± 0.08^{b}	0.92 ± 0.25^{a}	0.58 ± 0.12^{ab}	0.67 ± 0.25^{ab}
E. coli	0.2 ± 0.08^{b}	0.67 ± 0.28^{ab}	0.92 ± 0.12^{a}	1.08 ± 0.28^{a}	0.67 ± 0.14^{ab}	0.58 ± 0.14^{ab}
S. typhi	0.15 ± 0.08^{c}	0.42 ± 0.12^{bc}	1.08 ± 0.11^{a}	1.0 ± 0.22^{ab}	1.08 ± 0.26^{a}	0.92 ± 0.34^{ab}
P. aeruginosa	0.58 ± 0.12^{b}	0.83 ± 0.11^{ab}	0.67 ± 0.12^{b}	0.58 ± 0.08^{b}	1.08 ± 0.12^{a}	0.92 ± 0.12^{ab}

Each value represents the mean ± SE (n=4). Values with the same letter are not significantly different at ($p \leq 0.05$), and the comparison is done according to different treatments in the same column. ***T1****: Control (non-treated) (dw).* ***T2****: (dw + ZnO-NPs 75 mg/L).* ***T3****: (dw + ZnO-NPs 150 mg/L).* ***T4****: NaCl (150 mM).* ***T5****: (150 mM NaCl + ZnO-NPs 75 mg/L).* ***T6****: (150 mM NaCl + ZnO-NPs 150 mg/L).*

As illustrated in Table 29, the aqueous extract of different treatments exhibited the most potent activity with the lowest MIC value of 0.33 mg/mL, resulting from T2 aqueous extract, followed by T5 extract with 0.42 mg/mL against *A. flavus*. T1 aqueous extract had the highest activity against *A. niger* with 0.2 mg/mL, while *A. carbonarius* was highly affected by T2 and T1 extracts, with 0.15 mg/mL for both. T5 extract had the highest activity with the lowest MIC against *A. ochraceus* with 0.28 mg/mL. For *F. verticilioides* and *F. proliferatium*, both were highly affected by T1 aqueous extract with 0.58 mg/mL from both extracts.

Table 29. Minimum inhibitory concentration (mg/mL) of tomato leaf aqueous extracts against mycotoxigenic fungi.

Fungi	T1	T2	T3	T4	T5	T6
A. flavus	0.58 ± 0.12^{bc}	0.33 ± 0.04^{c}	1.08 ± 0.11^{a}	0.67 ± 0.12^{bc}	0.42 ± 0.08^{c}	0.83 ± 0.12^{ab}
A. niger	0.2 ± 0.07^{c}	0.42 ± 0.08^{bc}	0.67 ± 0.13^{abc}	0.58 ± 0.11^{abc}	0.92 ± 0.12^{a}	0.83 ± 0.15^{ab}
A. carbonarius	0.15 ± 0.08^{c}	0.15 ± 0.07^{c}	0.67 ± 0.15^{abc}	0.28 ± 0.08^{bc}	0.83 ± 0.15^{ab}	1.00 ± 0.22^{a}
A. ochraceus	0.67 ± 0.14^{ab}	0.58 ± 0.14^{ab}	0.67 ± 0.18^{ab}	0.83 ± 0.14^{a}	0.28 ± 0.10^{b}	0.83 ± 0.14^{a}
F. verticilioides	0.58 ± 0.12^{c}	1.08 ± 0.08^{bc}	1.33 ± 0.25^{b}	1.42 ± 0.12^{b}	2.16 ± 0.25^{a}	1.25 ± 0.22^{b}
F. proliferatium	0.58 ± 0.05^{c}	0.83 ± 0.12^{bc}	1.16 ± 0.12^{ab}	1.42 ± 0.12^{a}	1.17 ± 0.13^{ab}	1.33 ± 0.12^{a}

Each value represents the mean ± SE (n=4). Values with the same letter are not significantly different at ($p \leq 0.05$), and the comparison is done according to different treatments in the same column. ***T1****: Control (non-treated) (dw).* ***T2****: (dw + ZnO-NPs 75 mg/L).* ***T3****: (dw + ZnO-NPs 150 mg/L).* ***T4****: NaCl (150 mM).* ***T5****: (150 mM NaCl + ZnO-NPs 75 mg/L).* ***T6****: (150 mM NaCl + ZnO-NPs 150 mg/L).*

Table 30 shows the MIC results of the diethyl ether extracts from different treatments against the mycotoxigenic fungi. T2 diethyl ether extract had the highest activity against *A. flavus* with 0.33 mg/mL, while the same extract had also the highest effect against *A. niger* with 0.58 mg/mL compared to the other treatment extracts. *A. carbonarius* was highly affected by T1 extract with 0.58 mg/mL, and for *A. ochraceus*, extracts of T1, T3, T4, and T5 had the lowest MICs within the range of 0.58 to 0.67 mg/mL. For *F. verticilioides* and *F. proliferatium*, both were highly affected by T1 aqueous extract with 0.58 and 0.33 mg/mL, respectively.

Table 30. Minimum inhibitory concentration (mg/mL) of tomato leaf diethyl ether extracts against mycotoxigenic fungi.

Fungi	T1	T2	T3	T4	T5	T6
A. flavus	0.67 ± 0.12^{ab}	0.33 ± 0.08^{b}	1.08 ± 0.12^{a}	0.58 ± 0.12^{ab}	0.75 ± 0.22^{ab}	0.92 ± 0.14^{ab}
A. niger	1.33 ± 0.15^{a}	0.58 ± 0.08^{c}	0.83 ± 0.1^{2bc}	0.67 ± 0.11^{c}	1.08 ± 0.12^{ab}	0.92 ± 0.13^{bc}
A. carbonarius	0.58 ± 0.08^{b}	0.67 ± 0.12^{ab}	1.08 ± 0.13^{a}	0.67 ± 0.08^{ab}	0.83 ± 0.12^{ab}	1.0 ± 0.12^{ab}
A. ochraceus	0.67 ± 0.12^{b}	0.75 ± 0.15^{ab}	0.67 ± 0.14^{b}	0.58 ± 0.08^{b}	0.67 ± 0.12^{b}	1.16 ± 0.14^{a}
F. verticilioides	0.58 ± 0.12^{d}	0.67 ± 0.11^{cd}	1.16 ± 0.12^{bc}	1.33 ± 0.25^{b}	1.33 ± 0.13^{b}	2.33 ± 0.25^{a}
F. proliferatium	0.33 ± 0.08^{b}	0.58 ± 0.12^{ab}	0.75 ± 0.22^{ab}	0.67 ± 0.11^{ab}	0.83 ± 0.12^{ab}	1.0 ± 0.22^{a}

Each value represents the mean ± SE (n=4). Values with the same letter are not significantly different at ($p \leq 0.05$), and the comparison is done according to different treatments in the same column. ***T1****: Control (non-treated) (dw).* ***T2****: (dw + ZnO-NPs 75 mg/L).* ***T3****: (dw + ZnO-NPs 150 mg/L).* ***T4****: NaCl (150 mM).* ***T5****: (150 mM NaCl + ZnO-NPs 75 mg/L).* ***T6****: (150 mM NaCl + ZnO-NPs 150 mg/L).*

For the maize samples, according to the aqueous extract from maize leaves, it was reported in Figure 39 that M1, M3, and M4 extracts had the highest antibacterial activity against *B. cereus*, followed by M2 extracts. For *E. coli*, *Staph. aureus*, *L. monocytogenes*, and *P. aeruginosa* there was no significant difference between the four treatments' extracts (M1-M4) except the positive control (tetracycline), which had the highest effect. For *S. typhi*, M2, M3, and M4 extracts had the highest activity compared to M1. On the other hand, the diethyl ether extract from maize leaves showed no significant differences between the four different treatments extracts (M1-M4) with *B. cereus* (Figure 40). For *E. coli*, *Staph. aureus*, *L. monocytogenes*, and *P. aeruginosa* there was no significant difference between the four treatments' extracts (M1-M4) except the positive control (tetracycline), which had the highest effect. . For *S. typhi*, M2, M3, and M4 extracts had the highest activity compared to M1.

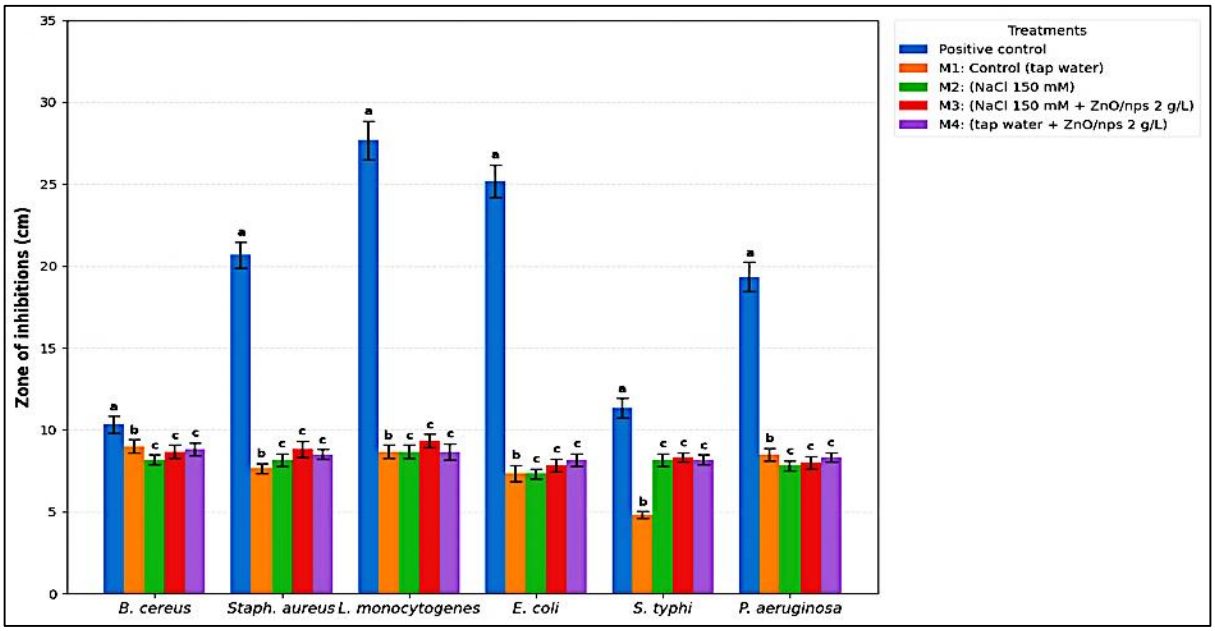

Figure 39. Antibacterial activity of maize aqueous extract against different bacterial strains by disc diffusion method.

+Ve Ctrl: tetracycline. Each value represents the mean ± SE (n=4). The significance of the numbers is shown by the lowercase letters that appear above them. Two values are not substantially different ($p < 0.05$) if they share a letter. All samples were statistically compared to each item (confidence intervals corrected using Tukey method).

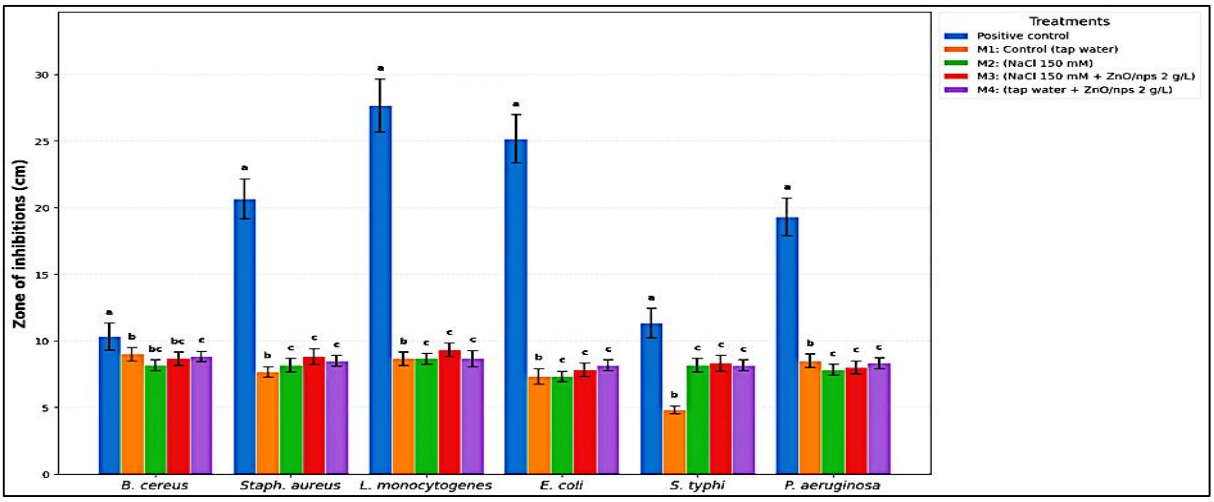

Figure 40. Antibacterial activity of maize diethyl ether extract against different bacterial strains by disc diffusion method.

+Ve Ctrl: tetracycline. Each value represents the mean ± SE (n=4). The significance of the numbers is shown by the lowercase letters that appear above them. Two values are not substantially different ($p < 0.05$) if they share a letter. All samples were statistically compared to each item (confidence intervals corrected using Tukey method).

Following the antifungal activity, the aqueous extract from the maize leaves showed no significant differences between the extracts of the M1-M4 treatments (Figure 41) with *A. flavus*, *A. niger*, *A. ocheraceus*, *F. verticilioides*, and *F. proliferatium*, and *P. vercosum*, except the positive control (nystatin). For the diethyl ether extract, there was no significant difference between the different extracts from all the treatments against the following fungi *A. flavus*, *A. niger*, *A. ocheraceus*, *F. verticilioides*, and *F. proliferatium* (Figure 42); except with *P. vercosum*, as the M4 diethyl extract showed the highest antifungal activity against it, followed by M3, then M1 and M2.

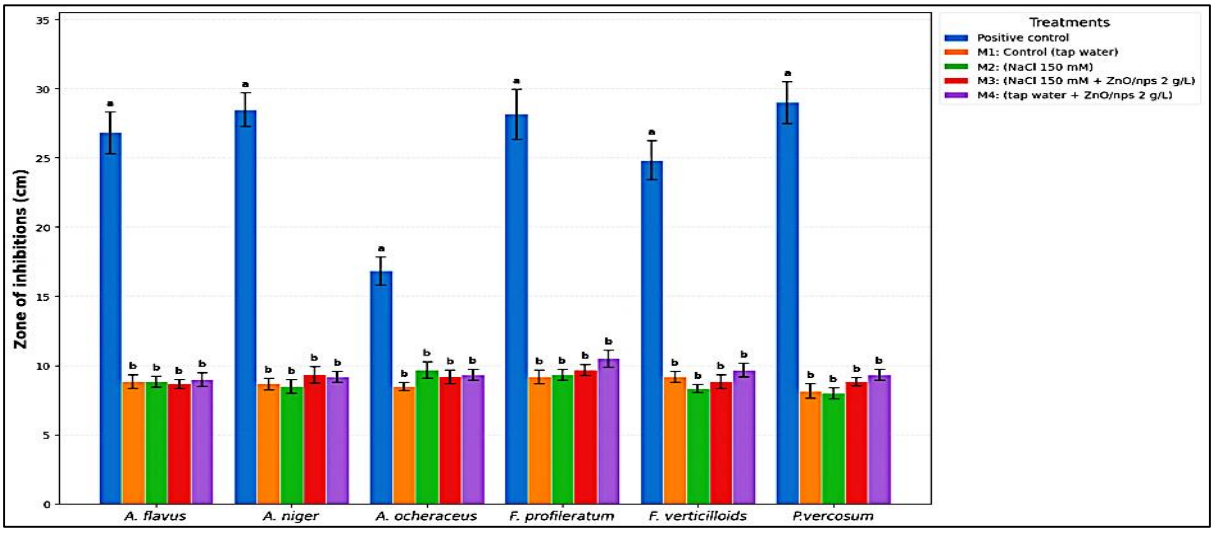

Figure 41. Antifungal activity of maize aqueous extract against different fungal strains by disc diffusion method.

+Ve Ctrl: nystatin. Each value represents the mean ± SE (n=4). The significance of the numbers is shown by the lowercase letters that appear above them. Two values are not substantially different ($p < 0.05$) if they share a letter. All samples were statistically compared to each item (confidence intervals corrected using Tukey method).

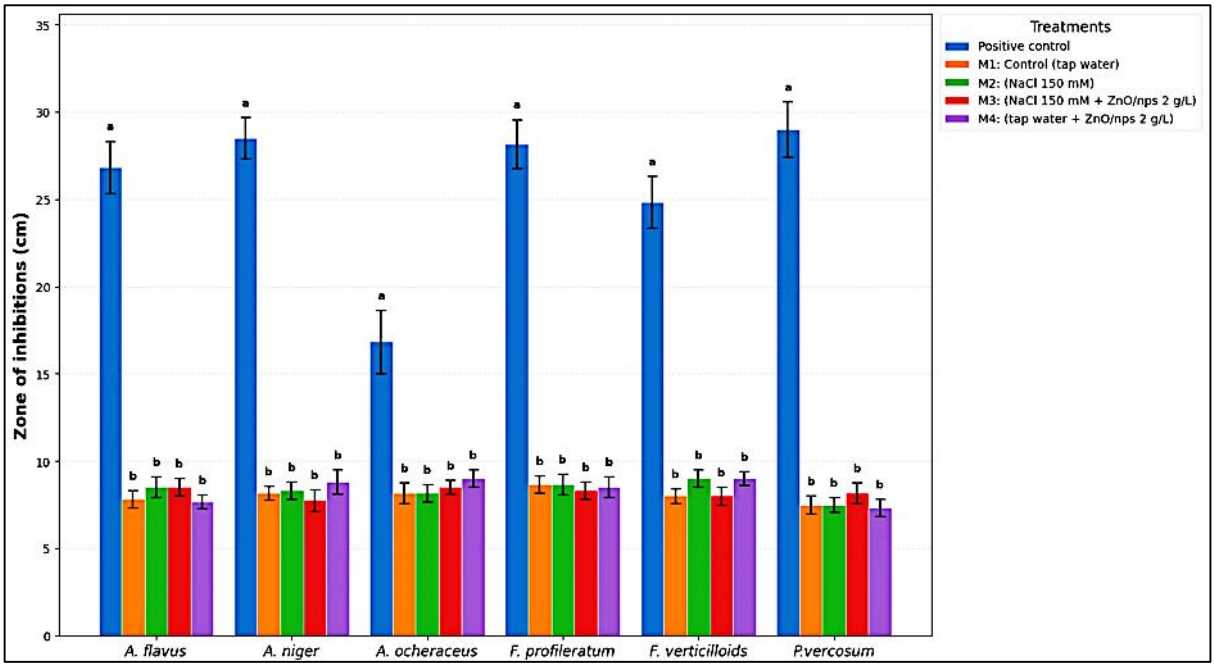

Figure 42. Antifungal activity of maize diethyl ether extract against different fungal strains by disc diffusion method.

+Ve Ctrl: nystatin. Each value represents the mean ± SE (n=4). The significance of the numbers is shown by the lowercase letters that appear above them. Two values are not substantially different ($p < 0.05$) if they share a letter. All samples were statistically compared to each item (confidence intervals corrected using Tukey method).

As illustrated in Table 31, the aqueous extract of different treatments exhibited minimum inhibitory concentration (MIC) values within the range of 1.08 to 0.67 mg/mL against *L. monocytogenes*, and the most potent activity with the lowest MIC value of 0.67 mg/mL resulted from M3 aqueous extract. No notable distinction was observed among various treatments concerning the following pathogenic bacteria: *B. cereus*, *Staph. aureus*, *E. coli*, and *P. aeruginosa*. The lowest MIC values against *S. typhi* resulted from M3 and M4 aqueous extracts with 0.92, and 0.83 mg/mL, respectively. Table 32 shows the MIC results of the diethyl ether extracts from different treatments against the pathogenic bacteria. M3 aqueous extract had the highest activity (lowest MIC) against *S. typhi* with 0.20 mg/mL. In case of *B. cereus*, *Staph. aureus*, and *P. aeruginosa* the diethyl ether extracts showed no notable distinction was observed among various treatments. M4 extract showed the lowest MIC value against *E. coli* with 0.33 mg/mL, while for *L. monocytogenes*, it was highly affected by the extract of M4 with 0.15 mg/mL, compared to the other treatment extracts.

Table 31. The minimal concentration (mg/mL) inhibiting the different bacterial strains using the maize leaf aqueous extracts.

Bacteria	M1	M2	M3	M4
B. cereus	0.58±0.13^{a}	0.67±0.13^{a}	0.58±0.13^{a}	0.33±0.13^{a}
Staph. aureus	1.25±0.22^{a}	0.92±0.13^{a}	0.83±0.13^{a}	0.92±0.13^{a}
L. monocytogenes	1.08±0.14^{a}	0.83±0.14^{ab}	0.67±0.14^{ab}	0.92±0.29^{b}
E. coli	1.83±0.26^{a}	1.67±0.26^{a}	1.58±0.34^{a}	0.92±0.13^{a}
S. typhi	1.67±0.29^{a}	1.17±0.26^{ab}	0.92±0.13^{b}	0.83±0.13^{b}
P. aeruginosa	1.83±0.26^{a}	2.17±0.26^{a}	2.33±0.26^{a}	1.67±0.26^{a}

Each value represents the mean ± SE (n=4). Values with the same letter are not significantly different at ($p \leq 0.05$), and the comparison is done according to different treatments in the same column. ***M1****: Control (tap water);* ***M2****: (NaCl 150 mM);* ***M3****: (NaCl 150 mM + ZnO-NPs 2 g/L); and* ***M4****: (tap water + ZnO-NPs 2 g/L).*

Table 32. The minimal concentration (mg/mL) inhibiting the different bacterial strains using the maize leaf diethyl ether extracts.

Bacteria	M1	M2	M3	M4
B. cereus	0.20±0.08^{a}	0.15±0.08^{a}	0.20±0.08^{a}	0.23±0.21^{a}
Staph. aureus	0.37±0.21^{a}	0.58±0.13^{a}	0.67±0.13^{a}	0.58±0.13^{a}
L. monocytogenes	0.83±0.13^{a}	0.33±0.13^{ab}	0.42±0.13^{ab}	0.15±0.08^{b}
E. coli	0.83±0.14^{a}	0.58±0.14^{b}	0.50±0.25^{b}	0.33±0.14^{b}
S. typhi	0.58±0.13^{a}	0.42±0.13^{ab}	0.20±0.08^{b}	0.15±0.08^{b}
P. aeruginosa	1.17±0.26^{a}	1.33±0.26^{a}	1.17±0.26^{a}	0.67±0.13^{a}

Each value represents the mean ± SE (n=4). Values with the same letter are not significantly different at ($p \leq 0.05$), and the comparison is done according to different treatments in the same column. ***M1****: Control (tap water);* ***M2****: (NaCl 150 mM);* ***M3****: (NaCl 150 mM + ZnO-NPs 2 g/L); and* ***M4****: (tap water + ZnO-NPs 2 g/L).*

As illustrated in Table 33, the aqueous extract of different treatments exhibited minimum inhibitory concentration (MIC) values within the range of 1.67 to 0.83 mg/mL against *F. verticilloids*, and the most potent activity with the lowest MIC value of 0.83 mg/mL resulted from M2 aqueous extract. No notable distinction was observed among various treatments concerning the following fungi: *A. niger*, *A. flavus*, *A. ochraceus*, *F. proliferatum*, and *P. vercosum*. As illustrated in Table 34, the aqueous extract of different treatments exhibited minimum inhibitory concentration (MIC) values within the range of 1.17 to 0.14 mg/mL against *A. flavus*, and the most potent activity with the lowest MIC value of 0.14 mg/mL resulted from M3 aqueous extract.

No notable distinction was observed against *A. niger* according to all the treatments. For *A. ocheraceus*, the lowest MIC which represented the highest activity was obtained from M2, M3, and M4 with 0.75, 0.14, and 0.42 mg/mL, respectively. While *F. proliferatum*, and *P. vercosum* were highly affected by the M3 and M4 extracts with 0.14 and 0.20 mg/mL for the first, 0.14 and 0.58 mg/mL for the second, respectively, and no significant differences were obtained at the effect of M1 and M2 extracts against both fungi.

Table 33. The minimal concentration (mg/mL) inhibiting the different fungal strains using the maize leaf aqueous extracts.

Fungi	M1	M2	M3	M4
A. flavus	1.83±0.58^{a}	1.25±0.25^{a}	1.33±0.29^{a}	1.83±0.29^{a}
A. niger	1.58±0.38^{a}	1.17±0.14^{a}	1.58±0.38^{a}	0.83±0.14^{a}
A. ocheraceus	1.67±0.29^{a}	1.67±0.76^{a}	1.17±0.14^{a}	0.92±0.14^{a}
F. profileratum	1.08±0.14^{a}	0.92±0.14^{a}	1.08±0.14^{a}	1.00±0.25^{a}
F. verticilloids	1.33±0.29^{ab}	0.83±0.14^{b}	1.50±0.43^{ab}	1.67±0.29^{a}
P. vercosum	1.67±1.04^{a}	2.17±0.29^{a}	1.33±0.29^{a}	1.83±0.29^{a}

Each value represents the mean ± SE (n=4). Values with the same letter are not significantly different at ($p \leq 0.05$), and the comparison is done according to different treatments in the same column. ***M1****: Control (tap water);* ***M2****: (NaCl 150 mM);* ***M3****: (NaCl 150 mM + ZnO-NPs 2 g/L); and* ***M4****: (tap water + ZnO-NPs 2 g/L).*

Table 34. The minimal concentration (mg/mL) inhibiting the different fungal strains using the maize leaf diethyl ether extracts.

Fungi	M1	M2	M3	M4
A. flavus	1.08±0.14^{ab}	1.17±0.29^{a}	0.92±0.14^{a}	0.67±0.14^{b}
A. niger	0.83±0.29^{a}	0.83±0.14^{a}	0.58±0.14^{b}	0.67±0.29^{a}
A. ocheraceus	1.33±0.14^{a}	0.75±0.25^{b}	0.58±0.14^{b}	0.42±0.29^{b}
F. profileratum	0.67±0.14^{a}	0.58±0.14^{a}	0.33±0.14^{b}	0.20±0.09^{b}
F. verticilloids	0.83±0.14^{a}	1.08±0.14^{a}	0.83±0.14^{ab}	0.42±0.14^{b}
P. vercosum	0.92±0.14^{ab}	1.08±0.14^{a}	0.83±0.14^{ab}	0.58±0.14^{b}

Each value represents the mean ± SE (n=4). Values with the same letter are not significantly different at ($p \leq 0.05$), and the comparison is done according to different treatments in the same column. ***M1****: Control (tap water);* ***M2****: (NaCl 150 mM);* ***M3****: (NaCl 150 mM + ZnO-NPs 2 g/L); and* ***M4****: (tap water + ZnO-NPs 2 g/L).*

Tomato and maize plants subjected to salt stress may exhibit altered leaf extract compositions, potentially affecting their efficacy in combating pathogens. Certain studies indicated that salt stress can induce leaves to synthesize increased levels of chemicals, including antioxidants and phenolic compounds. This may enhance the leaves' efficacy in combating pathogens. Conversely, additional studies indicated that salt stress might adversely affect certain plant traits, thereby diminishing their capacity to combat pathogens.

The activation of secondary metabolism is a hallmark of environmental stressors (Pirbalouti, 2019). Attia et al. (2021) used the following fungi in the antifungal test; *Aspergillus niger*; *Candida albicans* (yeast); *Penicillium frequentans*; *Fusarium roseum*; *Mucor plumbeus*, and *Rhizopus stolonifer*. The authors indicated that the constituents of safflower essential oils varied, with one principal compound (γ-cadinene in roots, myrtenal in stems, and β-caryophyllene in leaves) exhibiting a decline, while another compound (β-thujone and 1-pentadecene in roots, stems, and leaves, respectively) demonstrated an increase under saline conditions. The reduced concentrations of these compounds in various regions of salt-treated plants may be attributed to NaCl stress, which induces cellular dehydration. Their research indicated that safflower essential oils had a strong antifungal effect against *Aspergillus niger*. When salt was present, the effect was seen at the level of the leaves, and when salt was not present, it was shown at the level of the stems. The percentages of inhibition were 85% and 82%, respectively. At the root level, this inhibition was 70% for the concentration of essential oils, whether NaCl was present or not.

In a study on *Escherichia coli*, *Staphylococcus aureus*, *Bacillus subtilis*, *Pseudomonas aeruginosa*, and *Klebsiella pneumonia*, the antimicrobial activity was measured by the Kirby–Bauer testing (Forghani et al., 2024). That study examined the antibacterial mechanisms of *Salicornia persica* under salt stress to further understanding of its bacterial resistance. The authors demonstrated that *S. persica* exerted a markedly distinct effect on *E. coli* and *S. aureus* compared to other bacteria examined. They discovered that *E. coli* exhibited the greatest efficacy and possessed the highest antibacterial activity. Upon increasing the salt concentration in the medium, *S. persica* accumulated photosynthetic pigments, carotenoids, soluble carbohydrates, phenolic compounds, and anthocyanins.

Plants cultivated in a medium with 400 mM NaCl exhibited the highest lipid peroxidation, which was 46% and 39% more than that of the control and plants grown in a medium with 200 mM NaCl, respectively. This was associated with an enhancement in total antioxidant capacity and the activity of antioxidant enzymes. The augmented antibacterial activity appears to be associated with elevated concentrations of phenol, anthocyanin, carotenoids, and antioxidants in *S. persica* under salt stress. In another study, the broth microdilution technique was employed to assess the efficacy of the *Spirulina platensis* extracts in inhibiting the growth of *Yersinia ruckeri*, *Salmonella* sp., *Escherichia coli*, and *Vibrio cholerae* bacteria (Sanchooli & Rahdari, 2024). The study's findings indicated that as salt stress increased, the antibacterial efficacy of methanol extracts from spirulina algae against the tested bacteria also intensified.

In the current study, in case of tomato plants, the lowest MIC values against *S. typhi* resulted from T1, T2, and T5 aqueous extracts. While T3 aqueous extract had the highest activity (lowest MIC) against *P. aeruginosa*. It showed that spraying the ZnO-NPs enhanced the antibacterial activity against the afore-mentioned strains. It was also noticed that the fourth treatment (T4) that was completely stressed without any spraying with ZnO-NPs had high values of MIC (low activity) compared to the other aqueous extracts from the rest of the treatments. The same trend was also observed in the case of the antifungal activity, as the plants were sprayed with ZnO-NPs –especially T2 plants- had the lowest MIC values, sharing those highest activities with the control (T1) plants compared to the other treatments. The plants that were stressed with/without spraying ZnO-NPs were not as good as the T1 and T2 aqueous and diethyl ether extracts in inhibiting the mycotoxigenic fungi.

And, in case of maize plants, the most potent antibacterial activity with the lowest MIC value of 0.67 mg/mL resulted from M3 aqueous extract against *L. monocytogenes*. Convesly, it was noticed that the second treatment (M2) that was completely stressed without any spraying with ZnO-NPs had low values of MIC (high activity) compared to the other aqueous extracts from the rest of the treatments, as against *F. verticilloids*, the most potent antifungal activity with the lowest MIC value of 0.83 mg/mL was from aqueous extract of M2 plants.

Those findings were with the aqueous and diethyl ether extracts from tomato and mazie plants, and they may be explained by the lowest concentrations of the protein content in case of the stressed tomato and maize treatments (T4 and M2, respectively). The salinity stress may affect the abilities of the plant extracts against the different pathogenic strains.

The Food and Drug Administration (F.D.A., 2023) states that ZnO-NPs are inorganic substances and are "generally recognized as safe" (GRAS) materials (Sripo-ngam et al., 2024). They serve as a novel class of antibacterial agents against many pathogenic microorganisms. Numerous studies have shown that ZnO-NPs eradicate *Escherichia coli*, *Pseudomonas aeruginosa*, and *Staphylococcus aureus*. They are effective against both gram-positive and gram-negative bacteria (Wang et al., 2017). The antibacterial efficacy of ZnO against bacterial infections is correlated with its surface area. ZnO nanoparticles having a substantial specific surface area have been shown to be highly effective against *E. coli* and *S. aureus* (Babayevska et al., 2022).

Consequently, ZnO-NPs can be securely utilized as pharmaceuticals, preservatives in packaging, and antibacterial agents (Baum et al., 2000). It disseminates effortlessly throughout the meal, eradicates pathogens, and prevents illness. Therefore, it is frequently utilized as a preservative and incorporated into plastic packaging to avoid microbial contamination of food (Espitia et al., 2012).

A significant discovery in this study was that the untreated control plants had antibacterial levels comparable to or above those of the ZnO-treated salt-stressed plants. In a stress-free environment, plants allocate their carbon resources to primary growth and the continuous synthesis of secondary metabolites (Herms & Mattson, 1992; Huot et al., 2014). Even in the presence of ZnO-NPs, the plant undergoes a "metabolic pivot" when subjected to salt stress (Isah, 2019; Munns & Tester, 2008). This indicates that it produces primary osmolytes, such as proline, and antioxidant enzymes to sustain life. Although ZnO-NPs mitigated the detrimental effects of NaCl and aligned the antimicrobial profile with the control, they did not function as a hyper-stimulant (Zulfiqar and Ashraf, 2021). This indicates that the utilization of nanoparticles aids in preserving bioactivity during stress, rather than enhancing the metabolic state beyond ideal developmental settings.

The increased antibacterial efficacy of extracts from ZnO-treated plants is apparent, although the possible influence of residual zinc should be acknowledged. Zinc ions are recognized for their bioaccumulation in leaf tissues after foliar application (Rossi et al., 2019). Despite the mitigatory concentrations employed in this work (75 and 150 mg/L), it is conceivable that trace quantities of Zn^{2+} were sequestered in the extracts. The observed antibacterial activity should be viewed as a synergistic effect: a confluence of nanoparticle-induced metabolic flux (elevated phenolics and flavonoids) and the presence of trace bioactive zinc.

The significant enhancement in antibacterial activity following the application of ZnO-NPs cannot be attributed to a single factor. Our observations indicated a significant increase in phenolic and flavonoid concentrations; nevertheless, it is essential to recognize that bioaccumulated Zn^{2+} or nanoparticles absorbed by cells may be responsible for this phenomenon. Zinc is an acknowledged antibacterial agent; however, its role in our extracts likely functions as a potentiator rather than the sole active ingredient. We propose a synergistic mechanism wherein ZnO-induced metabolites (e.g., quercetin, gallic acid) undermine the structural integrity of the bacterial cell wall, hence increasing the pathogen's susceptibility to trace Zn^{2+} ions. The results should be interpreted as an enhanced plant-defense response that produces a more potent biocomposite extract.

4.12. Results of molecular docking

Table 35 demonstrates docking energy scores (kcal/mol) **for the detected phenolic compounds in tomato**, predicted interactions with key active site residues and their distances (Å) for molecules under investigation against DNA Gyrase inhibitor as an antibacterial target (PDB ID: 3TTZ). Similarly, Table 36 presents the results of the tested compounds against sterol 14-alpha demethylase (CYP51) enzyme (PDB ID: 5FSA), serving as an antifungal target. Accordingly, most of the compounds exhibited high affinity (docking scores) and comparable interactions to the original inhibitor (07N) within the antibacterial target's active site. With the antifungal target attaining some similar interactions within the active site to the native ligand (posaconazole), they did, however, demonstrate relatively high scores. 2D and 3D visualisations of these predicted interactions are shown in Figures 43 and 44 for DNA Gyrase and CYP51, respectively.

The interaction of 07N original ligand, caffeic acid, ferulic acid, and *p*-coumaric acid within DNA Gyrase's active site (as antibacterial targets) has been investigated and illustrated in both two and three dimensions, as shown in Figure 43a, 43b, 43c, and 43d, respectively. The native ligand coordinated two Hydrogen bond interactions to link with the key residues Asp81 and Arg144 at a distance of 2.80 and 3.51 Å, respectively, and a docking score value of −7.4 kcal\mol. When compared to tested compounds, rutin had the highest docking score for the antibacterial activity (−7.3 kcal\mol), followed by quercetin, sinapic, and apigenin-7-glucoside (−5.7, −5.6, and −5.6 kcal\mol, respectively). However, when considering their interactions, they showed only one hydrogen bond interaction with either ASP 81 or ARG 144. Three of the tested compounds (ferulic acid, caffeic acid and *p*-coumaric acid) scored lower binding affinities (−5.2, −5.1 and −4.6 kcal\mol, respectively), but attained the same mode of interaction like 07N, mediating two hydrogen bond interactions to bind with ASP 81 and ARG 144. All other compounds, apart from apigenin, which did not exhibit any interactions within the active site, were able to form at least one hydrogen bond with either ASP 81 or ARG 144, regardless of their scores.

Table 35. Docking energy scores (S), interactions and distances for the investigated molecules against DNA Gyrase inhibitor as an antibacterial target (PDB Id: 3TTZ).

Studied Compounds	**3TTZ docking site**		
	S (kcal/mol)	**Interaction**	**Distance (Å)**
Original ligand, 07N	−7.4	ASP 81 (H-donor)	2.80
		ARG 144 (H-acceptor)	3.51
Gallic acid	−4.2	ASP 81 (H-donor)	3.18
Protocatechuic acid	−4.4	ASP 81 (H-donor)	3.04

Table 35. *Continued.*			
***p*-hydroxybenzoic acid**	−4.2	ASP 81 (H-donor)	2.91
Caffeic acid	−5.1	ASP 81 (H-donor)	3.33
		ARG 144 (H-acceptor)	3.02
Syringic acid	−4.3	ARG 144 (acceptor)	3.07
		ARG 84 (ionic)	3.33
Vanillic acid	−4.4	ARG 144 (acceptor)	3.02
		ARG 84 (ionic)	3.53
Ferulic acid	−5.2	ASP 81 (H-donor)	3.38
		ARG 144 (H-acceptor)	2.99
		ARG 84 (ionic)	3.30
Sinapic acid	−5.6	ARG 144 (H-acceptor)	2.91
		ARG 84 (ionic)	2.91
Rutin	−7.3	ASP 81 (H-donor)	3.03
		ARG 84 (acceptor)	3.12
***p*-coumaric acid**	−4.9	ASP 81 (H-donor)	3.13
		ARG 144 (H-acceptor)	3.03
		ARG 84 (ionic)	3.65
Apigenin-7-glucoside	−5.6	ASP 81 (H-donor)	2.97
Cinnamic acid	−4.5	ARG 144 (H-acceptor)	2.92
		ARG 84 (ionic)	3.71
Quercetin	−5.7	ASP 81 (H-donor)	3.23
		GLY 85 (H-donor)	3.02
Apigenin	No ligand reactions		
Chrysin	−5.0	ASP 81 (H-donor)	3.14
Catechin	−5.7	ASP 81 (H-donor)	3.46 and 3.37
Chlorogenic acid	−4.9	ARG 144 (H-acceptor)	2.86

Dashes (-) refer to compounds that have no interactions within the active site.

Table 36. Docking energy scores (S), interactions and distances for the investigated molecules against sterol 14−alpha demethylase (CYP51) as an antifungal target (PDB Id: 5FSA).

Studied Compounds	**5FSA docking site**		
	S (kcal/mol)	**Interaction (Å)**	**Distance (Å)**
Original Ligand, X2N	−15.2	ARG 381 (H-acceptor)	3.17
		LYS 143 (H-acceptor)	2.92
		HIS 468 (H-acceptor)	3.01
		TYR 132 (H-acceptor)	2.20
		ARG 381 (ionic)	3.17
		LYS 143 (ionic)	2.92
		HIS 468 (ionic)	3.01
Gallic acid	−4.8	ARG 381 (H-acceptor)	2.80
		ARG 381 (ionic)	2.80
Protocatechuic acid	−4.3	TYR 118 (H-acceptor)	3.19
		ARG 381 (H-acceptor)	3.29

Table 36. *Continued.*			
***p*-hydroxybenzoic acid**	−4.7	ARG 381 (H-acceptor)	3.17
Caffeic acid	-5.0	TYR 118 (H-acceptor)	3.16
		ARG 381 (H-acceptor)	3.25 and 3.23
Syringic acid	−5.0	ARG 381 (H-acceptor)	2.98
		TYR 118 (H-acceptor)	3.17
Vanillic acid	−4.8	ARG 381 (H-acceptor)	2.79
		ARG 381 (ionic)	3.86
Ferulic acid	−5.1	TYR 132 (H-acceptor)	2.97
		HIS 468 (H-acceptor)	2.88
		LYS 143 (H-acceptor)	3.54
Sinapic acid	−5.6	TYR 132 (H-acceptor)	2.94
		HIS 468 (H-acceptor)	2.96
		LYS 143 (ionic)	3.97
Rutin	−7.3	MET 508 (H-donor)	3.34
***p*-coumaric acid**	−4.6	TYR 118 (H-acceptor)	3.26
		ARG 381 (H-acceptor)	2.97
		HIS 468 (ionic)	3.94
Apigenin-7-glucoside	−7.9	PRO 462 (H-donor)	3.09
		ARG 381 (H-acceptor)	3.29
Cinnamic acid	−5.3	ARG 381 (H-acceptor)	2.90
		ARG 381 (ionic)	3.51
Quercetin	−5.5	PRO 462 (H-donor)	3.07
Apigenin	−6.1	No ligand reactions	
Chrysin	−5.1	PRO 462 (H-donor)	3.06
Catechin	−5.5	MET 508 (H-donor)	3.50
		GLY 307 (H-donor)	3.05
Chlorogenic acid	−5.5	PRO 462 (H-donor)	2.76
		TYR 132 (H-acceptor)	2.77
		HIS 468 (H-acceptor)	3.04
		LYS 143 (H-acceptor)	2.91

Dashes (-) refer to compounds that have no interactions within the active site.

Similarly, the interaction between the original ligand (X2N), ferulic acid, sinapic acid, and Apigenin-7-glucoside.within the active site of CYP51 (as antifungal targets) has been studied and visualized (2D and 3D) in Figure 44a, 44b, 44c, and 44d, respectively. X2N showed high docking scores (−15.2 kcal/mol), mediating seven key residues ARG 381, LYS 143, HIS 468, TYR 132, ARG 381, LYS 143 and HIS 468 to form hydrogen and ionic interactions. Although docking energy scores for the tested compounds ranged between −4.3 to −7.9 kcal/mol, they exhibited interesting binding interactions in closed proximity to the active site pocket of CYP51, as listed in Table 36.

To illustrate, apigenin-7-glucoside showed the highest score (−7.9 kcal/mol), while protocatechuic acid showed the lowest score (−4.3 kcal/mol), but both have one hydrogen bond interaction within the active site pocket in conjunction with ARG 381 at a similar distance of 3.29 Å. Interestingly, ferulic acid (−5.1 kcal/mol) and sinapic acid (−5.6 kcal/mol) mediated three interactions with TYR 132 (H-bond interaction), HIS 468 (H-bond interaction), LYS 143 (ionic interaction) in the active site pocket. On the other hand, although rutin, apigenin, quercetin and chrysin followed apigenin-7-glucoside in docking score values (−7.3, −6.1, −5.5, and −5.1 kcal/mol), they presented interactions in the active site with residues that were different from that of the original ligand. To clarify, rutin had a single hydrogen bond with MET 508, apigenin has no interaction in the active site, quercetin and chrysin both have a single hydrogen bond with PRO 462. However, all the other tested compounds have at least one hydrogen bond interaction with ARG 381 or more, as shown in Table 36.

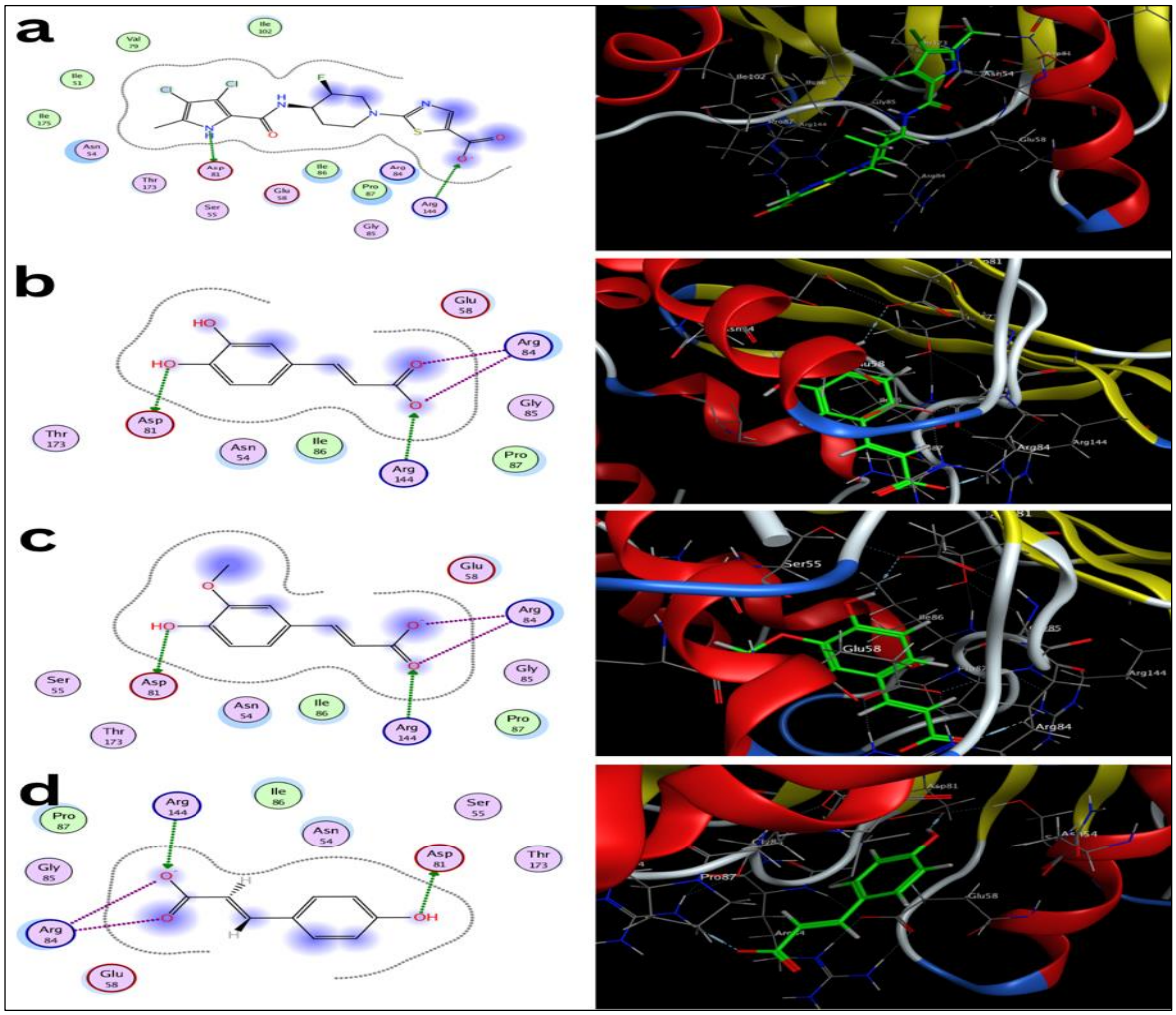

Figure 43. Selected 2D and 3D visualizations of the projected interaction modes and mechanisms of binding between studied compounds and DNA Gyrase Enzyme's active site.
(a) *original ligand 07N,* ***(b)*** *Caffeic acid,* ***(c)*** *Ferulic acid,* ***(d)*** *p-coumaric acid.*

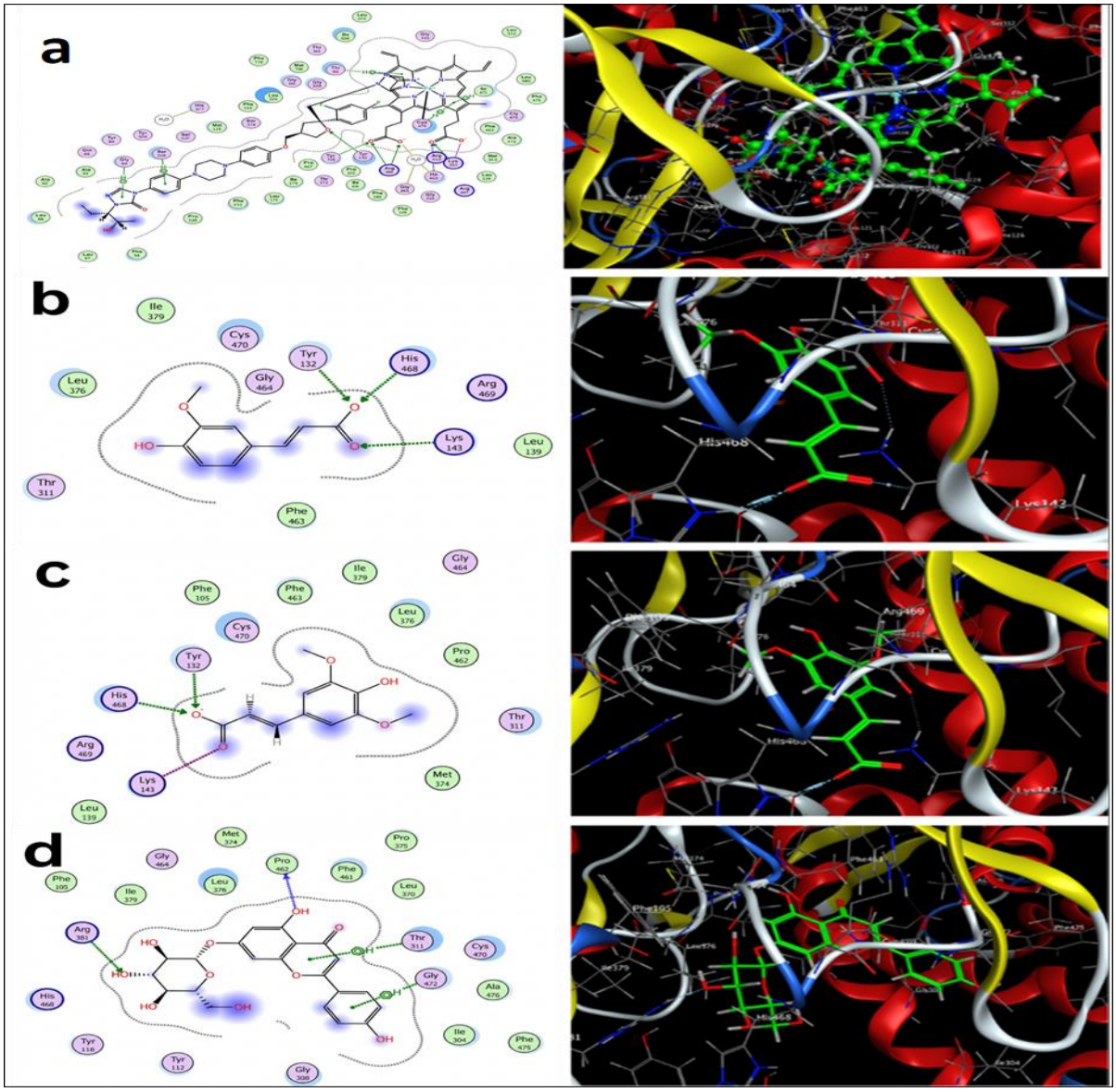

Figure 44. Selected 2D and 3D illustrations of the projected interaction modes and mechanisms of binding between the studied compounds and the sterol 14-alpha demethylase (CYP51) enzyme active site.
*(**a**) Original ligand, (**b**) Ferulic acid, (**c**) Sinapic acid, (**d**) Apigenin-7-glucoside.*

Similarly, **for the maize HPLC results**, Table 37 demonstrates the molecules under investigation against DNA gyrase inhibitor as an antibacterial target (PDB ID: 6F86). Similarly, Table 38 shows the results of tested compounds against alpha−L−fucosidase enzyme (PDB Id: 9LXL) as an antifungal target. 2D and 3D visualisations of these predicted interactions are shown in Figures 45 and 46 for DNA Gyrase and alpha−L−fucosidase, respectively. The interaction of original ligand CWW, Rutin, Apeginin-7-glucoside, and clorogenic acid within DNA Gyrase's active site (as antibacterial targets) has been investigated and illustrated in both two and three dimensions, as shown in Figure 45a, 45b, 45c, and 45d, respectively

The native ligand coordinated four hydrogen bond interactions to link with the key residues Asp73, Gly77, Asn46 and Arg76 at a distance of 2.79, 2.8, 2.86 and 2.81 Å, respectively, and a docking score value of −8.6 kcal\mol. Among the tested compounds, rutin had the highest docking score for antibacterial activity (−7.3 kcal/mol) with one hydrogen bond interaction at ASN46, followed by clorogenic acid and apigenin−7−glucoside with −6.5 and −6.51 kcal/mol, respectively.

When considering their interactions, the apigenin−7−glucoside showed no ligand reactions, and the clorogenic acid showed three hydrogen bond interactions with ASP73, ASN46, or ARG76. Catechin scored lower binding affinities with −5.6 kcal\mol, but attained the same mode of interaction like CWW, mediating four hydrogen bond interactions to bind with ASP73, GLY77, ASN46, and ARG76. Additionally, protocatechuic acid, *p*−hydroxybenzoic acid, syringic acid, ferulic acid, sinapic acid, *p*−coumaric acid, cinamic acid, and apegenin had only one hydrogen bond interaction with ARG76, ARG136, ARG76, ARG136, ARG136, ASP73, ARG136, and ASP73.

Similarly, the interaction between the original ligand (NAG), rutin, apeginin-7-glucoside, and clorogenic acid within the active site of alpha−L−fucosidase enzyme has been investigated and illustrated in both two and three dimensions, as shown in Figure 46a, 46b, 46c, and 46d, respectively. NAG showed high docking scores of −7.2 kcal/mol, mediating five key residues — GLU289, GLU47, ASP227, TRP48, and HIS128, to form four hydrogen and one ionic interaction at distances of 3.01, 2.64, 3, 2.97, and 3.08 Å, respectively.

Although docking energy scores for the tested compounds ranged between −3.9 and −7.6 kcal/mol, they exhibited interesting binding interactions near the active site pocket of alpha-L-fucosidase, as listed in Table 37. To illustrate, rutin showed the highest score (−7.6) compared to the ligand itself, followed by the apegenin-7-glucoside (−7.1), while cinnamic acid showed the lowest score (−3.9), but rutin had four hydrogen bond interactions within the active site pocket in conjunction with GLU289, ASP227, TRP312, HIS128 at distances of 2.94, 2.79, 3, and 3.03 Å, and the apegenin-7-glucoside had also four hydrogen bond interactions with GLU47, LYS273, HIS35, TRP48, at distances of 2.78, 3, 2.94, and 2.84 Å, while the cinnamic acid had only two hydrogen bond interactions with HIS35 and TRP48 at distances of 3.19 and 2.9 Å.

Interestingly, gallic acid and chrysin had no ligand interactions, but ferulic acid, sinapic acid, quercetin, apigenin, clorogenic acid, and catechin, they all had only one hydrogen bond interactions with HIS35, ASP227, GLU47, ASP227, GLU289, and GLU289, at scores of 2.94, 2.98, 2.89, 2.82, 3.1, and 2.9 Å, and in scores of −4.6, −4.9, −5.9, −5.2, −6.4, and −5.4 kcal/mol.

Despite sharing the same −4.2 kcal/mol score, vanillic acid had two H-interactions with TRP48 at 2.9 Å and HIS35 at 3.22 Å, while the *p*-coumaric acid had also two H-interactions, but with HIS35 at 2.85 Å and LYS273 at 3.13 Å.

Table 37. Docking energy scores (S), interactions and distances for the investigated molecules against DNA Gyrase inhibitor as an antibacterial target (PDB Id: 6F86).

Studied molecule	**Docking site in 6F86**				
	Interaction			**Distance (Å)**	**S (kcal/mol)**
Original ligand, CWW	ASP	73	H-donor	2.79	−8.6
	GLY	77	H-donor	2.8	
	ASN	46	H-acceptor	2.86	
	ARG	76	H-acceptor	2.81	
Gallic acid	ASP	73	H-donor	2.79	−4.2
	GLY	77	H-donor	2.8	
	ASN	46	H-acceptor	2.86	
	ARG	76	H-acceptor	2.81	
Protocatechuic acid	ARG	76	H-acceptor	3.17	−4.23
***p*-hydroxybenzoic acid**	ARG	136	H-acceptor	2.94	−3.95
Caffeic acid	ARG	136	H-acceptor	3.01	−4.6
	ARG	136	Ionic	3.01	
Syringic acid	ARG	76	H-acceptor	3.16	−5.02
Vanillic acid	No ligand reactions				−4.5
Ferulic acid	ARG	136	H-acceptor	3.12	−5.1
Sinapic acid	ARG	136	H-acceptor	3.06	−5.6
Rutin	ASN	46	H-donor	2.96	−7.3
***p*-coumaric acid**	ASP	73	H-donor	2.92	−5.1
Apigenin-7-glucoside	No ligand reactions				−6.5
Cinnamic acid	ARG	136	H-acceptor	2.99	−4.3
Quercetin					−5.5
Apigenin	ASP	73	H-donor	2.81	−6.04
Chrysin	No ligand reactions				−3.9
Clorogenic acid	ASP	73	H-donor	2.78	−6.5
	ASN	46	H-acceptor	3.05	
	ARG	76	H-acceptor	3.1	
Catechin	ASP	73	H-donor	2.79	−5.6
	GLY	77	H-donor	2.8	
	ASN	46	H-acceptor	2.86	
	ARG	76	H-acceptor	2.81	

Table 38. Docking energy scores (S), interactions and distances for the investigated molecules against alpha-L-fucosidase inhibitor as an antifungal target (PDB Id: 9LXL).

Studied molecule	**Docking site in 9LXL**				
	Interaction			**Distance (Å)**	**S (kcal/mol)**
Original ligand NAG	GLU	289	Ionic	3.01	−7.2
	GLU	47	H-donor	2.64	
	ASP	227	H-donor	3	
	TRP	48	H-acceptor	2.97	
	HIS	128	H-acceptor	3.08	
Gallic acid	No ligand reactions				−3.9
Protocatechuic acid	GLU	47	H-donor	2.86	−4.4
***p*-hydroxybenzoic acid**	HIS	35	H-acceptor	2.94	−4.1
Caffeic acid	GLU	47	H-donor	2.92	−4.6
	HIS	35	H-acceptor	2.85	
Syringic acid	ASP	227	H-donor	3.02	−4.8
	TRP	312	H-acceptor	2.93	
Vanillic acid	TRP	48	H-acceptor	2.9	−4.2
	HIS	35	H-acceptor	3.22	
Ferulic acid	HIS	35	H-acceptor	2.94	−4.6
Sinapic acid	ASP	227	H-donor	2.98	−4.9
Rutin	GLU	289	H-donor	2.94	−7.6
	ASP	227	H-donor	2.79	
	TRP	312	H-acceptor	3	
	HIS	128	H-acceptor	3.03	
***p*-coumaric acid**	HIS	35	H-acceptor	2.85	−4.2
	LYS	273	H-acceptor	3.13	
Apigenin-7-glucoside	ASP	304	H-donor	2.7	−7.1
	GLU	47	H-donor	2.78	
	LYS	273	H-acceptor	3	
	HIS	35	H-acceptor	2.94	
	TRP	48	H-acceptor	2.84	
Cinnamic acid	HIS	35	H-acceptor	3.19	−3.9
	TRP	48	H-acceptor	2.9	
Quercetin	GLU	47	H-donor	2.89	−5.9
Apigenin	ASP	227	H-donor	2.82	−5.2
Chrysin	No ligand reactions				−5.3
Clorogenic acid	GLU	289	H-donor	3.1	−6.4
Catechin	GLU	289	H-donor	2.9	−5.4

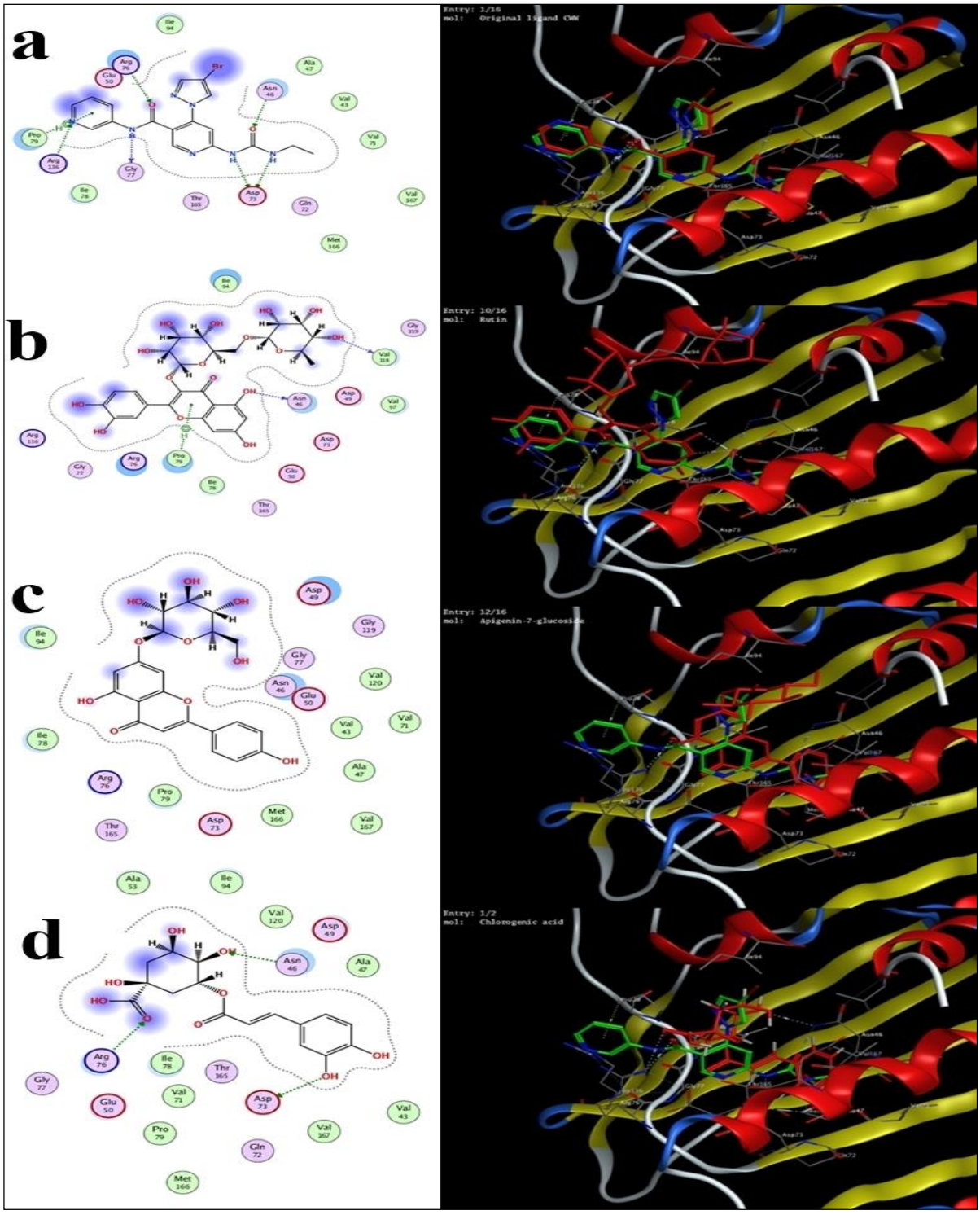

Figure 45. Selected 2D and 3D visualizations of the projected interaction modes and mechanisms of binding between studied compounds and DNA Gyrase Enzyme's active site.
***(a)** original ligand CWW, **(b)** Rutin, **(c)** Apeginin-7-glucoside, **(d)** clorogenic acid.*

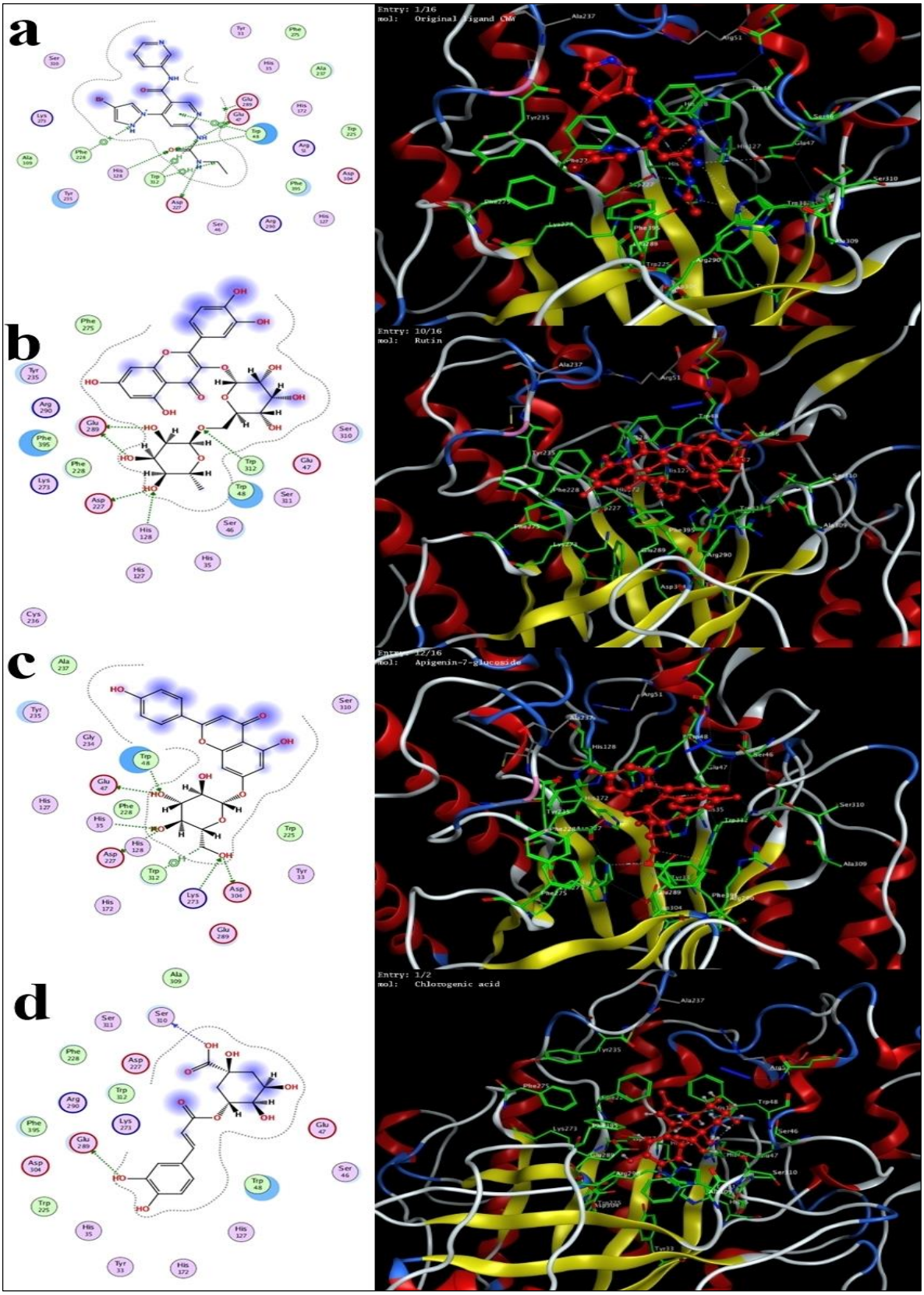

Figure 46. Selected 2D and 3D illustrations of the projected interaction modes and mechanisms of binding between the studied compounds and the alpha-L-fucosidase enzyme active site.
(a) *Original ligand NAG,* ***(b)*** *Rutin,* ***(c)*** *Apeginin-7-glucoside,* ***(d)*** *clorogenic acid.*

The HPLC-detected phenolics in the aqueous extracts of tomato and maize are suggested to have antibacterial and antifungal activities against various bacterial and fungal pathogens. Molecular docking can serve as a functional validation of the plant secondary metabolites. The obtained results can be explicitly integrated into the main narrative of ZnO-NP-mediated stress tolerance. The HPLC results in tables 15 and 16 demonstrated that ZnO-NPs treatments, especially T5 and T6 in tomato, and M3 in maize, significantly increased the content of phenolics compared to the salinity-stressed treatments (T4 and M2). It suggested that ZnO-NPs acted as elicitors, reprogramming plant secondary metabolites when stressed with 150 mM NaCl.

Since determining the antimicrobial activities is a standard metric to assess the biological potency of the stimulated secondary metabolites, it was found that the induction revealed by ZnO-NPs in the different extracts from tomato and maize plants supported the chemical shift of increasing molecules such as rutin, chlorogenic acid, apeginin-7-glucoside, and feulic acid, etc, which supports the hypothesis of induced cross-tolerance as the salt stress triggered a broad spectrum of biochemical shield which enhance reduced the susceptibility of the tomato and maize leaves to pathogens, and increased their abilities to act as antibacterial and antifungal agents. Molecular docking provided a mechanistic proof on how the cross-tolerance worked. The high binding affinities between some detected phenolics like rutin and the active sites of the proteins in the targeted pathogens, assumed a molecular-level explanation for the biological efficacy of the phenolic compounds that were upregulated in the treatments T5, T6, and M3, as they represented the salinity-stressed treatments but sprayed with the different concntrations of ZnO-NPs.

Molecular docking commonly used to discover the optimal orientation of a ligand (a single compound or a group) to a target receptor as well as to thoroughly examine the mode of interaction and binding energy for this ligand/s (Mostafa et al., 2025). In this investigation, docking was employed as a reliable and effective method to evaluate the antibacterial activity of tomato and maize leaves extracts *in silico* and validate the *in vitro* findings. Additionally, to comprehend how the molecules they contain will interact with DNA Gyrase (PDB Id: 3TTZ), CYP51 (PDB Id: 5FSA), DNA Gyrase (PDB ID: 6F86), and alpha−L−fucosidase enzyme (PDB Id: 9LXL), four possible antimicrobial targets. According to HPLC analysis, tomato and maize leaves included 17 polyphenols and flavonoids, which are naturally occurring substances that may be found in a variety of plant sources and have demonstrated promising antimicrobial action.

Phenolic compounds may have an antibacterial effect because they can permeabilize and destabilise the cytoplasmic membrane, block essential enzymes, and affect DNA synthesis (Borges et al., 2013). DNA Gyrase enzyme is a necessary component of bacterial cells and plays important roles in transcription, replication, and repair processes, all of which are critical to cell life and reproduction (Andrade-Pavón et al., 2024). Lanosterol 14α-demethylase (CYP51), an enzyme essential for preserving the integrity of fungal cell membranes, is inhibited by conventional antifungal drugs like azoles, which target ergosterol production (Zhang et al., 2024).

For the antibacterial action in tomato and maize leaves, rutin had the strongest affinity at −7.3 kcal\mol with one hydrogen bond interaction at ASN46 for both DNA Gyrase (PDB Id: 3TTZ) and DNA Gyrase (PDB ID: 6F86) targets, respectively, which was in line with the findings of Shaker et al. (2022). The researchers found that rutin has the highest binding energy with the 3TTZ active site, at −7.29 kcal\mol. Additionally, rutin showed a hydrogen bond interaction with ASP 81 in both investigations. Likewise, in both studies, ferulic acid interacted with ASP 81 and ARG 144 through two hydrogen bonds, with a docking score value of −5.2 kcal/mol. Interestingly, caffeic acid (5.1 kcal\mol) and *p*-coumaric (−4.6 kcal\mol) acid both had two H-bond interactions with the key residues ASP 81 and ARG 144.

According to Merlani et al. (2019), caffeic acid derivatives exhibit strong antibacterial action against a variety of bacteria, possibly by inhibiting DNA Gyrase (Merlani et al., 2019). In their study, they assessed the biological activity of caffeic acid derivatives against 8 Gram-positive and Gram-negative bacteria, and *in silico* against *E. coli* DNA GyrB (DNA Gyrase) (PDB ID: 1KZN), MurB (PDB ID: 2Q85), and Thymidylate Kinase (PDB ID: 4QGG). Their research indicated that all tested caffeic acid derivatives were effective against the studied bacteria, suggesting that DNA Gyrase inhibition is the key mechanism of antibacterial effect. Another study used both *in vitro* and *in silico* (molecular docking) methods to evaluate the antibacterial efficiency of the phytochemical quercetin compared to ciprofloxacin as a reference antibiotic. Several bacterial targets, including Sortase B, Toxic Shock Syndrome Toxin-1, Multidrug Efflux Pump AdeJ, and LasR, were employed by the researchers as antibacterial tagrets. Ciprofloxacin showed binding energies of −7.3 to −7.4 kcal/mol against the target proteins, but quercetin showed exceptionally high binding energies of -6.9 to −10.3 kcal/mol.

Furthermore, quercetin showed antibacterial activity against gram-positive (*Staph. aureus*, *Strept. pneumonia*) and gram-negative (*Acinetobacter baumannii*, *E. coli*, *Ps. aeruginosa*) bacteria. It also showed a synergistic effect with piperacillin and cefotaxime against most of the tested bacterial strains (Majumdar & Mandal, 2024). Notably, quercetin interacted with ASP 81 and GLY 85 through hydrogen bonds, achieving the second-highest energy scores in our study (−5.7 kcal/mol). Additionally, all tested compounds, except apigenin, had at least one interaction like the original DNA Gyrase within the active site. This similar and near the key residues in the active site may explain the tomato extracts' antibacterial activity. Moreover, ferulic acid, caffeic acid and *p*-coumaric acid may have similar mode of action to that of the original inhibitor as they mediated similar interaction with the same residues.

Regarding antifungal effect, potential sterol 14α-demethylase (CYP51) (Yuan et al., 2017) and foralpha-L-fucosidase (Mai et al., 2024) inhibitors have been found using *in silico* techniques such as pharmacophore-based virtual screening and molecular docking. Phytochemicals have been studied as possible 14α-demethylase inhibitors; several plant compounds have shown good binding affinities and comparable binding residues to well-known antifungal agents such as ketoconazole (Sama-ae et al., 2023). To assess phytochemicals' potential as antifungal drugs, a molecular docking study by Jadhav et al. (2020) was conducted on 60 plant-based compounds against CYP51 as an antifungal target.

The results of phenolic compounds detected in tomato leaves showed that majority of the compounds were able to establish hydrogen bond interactions with the CYP51 active site pocket, while 17 compounds had binding residues that were comparable to those of the antifungal drug ketoconazole. For instance, several phytochemicals showed repeated Hydrogen bond interactions with HIS468, TYR132, TYR 118, THR311, LYS143 and TYR132 amino acids, while ketoconazole interacted with LYS143 by a single H-bond. Similar interactions were also seen in some of the molecules in our investigation, including *p*-coumaric acid (HIS468, TYR 118, ARG381), protocatechuic acid (TYR 118, ARG 381), syringic acid (TYR 118, ARG 381), and ferulic acid (HIS468, TYR 132, LYS 143).

A study by Merlani et al. (2019) revealed that caffeic acid derivatives exhibit a strong antifungal effect, possibly by inhibiting 14α-demethylase enzyme. The research team assessed the antifungal activity of caffeic acid derivatives *in vitro* against 8 strains of fungi. They also assessed the activity *in silico* by performing molecular docking against Dihydrofolate reductase enzyme (PDB ID: 4HOF) and *C. albicans* lanosterol 14-αdemethylase CYP51 (PDB ID: 5V5Z).

According to their results, seven compounds of caffeic acid derivatives seemed to be more active than bifonazole, whereas all compounds were more active than ketoconazole. Moreover, they highlighted that the primary cause of the antifungal effect seems to be due to the inhibition of 14α-demethylase rather than Dihydrofolate reductase enzyme. Like the original ligand interaction (posaconazole), caffeic acid exhibited two interactions with the active site residues in our docking study.

Another study by Sama-ae et al. (2023) sought to identify novel natural-based antifungal agents that might successfully block CYP51's enzymatic activity (PDB ID: 5TZ1) while also having favourable pharmacokinetics. They studied forty-six molecules originating from algae, bacteria, plants, sponges, and fungi. Didymellamide compounds had the highest binding energy scores against CYP51 among the 15 candidate molecules studied by molecular docking. Through hydrophobic interactions with the HEM601 molecule and hydrogen bonding to Tyr132, Ser378, Met508, His377, and Ser507, didymellamide molecules bind to similar active-pocket poses of the antifungal drugs ketoconazole and itraconazole.

In case of tomato, ferulic acid and sinapic acid mediated H-bonds with TYR132 (together with HIS468 and LYS143), while rutin formed a single H-bond with MET 508 in the active site of CYP51 (PDB ID: 5FSA). However, it is well established that a molecule and protein/enzyme (antimicrobial target) must engage by some interaction, such as a H-bond interaction, to have an impact (Ruge et al., 2005). The antifungal activity of the tomato leaf extract may be explained by the fact that all the studied compounds have at least one interaction in the active site pocket similar to the original ligand.

The molecular docking research evaluated the inhibitory potential of several phytochemicals in maize leaves against two therapeutic targets: DNA gyrase (PDB ID: 6F86) for antibacterial activity and alpha-L-fucosidase (PDB ID: 9LXL) for antifungal activity. The DNA gyrase B subunit is an established target for antibacterial drugs due to its essential role in DNA replication (Gellert et al., 1976). This study revealed that the native ligand (CWW) achieved a docking score of −8.6 kcal/mol, forming four hydrogen bonds with essential residues: Asp73, Gly77, Asn46, and Arg76. Rutin exhibited the highest binding affinity (−7.3 kcal/mol) among the assessed chemicals, especially interacting with Asn46. Chlorogenic acid (−6.5 kcal/mol) and catechin (−5.6 kcal/mol) exhibited significant interactions.

Moreover, catechin replicated the exact binding profile of the native ligand by interacting with Asp73, Gly77, Asn46, and Arg76. The inhibitory effects of flavonoids, including rutin and catechin, on GyrB are well-documented. Studies demonstrate that these polyphenols compete with ATP for binding to the N-terminal region of the gyrase B subunit (Plaper et al., 2003).

The interaction with Asp73 is particularly important due to its conservation among various bacterial species and its function in anchoring the adenine ring of ATP; thus, the binding of catechin and chlorogenic acid in this study reinforces their potential as competitive inhibitors (Fikrika, 2016). Moreover, rutin's interaction with Asn46 supports earlier research emphasising the significance of this residue in stabilising the inhibitor-enzyme complex (Cushnie & Lamb, 2005; Plaper et al., 2003)

Alpha-L-fucosidase, an enzyme that cleaves fucose from glycoconjugates, is a target for suppression in fungal infection treatment (Intra et al., 2007). The endogenous ligand (NAG), with a docking score of −7.2 kcal/mol, interacted with Glu289, Glu47, Asp227, Trp48, and His128. Rutin, with a binding affinity score of −7.6 kcal/mol, demonstrated greater binding affinity than the native ligand. Rutin established hydrogen bonds with Glu289, Asp227, Trp312, and His128. Additionally, apigenin-7-glucoside exhibited a robust affinity (−7.1 kcal/mol), particularly engaging with Glu47, Lys273, His35, and Trp48.

The heightened binding affinities of rutin and apigenin-7-glucoside are presumably attributable to their glycosylated configurations. Prior research demonstrates that the inclusion of sugar moieties, such as the rutinoside group, enhances the surface area available for hydrogen bonding within the enzyme's catalytic pocket, frequently resulting in greater affinity compared to their corresponding aglycones (Limanto, 2025). The interaction between Asp227 and Glu289 is significant, as these acidic residues generally serve as the nucleophile and acid/base catalyst in the GH29 family of glycosidases, which includes alpha-L-fucosidase (Shaikh, 2013). Rutin efficiently obstructs the enzyme's catalytic machinery by occupying these residues (Limanto, 2025; McMillan, 2025).

The docking results indicate that the phytochemicals, especially rutin, exhibit multi-target potential. Their capacity to interact with conserved residues in both DNA gyrase and alpha-L-fucosidase, frequently matching or surpassing the efficacy of native ligands, indicates their potential as promising candidates for natural antibacterial development (Tiwari et al., 2011).

A study by Okechukwu et al. (2023) examined the efficacy of *Curcuma longa* phytochemicals in blocking or altering alpha-glucosidase enzymes, that preliminary study investigated the potential of methanolic extracts of *Curcuma longa* through *in vitro* inhibition assays against glucosidase, as well as the activities of the phytoconstituents via molecular docking and computational analyses of the X-ray protein crystal structure of alpha-glucosidase (PDB ID: 3W37).

The results of phenolic compounds detected **in maize leaves** showed several phytochemicals showed repeated Hydrogen bond interactions, and those results were in line with the study of Okechukwu et al. (2023) when the ligand library was docked to the alpha-glucosidase binding site using GLIDE's normal and extra-precision modules. Limonene, guaiacol, and others scored highest energy. Guaiacol, the highest-scoring compound, was studied in the protein's binding pocket and found surface charge interactions (both positive and negative), hydrogen bonding with Glu 792 and Ile 759, and pi-pi stacking between the aromatic ring and Tyr 659. Acarbose, a reference chemical, docked to alpha-glucosidase. Comparisons were made on binding pocket interaction. The docking score of acarbose was higher than that of turmeric phytochemicals. However, its large molecular architecture raises questions about its pharmacokinetics and safety. Furthermore, the foliar application of zinc oxide nanoparticles (ZnO-NPs) to tomato and maize plants can not only enhance the yields and fruits quality but also increase the antimicrobial activity of leaf extracts due to their higher concentrations of phenolic compounds.

Despite the identified metabolites demonstrating significant binding affinities for target proteins, these *in silico* predictions should not be considered conclusive evidence of biological activity. Crude plant extracts are complex mixtures; hence, the antimicrobial capabilities found may be affected by synergistic or antagonistic interactions that cannot only be clarified via the docking of an individual molecule. Furthermore, this data provides a theoretical basis for the proposed mechanism of action. Further study employing bio-guided separation and purification of these metabolites is essential to validate these computational predictions.

5. CONCLUSIONS AND RECOMMENDATIONS

Saline impacts arise from intricate interactions among morphological, physiological, and biochemical processes, encompassing seed germination, plant growth, and the uptake of water and nutrients. Plant growth is negatively affected by early salt stress. This ultimately decreases crop output in saline environments, affecting both the quality and quantity of plant products. This underscores the necessity of researching procedures for using manufactured nanoparticles to regulate plants' physiological responses to adverse environments.

In case of tomato plants, dosages of ZnO-NPs had a significant effect across treatments. ZnO-NPs also increased chlorophyll, reduced stress markers, and released phenolic chemicals and proteins in the leaves of tomatoes. ZnO-NPs reduce salt stress by promoting the uptake of minerals. ZnO-NPs had beneficial effects on tomato plants under salt stress, making them an alternative approach to enhance resilience in saline soils or low-quality irrigation water. This study examined how foliar application of chemically synthesized ZnO-NPs to the leaves affected biochemistry, morphology, and phenolic compound synthesis with and without NaCl. It would be beneficial to conduct further research on the impacts at the enzyme and molecular levels to obtain more comprehensive and precise findings. Furthermore, to further the investigation, it is possible to undertake studies that extend to fruit yield and ripening in plants to optimize the dosages of zinc oxide nanoparticles applied via foliar spray in an open-field experiment.

All treatments showed significant changes in maize plant growth and development after applying zinc oxide NPs. ZnO-NPs increased chlorophyll and lowered stress. ZnO-NPs enhanced the ability of maize plants to withstand the adverse conditions of saline soils or low-quality irrigation water. This field study investigated the effect of zinc oxide nanoparticles on maize plant leaves when saline water is used for irrigation during the growing season. This study also examined how this foliar treatment affected plant biochemistry, morphology, fatty acid synthesis, and crop production when NaCl is present and when it is not. Considering the characteristics of ZnO-NPs in maize plants under salt stress, it might be considered a feasible option for cultivating areas with restricted availability of high-quality irrigation water.

While the obtained results demonstrated the high potential of ZnO-NPs, it is important to note that the efficacy of the different treatments and their influences on tomato and maize crops may vary depending on soil type, environmental humidity, genotype of the crop under investigation, dosage of the salinity stressor, dosage of the sprayed nanoparticles, and the area of the experiment weather it is under the greenhouse or in the open field, etc.

6. FUTURE PRESPECTIVES AND LIMITATIONS

The current study provides a strong physiological and molecular basis for employing ZnO-NPs to alleviate salt stress; nonetheless, future investigations are expected to focus on the following aspects to strengthen the practical applicability to be discussed in a more explicit and critical manner:

1. Examining the sustained impacts of recurrent ZnO-NPs treatments on enzyme activity to confirm the absence of detrimental ecological consequences.
2. Performing comprehensive assessments of zinc buildup in consumable tissues (tomatoes and maize kernels) to guarantee consumer safety and adherence to international food regulations.
3. Real-environmental situations frequently involve synchronous pressures (e.g., salinity and heat). Future research should assess the effectiveness of ZnO-NPs in complex and multi-stress conditions.
4. Extending the study to a larger variety of tomato and maize cultivars in order to find genotypes that optimize the resource-use efficiency of nanoparticles.
5. Investigating novel formulations through the application of green synthesis of ZnO-NPs to improve biocompatibility and facilitate controlled release.
6. Performing cost-benefit studies to evaluate foliar ZnO-NPs treatments in comparison to conventional soil amendments and breeding programs oriented at enhancing salt tolerance.
7. Integrating foliar ZnO-NPs with soil-based organic amendments, such as charcoal or compost, may offer a multi-action defense, enhancing both soil structure and plant physiological stimulation.
8. Using new molecular insights to figure out the ultimate protein and metabolite changes triggered by ZnO-NPs through going beyond transcriptomics.

Like other advanced nano-agriculture studies, its global applicability is limited. These constraints do not invalidate the findings; rather, they improve practical use of this technology. The current study's parameters and boundaries guide further optimization:

1. Greenhouse and pot-trial conditions provided most tomato physiological and transcriptome data. These settings unable to replicate genotype-environment interactions in open-field agriculture, which has variable diurnal temperatures, light intensities, and complicated soil mineralogy.

2. The study focused on *Solanum lycopersicum* L. (Kecskeméti 549) and *Zea mays* L. (FAO P0023) cultivars. Because these crops are genetically heterogeneous, the recommended amounts (such as 2 g/L for maize or 75 and 150 mg/L for tomato) may need to be modified for each variety with different salt tolerance levels.
3. It is crucial to identify the dosage at which these produced ZnO-NPs switch from biostimulant to phytotoxicity under different soil pH or organic matter conditions.
4. ZnO-NPs were applied to foliage to reduce soil stress from NaCl (150 mM). However, the effects of nanoparticles on non-target species, such as pollinating insects, need further study.
5. The commercial viability of producing and using ZnO-NPs vs zinc sulfate or standard breeding programs for industrial agriculture has to be investigated.
6. Molecular docking showed strong binding affinities for rutin and apigenin-7-glucoside in the antimicrobial section, but more *in vivo* studies are needed to establish the molecular binding motifs of pathogens.

7. NOVEL SCIENTIFIC RESULTS

1. Understanding the potential benefits of using ZnO-NPs in the cultivation of *Solanum lycopersicum* L. and *Zea mays* L. ultimately contributes to enhancing agricultural resource-use efficiency and crop resilience under environmental constraints.
2. Exogenous foliar application of 75 & 150 mg/L and 2 g/L ZnO-NPs on *Solanum lycopersicum* L. and *Zea mays* L. is associated with measurable changes in chlorophyll-related traits, oxidative stress markers, phenolic compounds, fatty acids, and nutrient-related physiological parameters in the studied plants under salinity stress (150 mM NaCl).
3. Foliar treatment with 75 and 150 mg/L ZnO-NPs in *Solanum lycopersicum* L. provided a biochemical shield against 150 mM NaCl stress by counteracting salinity-induced inhibition of SOD, CAT, and GR enzymes. This treatment creates a better antioxidant balance by increasing the levels of POX and GST, which act together. This blocked ROS from damaging membranes and maintained photosynthesis.
4. The application of ZnO-NPs (2 g/L) in *Zea mays* L. established an optimal antioxidant equilibrium during stress induced by 150 mM NaCl. This is characterized by the reactivation of inhibited SOD, CAT, and GR activities, alongside a strategic reduction in the excessive activation of POX and GST (by 55–61%). This improved enzyme profile reduces the metabolic contribution to defense, hence decreasing lipid peroxidation and maintaining cellular health in saline conditions.
5. Foliar application of ZnO-NPs (75 and 150 mg/L) alleviated salinity stress (150 mM) in *Solanum lycopersicum* L. by activating a comprehensive transcriptome reconfiguration. This molecular priming effect was characterized by the upregulation of pathways for carbon and nitrogen assimilation and the activation of gene clusters for secondary metabolism. This triggered the antioxidant enzymatic defense system (such as SOD, CAT, and GST), which, at 150 mM NaCl salinity, would have otherwise slowed.
6. In *Zea mays* L., foliar ZnO-NP treatment (2 g/L) alleviated 150 mM NaCl stress by reversing the extensive transcriptional suppression of more than 8,000 genes. The nanoparticles stabilized metabolism by increasing the activity of pathways that generate energy (oxidative phosphorylation) and nitrogen (arginine/proline), while also improving maize's ability to respond to oxidative stress, thereby stimulating ROS-detoxifying pathways.

7. Under 150 mM NaCl stress, the application of 75 and 150 mg/L ZnO-NPs to the leaves of *Solanum lycopersicum* L. enhanced the efficacy of leaf extracts against bacterial and fungal pathogens such as *E. coli*, *Staph. aureus*, and *Aspergillus niger*, etc. The augmented synthesis of bioactive compounds like Rutin and Apeginin-7-glucoside, confirmed by molecular docking to exhibit substantial binding affinities (up to −7.0 kcal/mol) to pathogen target proteins (Topoisomerase II ATPase enzyme) (DNA Gyrase) (PDB Id: 3TTZ) and sterol 14-alpha demethylase (CYP51) (PDB Id: 5FSA), respectively.
8. In *Zea mays* L., under 150 mM NaCl stress, the application of 2 g/L ZnO-NPs to leaves enhanced the efficacy of leaf extracts against bacterial and fungal pathogens, including *B. cereus*, *S. typhi*, *A. flavus*, and *P. vercosum*, etc. The molecular docking analysis confirmed that the augmented synthesis of bioactive compounds, such as Rutin, exhibited significant binding affinities (up to −7.0 kcal/mol) to both pathogen target proteins (Topoisomerase II ATPase enzyme) (DNA Gyrase) (PDB Id: 6F86), and the alpha-L-fucosidase (PDB Id: 9LXL). This demonstrated a novel link between ZnONPs-mediated salt tolerance and enhanced biotic defense.

8. SUMMARY

Abiotic stress conditions impede worldwide agricultural production. Salt disrupts the ecological balance of the region and reduces the productivity of most crops. Increased salinity reduces the amount of water that plants can obtain. It also affects the physicochemical qualities of the ground. Salt diminishes agricultural yield, degrades the soil, and adversely impacts the economy. The present study demonstrated the mitigating impact of chemically produced zinc oxide nanoparticles and their ability to counteract the detrimental effects of the 150 mM NaCl stressor against tomato and maize plants.

The greenhouse study aimed to assess the impact of chemically generated ZnO-NPs foliar spray at several concentrations on the tomato plants under salt stress. The results were analyzed in terms of numerous morphological and biochemical factors. A notable decline in plant growth characteristics and development was seen in correlation with the salt stress. Applying ZnO-NPs externally to the leaves enhanced the ability of the plants to withstand salt stress. Zinc oxide nanoparticles (ZnO-NPs) play a protective role in the plants exposed to salt stress. They help safeguard the integrity of the plant's cell membranes, enhance chlorophyll content, increase the accumulation of polyphenolic compounds, induce changes in biochemical stress indicators, and regulate mineral levels. Therefore, due to the therapeutic properties of ZnO-NPs in tomato/maize plants exposed to salt stress, it can be regarded as a viable alternative for cultivation in regions with limited access to high-quality irrigation water.

The open-field study of maize plants aimed to investigate the aggressive behavior of ZnO nanoparticles on maize plants when saline water fulfills the water needs during the growing season. This study sought to investigate the impact of applying saline water to the leaves on plants' biochemistry, morphology, and phenolics and fatty acid production under both sodium chloride-free and sodium chloride-rich conditions. The results were analyzed regarding numerous morphological, biochemical, and quality parameters. An evident decrease in traits and stages of plant development was observed in conjunction with salt stress. External application of ZnO-NPs to the leaves improved the salt stress tolerance of maize plants. Zinc oxide nanoparticles (ZnO-NPs) protect maize plants when exposed to salinity stress. They contribute to the protection of the cell membranes, increase the amount of chlorophyll, cause alterations in stress markers, strengthen the crop's productivity and quality, and favorably impact the lipid composition.

In the current study, the foliar spray of chemically synthesized zinc oxide nanoparticles showed a significant contribution in maintaining the levels of antioxidative enzymes in the

leaves of tomato plants that were stressed with the sodium chloride solution. They also showed a significant increase in the level of those enzymes in the treatments that were not stressed but sprayed with the ZnO nanoparticles. Since the tomato plants are moderately sensitive to the salinity stress, so the salt stressed treatments showed the lowest values of the antioxidative enzymes, and those results were matching the protein content in the salt-stressed tomato plants that were not sprayed with the ZnO-NPs at all. On the other hand, maize is considered a moderately tolerant crop, so the salt-stressed treatment that was not sprayed showed an increase in the level of the antioxidative enzymes compared to the other treatments. Thus, may explain why the level of the antioxidative enzymes was decreased in the fourth tomato treatment that was stressed with 150 mM NaCl without spraying ZnO-NPs, while it was increased in case of the maize second treatment.

The expression levels of set genes that may contribute to different metabolic pathways were studied. It was found that foliar spraying ZnO-NPs on salinity-stressed tomato plants positively affected the expression levels of stress-responsive genes, triggering the plants to accumulate beneficial biomolecules such as proline, thiamine, purine, and arginine, which are crucial for stress tolerance. Further studies on the combination of salted-soil amendments and foliar application of ZnO-NPs would be useful in the future to elucidate the molecular mechanisms underlying ZnO-NPs-induced alterations in soil microorganisms' diversity and functions related to salinity and ZnO-NPs, suggesting that this pathway is crucial for the adaptive response to salinity stress in tomato.

Molecular docking showed that caffeic acid, ferulic acid, p-coumaric acid, sinapic acid, and apigenin-7-glucoside are essential chemicals with antibacterial and antifungal activity against the DNA Gyrase inhibitor and the sterol 14-alpha demethylase (CYP51) enzyme, respectively. It is concluded that salt stress can negatively affect the growth, quality, and variant plant features.

9. APPENDICES

A1: Bibliography

Abbasi, G. H., Akhtar, J., Ahmad, R., Jamil, M., Anwar-Ul-Haq, M., Ali, S., & Ijaz, M. (2015). Potassium application mitigates salt stress differentially at different growth stages in tolerant and sensitive maize hybrids. *Plant Growth Regul*, *76*, 111–125.

Abdel Latef, A. A. H., Abu Alhmad, M. F., & Abdelfattah, K. E. (2017). The Possible Roles of Priming with ZnO Nanoparticles in Mitigation of Salinity Stress in Lupine (Lupinus termis. *Plants. J. Plant Growth Regul*, *36*, 60–70. https://doi.org/10.1007/s00344

Abogadallah, G. M. (2010). Antioxidative defense under salt stress. *Plant Signaling & Behavior*, *5*(4), 369–374. https://doi.org/10.4161/psb.5.4.10873

Adil, M., Bashir, S., Bashir, S., Aslam, Z., Ahmad, N., Younas, T., Asghar, R. M. A., Alkahtani, J., Dwiningsih, Y., & Elshikh, M. S. (2022). Zinc oxide nanoparticles improved chlorophyll contents, physical parameters, and wheat yield under salt stress. *Front. Plant Sci*, *13*, 932861.

Adly, A. A. M. (2010). Oxidative stress and disease: An updated review. *Res. J. Immunol*, *3*, 129–145.

Adrees, M., Khan, Z. S., Hafeez, M., Rizwan, M., Hussain, K., Asrar, M., Alyemeni, M. N., Wijaya, L., & Ali, S. (2021). Foliar exposure of zinc oxide nanoparticles improved the growth of wheat (Triticum aestivum L.) and decreased cadmium concentration in grains under simultaneous Cd and water deficient stress. *Ecotoxicol. Environ. Saf*, *208*, 111627.

Afzal, S., Singh, N. K., Lal, A. F., Sohrab, S., Singh, N., Gupta, P. S., Mishra, S. K., Adeel, M., & Faizan, M. (2024). Nanostructure and plant uptake: Assessing the ecological footprint and root-to-leaf dynamics. *Plant Nano Biology*, *10*, 100122. https://doi.org/10.1016/j.plana.2024.100122

Aghighi Shahverdi, M., Omidi, H., & Tabatabaei, S. J. (2018). Plant growth and steviol glycosides as affected by foliar application of selenium, boron, and iron under NaCl stress in Stevia rebaudiana Bertoni. *Ind. Crops Prod*, *125*, 408–415.

Ahanger, M. A., Agarwal, R. M., Tomar, N. S., & Shrivastava, M. (2015). Potassium induces positive changes in nitrogen metabolism and antioxidant system of oat (Avena sativa L. cultivar Kent. *J. Plant Interact*, *10*, 211–223.

Ahemad, M., & Kibret, M. (2014). Mechanisms and applications of plant growth promoting rhizobacteria: Current perspective. *Journal of King Saud University - Science*, *26*(1), 1–20. https://doi.org/10.1016/j.jksus.2013.05.001

Ahmad, A., Tola, E., Alshahrani, T. S., & Seleiman, M. F. (2023). Enhancement of Morphological and Physiological Performance of Zea mays L. under Saline Stress Using ZnO Nanoparticles and 24-Epibrassinolide Seed Priming. *Agronomy*, *13*(3), Article 3. https://doi.org/10.3390/agronomy13030771

Ahmad, M., Zahir, Z. A., Naeem Asghar, H., & Asghar, M. (2011). Inducing salt tolerance in mung bean through coinoculation with rhizobia and plant-growth-promoting rhizobacteria containing 1- aminocyclopropane-1-carboxylate deaminase. *Can. J. Microbiol*, *57*(7), 578–589.

Ahmadi, F. I., Karimi, K., & Struik, P. C. (2018). Effect of exogenous application of methyl jasmonate on physiological and biochemical characteristics of Brassica napus L. cv. Talaye under salinity stress. *S. Afr. J. Bot*, *115*, 5–11.

Ahmed, M., Abd-El Fatah, S. I., Shaker, A. S., Tóth, Z., & Decsi, K. (2026). The Role of Zinc Oxide Nanoparticles in Boosting Tomato Leaf Quality and Antimicrobial Potency. *Oxygen*, *6*(1), 2. https://doi.org/10.3390/oxygen6010002

Ahmed, M., Decsi, K., Tóth, Z., 2023a. Different Tactics of Synthesized Zinc Oxide Nanoparticles, Homeostasis Ions, and Phytohormones as Regulators and Adaptatively Parameters to Alleviate the Adverse Effects of Salinity Stress on Plants. Life 13, 73. https://doi.org/10.3390/life13010073

Ahmed, M., Marrez, D.A., Abdelmoeen, N.M., Mahmoud, E.A., Abdel-Shakur Ali, M., Decsi, K., Tóth, Z., 2023b. Proximate Analysis of Moringa oleifera Leaves and the Antimicrobial Activities of Successive Leaf Ethanolic and Aqueous Extracts Compared with Green Chemically Synthesized Ag-NPs and Crude Aqueous Extract against Some Pathogens. International Journal of Molecular Sciences 24, 3529. https://doi.org/10.3390/ijms24043529

Ahmed, M., Marrez, D.A., Mohamed Abdelmoeen, N., Abdelmoneem Mahmoud, E., Ali, M.A.-S., Decsi, K., Tóth, Z., 2023c. Studying the Antioxidant and the Antimicrobial Activities of Leaf Successive Extracts Compared to the Green-Chemically Synthesized Silver Nanoparticles and the Crude Aqueous Extract from Azadirachta indica. Processes 11, 1644. https://doi.org/10.3390/pr11061644

hmed, M., Tóth, Z., Decsi, K., 2024a. The Impact of Salinity on Crop Yields and the Confrontational Behavior of Transcriptional Regulators, Nanoparticles, and Antioxidant Defensive Mechanisms under Stressful Conditions: A Review. International Journal of Molecular Sciences 25, 2654. https://doi.org/10.3390/ijms25052654

Ahmed, M., Marrez, D.A., Rizk, R., Zedan, M., Abdul-Hamid, D., Decsi, K., Kovács, G.P., Tóth, Z., 2024b. The Influence of Zinc Oxide Nanoparticles and Salt Stress on the Morphological and Some Biochemical Characteristics of Solanum lycopersicum L. Plants. Plants 13, 1418. https://doi.org/10.3390/plants13101418

Ahmed, M., Marrez, D.A., Rizk, R., Abdul-Hamid, D., Tóth, Z., Decsi, K., 2024c. Interventional Effect of Zinc Oxide Nanoparticles with Zea mays L. Plants When Compensating Irrigation Using Saline Water. Nanomaterials 14, 1341. https://doi.org/10.3390/nano14161341

Ahmed, M., Tóth, Z., Marrez, D.A., Rizk, R., Abdul-Hamid, D., Decsi, K., 2025. Transcriptome datasets of salt-stressed tomato plants treated with zinc oxide nanoparticles. Data in Brief 58, 111282. https://doi.org/10.1016/j.dib.2025.111282

Akhavan, H., Torfeh, P., Latifeh, R., & Fatemeh, A. H. (2020). Effects of ZnO NPs on phenolic compounds of rapeseed seeds under salinity stress. *J. Plant Proc. Func*, *8*, 11–18.

Alabdallah, N. M., & Alzahrani, H. S. (2020). The Potential Mitigation Effect of ZnO Nanoparticles on [Abelmoschus Esculentus L. Moench] Metabolism under Salt Stress Conditions. *Saudi J. Biol. Sci*, *27*, 3132–3137. https://doi.org/10.1016/j.sjbs.2020.08.005.

Alexieva, V., Sergiev, I., Mapelli, S., & Karanov, E. (2001). The effect of drought and ultraviolet radiation on growth and stress markers in pea and wheat. *Plant, Cell & Environment*, *24*, 1337–1344. https://doi.org/10.1046/j.1365-3040.2001.00778.x

Ali, A. A. M., Romdhane, W. B., Tarroum, M., Al-Dakhil, M., Al-Doss, A., Alsadon, A. A., & Hassairi, A. (2021). Analysis of Salinity Tolerance in Tomato Introgression Lines Based on Morpho-Physiological and Molecular Traits. *Plants*, *10*(12), Article 12. https://doi.org/10.3390/plants10122594

Ali, L., Shaheen, M. R., Ihsan, M. Z., Masood, S., Zubair, M., Shehzad, F., & Khalid, A.-U.-H. (2022). Growth, photosynthesis and antioxidant enzyme modulations in broccoli (*Brassica oleracea* L. var. *Italica*) under salinity stress. *South African Journal of Botany*, *148*, 104–111. https://doi.org/10.1016/j.sajb.2022.03.050

Aljutheri, H., Habeeb, K., Al-Taey, D., Rahman, A., Al Tawaha, A. R., & Kadhim, F. (2020). *Effect of foliar application of different sources of nano-fertilizers on growth and yield of wheatEffect of foliar application of different sources of nano-fertilizers on growth and yield of wheat*.

Almeida, D. M., Oliveira, M. M., & Saibo, N. J. M. (2017). Regulation of Na^+ and K^+ homeostasis in plants: Towards improved salt stress tolerance in crop plants. *Genetics and Molecular Biology*, *40*, 326–345. https://doi.org/https://doi.org/10.1590/1678-4685-GMB-2016-0106

Al-shareef, N. O., & Tester, M. (2019). Plant Salinity Tolerance. In *Encyclopedia of Life Sciences* (pp. 1–6). Wiley. https://doi.org/10.1002/9780470015902.a0001300.pub3

Ambrosone, A., Mattera, L., Marchesano, V., Quarta, A., Susha, A. S., Tino, A., Rogach, A. L., & Tortiglione, C. (2012). Mechanisms underlying toxicity induced by CdTe quantum dots determined in an invertebrate model organism. *Biomaterials*, *33*(7), 1991–2000. https://doi.org/10.1016/j.biomaterials.2011.11.041

Amini, F., Ehsanpour, A. A., Hoang, Q. T., & Shin, J. Sh. (2007). Protein pattern changes in tomato under in vitro salt stress. *Russian Journal of Plant Physiology*, *54*(4), 464–471. https://doi.org/10.1134/S102144370704005X

Amthor, J. (2000). The McCree–de Wit–penning de Vries–Thornley respiration paradigms: 30 years later. *Annals of Botany*, *86*(1), 1–20. https://doi.org/10.1006/anbo.2000.1175

Andrade-Pavón, D., Gómez-García, O., & Villa-Tanaca, L. (2024). Review and Current Perspectives on DNA Topoisomerase I and II Enzymes of Fungi as Study Models for the Development of New Antifungal Drugs. *Journal of Fungi*, *10*(9), 629. https://doi.org/10.3390/jof10090629

Andrews, S., Krueger, F., Segonds-Pichon, A., Biggins, L., Krueger, C., Wingett, S., & FastQC. (2010). A quality control tool for high throughput sequence data. *Babraham Bioinformatics*, 370.

Anjum, N., Gill, S., Corpas, F., Ortega Villasante, C., Hernández, L. E., Tuteja, N., Sofo, A., Hasanuzzaman, M., & Fujita, M. (2022). Editorial: Recent Insights Into the Double Role of Hydrogen Peroxide in Plants. *Frontiers in Plant Science*, *13*, 843274. https://doi.org/10.3389/fpls.2022.843274

Antony Lilly Grace, M., Veerabhadra Rao, K., Anuradha, K., Judith Jayarani, A., Arun kumar, A., & Rathika, A. (2023). X-ray analysis and size-strain plot of zinc oxide nanoparticles by Williamson-Hall. *Materials Today: Proceedings*, *2nd International Conference on Multifunctional Materials*, *92*, 1334–1339. https://doi.org/10.1016/j.matpr.2023.05.492

A.O.A.C. (2019). *Official Methods of Analysis of the Association of Official Analytical Chemists: Official Methods of Analysis of AOAC International* (21st edn).

Aqeel, U., Aftab, T., Khan, M. M. A., Naeem, M., & Khan, M. N. (2022). A comprehensive review of impacts of diverse nanoparticles on growth, development and physiological adjustments in plants under changing environment. *Chemosphere*, *291*, 132672.

Asada, K. (1994). Causes of Photooxidative Stress and Amelioration of Defense Systems in Plants. In *Production and Action of Active Oxygen Species in Photosynthetic Tissues* (pp. 77–104). CRC press.

Ashraf, M. (2001). Relationships between growth and gas exchange characteristics in some salt-tolerant amphidiploid *Brassica* species in relation to their diploid parents. *Environmental and Experimental Botany*, *45*(2), 155–163. https://doi.org/10.1016/S0098-8472(00)00090-3

Ashraf, M., & Foolad, M. R. (2007). Roles of glycine betaine and proline in improving plant abiotic stress resistance. *Environmental and Experimental Botany*, *59*(2), 206–216. https://doi.org/https://doi.org/10.1016/j.envexpbot.2005.12.006

A.T.C.C. (1984). *American Type Culture Collection* (13th edn). USA.

Attia, H., Harrathi, J., Alamer, K. H., Alsalmi, F. A., Magné, C., & Khalil, M. (2021). Effects of NaCl on Antioxidant, Antifungal, and Antibacterial Activities in Safflower Essential Oils. *Plants*, *10*(12), 2809. https://doi.org/10.3390/plants10122809

Azeem, M., Pirjan, K., & Qasim, M. (2023). Salinity stress improves antioxidant potential by modulating physio-biochemical responses in Moringa oleifera Lam. *Sci Rep*, *13*, 2895. https://doi.org/10.1038/s41598-023-29954-6

Babayevska, N., Przysiecka, Ł., Iatsunskyi, I., Nowaczyk, G., Jarek, M., Janiszewska, E., & Jurga, S. (2022). ZnO size and shape effect on antibacterial activity and cytotoxicity profile. *Scientific Reports*, *12*(1), 8148. https://doi.org/10.1038/s41598-022-12134-3

Badawy, S. A., Zayed, B. A., Bassiouni, S. M. A., Mahdi, A. H. A., Majrashi, A., Ali, E. F., & Seleiman, M. F. (2021). Influence of Nano Silicon and Nano Selenium on Root Characters, Growth, Ion Selectivity, Yield, and Yield Components of Rice (Oryza sativa L.) under Salinity Conditions. *Plants*, *10*(8), Article 8. https://doi.org/10.3390/plants10081657

Bahr, G., Tomatis, P. E., & Vila, A. J. (2023). 2.10—The biochemistry and enzymology of zinc enzymes. In J. Reedijk & K. R. Poeppelmeier (Eds), *Comprehensive Inorganic Chemistry III (Third Edition)* (pp. 231–267). Elsevier. https://doi.org/10.1016/B978-0-12-823144-9.00148-5

Balasubramaniam, T., Shen, G., Esmaeili, N., & Zhang, H. (2023). Plants' Response Mechanisms to Salinity Stress. *Plants*, *12*(12), 2253. https://doi.org/10.3390/plants12122253

Balibrea, M. E., Martínez-Andújar, C., Cuartero, J., Bolarín, M. C., & Pérez-Alfocea, F. (2006). The high fruit soluble sugar content in wild Lycopersicon species and their hybrids with cultivars depends on sucrose import during ripening rather than on sucrose metabolism. *Functional Plant Biology: FPB*, *33*(3), 279–288. https://doi.org/10.1071/FP05134

Balibrea, M., Parra, M., Bolarín, M., & Pérez-Alfocea, F. (1999). Cytoplasmic sucrolytic activity controls tomato fruit growth under salinity. *Australian Journal of Plant Physiology*, *26*, 561–568.

Balibrea, M., Santa Cruz, A., Bolarín, M., & Pérez-Alfocea, F. (1996). Sucrolytic activities in relation to sink strength and carbohydrate composition in tomato fruit growing under salinity. *Plant Science*, *118*, 47–55.

Balusamy, S. R., Joshi, A. S., Perumalsamy, H., Mijakovic, I., & Singh, P. (2023). Advancing sustainable agriculture: A critical review of smart and eco-friendly nanomaterial applications. *Journal of Nanobiotechnology*, *21*, 372. https://doi.org/10.1186/s12951-023-02135-3

Barbes, L., Barbulescu, A., Radulescu, C., Stihi, C., & Chelarescu, E. (2014). Determination of Heavy Metals in Leaves and Bark of Populus Nigra L. by Atomic Absorption Spectrometry. *Romanian Reports in Physics*, *66*.

Bates, L. S., Waldren, R. P., & Teare, I. D. (1973). Rapid determination of free proline for water-stress studies. In *Plant and Soil* (Vol. 39, Issue 1, pp. 205–207). https://doi.org/10.1007/BF00018060

Bauer, A., Kirby, W., Sheriss, J., & Turck, M. (1996). Antibiotic susceptibility testing by standardized single method. *Am. J. Clin. Pathol*, *45*, 493–496.

Baum, M. K., Shor-Posner, G., & Campa, A. (2000). Zinc Status in Human Immunodeficiency Virus Infection. *The Journal of Nutrition*, *130*(5), 1421S-1423S. https://doi.org/10.1093/jn/130.5.1421S

Beauchamp, C., & Fridovich, I. (1971). Superoxide dismutase: Improved assays and an assay applicable to acrylamide gels. *Analytical Biochemistry*, *44*(1), 276–287. https://doi.org/10.1016/0003-2697(71)90370-8

Beauchemin, K. A. (1996). Using ADF and NDF in dairy cattle diet formulation—A western Canadian perspective. *Animal Feed Science and Technology*, *N. American Nutrition Conferences*, *58*(1), 101–111. https://doi.org/10.1016/0377-8401(95)00877-2

Ben-Ghedalia, D., Solomon, R., Miron, J., Yosef, E., Zomberg, Z., Zukerman, E., Greenberg, A., & Kipnis, T. (2001). Effect of water salinity on the composition and in vitro digestibility of winter-annual ryegrass grown in the Arava desert. *Animal Feed Science and Technology*, *91*(3–4), 139–147. Scopus. https://doi.org/10.1016/S0377-8401(01)00218-8

Berkhout, S. W., Haaf, J. M., Gronau, Q. F., Heck, D. W., & Wagenmakers, E.-J. (2024). A tutorial on Bayesian model-averaged meta-analysis in JASP. *Behavior Research Methods*, *56*(3), 1260–1282. https://doi.org/10.3758/s13428-023-02093-6

Bihmidine, S., Hunter, C. T., Johns, C. E., Koch, K. E., & Braun, D. M. (2013). Regulation of assimilate import into sink organs: Update on molecular drivers of sink strength. *Frontiers in Plant Science*, *4*. https://doi.org/10.3389/fpls.2013.00177

Boga, M., Yurtseven, S., Kilic, U., Aydemir, S., & Polat, T. (2014). Determination of nutrient contents and in vitro gas production values of some legume forages grown in the harran plain saline soils. *Asian-Australasian Journal of Animal Sciences*, *27*(6), 825–831. Scopus. https://doi.org/10.5713/ajas.2013.13718

Bolger, A. M., Lohse, M., & Usadel, B. (2014). Trimmomatic: A flexible trimmer for Illumina sequence data. *Bioinformatics*, *30*(15), 2114–2120. https://doi.org/10.1093/bioinformatics/btu170

Bonnichsen, R. K., Chance, B., & Theorell, H. (1947). Catalase Activity. *Acta Chem. Scand*, *1*, 685–709. https://doi.org/10.1016/j.abb.2012.01.015

Borges, A., Ferreira, C., Saavedra, M. J., & Simões, M. (2013). Antibacterial activity and mode of action of ferulic and gallic acids against pathogenic bacteria. *Microbial Drug Resistance*, *19*(4), 256–265. https://doi.org/10.1089/mdr.2012.0244

Bradford, M. M. (1976). A rapid and sensitive method for the quantitation of microgram quantities of protein utilizing the principle of protein-dye binding. In *Analytical Biochemistry* (Vol. 72, Issues 1–2, pp. 248–254). https://doi.org/10.1016/0003-2697(76)90527-3

Buchanan, B. B., Gruissem, W., & Jones, R. L. (Eds). (2015). *Biochemistry and molecular biology of plants* (2nd edn). Wiley-Blackwell.

Burmistrov, D. E., Serov, D. A., Simakin, A. V., Baimler, I. V., Uvarov, O. V., & Gudkov, S. V. (2022). A Polytetrafluoroethylene (PTFE) and Nano-Al2O3 Based Composite Coating with a Bacteriostatic Effect against E. coli and Low Cytotoxicity. *Polymers*, *14*(21), Article 21. https://doi.org/10.3390/polym14214764

Butcher, K., Wick, A., DeSutter, T., Chatterjee, A., & Harmon, J. (2016). Soil Salinity: A Threat to Global Food Security. *Agronomy Journal*, *108*, 2189–2200. https://doi.org/10.2134/agronj2016.06.0368

Byrt, C. S., Platten, J. D., Spielmeyer, W., James, R. A., Lagudah, E. S., Dennis, E. S., Tester, M., & Munns, R. (2007). *HKT1;5-like cation transporters linked to Na+ exclusion loci in wheat, Nax2 and Kna1*.

Cai, L., Liu, C., Fan, G., Liu, C., & Sun, X. (2019). Preventing viral disease by ZnONPs through directly deactivating TMV and activating plant immunity in Nicotiana benthamiana. *Environmental Science: Nano*, *6*(12), 3653–3669. https://doi.org/10.1039/C9EN00850K

Cakmak, I. (2000). Tansley Review No. 111. *New Phytologist*, *146*(2), 185–205. https://doi.org/10.1046/j.1469-8137.2000.00630.x

Cakmak, I. (2008). Enrichment of cereal grains with zinc: Agronomic or genetic biofortification? *Plant and Soil*, *302*(1), 1–17. https://doi.org/10.1007/s11104-007-9466-3

Cantabella, D., Piqueras, A., Acosta-Motos, J. R., Bernal-Vicente, A., Hernández, J. A., & Díaz-Vivancos, P. (2017). Salt-tolerance mechanisms induced in Stevia rebaudiana Bertoni: Effects on mineral nutrition, antioxidative metabolism and steviol glycoside content. *Plant Physiol. Biochem*, *115*, 484–496.

Cao, Y., Turk, K., Bibi, N., Ghafoor, A., Ahmed, N., Azmat, M., Ahmed, R., Ghani, M. I., & Ahanger, M. A. (2025). Nanoparticles as catalysts of agricultural revolution: Enhancing crop tolerance to abiotic stress: a review. *Frontiers in Plant Science*, *15*, 1510482. https://doi.org/10.3389/fpls.2024.1510482

Carmassi, G., Incrocci, L., Incrocci, G., & Pardossi, A. (2010). *NON-DESTRUCTIVE ESTIMATION OF LEAF AREA IN (SOLANUM LYCOPERSICUM L.) AND GERBERA (GERBERA JAMESONII H. BOLUS)*. https://www.semanticscholar.org/paper/NON-DESTRUCTIVE-ESTIMATION-OF-LEAF-AREA-IN-(SOLANUM-Carmassi-Incrocci/e019f2759b61e7aed2b7e79131139ef253dc8076

Cequier-Sánchez, E., Rodríguez, C., Ravelo, Á. G., & Zárate, R. (2008). Dichloromethane as a Solvent for Lipid Extraction and Assessment of Lipid Classes and Fatty Acids from Samples of Different Natures. *Journal of Agricultural and Food Chemistry*, *56*(12), 4297–4303. https://doi.org/10.1021/jf073471e

Chabi, I. B., Zannou, O., Dedehou, E. S. C. A., Ayegnon, B. P., Oscar Odouaro, O. B., Maqsood, S., Galanakis, C. M., & Pierre Polycarpe Kayodé, A. (2024). Tomato pomace as a source of valuable functional ingredients for improving physicochemical and sensory properties and extending the shelf life of foods: A review. *Heliyon*, *10*(3), e25261. https://doi.org/10.1016/j.heliyon.2024.e25261

Chance, B., & Maehly, A. C. (1955). [136] Assay of catalases and peroxidases: In *Methods in Enzymology* (Vol. 2, pp. 764–775). Academic Press. https://doi.org/10.1016/S0076-6879(55)02300-8

Chanu Thounaojam, T., Thounaojam, T. M., & Upadhyaya, H. (2021). Chapter 16—Role of zinc oxide nanoparticles in mediating abiotic stress responses in plant. In K. A. Abd-Elsalam (Ed.), *Zinc-Based Nanostructures for Environmental and Agricultural Applications* (pp. 323–337). Elsevier. https://doi.org/10.1016/B978-0-12-822836-4.00027-6

Chaudhary, D., Kumar, A., Kumar, R., Singode, A., Mukri, G., Sah, R., Tiwana, U., & Kumar, B. (2016). Evaluation of normal and specialty corn for fodder yield and quality traits. *Range Management and Agroforestry*, *37*, 79–83.

Chawla, L. S., Beers-Mulroy, B., & Tidmarsh, G. F. (2019). Therapeutic Opportunities for Hepcidin in Acute Care Medicine. *Critical Care Clinics, Modern Critical Care Endocrinology*, *35*(2), 357–374. https://doi.org/10.1016/j.ccc.2018.11.014

Chen, Z., Yuan, Y., Fu, D., Shen, C., & Yang, Y. (2017). Identification and Expression Profiling of the Auxin Response Factors in Dendrobium officinale under Abiotic Stresses. *International Journal of Molecular Sciences*, *18*(5), Article 5. https://doi.org/10.3390/ijms18050927

Childs, B. G., Durik, M., Baker, D. J., & van Deursen, J. M. (2015). Cellular senescence in aging and age-related disease: From mechanisms to therapy. *Nature Medicine*, *21*(12), 1424–1435. https://doi.org/10.1038/nm.4000

Christie, W. (1993). Preparation of ester derivatives of fatty acids for chromatographic analysis. In W. Ed. Christie (Ed.), *Advances in Lipid Methodology—Two* (pp. 69–111). Oily Press.

Cohu, C. M., Abdel-Ghany, S. E., Gogolin Reynolds, K. A., Onofrio, A. M., Bodecker, J. R., Kimbrel, J. A., Niyogi, K. K., & Pilon, M. (2009). Copper Delivery by the Copper Chaperone for Chloroplast and Cytosolic Copper/Zinc-Superoxide Dismutases: Regulation and Unexpected Phenotypes in an *Arabidopsis* Mutant. *Molecular Plant*, *2*(6), 1336–1350. https://doi.org/10.1093/mp/ssp084

Csiszár, J., Horváth, E., Váry, Z., Gallé, Á., Bela, K., Brunner, S., & Tari, I. (2014). Glutathione transferase supergene family in tomato: Salt stress-regulated expression of representative genes from distinct GST classes in plants primed with salicylic acid. *Plant Physiology and Biochemistry*, *78*, 15–26. https://doi.org/10.1016/j.plaphy.2014.02.010

Cuajungco, M. P., Ramirez, M. S., & Tolmasky, M. E. (2021). Zinc: Multidimensional Effects on Living Organisms. *Biomedicines*, *9*(2), 208. https://doi.org/10.3390/biomedicines9020208

Cuin, T. A., Bose, J., Stefano, G., Jha, D., Tester, M., Mancuso, S., & Shabala, S. (2011). Assessing the role of root plasma membrane and tonoplast Na+ /H+ exchangers in salinity tolerance in wheat: In planta quantification methods: Cytosolic Na+ exclusion in wheat. *Plant, Cell & Environment*, *34*(6), 947–961. https://doi.org/10.1111/j.1365-3040.2011.02296.x

Cushnie, T. P. T., & Lamb, A. J. (2005). Antimicrobial activity of flavonoids. *International Journal of Antimicrobial Agents*, *26*(5), 343–356. https://doi.org/10.1016/j.ijantimicag.2005.09.002

de Lima, R. B., dos Santos, T. B., Vieira, L. G. E., de Lourdes Lúcio Ferrarese, M., Ferrarese-Filho, O., Donatti, L., Boeger, M. R. T., & de Oliveira Petkowicz, C. L. (2014). Salt stress alters the cell wall polysaccharides and anatomy of coffee (*Coffea arabica* L.) leaf cells. *Carbohydrate Polymers*, *112*, 686–694. https://doi.org/10.1016/j.carbpol.2014.06.042

De Sio, F., Rapacciuolo, M., De Giorgi, A., Sandei, L., Giuliano, B., Tallarita, A., Golubkina, N., Sekara, A., Stoleru, V., Cuciniello, A., Morano, G., & Caruso, G. (2021). Industrial Processing Affects Product Yield and Quality of Diced Tomato. *Agriculture*, *11*(3), Article 3. https://doi.org/10.3390/agriculture11030230

Decsi, K., Ahmed, M., Abdul-Hamid, D., Rizk, R., & Tóth, Z. (2025). Verification of Seed-Priming-Induced Stress Memory by Genome-Wide Transcriptomic Analysis in Wheat (Triticum aestivum L.). *Agronomy*, *15*(6), Article 6. https://doi.org/10.3390/agronomy15061365

Decsi, K., Ahmed, M., & Tóth, Z. (2025). Genome-Wide Transcriptional Analysis Reveals Gamma-Aminobutyric Acid (GABA) Priming Induces Long-Term Stress Memory in Tomato (Solanum lycopersicum). *Agriculture*, *15*(19), 2012. https://doi.org/10.3390/agriculture15192012

De-la-Cruz Chacón, I., Riley-Saldaña, C. A., & González-Esquinca, A. R. (2013). Secondary metabolites during early development in plants. *Phytochemistry Reviews*, *12*(1), 47–64. https://doi.org/10.1007/s11101-012-9250-8

Demidchik, V. (2015). Mechanisms of oxidative stress in plants: From classical chemistry to cell biology. *Environmental and Experimental Botany*, *109*, 212–228. https://doi.org/10.1016/j.envexpbot.2014.06.021

Demiral, T., & Türkan, I. (2005). Comparative lipid peroxidation, antioxidant defense systems and proline content in roots of two rice cultivars differing in salt tolerance. *Environ. Exp. Bot*, *53*, 247–257.

Di Caterina, R., Giuliani, M. m., Rotunno, T., De Caro, A., & Flagella, Z. (2007). Influence of salt stress on seed yield and oil quality of two sunflower hybrids. *Annals of Applied Biology*, *151*(2), 145–154. https://doi.org/10.1111/j.1744-7348.2007.00165.x

Dixon, D. P., & Edwards, R. (2010). Glutathione Transferases. *The Arabidopsis Book*, *2010*(8). https://doi.org/10.1199/tab.0131

Dola, D. B., & Mannan, M. A. (2022). Foliar Application Effects of Zinc Oxide Nanoparticles on Growth, Yield and Drought Tolerance of Soybean. *Bangladesh Agronomy Journal*, *25*(2), 73–82. (Bangladesh). https://doi.org/10.3329/baj.v25i2.65940

Dombrowski, J. E. (2003). Salt Stress Activation of Wound-Related Genes in Tomato Plants. *Plant Physiology*, *132*(4), 2098–2107. https://doi.org/10.1104/pp.102.019927

Dresselhaus, T., & Hückelhoven, R. (2018). Biotic and Abiotic Stress Responses in Crop Plants. *Agronomy*, *8*(11), Article 11. https://doi.org/10.3390/agronomy8110267

Dziergowska, K., & Michalak, I. (2022). Chapter 9—The role of nanoparticles in sustainable agriculture. In K. Chojnacka & A. Saeid (Eds), *Smart Agrochemicals for Sustainable Agriculture* (pp. 225–278). Academic Press. https://doi.org/https://doi.org/10.1016/B978-0-12-817036-6.00007-8

El-Badri, A. M. A., Batool, M., Mohamed, I. A. A., Khatab, A., Sherif, A., Wang, Z., Salah, A., Nishawy, E., Ayaad, M., Kuai, J., Wang, B., & Zhou, G. (2021). Modulation of salinity impact on early seedling stage via nano-priming application of zinc oxide on rapeseed (Brassica napus L.). *Plant Physiology and Biochemistry: PPB*, *166*, 376–392. https://doi.org/10.1016/j.plaphy.2021.05.040

Elinder, F., & Liin, S. I. (2017). Actions and mechanisms of polyunsaturated fatty acids on voltage-gated ion channels. *Frontiers in Physiology*, *8*. https://doi.org/10.3389/fphys.2017.00043

Elkelish, A. A., Soliman, M. H., Alhaithloul, H. A., & El-Esawi, M. A. (2019). Selenium protects wheat seedlings against salt stress-mediated oxidative damage by up-regulating antioxidants and osmolytes metabolism. *Plant Physiol. Biochem*, *137*, 144–153.

Elsheery, N. I., Sunoj, V. S. J., Wen, Y., Zhu, J. J., Muralidharan, G., & Cao, K. F. (2020). Foliar application of nanoparticles mitigates the chilling effect on photosynthesis and photoprotection in sugarcane. *Plant Physiology and Biochemistry*, *149*, 50–60. https://doi.org/10.1016/j.plaphy.2020.01.035

El-Zohri, M., Al-Wadaani, N. A., & Bafeel, S. O. (2021). Foliar Sprayed Green Zinc Oxide Nanoparticles Mitigate Drought-Induced Oxidative Stress in Tomato. *Plants*, *10*(11), Article 11. https://doi.org/10.3390/plants10112400

Espitia, P. J. P., Soares, N. de F. F., Coimbra, J. S. dos R., de Andrade, N. J., Cruz, R. S., & Medeiros, E. A. A. (2012). Zinc Oxide Nanoparticles: Synthesis, Antimicrobial Activity and Food Packaging Applications. *Food and Bioprocess Technology*, *5*(5), 1447–1464. https://doi.org/10.1007/s11947-012-0797-6

Evelin, H., Kapoor, R., & Giri, B. (2009). Arbuscular mycorrhizal fungi in alleviation of salt stress: A review. *Ann. Bot*, *104*, 1263–1280.

Fabregat, A., Jupe, S., Matthews, L., Sidiropoulos, K., Gillespie, M., Garapati, P., Haw, R., Jassal, B., Korninger, F., May, B., Milacic, M., Roca, C. D., Rothfels, K., Sevilla, C., Shamovsky, V., Shorser, S., Varusai, T., Viteri, G., Weiser, J., … D'Eustachio, P. (2018). The Reactome Pathway Knowledgebase. *Nucleic Acids Research*, *46*(D1), D649–D655. https://doi.org/10.1093/nar/gkx1132

Fageria, V. D. (2001). Nutrient Interactions in Crop Plants. *Journal of Plant Nutrition*, *24*(8), 1269–1290. https://doi.org/10.1081/PLN-100106981

Faizan, M. (2020). Zinc Oxide Nanoparticles Ameliorate the Adverse Effects of Abiotic Stresses by Improving Growth, Photosynthesis and Antioxidant Defense System. *Ecotoxicology and Environmental Safety*, *184*, 109644.

Faizan, M., Bhat, J. A., Chen, C., Alyemeni, M. N., Wijaya, L., Ahmad, P., & Yu, F. (2021). Zinc oxide nanoparticles (ZnO-NPs) induce salt tolerance by improving the antioxidant system and photosynthetic machinery in tomato. *Plant Physiology and Biochemistry*, *161*, 122–130. https://doi.org/10.1016/j.plaphy.2021.02.002

Faizan, M., & Hayat, S. (2019). Effect of foliar spray of ZnO-NPs on the physiological parameters and antioxidant systems of Lycopersicon esculentum. *Polish Journal of Natural Sciences*, *34*(1). http://yadda.icm.edu.pl/yadda/element/bwmeta1.element.agro-668f9bf8-3d05-4497-85c5-bd3d9e14a40e

FAOStat. (2021). *FAO Stat*. FAO.

Farhangi-Abriz, S., & Ghassemi-Golezani, K. (2018). How can salicylic acid and jasmonic acid mitigate salt toxicity in soybean plants? *Ecotoxicol. Environ. Saf*, *154*, 1010–1016.

Farmer, E. E., & Mueller, M. J. (2013). ROS-Mediated Lipid Peroxidation and RES-Activated Signaling. *Ann. Rev. Plant Biol*, *64*, 429–450.

Fathi, A., Zahedi, M., & Torabian, S. (2017). Effect of Interaction between Salinity and Nanoparticles (Fe2O3 and ZnO) on Physiological Parameters Of Zea mays L. *J. Plant Nutr*, *40*, 2745–2755. https://doi.org/10.1080/01904167.2017.1381731.

F.D.A. (2023). *CFR—Code of Federal Regulations Title 21*. https://www.accessdata.fda.gov/scripts/cdrh/cfdocs/cfcfr/CFRSearch.cfm?fr=182.8991

Fikrika, H. (2016). Molecular docking studies of catechin and its derivatives as anti-bacterial inhibitors. *IOP Conference Series: Earth and Environmental Science*, *31*(1), 012019.

Foley, J. A., Ramankutty, N., Brauman, K. A., Cassidy, E. S., Gerber, J. S., & Johnston, M. (2011). Solutions for a cultivated planet. *Nature*, *478*(7369), 337–342.

Food, & Organization, A. (1998). *Crop Evapo-transpiration-Guidelines for Computing Crop Water Requirements, FAO Irrigation and Drainage Paper 56*. FAO.

Forghani, A. H., Mohebatinejad, H., & Fazilati, M. (2024). The Effect of Salt Stress on Antimicrobial Activity and Potential Production of Anthocyanin and Total Phenolic of Salicornia in Hydroponic Culture. *Proceedings of the National Academy of Sciences, India Section B: Biological Sciences*, *94*(4), 793–801. https://doi.org/10.1007/s40011-024-01643-y

Foyer, C. H., & Noctor, G. (2003). Redox sensing and signalling associated with reactive oxygen in chloroplasts, peroxisomes and mitochondria. *Physiol. Plant*, *119*, 355–364.

Gaafar, R., Diab, R., Halawa, M., Elshanshory, A., El-Shaer, A., & Hamouda, M. (2020). Role of Zinc Oxide Nanoparticles in Ameliorating Salt Tolerance in Soybean. *Egyptian Journal of Botany*. https://doi.org/10.21608/ejbo.2020.26415.1475

Gaikwad, S. (2023). Computational evaluation of phytochemicals as DNA gyrase inhibitors: A new frontier in antibiotic discovery. *Journal of Molecular Graphics and Modelling*, *118*, 108–115.

Galva, C., Artigas, P., & Gatto, C. (2012). Nuclear Na+/K+-ATPase plays an active role in nucleoplasmic Ca2+ homeostasis. *Journal of Cell, Science125*, 6137–6147.

Gao, Y., Lu, Y., Wu, M., Liang, E., Li, Y., Zhang, D., Yin, Z., Ren, X., Dai, Y., Deng, D., & Chen, J. (2016). Ability to Remove Na+ and Retain K+ Correlates with Salt Tolerance in Two Maize Inbred Lines Seedlings. *Frontiers in Plant Science*, *7*. https://doi.org/10.3389/fpls.2016.01716

García, A. B., Cuesta, A., Montes-Morán, M. A., Martínez-Alonso, A., & Tascón, J. M. D. (1997). Zeta Potential as a Tool to Characterize Plasma Oxidation of Carbon Fibers. *Journal of Colloid and Interface Science*, *192*(2), 363–367. https://doi.org/10.1006/jcis.1997.5007

Geilfus, C.-M., Tenhaken, R., & Carpentier, S. C. (2017). Transient alkalinization of the leaf apoplast stiffens the cell wall during onset of chloride salinity in corn leaves. *Journal of Biological Chemistry*, *292*(46), 18800–18813. https://doi.org/10.1074/jbc.M117.799866

Gellert, M., Mizuuchi, K., O'Dea, M. H., & Nash, H. A. (1976). DNA gyrase: An enzyme that introduces superhelical turns into DNA. *Proceedings of the National Academy of Sciences*, *73*(11), 3872–3876.

Gengmao, Z., Shihui, L., Xing, S., Yizhou, W., & Zipan, C. (2015). The role of silicon in physiology of the medicinal plant (Lonicera japonica L.) under salt stress. *Sci. Rep*, *5*, 12696.

Gerona, M. E. B., Deocampo, M. P., Egdane, J. A., Ismail, A. M., & Dionisio-Sese, M. L. (2019). Physiological Responses of Contrasting Rice Genotypes to Salt Stress at Reproductive Stage. *Rice Science*, *26*(4), 207–219. https://doi.org/10.1016/j.rsci.2019.05.001

Ghani, M. I., Saleem, S., Rather, S. A., Rehmani, M. S., Alamri, S., & Rajput, V. D. (2022). Foliar application of zinc oxide nanoparticles: An effective strategy to mitigate drought stress in cucumber seedling by modulating antioxidant defense system and osmolytes accumulation. *Chemosphere*, *289*(133202).

Ghannoum, O. (2009). C4 photosynthesis and water stress. *Annals of Botany*, *103*(4), 635–644. https://doi.org/10.1093/aob/mcn093

Ghiyasi, M., Rezaee Danesh, Y., Amirnia, R., Najafi, S., Mulet, J. M., & Porcel, R. (2023). Foliar Applications of ZnO and Its Nanoparticles Increase Safflower (Carthamus tinctorius L.) Growth and Yield under Water Stress. *Agronomy*, *13*(1), 192. https://doi.org/10.3390/agronomy13010192

Gogna, M., Choudhary, A., Mishra, G., Kapoor, R., & Bhatla, S. C. (2020). Changes in lipid composition in response to salt stress and its possible interaction with intracellular Na+-K+ ratio in sunflower (*Helianthus annuus* L.). *Environmental and Experimental Botany*, *178*, 104147. https://doi.org/10.1016/j.envexpbot.2020.104147

Goharrizi, K. J., Baghizadeh, A., Kalantar, M., & Fatehi, F. (2020). Combined effects of salinity and drought on physiological and biochemical characteristics of pistachio rootstocks. *Scientia Horticulturae*, *261*, 108970. https://doi.org/https://doi.org/10.1016/j.scienta.2019.108970

Goyer, A. (2010). Thiamine in plants: Aspects of its metabolism and functions. *Phytochemistry*, *71*(14), 1615–1624. https://doi.org/10.1016/j.phytochem.2010.06.022

Grigore, M. N., Toma, C., Grigore, M. N., & Toma, C. (2017). *Saline environments*. Springer International Publishing.

Gudkov, S. V., Li, R., Serov, D. A., Burmistrov, D. E., Baimler, I. V., Baryshev, A. S., Simakin, A. V., Uvarov, O. V., Astashev, M. E., Nefedova, N. B., Smolentsev, S. Y., Onegov, A. V., Sevostyanov, M. A., Kolmakov, A. G., Kaplan, M. A., Drozdov, A., Tolordava, E. R., Semenova, A. A., Lisitsyn, A. B., & Lednev, V. N. (2023). Fluoroplast Doped by Ag2O Nanoparticles as New Repairing Non-Cytotoxic Antibacterial Coating for Meat Industry. *International Journal of Molecular Sciences*, *24*(1), Article 1. https://doi.org/10.3390/ijms24010869

Gudkov, S. V., Sarimov, R. M., Astashev, M. E., Pishchalnikov, R. Y., Yanykin, D. V., Simakin, A. V., Shkirin, A. V., Serov, D. A., Konchekov, E. M., Ogly, G. N. G., Lednev, V. N., Grishin, M. Y., Sdvizhenskii, P. A., Pershin, S. M., Bunkin, A. F., Ashurov, M. K., Aksenov, A. G., Chilingaryan, N. O., Smirnov, I. G., … Izmailov, A. Y. (2024). Modern physical methods and technologies in agriculture. *Physics-Uspekhi*, *67*(2), 194–210.

Guo, Q., Liu, L., & Uppalapati, S. R. (2019). Membrane lipid metabolism and its adaptation to environmental abiotic stresses in plants. *International Journal of Molecular Sciences*, *20*(16), 3930.

Gupta, A., Bharati, R., Kubes, J., Popelkova, D., Praus, L., Yang, X., Severova, L., Skalicky, M., & Brestic, M. (2024). Zinc oxide nanoparticles application alleviates salinity stress by modulating plant growth, biochemical attributes and nutrient homeostasis in Phaseolus vulgaris L. *Frontiers in Plant Science*, *15*. https://doi.org/10.3389/fpls.2024.1432258

Gururani, M. A., Venkatesh, J., & Tran, L. S. P. (2015). Regulation of photosynthesis during abiotic stress-induced photoinhibition. *Mol. Plant*, *8*, 1304–1320.

Habig, W. H., Pabst, M. J., & Jakoby, W. B. (1974). Glutathione S-transferases: The first enzymatic step in mercapturic acid formation. *J. Biol. Chem*, *249*, 7130–7139.

Hajiboland, R., Norouzi, F., & Poschenrieder, C. (2014). Growth, physiological, biochemical and ionic responses of pistachio seedlings to mild and high salinity. *Trees Struct. Funct*, *28*, 1065–1078.

Hameed, A., Ahmed, M. Z., Hussain, T., Aziz, I., Ahmad, N., Gul, B., & Nielsen, B. L. (2021). Effects of Salinity Stress on Chloroplast Structure and Function. *Cells*, *10*(8), 2023. https://doi.org/10.3390/cells10082023

Hamzah Saleem, M., Usman, K., Rizwan, M., Al Jabri, H., & Alsafran, M. (2022). Functions and strategies for enhancing zinc availability in plants for sustainable agriculture. *Frontiers in Plant Science*, *13*. https://doi.org/10.3389/fpls.2022.1033092

Hasanuzzaman, M., Bhuyan, M. H. M. B., Nahar, K., Hossain, M. S., Mahmud, J. A., Hossen, M. S., Masud, A. A. C., Moumita, & Fujita, M. (2018). Potassium: A Vital Regulator of Plant Responses and Tolerance to Abiotic Stresses. *Agronomy*, *8*(3), Article 3. https://doi.org/10.3390/agronomy8030031

Hasanuzzaman, M., Bhuyan, M. H. M. B., Zulfiqar, F., Raza, A., Mohsin, S. M., Mahmud, J. A., Fujita, M., & Fotopoulos, V. (2020). Reactive Oxygen Species and Antioxidant Defense in Plants under Abiotic Stress: Revisiting the Crucial Role of a Universal Defense Regulator. *Antioxidants*, *9*(8), 681. https://doi.org/10.3390/antiox9080681

Hassan, N. S., Salah El Din, T. A., Hendawey, M. H., Borai, I. H., & Mahdi, A. A. (2018). Magnetite and zinc oxide nanoparticles alleviated heat stress in wheat plants. *Current Nanomaterials*, *3*(1), 32–43.

Hauser, F., & Horie, T. (2010). A conserved primary salt tolerance mechanism mediated by HKT transporters: A mechanism for sodium exclusion and maintenance of high K/Na ratio in leaves during salinity stress. *Plant Cell Environ*, *33*, 552–565.

Hayat, S., Hayat, Q., Alyemeni, M. N., Wani, A. S., Pichtel, J., & Ahmad, A. (2012). Role of proline under changing environments. *Plant Signaling & Behavior*, *7*(11), 1456–1466. https://doi.org/10.4161/psb.21949

Heath, R. L., & Packer, L. (1968). Photoperoxidation in isolated chloroplasts. I. Kinetics and stoichiometry of fatty acid peroxidation. *Archives of Biochemistry and Biophysics*, *125*(1), 189–198. https://doi.org/10.1016/0003-9861(68)90654-1

Herms, D. A., & Mattson, W. J. (1992). The Dilemma of Plants: To Grow or Defend. *The Quarterly Review of Biology*, *67*(3), 283–335.

Hernández-Fuentes, A. D., López-Vargas, E. R., Pinedo-Espinoza, J. M., Campos-Montiel, R. G., Valdés-Reyna, J., & Juárez-Maldonado, A. (2017). Postharvest Behavior of Bioactive Compounds in Tomato Fruits Treated with Cu Nanoparticles and NaCl Stress. *Applied Sciences*, *7*(10), Article 10. https://doi.org/10.3390/app7100980

Hezaveh, T. A., Pourakbar, L., Rahmani, F., & Alipour, H. (2019). Interactive Effects of Salinity and ZnO Nanoparticles on Physiological and Molecular Parameters of Rapeseed (Brassica napus L. *Commun. Soil Sci. Plant Anal*, *50*, 698–715. https://doi.org/10.1080/00103624.2019.1589481.

Hoffmann, T., Hofman, A., & Wagenmakers, E.-J. (2022). Bayesian Tests of Two Proportions: A Tutorial With R and JASP. *Methodology*, *18*(4), Article 4. https://doi.org/10.5964/meth.9263

Hong, Y., Zhao, J., Guo, L., Kim, S.-C., Deng, X., Wang, G., Zhang, G., Li, M., & Wang, X. (2016). Plant phospholipases D and C and their diverse functions in stress responses. *Progress in Lipid Research*, *62*, 55–74. https://doi.org/10.1016/j.plipres.2016.01.002

Hoppe, K., & Carlson, Z. (2023). *Quality Forage Series: Interpreting Composition and Determining Market Value*. North Dakota State University.

Houot, V., Etienne, P., Petitot, A. S., Barbier, S., Blein, J. P., & Suty, L. (2001). Hydrogen peroxide induces programmed cell death features in cultured tobacco BY-2 cells, in a dose-dependent manner. *J. Exp. Bot*, *52*, 1721–1730.

Hsu, S. Y., & Kao, C. H. (2003). Differential effect of sorbitol and polyethylene glycol on antioxidant enzymes in rice leaves. *Plant Growth Regulation*, *39*, 83–90. https://doi.org/10.1023/A:1021830926902

Huot, B., Yao, J., Montgomery, B. L., & He, S. Y. (2014). Growth–Defense Tradeoffs in Plants: A Balancing Act to Optimize Fitness. *Molecular Plant*, *7*(8), 1267–1287.

Hussain, S., Bai, Z., Huang, J., Cao, X., Zhu, L., Zhu, C., Khaskheli, M. A., Zhong, C., Jin, Q., & Zhang, J. (2019). 1-methylcyclopropene modulates physiological, biochemical, and antioxidant responses of rice to different salt stress levels. *Front. Plant Sci*, 10.

Hussain, S., Cao, X., Zhong, C., Zhu, L., Khaskheli, M. A., Fiaz, S., Zhang, J., & Jin, Q. (2018). Sodium chloride stress during early growth stages altered physiological and growth characteristics of rice. *Chilean Journal of Agricultural Research*, *78*(2), 183–197. https://doi.org/10.4067/s0718-58392018000200183

Hussain, S., Zhang, J. H., Zhong, C., Zhu, L. F., Cao, X. C., YU, S. M., Allen Bohr, J., Hu, J. J., & Jin, Q. Y. (2017). Effects of salt stress on rice growth, development characteristics, and the regulating ways: A review. *J. Integr. Agric*, *16*, 2357–2374.

Hussain, S., Zhong, C., Bai, Z., Cao, X., Zhu, L., Hussain, A., Zhu, C., Fahad, S., James, A. B., & Zhang, J. (2018). Effects of 1-Methylcyclopropene on Rice Growth Characteristics and Superior and Inferior Spikelet Development Under Salt Stress. *J. Plant Growth Regul*, *37*, 1368–1384.

Hussein, M. M., & Abou-Baker, N. H. (2018). The contribution of nano-zinc to alleviate salinity stress on cotton plants. *Royal Society Open Science*, *5*(8), 171809. https://doi.org/10.1098/rsos.171809

Ibrahim, E. A. (2016). Seed priming to alleviate salinity stress in germinating seeds. *J. Plant Physiol*, *192*, 38–46.

Ihme, N., Kiesewetter, H., Jung, F., Hoffmann, K. H., Birk, A., Müller, A., & Grützner, K. I. (1996). Leg oedema protection from a buckwheat herb tea in patients with chronic venous insufficiency: A single-centre, randomised, double-blind, placebo controlled clinical trial. *European Journal of Clinical Pharmacology*, *50*(6), 443–447. Scopus. https://doi.org/10.1007/s002280050138

Imakumbili, M. L. E., Semu, E., Semoka, J. M. R., Abass, A., & Mkamilo, G. (2021). Managing cassava growth on nutrient poor soils under different water stress conditions. *Heliyon*, *7*(6), e07331. https://doi.org/https://doi.org/10.1016/j.heliyon.2021.e07331

Inculet, C.-S., Mihalache, G., Sellitto, V. M., Hlihor, R.-M., & Stoleru, V. (2019). The Effects of a Microorganisms-Based Commercial Product on the Morphological, Biochemical and Yield of Tomato Plants under Two Different Water Regimes. *Microorganisms*, *7*(12), Article 12. https://doi.org/10.3390/microorganisms7120706

Ingrao, C., Strippoli, R., Lagioia, G., & Huisingh, D. (2023). Water scarcity in agriculture: An overview of causes, impacts and approaches for reducing the risks. *Heliyon*, *9*(8), e18507. https://doi.org/https://doi.org/10.1016/j.heliyon.2023.e18507

Intra, J., Pescatori, M., & Bernasconi, S. (2007). Alpha-L-fucosidase: Structure, genetics and role in biology. *Glycobiology*, *17*(9), 958–971.

Isah, T. (2019). Stress Responses of Secondary Metabolites in Plants: A Review. *Frontiers in Plant Science*, *10*, 21.

Jadhav, A. K., Khan, P. K., & Karuppayil, S. M. (2020). PHYTOCHEMICALS AS POTENTIAL INHIBITORS OF LANOSTEROL 14 A-DEMETHYLASE (CYP51) ENZYME: AN IN SILICO STUDY ON SIXTY MOLECULES. *International Journal of Applied Pharmaceutics*, 18–30. https://doi.org/10.22159/ijap.2020.v12s4.40100

Jaime-Pérez, N., Pineda, B., García-Sogo, B., Atares, A., Athman, A., Byrt, C. S., Olías, R., Asins, M. J., Gilliham, M., Moreno, V., & Belver, A. (2017). The sodium transporter encoded by the HKT1;2 gene modulates sodium/potassium homeostasis in tomato shoots under salinity. *Plant, Cell & Environment*, *40*(5), 658–671. https://doi.org/10.1111/pce.12883

Jain, D., Shivani, Bhojiya, A. A., Singh, H., Daima, H. K., Singh, M., Mohanty, S. R., Stephen, B. J., & Singh, A. (2020). Microbial Fabrication of Zinc Oxide Nanoparticles and Evaluation of Their Antimicrobial and Photocatalytic Properties. *Frontiers in Chemistry*, *8*. https://doi.org/10.3389/fchem.2020.00778

James, R. A., Blake, C., Byrt, C. S., & Munns, R. (2011). Major genes for Na+ exclusion, Nax1 and Nax2 (wheat HKT1;4 and HKT1;5), decrease Na+ accumulation in bread wheat leaves under saline and waterlogged conditions. *J. Exp. Bot*, *62*, 2939–2947.

Jayarambabu, N. (2014). Germination and Growth Characteristics of Mungbean Seeds (Vigna radiata L.) affected by Synthesized Zinc Oxide Nanoparticles. *International Journal of Current Engineering and Technology*, *4*, 5.

Jethva, J., Schmidt, R. R., Sauter, M., & Selinski, J. (2022). Try or Die: Dynamics of Plant Respiration and How to Survive Low Oxygen Conditions. *Plants*, *11*(2), 205. https://doi.org/10.3390/plants11020205

Jiang, C., Zu, C., Lu, D., Zheng, Q., Shen, J., Wang, H., & Li, D. (2017). Effect of exogenous selenium supply on photosynthesis, Na+ accumulation and antioxidative capacity of maize (Zea mays L.) under salinity stress. *Sci. Rep*, *7*, 42039.

Johnson, R., Vishwakarma, K., Hossen, M. S., Kumar, V., Shackira, A. M., Puthur, J. T., Abdi, G., Sarraf, M., & Hasanuzzaman, M. (2022). Potassium in plants: Growth regulation, signaling, and environmental stress tolerance. *Plant Physiology and Biochemistry: PPB*, *172*, 56–69. https://doi.org/10.1016/j.plaphy.2022.01.001

Kamran, M., Malik, Z., Parveen, A., Huang, L., Riaz, M., Bashir, S., Mustafa, A., Abbasi, G. H., Xue, B., & Ali, U. (2019a). Ameliorative Effects of Biochar on Rapeseed (Brassica napus L.) Growth and Heavy Metal Immobilization in Soil Irrigated with Untreated Wastewater. *Journal of Plant Growth Regulation*, 1–16.

Kamran, M., Parveen, A., Ahmar, S., Malik, Z., Hussain, S., Chattha, M. S., Saleem, M. H., Adil, M., Heidari, P., & Chen, J.-T. (2019b). An Overview of Hazardous Impacts of Soil Salinity in Crops, Tolerance Mechanisms, and Amelioration through Selenium Supplementation. *International Journal of Molecular Sciences*, *21*(1), 148. https://doi.org/10.3390/ijms21010148

Kanehisa, M., & Goto, S. (2000). KEGG: kyoto encyclopedia of genes and genomes. *Nucleic Acids Res, 1;28(1):27-30*. https://doi.org/10.1093/nar/28.1.27.

Kang, Y., & Wan, S. (2005). Effect of soil water potential on radish (*Raphanus sativus* L.) growth and water use under drip irrigation. *Scientia Horticulturae*, *106*(3), 275–292. https://doi.org/10.1016/j.scienta.2005.03.012

Katerji, N., Hoorn, J. W. van, Hamdy, A., & Mastrorilli, M. (2001). Salt tolerance of crops according to three classification methods and examination of some hypothesis about salt tolerance. *Agricultural Water Management*, *47*(1), 1–8. https://doi.org/https://doi.org/10.1016/S0378-3774(00)00099-8

Kerepesi, I., & Galiba, G. (2000). Osmotic and salt stress-induced alteration in soluble carbohydrate content in wheat seedlings. *Crop Science*, *40*(2), 482–487. Scopus. https://doi.org/10.2135/cropsci2000.402482x

Khan, M. I. R., Asgher, M., & Khan, N. A. (2014). Alleviation of salt-induced photosynthesis and growth inhibition by salicylic acid involves glycinebetaine and ethylene in mungbean (Vigna radiata L. *Plant Physiol. Biochem*, *80*, 67–74.

Khan, M. T. (2021). Molecular docking and dynamics simulation of plant-derived protease inhibitors against multidrug-resistant bacteria. *Frontiers in Molecular Biosciences*, *8*, 642–651.

Khan, S. T., Malik, A., Alwarthan, A., & Shaik, M. R. (2022). The enormity of the zinc deficiency problem and available solutions; an overview. *Arabian Journal of Chemistry*, *15*(3), 103668. https://doi.org/10.1016/j.arabjc.2021.103668

Khanm, H., Vaishnavi, B. A., & Shankar, A. G. (2018). Raise of Nano-Fertilizer Era: Effect of Nano Scale Zinc Oxide Particles on the Germination, Growth and Yield of Tomato (Solanum lycopersicum). *International Journal of Current Microbiology and Applied Sciences*, *7*(5), 1861–1871. https://doi.org/10.20546/ijcmas.2018.705.219

Khatkar, D., & Kuhad, M. S. (2000). Short-term salinity induced changes in two wheat cultivars at different growth stages. *Biologia Plantarum*, *43*(4), 629–632. Scopus. https://doi.org/10.1023/A:1002868519779

Khattak, S. G., Dominy, P. J., & Ahmad, W. (2015). *Effect of Zn as soil addition and foliar application on yield and protein content of wheat in alkaline soil* (No. 4). *43*(4), Article 4. https://doi.org/10.4038/jnsfsr.v43i4.7965

Khodakovskaya, M., Dervishi, E., Mahmood, M., Xu, Y., Li, Z., Watanabe, F., & Biris, A. S. (2009). Carbon nanotubes are able to penetrate plant seed coat and dramatically affect seed germination and plant growth. *ACS Nano*, *3*, 3221–3227.

Kim, D. Y., Kwon, S. I., Choi, C., Lee, H., Ahn, I., Park, S. R., Bae, S. C., Lee, S. C., & Hwang, D. J. (2013). Expression analysis of rice VQ genes in response to biotic and abiotic stresses. *Gene*, *529*(2), 208–214. https://doi.org/10.1016/j.gene.2013.08.023

Kim, H.-J., Fonseca, J. M., Kubota, C., Kroggel, M., & Choi, J.-H. (2008). Quality of fresh-cut tomatoes as affected by salt content in irrigation water and post-processing ultraviolet-C treatment. *Journal of the Science of Food and Agriculture*, *88*(11), 1969–1974. https://doi.org/10.1002/jsfa.3305

Kim, K.-H., Tsao, R., Yang, R., & Cui, S. W. (2006). Phenolic acid profiles and antioxidant activities of wheat bran extracts and the effect of hydrolysis conditions. *Food Chemistry*, *95*(3), 466–473. https://doi.org/10.1016/j.foodchem.2005.01.032

Kinraide, T. B. (1999). Interactions among Ca2+, Na+ and K+ in salinity toxicity: Quantitative resolution of multiple toxic and ameliorative effects. *Journal of Experimental Botany*, *50*(338), 1495–1505. https://doi.org/10.1093/jxb/50.338.1495

Kitchener, R. L. (2021). Molecular Docking Studies of Plant Metabolites against Microbial Targets. *Computational Biology and Chemistry*, *91*, 107452.

Kong-Ngern, K., Daduang, S., Wongkham, C. H., Bunnag, S., Kosittrakun, M., & Theerakulpisut, P. (2005). *Protein Profiles in Response to Salt Stress in Leaf Sheaths of Rice Seedlings*, *Sci* (Vol. 31, pp. 403–408).

Korban, S., Bobrov, K., Borshchevskiy, V., Pospelov, V., Shvetsov, A., Titov, A., Eneyskaya, E., & Kulminskaya, A. (2025). Structure and biochemical characterization of GH29 family α-l-fucosidase from *Fusarium*

proliferatum LE1. *Biochemical and Biophysical Research Communications*, *779*, 152451. https://doi.org/10.1016/j.bbrc.2025.152451

Kozukue, N., Han, J.-S., Lee, K.-R., & Friedman, M. (2004). Dehydrotomatine and alpha-tomatine content in tomato fruits and vegetative plant tissues. *Journal of Agricultural and Food Chemistry*, *52*(7), 2079–2083. https://doi.org/10.1021/jf0306845

Krauss, S., Schnitzler, W. H., Grassmann, J., & Woitke, M. (2006). The Influence of Different Electrical Conductivity Values in a Simplified Recirculating Soilless System on Inner and Outer Fruit Quality Characteristics of Tomato. *Journal of Agricultural and Food Chemistry*, *54*(2), 441–448. https://doi.org/10.1021/jf051930a

Krishnaiah, D., Sarbatly, R., & Nithyanandam, R. (2011). A review of the antioxidant potential of medicinal plant species. *Food Bioprod. Process*, *89*, 217–233.

Ksouri, R., Megdiche, W., Debez, A., Falleh, H., Grignon, C., & Abdelly, C. (2007). Salinity effects on polyphenol content and antioxidant activities in leaves of the halophyte *Cakile maritima*. *Plant Physiology and Biochemistry*, *45*(3), 244–249. https://doi.org/10.1016/j.plaphy.2007.02.001

Kumar, D., Yusuf, M. A., Singh, P., Sardar, M., & Sarin, N. B. (2013). Modulation of antioxidant machinery in α-tocopherol-enriched transgenic Brassica juncea plants tolerant to abiotic stress conditions. *Protoplasma*, *250*(5), 1079–1089. Scopus. https://doi.org/10.1007/s00709-013-0484-0

Kumar, K. H., Adithya, S., & Savalgi, V. P. (2021). Evaluation of foliar application of zinc nanoparticles on growth and yield parameters of maize (Zea mays L.) grown under greenhouse conditions. *International Journal of Chemical Studies*, *9*(1), 1464–1467. https://doi.org/10.22271/chemi.2021.v9.i1u.11428

Lai, Z., Li, Y., Wang, F., Cheng, Y., Fan, B., Yu, J.-Q., & Chen, Z. (2011). Arabidopsis sigma factor binding proteins are activators of the WRKY33 transcription factor in plant defense. *The Plant Cell*, *23*(10), 3824–3841. https://doi.org/10.1105/tpc.111.090571

Lalarukh, I., Zahra, N., Al Huqail, A. A., Amjad, S. F., Al−Dhumri, S. A., Ghoneim, A. M., Alshahri, A. H., Almutari, M. M., Alhusayni, F. S., & Al−Shammari, W. B. (2022). Exogenously Applied ZnO Nanoparticles Induced Salt Tolerance in Potentially High Yielding Modern Wheat (Triticum aestivum L.) Cultivars. *Environ. Technol. Innov*, *27*, 102799. https://doi.org/10.1016/j.eti.2022.102799.

Lee, D. G., Park, K. W., An, J. Y., Sohn, Y. G., Ha, J. K., Kim, H. Y., Bae, D. W., Lee, K. H., Kang, N. J., & Lee, B. H. (2011). Proteomics analysis of salt-induced leaf proteins in two rice germplasms with different salt sensitivity. *Can. J. Plant Sci*, *91*, 337–349.

Lefoulon, C. (2021). The bare necessities of plant K+ channel regulation. *Plant Physiology*, *187*(4), 2092–2109. https://doi.org/10.1093/plphys/kiab266

Levitt, J. (1985). Responses of Plants to Environmental Stresses. *J. Range Manag*, *38*(480). https://doi.org/10.2307/3899731.

Li, B., & Dewey, C. N. (2011). RSEM: Accurate transcript quantification from RNA-Seq data with or without a reference genome. *BMC Bioinformatics*, *12*(1), 323. https://doi.org/10.1186/1471-2105-12-323

Li, J., Chen, J., Jin, J., Wang, S., & Du, B. (2019). Effects of Irrigation Water Salinity on Maize (Zea may L.) Emergence, Growth, Yield, Quality, and Soil Salt. *Water*, *11*(10), Article 10. https://doi.org/10.3390/w11102095

Li, M., Guo, S., Xu, Y., Meng, Q., Li, G., & Yang, X. (2014). Glycine betaine-mediated potentiation of HSP gene expression involves calcium signaling pathways in tobacco exposed to NaCl stress. *Physiol. Plant*, *150*, 63–75.

Li, N., Wu, X., Zhuang, W., Xia, L., Chen, Y., Wu, C., Rao, Z., Du, L., Zhao, R., Yi, M., Wan, Q., & Zhou, Y. (2021). Tomato and lycopene and multiple health outcomes: Umbrella review. *Food Chemistry*, *343*, 128396. https://doi.org/10.1016/j.foodchem.2020.128396

Li, W., Mi, X., Jin, X., Zhang, D., Zhu, G., Shang, X., Zhang, D., & Guo, W. (2022). Thiamine functions as a key activator for modulating plant health and broad-spectrum tolerance in cotton. *The Plant Journal*, *111*(2), 374–390. https://doi.org/10.1111/tpj.15793

Li, Y. (2009). Physiological Responses of Tomato Seedlings (Lycopersicon Esculentum) to Salt Stress. *Modern Applied Science*, *3*(3), Article 3. https://doi.org/10.5539/mas.v3n3p171

Li, Y., Ye, Z., Xiang, J., Li, S., Zheng, Z., Li, Y., Fang, Y., Zhang, X., Chen, X., & Xue, D. (2025). Purine nucleotide metabolism response to drought stress in rice. *Plant Growth Regulation*. https://doi.org/10.1007/s10725-025-01309-3

Limanto, A. (2025). *Antioxidant, alpha-glucosidase inhibitory activity and molecular docking study of gallic acid, quercetin and rutin*. Cell and BioPharmaceutical Institute.

Lin, D., & Xing, B. (2008). Root uptake and phytotoxicity of ZnO nanoparticles. *Environmental Science and Technology*, *42*(15), 5580–5585. Scopus. https://doi.org/10.1021/es800422x

Liu, X., Ma, D., Zhang, Z., Wang, S., Du, S., Deng, X., & Yin, L. (2019). Plant lipid remodeling in response to abiotic stresses. *Environmental and Experimental Botany*, *165*, 174–184. https://doi.org/10.1016/j.envexpbot.2019.06.005

Lu, W., Zhao, Y., Liu, J., Zhou, B., Wei, G., Ni, R., Zhang, S., & Guo, J. (2023). Comparative Analysis of Antioxidant System and Salt-Stress Tolerance in Two Hibiscus Cultivars Exposed to NaCl Toxicity. *Plants*, *12*(7), 1525. https://doi.org/10.3390/plants12071525

Lucas, J. R., & Dupree, B. (n.d.). Stomatal pore width and area measurements in Zea mays. *microPublication Biology*, *2023*, 10.17912/micropub.biology.000893. https://doi.org/10.17912/micropub.biology.000893

Lunde, C., Drew, D. P., Jacobs, A. K., & Tester, M. (2007). Exclusion of Na+ via sodium ATPase (PpENA1) ensures normal growth of Physcomitrella patens under moderate salt stress. *Plant*, (ysiology144), 1786–1796.

Lv, Y., Pan, J., Wang, H., Reiter, R. J., Li, X., Mou, Z., Zhang, J., Yao, Z., Zhao, D., & Yu, D. (2021). Melatonin inhibits seed germination by crosstalk with abscisic acid, gibberellin, and auxin in Arabidopsis. *Journal of Pineal Research*, *70*(4), e12736. https://doi.org/10.1111/jpi.12736

Ma, Y., Dias, M. C., & Freitas, H. (2020). Drought and Salinity Stress Responses and Microbe-Induced Tolerance in Plants. *Frontiers in Plant Science*, *11*, 591911. https://doi.org/10.3389/fpls.2020.591911

Maas, E. V. (1990). Crop salt tolerance. In *Agricultural salinity assessment and management; ASCE Manuals and Reports on Engineering Practice*. American Society of Civil Engineers.

Maehly, A. C. (1954). The assay of catalases and peroxidases. In *Methods of Biochemical Analysis* (pp. 357–424). Wiley. https://doi.org/10.1002/9780470110171.ch14

Mahalakshmi, H. & Vijaya. (2020). In vitro biocompatibility and antimicrobial activities of zinc oxide nanoparticles (ZnO NPs) prepared by chemical and green synthetic route—A comparative study. *BioNanoScience*, *10*(1), 112–121. https://doi.org/10.1007/s12668-019-00698-w

Mahawar, L., Živčák, M., Barboricova, M., Kovár, M., Filaček, A., Ferencova, J., Vysoká, D. M., & Brestič, M. (2024). Effect of copper oxide and zinc oxide nanoparticles on photosynthesis and physiology of *Raphanus sativus* L. under salinity stress. *Plant Physiology and Biochemistry*, *206*, 108281. https://doi.org/10.1016/j.plaphy.2023.108281

Mai, T. T. N., Minh, P. N., Phat, N. T., Chi, M. T., Hien, D. C., Nguyen, V.-K., Duong, T. H., Nha, T. T., An, T. N. M., Tran, N. N. H., & Tri, M. D. (2024). In vitro and in silico studies of alpha glucosidase inhibition and antifungal activity of coffea canephora husk. *RSC Advances*, *14*(37), 27252–27264. https://doi.org/10.1039/D4RA04405C

Majumdar, G., & Mandal, S. (2024). Evaluation of broad-spectrum antibacterial efficacy of quercetin by molecular docking, molecular dynamics simulation and in vitro studies. *Chemical Physics Impact*, *8*, 100501. https://doi.org/10.1016/j.chphi.2024.100501

Mallahi, T., Saharkhiz, M. J., & Javanmardi, J. (2018). Salicylic acid changes morpho-physiological attributes of feverfew (Tanacetum parthenium L.) under salinity stress. *Acta Ecol. Sin*, *38*, 351–355.

Mandal, A. K., Katuwal, S., Tettey, F., Gupta, A., Bhattarai, S., Jaisi, S., Bhandari, D. P., Shah, A. K., Bhattarai, N., & Parajuli, N. (2022). Current Research on Zinc Oxide Nanoparticles: Synthesis, Characterization, and Biomedical Applications. *Nanomaterials*, *12*(17), 3066. https://doi.org/10.3390/nano12173066

Manigopa, C., & Sah, R. (2012). *Genetic component in baby corn (Zea Mays L.)*. *12*, 291–294.

Mansour, M. M. F., & Ali, E. F. (2017). Evaluation of proline functions in saline conditions. *Phytochemistry*, *140*, 52–68. https://doi.org/https://doi.org/10.1016/j.phytochem.2017.04.016

Marrez, D. A., El-Ssayad, M. F., Shaker, A. S., Elaaser, M., & Badr, A. N. (2024). Antimicrobial Synergy Interaction of Microalgae and Nisin to Improve Ice Cream Shelf Life and Retaining Quality. *Food Bioscience*, *105638*. https://doi.org/10.1016/j.fbio.2024.105638

Mashat, K. H., Babgi, B. A., Hussien, M. A., Arshad, M. N., & Abdellattif, M. H. (2019). Synthesis, structures, DNA-binding and anticancer activities of some copper (I)-phosphine complexes. *Polyhedron*, *158*, 164–172. https://doi.org/10.1016/j.poly.2018.10.062

McMillan, J. (2025). In silico docking and ADMET studies on clinical targets by rutin and phenolic acids. In *Silico Pharmacology*.

Medeiros, F. H. V., Martins, S. J., Zucchi, T. D., Melo, I. S., Batista, L. R., & Machado, J. C. (2011). Biological control of mycotoxin-producing molds. *Cienc. Agrotecnol*, *36*, 483–497.

Mendes, A. R., Granadeiro, C. M., Leite, A., Geiss, O., Bianchi, I., Ponti, J., Mehn, D., Pereira, E., Teixeira, P., & Poças, F. (2025). Functional Properties and Safety Considerations of Zinc Oxide Nanoparticles Under Varying Conditions. *Nanomaterials*, *15*(12), 892. https://doi.org/10.3390/nano15120892

Meneguzzo, S., Navari-Izzo, F., & Izzo, R. (1999). Antioxidative responses of shoots and roots of wheat to increasing NaCl concentrations. *Journal of Plant Physiology*, *155*(2), 274–280. Scopus. https://doi.org/10.1016/S0176-1617(99)80019-4

Merlani, M., Barbakadze, V., Amiranashvili, L., Gogilashvili, L., Poroikov, V., Petrou, A., & Sokovic, M. (2019). New caffeic acid derivatives as antimicrobial agents: Design, synthesis, evaluation and docking. *Current Topics in Medicinal Chemistry*, *19*(4), 292–304. https://doi.org/10.2174/1568026619666190122152957

Mirzajani, F., Askari, H., Hamzelou, S., Schober, Y., Römpp, A., Ghassempour, A., & Spengler, B. (2014). Proteomics study of silver nanoparticles toxicity on Oryza sativa L. *Ecotoxicol. Environ. Saf*, *108*, 335–339.

Mishra, N., Jiang, C., Chen, L., Paul, A., Chatterjee, A., & Shen, G. (2023). Achieving abiotic stress tolerance in plants through antioxidative defense mechanisms. *Frontiers in Plant Science*, *14*. https://doi.org/10.3389/fpls.2023.1110622

Mittal, S., Kumari, N., & Sharma, V. (2012). Differential response of salt stress on Brassica juncea: Photosynthetic performance, pigment, proline, D1 and antioxidant enzymes. *Plant Physiol. Biochem*, *54*, 17–26.

Mittova, V., Guy, M., Tal, M., & Volokita, M. (2004). Salinity up-regulates the antioxidative system in root mitochondria and peroxisomes of the wild salt-tolerant tomato species Lycopersicon pennellii. *Journal of Experimental Botany*, *55*(399), 1105–1113. https://doi.org/10.1093/jxb/erh113

Modena, M. M., Rühle, B., Burg, T. P., & Wuttke, S. (2019). Nanoparticle Characterization: What to Measure? *Advanced Materials*, *31*(32), 1901556. https://doi.org/10.1002/adma.201901556

Mogazy, A. M., & Hanafy, R. S. (2022). Foliar Spray of Biosynthesized Zinc Oxide Nanoparticles Alleviate Salinity Stress Effect on Vicia faba Plants. *Journal of Soil Science and Plant Nutrition*, *22*(2), 2647–2662. https://doi.org/10.1007/s42729-022-00833-9

Moles, T. M., de Brito Francisco, R., Mariotti, L., Pompeiano, A., Lupini, A., Incrocci, L., Carmassi, G., Scartazza, A., Pistelli, L., Guglielminetti, L., Pardossi, A., Sunseri, F., Hörtensteiner, S., & Santelia, D. (2019). Salinity in Autumn-Winter Season and Fruit Quality of Tomato Landraces. *Frontiers in Plant Science*, *10*. https://doi.org/10.3389/fpls.2019.01078

Montalvo, D., Degryse, F., da Silva, R. C., Baird, R., & McLaughlin, M. J. (2016). Chapter Five—Agronomic Effectiveness of Zinc Sources as Micronutrient Fertilizer. In D. L. Sparks (Ed.), *Advances in Agronomy* (Vol. 139, pp. 215–267). Academic Press. https://doi.org/10.1016/bs.agron.2016.05.004

Mostafa, H. S., Shaker, A. S., & El-Shaboury, G. A. (2025). Inhibitory effect of green coffee extracts on Rhizopus stolonifer: In-silico and in-situ evidence. *European Food Research and Technology*. https://doi.org/10.1007/s00217-025-04717-x

Munir, N., Hanif, M., Dias, D. A., & Abideen, A. (2021). The role of halophytic nanoparticles towards the remediation of degraded and saline agricultural lands. *Environ. Sci. Pollut. Res*, *28*, 60383–60405.

Munns, R. (1993). Physiological processes limiting plant growth in saline soils: Some dogmas and hypotheses. *Plant Cell Environ*, *16*, 15–24. https://doi.org/10.1111/j.1365-3040.1993.tb00840.x.

Munns, R. (2005). Genes and salt tolerance: Bringing them together. *New Phytol*, *167*, 645–663. https://doi.org/%5BPubMed%5D

Munns, R., & Gilliham, M. (2015). Salinity tolerance of crops – what is the cost? *New Phytologist*, *208*(3), 668–673. https://doi.org/10.1111/nph.13519

Munns, R., James, R. A., & Läuchli, A. (2006). Approaches to increasing the salt tolerance of wheat and other cereals. *Journal of Experimental Botany*, *57*(5), 1025–1043. https://doi.org/10.1093/jxb/erj100

Munns, R., James, R. A., & Xu, B. (2012). Wheat grain yield on saline soils is improved by an ancestral Na+ transporter gene. *Nature*, (nology30), 360–364.

Munns, R., & Tester, M. (2008). Mechanisms of salinity tolerance. *Annual Review of Plant Biology*, *59*, 651–681. https://doi.org/10.1146/annurev.arplant.59.032607.092911

Murdock, R. C., Braydich-Stolle, L., Schrand, A. M., Schlager, J. J., & Hussain, S. M. (2008). Characterization of nanomaterial dispersion in solution prior to in vitro exposure using dynamic light scattering technique. *Toxicological Sciences: An Official Journal of the Society of Toxicology*, *101*(2), 239–253. https://doi.org/10.1093/toxsci/kfm240

Musa, U., & Hassan, U. (2016). LEAF AREA DETERMINATION FOR MAIZE (Zea mays L), OKRA (Abelmoschus esculentus L) AND COWPEA (Vigna unguiculata L) CROPS USING LINEAR MEASUREMENTS. *Journal of Biology, Agriculture and Healthcare*. https://www.semanticscholar.org/paper/LEAF-AREA-DETERMINATION-FOR-MAIZE-(Zea-mays-L)%2C-L)-Musa-Hassan/b7ba0196db4fd0470c0852669a0ac0ad5358f153

Nabati, J., Kafi, M., Nezami, A., Moghaddam, P. R., Ali, M., & Mehrjerdi, M. Z. (2011). Effect of salinity on biomass production and activities of some key enzymatic antioxidants in Kochia (Kochia scoparia. *Pak. J. Bot*, *43*, 539–548.

Nachshon, U. (2018). Cropland Soil Salinization and Associated Hydrology: Trends, Processes and Examples. *Water*, *10*, 1030. https://doi.org/10.3390/w10081030

Narramore, S., Stevenson, C. E. M., Maxwell, A., Lawson, D. M., & Fishwick, C. W. G. (2019). New insights into the binding mode of pyridine-3-carboxamide inhibitors of *E. coli* DNA gyrase. *Bioorganic & Medicinal Chemistry*, *27*(16), 3546–3550. https://doi.org/10.1016/j.bmc.2019.06.015

Naseer, I., Javad, S., Iqbal, S., Shah, A. A., Alwutayd, K., & AbdElgawad, H. (2023). Deciphering the role of zinc oxide nanoparticles on physiochemical attributes of *Zea mays* exposed to saline conditions through modulation in antioxidant enzyme defensive system. *South African Journal of Botany*, *160*, 469–482. https://doi.org/10.1016/j.sajb.2023.07.035

Natasha, N., Shahid, M., Bibi, I., Iqbal, J., Khalid, S., Murtaza, B., Bakhat, H. F., Farooq, A. B. U., Amjad, M., Hammad, H. M., Niazi, N. K., & Arshad, M. (2022). Zinc in soil-plant-human system: A data-analysis review. *Science of The Total Environment*, *808*, 152024. https://doi.org/10.1016/j.scitotenv.2021.152024

Negacz, K., Malek, Ž., Vos, A. de, & Vellinga, P. (2022). Saline soils worldwide: Identifying the most promising areas for saline agriculture. *Journal of Arid Environments*, *203*, 104775. https://doi.org/https://doi.org/10.1016/j.jaridenv.2022.104775

Nejati, K., Rezvani, Z., & Pakizevand, R. (2011). Synthesis of ZnO nanoparticles and investigation of the ionic template effect on their size and shape. *International Nano Letters*, *1*, 75–81.

Netondo, G. W., Onyango, J. C., Beck, E. S., & salinity, I. (2004). Gas exchange and chlorophyll fluorescence of sorghum under salt stress. *Crop Sci*, *44*, 806.

Nguyen, K. C., Rippstein, P., Tayabali, A. F., & Willmore, W. G. (2015). Mitochondrial Toxicity of Cadmium Telluride Quantum Dot Nanoparticles in Mammalian Hepatocytes. *Toxicological Sciences: An Official Journal of the Society of Toxicology*, *146*(1), 31–42. https://doi.org/10.1093/toxsci/kfv068

Nishiuchi, T., & Iba, K. (1998). Roles of plastid ε-3 fatty acid desaturases in defense response of higher plants. *Journal of Plant Research*, *111*(4), 481–486. https://doi.org/10.1007/BF02507782

Nivatya, H. K., Singh, A., Kumar, N., Sonam, Sharma, L., Singh, V., Mishra, R., Gaur, N., & Mishra, A. K. (2025). Assessing molecular docking tools: Understanding drug discovery and design. *Future Journal of Pharmaceutical Sciences*, *11*(1), 111. https://doi.org/10.1186/s43094-025-00862-y

Noctor, G., & Foyer, C. H. (1998). Ascorbate and Glutathione: Keeping Active Oxygen Under Control. Ann. *Rev. Plant Physiol. Plant Mol. Biol*, *49*, 249–279.

Norbert, M. (2023, June 1). Kecskeméti 549 paradicsom termesztése. *Kertészkedj*. https://kerteszkedj.hu/kecskemeti-549-paradicsom-termesztese/

Noreen, S., & Ashraf, M. (2010). Modulation of salt (NaCl)-induced effects on oil composition and fatty acid profile of sunflower (Helianthus annuus L.) by exogenous application of salicylic acid. *Journal of the Science of Food and Agriculture*, *90*(15), 2608–2616. Scopus. https://doi.org/10.1002/jsfa.4129

Okechukwu, A.-J. M., Okeke, E. S., Eze, K. N., Ezeorba, W. F. C., & Ezeorba, T. P. C. (2023). Insight into the Alpha-Glucosidase Inhibitory Potentials of Curcuma longa Methanolic Extracts and Phytochemicals: An In Vitro and In Silico Study. *Biology and Life Sciences Forum*, *26*(1), 92. https://doi.org/10.3390/Foods2023-15514

OmicsBox. (2019). *Bioinformatics Made Easy*. Valencia.

Orfei, B., Scian, A., Del Buono, D., Paglialunga, M., Tolisano, C., Priolo, D., Moretti, C., & Buonaurio, R. (2025). Biogenic Zinc Oxide Nanoparticles Protect Tomato Plants Against Pseudomonas syringae pv. Tomato. *Horticulturae*, *11*(4), Article 4. https://doi.org/10.3390/horticulturae11040431

Pandit, M., Chakraborty, M., Haider, Z. A., Pande, A., Sah, R. P., & Sourav, K. (2016). Genetic diversity assay of maize (Zea mays L.) inbreds based on morphometric traits and SSR markers. *African Journal of Agricultural Research*, *11*(24), 2118–2128. https://doi.org/10.5897/AJAR2015.10404

Paramo, L. A., Feregrino-Pérez, A. A., Guevara, R., Mendoza, S., & Esquivel, K. (2020). Nanoparticles in agroindustry: Applications, toxicity, challenges, and trends. *Nanomaterials*, *10*(9).

Pardo, J. M., & Rubio, F. (2011). Na+ and K+ Transporters in Plant Signaling. In M. Geisler & K. Venema (Eds), *Transporters and Pumps in Plant Signaling* (pp. 65–98). Springer. https://doi.org/10.1007/978-3-642-14369-4_3

Parkhomchuk, D., Borodina, T., Amstislavskiy, V., Banaru, M., Hallen, L., Krobitsch, S., Lehrach, H., & Soldatov, A. (2009). Transcriptome analysis by strand-specific sequencing of complementary DNA. *Nucleic Acids Research*, *37*(18), e123. https://doi.org/10.1093/nar/gkp596

Pattanayak, G. K., & Tripathy, B. C. (2011). Overexpression of protochlorophyllide oxidoreductase c regulates oxidative stress in arabidopsis. *PLoS ONE*, *6*, 26532.

Paulucci, N. S., Medeot, D. B., Dardanelli, M. S., & De Lema, M. G. (2011). Growth temperature and salinity impact fatty acid composition and degree of unsaturation in peanut-nodulating rhizobia. *Lipids*, *46*(5), 435–441. Scopus. https://doi.org/10.1007/s11745-011-3545-1

Perrucci, A., Okmen, A., Gulluce, M., Akpulat, H., & Dafera, D. (2004). The in vitro antimicrobial and antioxidant activities of the essential oils and methanol extracts of endemic Thymus spathulifolius. *Food Contl*, *15*, 627–634.

Perumal, V., Priyanka, N., Kathiravan, M., Irulappan, G., Indiraarulselvi, P., Geetha, N., Koramutla, M., Bhattacharya, R., Tiwari, M., Sharma, N., & Sahi, S. (2016). Enhanced plant growth promoting role of phycomolecules coated zinc oxide nanoparticles with P supplementation in cotton (Gossypium hirsutum L.). *Plant Physiology and Biochemistry*, *110*. https://doi.org/10.1016/j.plaphy.2016.09.004

Pirbalouti, A. G. (2019). Phytochemical and bioactivity diversity in the extracts from bulbs and leaves of different populations of Allium jesdianum, a valuable underutilized vegetable. *Acta Sci. Pol. Hortorum Cultus*, *18*, 115–122. https://doi.org/10.24326/asphc.2019.2.11.

Pitzschke, A., Forzani, C., & Hirt, H. (2006). Reactive oxygen species signaling in plants. *Antioxid. Redox Signal*, *8*, 1757–1764.

Plaksenkova, I., Kokina, I., Petrova, A., Jermaļonoka, M., Gerbreders, V., & Krasovska, M. (2020). The Impact of Zinc Oxide Nanoparticles on Cytotoxicity, Genotoxicity, and miRNA Expression in Barley (Hordeum vulgare L.) Seedlings. *TheScientificWorldJournal*, *2020*, 6649746. https://doi.org/10.1155/2020/6649746

Plaper, A., Golob, M., Hafner, I., Oblak, M., Šolmajer, T., & Jerala, R. (2003). Quercetin and rutin as inhibitors of DNA gyrase. *Biochemical and Biophysical Research Communications*, *306*(2), 530–536.

Pritchard, J., & Du, L. (2023). From Forest to Formula: The role of in silico modeling in validating ethnobotanical antibacterial agents. *Phytochemistry Reviews*, *22*(4), 891–905.

Prud'homme, M.-P., Gonzalez, B., Billard, J.-P., & Boucaud, J. (1992). Carbohydrate Content, Fructan and Sucrose Enzyme Activities in Roots, Stubble and Leaves of Ryegrass (*Lolium perenne* L.) as Affected by Source/Sink Modification after Cutting. *Journal of Plant Physiology*, *140*(3), 282–291. https://doi.org/10.1016/S0176-1617(11)81080-1

Qados, A. M. S. A. (2011). Effect of salt stress on plant growth and metabolism of bean plant Vicia faba (L. *J. Saudi Soc. Agric. Sci*, *10*, 7–15.

Qiao, M., Hong, C., Jiao, Y., Hou, S., & Gao, H. (2024). Impacts of Drought on Photosynthesis in Major Food Crops and the Related Mechanisms of Plant Responses to Drought. *Plants (Basel, Switzerland)*, *13*(13), 1808. https://doi.org/10.3390/plants13131808

Quddus, M., Uddin, M., Kasim, S., MohdYusoff, K., Hossain, M. A., Solaiman, Z., & Haque, A. N. A. (2024). Influence of Zinc Oxide Nanoparticles on the Productivity, Mineral Element Accumulation, and Fruit Quality of Tomato (Solanum lycopersicum L.). *Journal of Experimental Biology and Agricultural Sciences*, *12*, 887–904. https://doi.org/10.18006/2024.12(6).887.904

Quintero, J. M., Fournier, J. M., & Benlloch, M. (2007). Na+ accumulation in shoot is related to water transport in K+-starved sunflower plants but not in plants with a normal K+ status. *J. Plant Physiol*, *164*, 60–67.

Raddy, R., Salimath, M., Geetha, K. N., & Shankar, A. (2018). ZnO Nanoparticle Improves Maize Growth, Yield and Seed Zinc under High Soil pH Condition. *International Journal of Current Microbiology and Applied Sciences*, *7*, 1593–1601. https://doi.org/10.20546/ijcmas.2018.712.187

Raha, S., & Ahmaruzzaman, M. (2022). ZnO nanostructured materials and their potential applications: Progress, challenges and perspectives. *Nanoscale Advances*, *4*(8), 1868–1925. https://doi.org/10.1039/D1NA00880C

Rai, P. K., Kumar, V., Lee, S., Raza, N., Kim, K.-H., & Ok, Y. S. (2018). Nanoparticleplant interaction: Implications in energy, environment, and agriculture. *Environment International*, *119*, 1–19.

Rai-Kalal, P., & Jajoo, A. (2021). Priming with zinc oxide nanoparticles improve germination and photosynthetic performance in wheat. *Plant Physiology and Biochemistry*, *160*, 341–351. Scopus. https://doi.org/10.1016/j.plaphy.2021.01.032

Rajput, V. D. (2018). Effects of high concentrations of ZnO nanoparticles on growth and antioxidant system of Fagus sylvatica L. seedlings. *Applied Geochemistry*, *97*, 177–184.

Rajput, V. D., Minkina, T. M., Behal, A., Sushkova, S. N., Mandzhieva, S., Singh, R., Gorovtsov, A., Tsitsuashvili, V. S., Purvis, W. O., Ghazaryan, K. A., & Movsesyan, H. S. (2018). Effects of zinc-oxide nanoparticles on soil, plants, animals and soil organisms: A review. *Environmental Nanotechnology, Monitoring & Management*, *9*, 76–84. https://doi.org/10.1016/j.enmm.2017.12.006

Rakgotho, T., Ndou, N., Mulaudzi, T., Iwuoha, E., Mayedwa, N., & Ajayi, R. F. (2022). Green-Synthesized Zinc Oxide Nanoparticles Mitigate Salt Stress in Sorghum bicolor. *Agriculture*, *12*(5), Article 5. https://doi.org/10.3390/agriculture12050597

Raliya, R., & Tarafdar, J. C. (2013). ZnO Nanoparticle Biosynthesis and Its Effect on Phosphorous-Mobilizing Enzyme Secretion and Gum Contents in Clusterbean (Cyamopsis tetragonoloba L.). *Agricultural Research*, *2*(1), 48–57. Scopus. https://doi.org/10.1007/s40003-012-0049-z

Ramachandra Reddy, A., Chaitanya, K. V., Jutur, P. P., & Sumithra, K. (2004). Differential antioxidative responses to water stress among five mulberry (Morus alba L.) cultivars. *Environ. Exp. Bot*, *52*, 33–42.

Rasha, E., Monerah, A., Manal, A., Rehab, A., Mohammed, D., & Doaa, E. (2021). Biosynthesis of Zinc Oxide Nanoparticles from Acacia nilotica (L.) Extract to Overcome Carbapenem-Resistant Klebsiella Pneumoniae. *Molecules*, *26*(7), Article 7. https://doi.org/10.3390/molecules26071919

Rastogi, A., Zivcak, M., Sytar, O., Kalaji, H. M., He, X., Mbarki, S., & Brestic, M. (2017). Impact of Metal and Metal Oxide Nanoparticles on Plant: A Critical Review. *Frontiers in Chemistry*, *5*, 78. https://doi.org/10.3389/fchem.2017.00078

Raza, A., Razzaq, A., Mehmood, S. S., Zou, X., Zhang, X., Lv, Y., & Xu, J. (2019). Impact of Climate Change on Crops Adaptation and Strategies to Tackle Its Outcome: A Review. *Plants (Basel, Switzerland)*, *8*(2), 34. https://doi.org/10.3390/plants8020034

Rehman, F. ur, Paker, N. P., Rehman, S. ur, Javed, M. T., Farooq Hussain Munis, M., & Chaudhary, H. J. (2024). Zinc oxide nanoparticles: Biogenesis and applications against phytopathogens. *Journal of Plant Pathology*, *106*(1), 45–65. https://doi.org/10.1007/s42161-023-01522-x

Ren, X., Jia, Z., & Chen, X. (2008). Rainfall concentration for increasing corn production under semiarid climate. *Agricultural Water Management*, *95*, 1293–1302. https://doi.org/10.1016/j.agwat.2008.05.007

Rossi, L. (2019). Impact of ZnO Nanoparticles and $ZnCl_2$ on Gene Expression and Elemental Composition in Plants. *Environmental Science & Technology*, *53*(19), 11524–11535.

Rossi, L., Fedenia, L. N., Sharifan, H., Ma, X., & Lombardini, L. (2019). Effects of Foliar Application of Zinc Sulfate and Zinc Nanoparticles in Coffee (Coffea Arabica L.) Plants. *Plant Physiol. Biochem*, *135*, 160–166. https://doi.org/10.1016/j.plaphy.2018.12.005.

Rozeff, N. (1995). Sugarcane and salinity—A review paper. *Sugar Cane*.

Rozov, A., Khusainov, I., El Omari, K., Duman, R., Mykhaylyk, V., Yusupov, M., Westhof, E., Wagner, A., & Yusupova, G. (2019). Importance of potassium ions for ribosome structure and function revealed by long-wavelength X-ray diffraction. *Nature Communications*, *10*, 2519. https://doi.org/10.1038/s41467-019-10409-4

Ruge, E., Korting, H. C., & Borelli, C. (2005). Current state of three-dimensional characterisation of antifungal targets and its use for molecular modelling in drug design. *International Journal of Antimicrobial Agents*, *26*(6), 427–441. https://doi.org/10.1016/j.ijantimicag.2005.09.006

Sabagh, A. E., Hossain, A., Iqbal, M. A., Barutçular, C., Islam, M. S., Çiğ, F., Erman, M., Sytar, O., Brestic, M., Wasaya, A., Jabeen, T., Bukhari, M. A., Mubeen, M., Athar, H.-R., Azeem, F., Akdeniz, H., Konuşkan, Ö., Kizilgeci, F., Ikram, M., … Saneoka, H. (2020). Maize Adaptability to Heat Stress under Changing Climate. In *Plant Stress Physiology*. IntechOpen. https://doi.org/10.5772/intechopen.92396

Sah, R., Ahmed, S., Malaviya, D., & Saxena, P. (2016). Identification of consistence performing dual purpose maize (Zea mays L.) genotypes under semi-arid condition. *Range Management and Agroforestry*, *37*, 162–166.

Sah, R. P., Chakraborty, M., Prasad, K., Pandit, M., Tudu, V. K., Chakravarty, M. K., Narayan, S. C., Rana, M., & Moharana, D. (2020). Impact of water deficit stress in maize: Phenology and yield components. *Scientific Reports*, *10*(1), 2944. https://doi.org/10.1038/s41598-020-59689-7

Sakalova, G. V. (1979). *Environment and experimental of plant growth*. Academic Press.

Salama, D. M., Osman, S. A., Abd El-Aziz, M. E., Abd Elwahed, M. S. A., & Shaaban, E. A. (2019). Effect of zinc oxide nanoparticles on the growth, genomic DNA, production and the quality of common dry bean (*Phaseolus vulgaris*). *Biocatalysis and Agricultural Biotechnology*, *18*, 101083. https://doi.org/10.1016/j.bcab.2019.101083

Salih, A. M., Al-Qurainy, F., Khan, S., Tarroum, M., Nadeem, M., Shaikhaldein, H. O., Gaafar, A.-R. Z., & Alfarraj, N. S. (2021). Biosynthesis of zinc oxide nanoparticles using Phoenix dactylifera and their effect on biomass and phytochemical compounds in Juniperus procera. *Scientific Reports*, *11*(1), 19136. https://doi.org/10.1038/s41598-021-98607-3

Sama-ae, I., Pattaranggoon, N. C., & Tedasen, A. (2023). In silico prediction of Antifungal compounds from Natural sources towards Lanosterol 14-alpha demethylase (CYP51) using Molecular docking and Molecular dynamic simulation. *Journal of Molecular Graphics and Modelling*, *121*, 108435. https://doi.org/10.1016/j.jmgm.2023.108435

Sánchez-Rodríguez, E., Ruiz, J. M., Ferreres, F., & Moreno, D. A. (2012). Phenolic profiles of cherry tomatoes as influenced by hydric stress and rootstock technique. *Food Chemistry*, *134*(2), 775–782. https://doi.org/10.1016/j.foodchem.2012.02.180

Sanchooli, N., & Rahdari, A. (2024). *The Effect of Salinity Stress on the Antibacterial Activity of SpirulinaPlatensis Algae.Gene Cell Tissue.11(3):e148559.https://doi.org/10.5812/gct-148559*.

Santos, M. G., Ribeiro, R. V., Machado, E. C., & Pimentel, C. (2009). Photosynthetic parameters and leaf water potential of five common bean genotypes under mild water deficit. *Biol. Plant*, *53*, 229–236.

Sardans, J., & Peñuelas, J. (2021). Potassium Control of Plant Functions: Ecological and Agricultural Implications. *Plants*, *10*(2), 419. https://doi.org/10.3390/plants10020419

Sarraf, M., Vishwakarma, K., Kumar, V., Arif, N., Das, S., & Johnson, R. (2022). Metal/ metalloid-based nanomaterials for plant abiotic stress tolerance: An overview of the mechanisms. *Plants*, *11*(3).

Sarwar, M., Anjum, S., Ali, Q., Alam, M. W., Haider, M. S., & Mehboob, W. (2021). Triacontanol modulates salt stress tolerance in cucumber by altering the physiological and biochemical status of plant cells. *Scientific Reports*, *11*(1), 24504. https://doi.org/10.1038/s41598-021-04174-y

Satdev, Zinzala, V. J., Chavda, B. N., & Saini, L. K. (2020). Effect of nano ZnO on growth and yield of sweet corn under South Gujarat condition. *International Journal of Chemical Studies*, *8*(1), 2020–2023. https://doi.org/10.22271/chemi.2020.v8.i1ad.8563

Sekhon, B. S. (2014). Nanotechnology in Agri-food production: An overview. *Nanotechnology, Science and Applications*, *7*, 31–53.

Seleiman, M. F., Ahmad, A., Alhammad, B. A., & Tola, E. (2023). Exogenous Application of Zinc Oxide Nanoparticles Improved Antioxidants, Photosynthetic, and Yield Traits in Salt-Stressed Maize. *Agronomy*, *13*(10), Article 10. https://doi.org/10.3390/agronomy13102645

Seleiman, M. F., Ahmad, A., Battaglia, M. L., Bilal, H. M., Alhammad, B. A., & Khan, N. (2023). Zinc oxide nanoparticles: A unique saline stress mitigator with the potential to increase future crop production. *South African Journal of Botany*, *159*, 208–218. https://doi.org/10.1016/j.sajb.2023.06.009

Seleiman, M. F., Al-Selwey, W. A., Ibrahim, A. A., Shady, M., & Alsadon, A. A. (2023). Foliar Applications of ZnO and SiO2 Nanoparticles Mitigate Water Deficit and Enhance Potato Yield and Quality Traits. *Agronomy*, *13*(2), Article 2. https://doi.org/10.3390/agronomy13020466

Seoudi, O. A., Atalla, K. M., & Helmy, A. M. (2013). Bioconversion of some agricultural wastes into animal feed by Trichoderma spp. *J. Am. Sci*, *9*(6), 203–212.

Serov, D. A., Baimler, I. V., Burmistrov, D. E., Baryshev, A. S., Yanykin, D. V., Astashev, M. E., Simakin, A. V., & Gudkov, S. V. (2022). The Development of New Nanocomposite Polytetrafluoroethylene/Fe2O3 NPs to Prevent Bacterial Contamination in Meat Industry. *Polymers*, *14*(22), Article 22. https://doi.org/10.3390/polym14224880

Serov, D. A., Burmistrov, D. E., Simakin, A. V., Astashev, M. E., Uvarov, O. V., Tolordava, E. R., Semenova, A. A., Lisitsyn, A. B., & Gudkov, S. V. (2022). Composite Coating for the Food Industry Based on Fluoroplast and ZnO-NPs: Physical and Chemical Properties, Antibacterial and Antibiofilm Activity, Cytotoxicity. *Nanomaterials*, *12*(23), Article 23. https://doi.org/10.3390/nano12234158

Sgherri, C., Navari-Izzo, F., Pardossi, A., Soressi, G. P., & Izzo, R. (2007). The Influence of Diluted Seawater and Ripening Stage on the Content of Antioxidants in Fruits of Different Tomato Genotypes. *Journal of Agricultural and Food Chemistry*, *55*(6), 2452–2458. https://doi.org/10.1021/jf0634451

Shaba.Zahra, Baghizadeh, A., Mohamadali, V., Yazdanpanah, A., & Yousefi, M. (2010). The salicylic acid effect on the tomato (lycopersicum esculentum Mill) sugar, protein and proline contents under salinity stress (Nacl). *Journal of Biophysics and Structural Biology*.

Shahrajabian, M. H., Khoshkharam, M., Sun, W., & Cheng, Q. (2019). *Germination and seedlings growth of Corn (Zea mays L.) to allelopathic effects of rice (Oryza sativa L.)*. *6*, 152–156. https://doi.org/10.22271/tpr.2019.v6.i1.022

Shahzad, R., Harlina, P. W., Ewas, M., Zhenyuan, P., Nie, X., Gallego, P. P., Ullah Khan, S., Nishawy, E., Khan, A. H., & Jia, H. (2021). Foliar applied 24-epibrassinolide alleviates salt stress in rice (Oryza sativa L.) by suppression of ABA levels and upregulation of secondary metabolites. *Journal of Plant Interactions*, *16*(1), 533–549. https://doi.org/10.1080/17429145.2021.2002444

Shaikh, F. A. (2013). Mechanistic analysis of the GH29 alpha-L-fucosidase. *Biochemistry*, *52*(34), 5857–5869.

Shaker, A. S., Marrez, D. A., Ali, M. A., & Fathy, H. M. (2022). Potential synergistic effect of Alhagi graecorum ethanolic extract with two conventional food preservatives against some foodborne pathogens. *Archives of Microbiology*, *204*(11), 686. https://doi.org/10.1007/s00203-022-03302-0

Shalata, A., & Neumann, P. M. (2001). Exogenous ascorbic acid (vitamin C) increases resistance to salt stress and reduces lipid peroxidation. *Journal of Experimental Botany*, *52*(364), 2207–2211. https://doi.org/10.1093/jexbot/52.364.2207

Shan, N., Xiang, Z., Sun, J., Zhu, Q., Xiao, Y., Wang, P., Chen, X., Zhou, Q., & Gan, Z. (2021). Genome-wide analysis of valine-glutamine motif-containing proteins related to abiotic stress response in cucumber (Cucumis sativus L.). *BMC Plant Biology*, *21*(1), 492. https://doi.org/10.1186/s12870-021-03242-9

Sharma, S., & Singh, S. (2023). *Synthetic Aspect of Quinoline & Indole Analogues Having Antibacterial & Antifungal Properties: Molecular Docking Study of 2-Chloro-3-Formylquinoline & 2-Chloro-3-Formylindole*.

Sharma, S., Zhang, X., Azhar, G., Patyal, P., Verma, A., KC, G., & Wei, J. Y. (2023). Valine improves mitochondrial function and protects against oxidative stress. *Bioscience, Biotechnology, and Biochemistry*, *88*(2), 168–176. https://doi.org/10.1093/bbb/zbad169

Shebl, A., Hassan, A. A., Salama, D. M., Abd El-Aziz, M. E., & Abd Elwahed, M. S. A. (2019). Green Synthesis of Nanofertilizers and Their Application as a Foliar for *Cucurbita pepo* L. *Journal of Nanomaterials*, *2019*, e3476347. https://doi.org/10.1155/2019/3476347

Shen, M., Liu, W., Zeb, A., Lian, J., Wu, J., & Lin, M. (2022). Bioaccumulation and phytotoxicity of ZnO nanoparticles in soil-grown Brassica chinensis L. and potential risks. *Journal of Environmental Management*, *306*, 114454. https://doi.org/10.1016/j.jenvman.2022.114454

Shi, Q., Ding, F., Wang, X., & Wei, M. (2007). Exogenous nitric oxide protects cucumber roots against oxidative stress induced by salt stress. *Plant Physiol. Biochem*, *45*, 542–550.

Shin, Y. K., Bhandari, S. R., Cho, M. C., & Lee, J. G. (2020). Evaluation of chlorophyll fluorescence parameters and proline content in tomato seedlings grown under different salt stress conditions. *Horticulture, Environment, and Biotechnology*, *61*(3), 433–443. https://doi.org/10.1007/s13580-020-00231-z

Shrivastava, P., & Kumar, R. (2015). Soil salinity: A serious environmental issue and plant growth promoting bacteria as one of the tools for its alleviation. *Saudi Journal of Biological Sciences*, *22*(2), 123–131. https://doi.org/https://doi.org/10.1016/j.sjbs.2014.12.001

Siddiqi, K. S., ur Rahman, A., Tajuddin, & Husen, A. (2018). Properties of Zinc Oxide Nanoparticles and Their Activity Against Microbes. *Nanoscale Research Letters*, *13*(1), 141. https://doi.org/10.1186/s11671-018-2532-3

Singam, K., Juntawong, N., Cha-Um, S., & Kirdmanee, C. (2011). Salt stress induced ion accumulation, ion homeostasis, membrane injury and sugar contents in salt-sensitive rice (Oryza sativa L. spp. Indica) roots under isoosmotic conditions. *Afr. J. Biotechnol*, *10*, 1340–1346.

Singh, A. (2021). Soil salinization management for sustainable development: A review. *Journal of Environmental Management*, *277*, 111383. https://doi.org/10.1016/j.jenvman.2020.111383

Singh, A. (2022). Soil salinity: A global threat to sustainable development. *Soil Use and Management*, *38*(1), 39–67. https://doi.org/10.1111/sum.12772

Singh, B. R., Singh, B. N., Khan, W., Singh, H. B., & Naqvi, A. H. (2012). ROS-mediated apoptotic cell death in prostate cancer LNCaP cells induced by biosurfactant stabilized CdS quantum dots. *Biomaterials*, *33*(23), 5753–5767. https://doi.org/10.1016/j.biomaterials.2012.04.045

Smaoui, S., Chérif, I., Ben Hlima, H., Khan, M. U., Rebezov, M., Thiruvengadam, M., Sarkar, T., Shariati, M. A., & Lorenzo, J. M. (2023). Zinc oxide nanoparticles in meat packaging: A systematic review of recent literature. *Food Packaging and Shelf Life*, *36*, 101045. https://doi.org/10.1016/j.fpsl.2023.101045

Smirnoff, N. (1998). Plant resistance to environmental stress. *Current Opinion in Biotechnology*, *9*(2), 214–219. https://doi.org/10.1016/S0958-1669(98)80118-3

Sofy, A. R., Sofy, M. R., Hmed, A. A., Dawoud, R. A., Alnaggar, A. E.-A. M., Soliman, A. M., & El-Dougdoug, N. K. (2021). Ameliorating the Adverse Effects of Tomato mosaic tobamovirus Infecting Tomato Plants in Egypt by Boosting Immunity in Tomato Plants Using Zinc Oxide Nanoparticles. *Molecules*, *26*(5), Article 5. https://doi.org/10.3390/molecules26051337

Solaiman, M. A., Ali, M. A., Abdel-Moein, N. M., & Mahmoud, E. A. (2020). Synthesis of Ag-NPs developed by green-chemically method and evaluation of antioxidant activities and anti-inflammatory of synthesized nanoparticles against LPS-induced NO in RAW 264.7 macrophages. *Biocatalysis and Agricultural Biotechnology*, *29*, 101832. https://doi.org/10.1016/j.bcab.2020.101832

Soliman, M., Elkelish, A., Souad, T., Alhaithloul, H., & Farooq, M. (2020). Brassinosteroid Seed Priming with Nitrogen Supplementation Improves Salt Tolerance in Soybean. *Physiol. Mol. Biol. Plants*, *26*, 501–511. https://doi.org/10.1007/s12298

Song, W., Zhao, H., Zhang, X., Lei, L., & Lai, J. (2016). Genome-Wide Identification of VQ Motif-Containing Proteins and their Expression Profiles Under Abiotic Stresses in Maize. *Frontiers in Plant Science*, *6*. https://doi.org/10.3389/fpls.2015.01177

Song, Y., Jiang, M., Zhang, H., & Li, R. (2021). Zinc oxide nanoparticles alleviate chilling stress in rice (Oryza sativa L.) by regulating antioxidative system and chilling response transcription factors. *Molecules*, *26*(8).

Sripo-ngam, S., Khaengraeng, C., Kasem, S., & Chatnaparat, T. (2024). Antibacterial activity of high surface area zinc oxide nanoparticles for controlling black rot disease of Chinese kale. *Plant Pathology*, *73*(7), 1957–1968. https://doi.org/10.1111/ppa.13923

Stępień, A., Wojtkowiak, K., Kolankowska, E., & Pietrzak-Fiećko, R. (2024). Corn Grain Fatty Acid Contents in Response to Organic Fertilisers from Meat Industry Waste. *Sustainability*, *16*(3), Article 3. https://doi.org/10.3390/su16030952

Stewart, A. J., Bozonnet, S., Mullen, W., Jenkins, G. I., Lean, M. E. J., & Crozier, A. (2000). Occurrence of Flavonols in Tomatoes and Tomato-Based Products. *Journal of Agricultural and Food Chemistry*, *48*(7), 2663–2669. https://doi.org/10.1021/jf000070p

Sturikova, H. (2018). Zinc, Zinc Nanoparticles and Plants. *Journal of Hazardous Materials*, *349*, 101–122.

Subramanyam, K., Laing, G., & Damme, E. J. M. (2019). Sodium selenate treatment using a combination of seed priming and foliar spray alleviates salinity stress in rice. *Front. Plant Sci*, *10*, 116.

Sukhanova, A., Bozrova, S., Sokolov, P., Berestovoy, M., Karaulov, A., & Nabiev, I. (2018). Dependence of nanoparticle toxicity on their physical and chemical properties. *Nanoscale Research Letters*, *13*(1), 1–21.

Sun, L. R., Zhao, Z. J., & Hao, F. S. (2019). NADPH oxidases, essential players of hormone signalings in plant development and response to stresses. *Plant Signaling & Behavior*, *14*(11), 1657343. https://doi.org/10.1080/15592324.2019.1657343

Sun, L., Wang, Y., Wang, R., Wang, R., Zhang, P., Ju, Q., & Xu, J. (2020). Physiological, transcriptomic, and metabolomic analyses reveal zinc oxide nanoparticles modulate plant growth in tomato. *Environmental Science: Nano*, *7*(11), 3587–3604. https://doi.org/10.1039/D0EN00723D

Sun, Y., Ma, R., Yang, X., & Zhang, G. (2024). A Metabolomic Analysis of Tomato Fruits in Response to Salt Stress. *Horticulturae*, *10*(12), Article 12. https://doi.org/10.3390/horticulturae10121303

Surjus, A., & Durand, M. (1996). Lipid changes in soybean root membranes in response to salt treatment. *Journal of Experimental Botany*, *47*(1), 17–23. https://doi.org/10.1093/jxb/47.1.17

Tam, C. C., Nguyen, K., Nguyen, D., Hamada, S., Kwon, O., Kuang, I., Gong, S., Escobar, S., Liu, M., Kim, J., Hou, T., Tam, J., Cheng, L. W., Kim, J. H., Land, K. M., & Friedman, M. (2021). Antimicrobial properties of tomato leaves, stems, and fruit and their relationship to chemical composition. *BMC Complementary Medicine and Therapies*, *21*(1), 229. https://doi.org/10.1186/s12906-021-03391-2

Tang, H., Zhang, X., Gong, B., Yan, Y., & Shi, Q. (2020). Proteomics and metabolomics analysis of tomato fruit at different maturity stages and under salt treatment. *Food Chemistry*, *311*, 126009. https://doi.org/10.1016/j.foodchem.2019.126009

Tang, R.-J., Yang, Y., Yan, Y.-W., Mao, D.-D., Yuan, H.-M., Wang, C., Zhao, F.-G., & Luan, S. (2022). Two transporters mobilize magnesium from vacuolar stores to enable plant acclimation to magnesium deficiency. *Plant Physiology*, *190*(2), 1307–1320. https://doi.org/10.1093/plphys/kiac330

Taran, N., Storozhenko, V., Svietlova, N., Batsmanova, L., Shvartau, V., & Kovalenko, M. (2017). Effect of zinc and copper nanoparticles on drought resistance of wheat seedlings. *Nanoscale Research Letters*, *12*(1), 1–6.

Tavakkoli, E., Rengasamy, P., & McDonald, G. K. (2010). High concentrations of Na+ and Cl– ions in soil solution have simultaneous detrimental effects on growth of faba bean under salinity stress. *Journal of Experimental Botany*, *61*(15), 4449–4459. https://doi.org/10.1093/jxb/erq251

Tavallali, V., Rahemi, M., Eshghi, S., Kholdebarin, B., & Ramezanian, A. (2010). Zinc alleviates salt stress and increases antioxidant enzyme activity in the leaves of pistachio (Pistacia vera L. 'Badami') seedlings. *Turkish Journal of Agriculture and Forestry*, *34*(4), 349–359. Scopus. https://doi.org/10.3906/tar-0905-10

Tavallali, V., Rahemi, M., Maftoun, M., Panahi, B., Karimi, S., Ramezanian, A., & Vaezpour, M. (2009). Zinc influence and salt stress on photosynthesis, water relations, and carbonic anhydrase activity in pistachio. *Scientia Horticulturae*, *123*(2), 272–279. Scopus. https://doi.org/10.1016/j.scienta.2009.09.006

Tavanti, T. R., Melo, A. A. R. D., Moreira, L. D. K., Sanchez, D. E. J., Silva, R. D. S., Silva, R. M. D., & Reis, A. R. D. (2021). Micronutrient fertilization enhances ROS scavenging system for alleviation of abiotic stresses in plants. *Plant Physiology and Biochemistry*, *160*, 386–396. Scopus. https://doi.org/10.1016/j.plaphy.2021.01.040

Tester, M., & Langridge, P. (2010). Breeding technologies to increase crop production in a changing world. *Science (New York, N.Y.)*, *327*(5967), 818–822. https://doi.org/10.1126/science.1183700

Tiwari, P., Kumar, B., Kaur, M., Kaur, G., & Kaur, H. (2011). Phytochemical screening and extraction: A review. *Internationale Pharmaceutica Sciencia*, *1*(1), 98–106.

Tomás-Barberán, F. A., & Espín, J. C. (2001). Phenolic compounds and related enzymes as determinants of quality in fruits and vegetables. *Journal of the Science of Food and Agriculture*, *81*(9), 853–876. Scopus. https://doi.org/10.1002/jsfa.885

Tondey, M., Kalia, A., Singh, A., Dheri, G. S., Taggar, M. S., Nepovimova, E., Krejcar, O., & Kuca, K. (2021). Seed Priming and Coating by Nano-Scale Zinc Oxide Particles Improved Vegetative Growth, Yield and Quality of Fodder Maize (Zea mays). *Agronomy*, *11*(4), Article 4. https://doi.org/10.3390/agronomy11040729

Toscano, S., Trivellini, A., Cocetta, G., Bulgari, R., Francini, A., Romano, D., & Ferrante, A. (2019). Effect of Preharvest Abiotic Stresses on the Accumulation of Bioactive Compounds in Horticultural Produce. *Frontiers in Plant Science*, *10*. https://doi.org/10.3389/fpls.2019.01212

Trombetta, D. (2022). Mechanisms of Antibacterial Action of Plant Polyphenols: A Review of In Vitro and In Silico Evidence. *Antibiotics*, *11*(8), 1023.

Tsubouchi, H., Yamamoto, K., Hisada, K., Sakabe, Y., & Udagawa, S. (1987). Effect of roasting on ochratoxin A level in green coffee beans inoculated with Aspergillus ochraceus. *Mycopathologia*, *97*, 111–115.

Tunc-Ozdemir, M., Miller, G., Song, L., Kim, J., & A, S. (2009). Thiamin confers enhanced tolerance to oxidative stress in arabidopsis. *Plant Physiol*, *151*(1), 421–432.

Tuomisto, H. L., Scheelbeek, P. F. D., Chalabi, Z., Green, R., Smith, R. D., Haines, A., & Dangour, A. D. (2017). Effects of environmental change on agriculture, nutrition and health: A framework with a focus on fruits and vegetables. *Wellcome Open Research*, *2*, 21. https://doi.org/10.12688/wellcomeopenres.11190.2

Umair Hassan, M., Aamer, M., Umer Chattha, M., Haiying, T., Shahzad, B., Barbanti, L., Nawaz, M., Rasheed, A., Afzal, A., Liu, Y., & Guoqin, H. (2020). The Critical Role of Zinc in Plants Facing the Drought Stress. *Agriculture*, *10*(9), Article 9. https://doi.org/10.3390/agriculture10090396

Uresti-Porras, J.-G., Cabrera-De-La Fuente, M., Benavides-Mendoza, A., Olivares-Sáenz, E., Cabrera, R. I., & Juárez-Maldonado, A. (2021). Effect of Graft and Nano ZnO on Nutraceutical and Mineral Content in Bell Pepper. *Plants*, *10*(12), 2793. https://doi.org/10.3390/plants10122793

Vago, M. E., Jaurena, G., Estevez, J. M., Castro, M. A., Zavala, J. A., & Ciancia, M. (2021). Salt Stress on Lotus tenuis Triggers Cell Wall Polysaccharide Changes Affecting Their Digestibility by Ruminants. *Plant Physiol. Biochem*, *166*, 405–415. https://doi.org/10.1016/j.plaphy.2021.05.049.

van Dijk, E. L., Jaszczyszyn, Y., & Thermes, C. (2014). Library preparation methods for next-generation sequencing: Tone down the bias. *Experimental Cell Research*, *322*(1), 12–20. https://doi.org/10.1016/j.yexcr.2014.01.008

Van Soest, P. J., Robertson, J. B., & Lewis, B. A. (1991). Methods for dietary fiber, neutral detergent fiber, and nonstarch polysaccharides in relation to animal nutrition. *Journal of Dairy Science*, *74*(10), 3583–3597. https://doi.org/10.3168/jds.S0022-0302(91)78551-2

Venisse, J.-S., Gullner, G., & Brisset, M.-N. (2001). Evidence for the Involvement of an Oxidative Stress in the Initiation of Infection of Pear by Erwinia amylovora 1. *Plant Physiology*, *125*(4), 2164–2172. https://doi.org/10.1104/pp.125.4.2164

Venkatachalam, P., Jayaraj, M., Manikandan, R., Geetha, N., Rene, E. R., & Sharma, N. (2017). Zinc oxide nanoparticles (ZnONPs) alleviate heavy metal-induced toxicity in Leucaena leucocephala seedlings: A physiochemical analysis. *Plant Physiology and Biochemistry*, *110*, 59–69.

Venzhik, Y. (2024). Zinc Oxide Nanoparticles: Impact on Plants, Phytotoxicity and Alleviation of Abiotic Stress. *Plants*, *13*(2), 263.

Vokkaliga T, H., Wu, T.-M., & Hong, C.-Y. (2017). Glutathione Reductase and Abiotic Stress Tolerance in Plants. In *Glutathione in Plant Growth, Development, and Stress Tolerance* (pp. 265–286). https://doi.org/10.1007/978-3-319-66682-2_12

Wang, Q., Xu, S., Zhong, L., Zhao, X., & Wang, L. (2023). Effects of Zinc Oxide Nanoparticles on Growth, Development, and Flavonoid Synthesis in Ginkgo biloba. *International Journal of Molecular Sciences*, *24*(21), Article 21. https://doi.org/10.3390/ijms242115775

Wang, S., Zhang, X., Gong, D.-H., Huang, Q.-Q., Kandegama, W. M. W. W., Georgiev, M. I., Gao, Y.-Y., Liao, P., & Hao, G.-F. (2025). Sophisticated crosstalk of tryptophan-derived metabolites in plant stress responses. *Plant Communications*, *6*(9), 101425. https://doi.org/10.1016/j.xplc.2025.101425

Wang, W., Vinocur, B., & Altman, A. (2003). Plant responses to drought, salinity and extreme temperatures: Towards genetic engineering for stress tolerance. *Planta*, *218*, 1–14.

Wang, Y., Hu, Q., Wu, Z., Wang, H., Han, S., Jin, Y., & Yang, W. (2017). HISTONE DEACETYLASE 6 Represses Pathogen Defence Responses in Arabidopsis Thaliana. *Plant Cell Environ*, *40*, 2972–2986.

Wasternack, C., & Feussner, I. (2018). The oxylipin pathways: Biochemistry and function. *Annual Review of Plant Biology*, *69*, 363–386.

Watanabe, S., Matsumoto, M., Hakomori, Y., Takagi, H., Shimada, H., & Sakamoto, A. (2014). The purine metabolite allantoin enhances abiotic stress tolerance through synergistic activation of abscisic acid metabolism. *Plant, Cell & Environment*, *37*(4), 1022–1036. https://doi.org/10.1111/pce.12218

Weinberg, Z. G., Yan, Y., Chen, Y., Finkelman, S., Ashbell, G., & Navarro, S. (2008). The effect of moisture level on high-moisture maize (*Zea mays* L.) under hermetic storage conditions—*In vitro* studies. *Journal of Stored Products Research*, *44*(2), 136–144. https://doi.org/10.1016/j.jspr.2007.08.006

Werf, A., Kooijman, A., Welschen, R., & Lambers, H. (1988). Respiratory energy costs for the maintenance of biomass, for growth and for ion uptake in roots ofCarex diandraandCarex acutiformis. *Physiologia Plantarum*, *72*(3), 483–491. https://doi.org/10.1111/j.1399-3054.1988.tb09155.x

Werner, A. K., & Witte, C.-P. (2011). The biochemistry of nitrogen mobilization: Purine ring catabolism. *Trends in Plant Science*, *16*(7), 381–387. https://doi.org/10.1016/j.tplants.2011.03.012

Wiegand, I., Hilpert, K., & Hancock, R. E. W. (2008). Agar and broth dilution methods to determine the minimal inhibitory concentration (MIC) of antimicrobial substances. *Nature Protocols*, *3*(2), 163–175. https://doi.org/10.1038/nprot.2007.521

Wu, H., Shabala, L., Azzarello, E., Huang, Y., Pandolfi, C., Su, N., Wu, Q., Cai, S., Bazihizina, N., Wang, L., Zhou, M., Mancuso, S., Chen, Z., & Shabala, S. (2018). Na+ extrusion from the cytosol and tissue-specific Na+ sequestration in roots confer differential salt stress tolerance between durum and bread wheat. *Journal of Experimental Botany*, *69*(16), 3987–4001. https://doi.org/10.1093/jxb/ery194

Xu, D., Sanden, N. C. H., Hansen, L. L., Belew, Z. M., Madsen, S. R., Meyer, L., Jørgensen, M. E., Hunziker, P., Veres, D., Crocoll, C., Schulz, A., Nour-Eldin, H. H., & Halkier, B. A. (2023). Export of defensive glucosinolates is key for their accumulation in seeds. *Nature*, *617*(7959), 132–138. https://doi.org/10.1038/s41586-023-05969-x

Xue, F., Liu, W., Cao, H., Song, L., Ji, S., Tong, L., & Ding, R. (2021). Stomatal conductance of tomato leaves is regulated by both abscisic acid and leaf water potential under combined water and salt stress. *Physiologia Plantarum*, *172*(4), 2070–2078. https://doi.org/10.1111/ppl.13441

Yang, L., Wen, K.-S., Ruan, X., Zhao, Y.-X., Wei, F., & Wang, Q. (2018). Response of plant secondary metabolites to environmental factors. *Molecules*, *23*(4).

Yang, Z., Li, J.-L., Liu, L.-N., Xie, Q., & Sui, N. (2020). Photosynthetic Regulation Under Salt Stress and Salt-Tolerance Mechanism of Sweet Sorghum. *Frontiers in Plant Science*, *10*. https://doi.org/10.3389/fpls.2019.01722

Yedurkar, S., Maurya, C., & Mahanwar, P. (2016). Biosynthesis of Zinc Oxide Nanoparticles Using Ixora Coccinea Leaf Extract—A Green Approach. *Open Journal of Synthesis Theory and Applications*, *5*(1), Article 1. https://doi.org/10.4236/ojsta.2016.51001

Yildirim, E., Ekinci, M., Turan, M., Ors, S., & Dursun, A. (2023). Physiological, Morphological and Biochemical Responses of Exogenous Hydrogen Sulfide in Salt-Stressed Tomato Seedlings. *Sustainability*, *15*(2), Article 2. https://doi.org/10.3390/su15021098

Yin, Y.-G., Kobayashi, Y., Sanuki, A., Kondo, S., Fukuda, N., Ezura, H., Sugaya, S., & Matsukura, C. (2010). Salinity induces carbohydrate accumulation and sugar-regulated starch biosynthetic genes in tomato (Solanum lycopersicum L. cv. 'Micro-Tom') fruits in an ABA- and osmotic stress-independent manner. *Journal of Experimental Botany*, *61*(2), 563–574. https://doi.org/10.1093/jxb/erp333

Yu, B. J., Gong, H. M., & Liu, Y. L. (1999). Effects of exogenous fatty acids on H+-ATPase activity and lipid composition of plasma membrane vesicles isolated from roots of barley seedlings under salt stress. *Journal of Plant Physiology*, *155*(4–5), 646–651. Scopus. https://doi.org/10.1016/S0176-1617(99)80067-4

Yu, D., Boughton, B. A., Hill, C. B., Feussner, I., Roessner, U., & Rupasinghe, T. W. T. (2020). Insights Into Oxidized Lipid Modification in Barley Roots as an Adaptation Mechanism to Salinity Stress. *Frontiers in Plant Science*, *11*. https://doi.org/10.3389/fpls.2020.00001

Yuan, G., Qian, Y., Ren, Y., Guan, Y., Wu, X., Ge, C., & Ding, H. (2021). The role of plant-specific VQ motif-containing proteins: An ever-thickening plot. *Plant Physiology and Biochemistry*, *159*, 12–16. https://doi.org/10.1016/j.plaphy.2020.12.005

Yuan, Y., Han, R., Cao, Q., Yu, J., Mao, J., Zhang, T., & Liu, D. (2017). Pharmacophore-based virtual screening of novel inhibitors and docking analysis for CYP51A from Penicillium italicum. *Marine Drugs*, *15*(4), 107. https://doi.org/10.3390/md15040107

Yusof, Z. N. B. (2019). Thiamine and Its Role in Protection Against Stress in Plants (Enhancement in Thiamine Content for Nutritional Quality Improvement). In P. K. Jaiwal, A. K. Chhillar, D. Chaudhary, & R. Jaiwal (Eds), *Nutritional Quality Improvement in Plants* (pp. 177–186). Springer International Publishing. https://doi.org/10.1007/978-3-319-95354-0_7

Zafar, S., Hasnain, Z., Aslam, N., Mumtaz, S., Jaafar, H. Z., Wahab, P. E. M., Qayum, M., & Ormenisan, A. N. (2021). Impact of Zn Nanoparticles Synthesized via Green and Chemical Approach on Okra (Abelmoschus esculentus L.) Growth under Salt Stress. *Sustainability*, *13*(7), Article 7. https://doi.org/10.3390/su13073694

Zafar, S., Perveen, S., Kamran Khan, M., Shaheen, M. R., Hussain, R., Sarwar, N., Rashid, S., Nafees, M., Farid, G., Alamri, S., Shah, A. A., Javed, T., Irfan, M., & Siddiqui, M. H. (2022). Effect of zinc nanoparticles seed priming and foliar application on the growth and physio-biochemical indices of spinach (Spinacia oleracea L.) under salt stress. *PLoS ONE*, *17*(2), e0263194. https://doi.org/10.1371/journal.pone.0263194

Zahedi, S. M., Abdelrahman, M., Hosseini, M. S., Hoveizeh, N. F., & Tran, L. P. (2019). Alleviation of the effect of salinity on growth and yield of strawberry by foliar spray of selenium-nanoparticles. In *Environmental Pollution*. Amsterdam.

Zak, A. K., Abrishami, M. E., Majid, W. H. Abd., Yousefi, R., & Hosseini, S. M. (2011). Effects of annealing temperature on some structural and optical properties of ZnO nanoparticles prepared by a modified sol–gel combustion method. *Ceramics International*, *37*(1), 393–398. https://doi.org/10.1016/j.ceramint.2010.08.017

Zak, A. K., Majid, W. H. Abd., Darroudi, M., & Yousefi, R. (2011). Synthesis and characterization of ZnO nanoparticles prepared in gelatin media. *Materials Letters*, *65*(1), 70–73. https://doi.org/10.1016/j.matlet.2010.09.029

Zak, A. K., Razali, R., Majid, W. A., & Darroudi, M. (2011). Synthesis and characterization of a narrow size distribution of zinc oxide nanoparticles. *International Journal of Nanomedicine*, *6*, 1399–1403. https://doi.org/10.2147/IJN.S19693

Zhang, C. W., Huang, D. Y., Rajoka, M. S. R., Wu, Y., He, Z. D., Ye, L., & Song, X. (2024). The antifungal effects of berberine and its proposed mechanism of action through CYP51 inhibition, as predicted by molecular docking and binding analysis. *Molecules*, *29*(21), 5079. https://doi.org/10.3390/molecules29215079

Zhang, H., Zhao, Y., & Zhu, J.-K. (2020). Thriving under Stress: How Plants Balance Growth and the Stress Response. *Developmental Cell*, *55*(5), 529–543. https://doi.org/10.1016/j.devcel.2020.10.012

Zhao, S., Zhang, Q., Liu, M., Zhou, H., Ma, C., & Wang, P. (2021). Regulation of Plant Responses to Salt Stress. *International Journal of Molecular Sciences*, *22*(9), 4609. https://doi.org/10.3390/ijms22094609

Zhou, D., Jin, S., Li, L., Wang, Y., & Weng, N. (2011). Quantifying the adsorption and uptake of CuO nanoparticles by wheat root based on chemical extractions. *Journal of Environmental Sciences*, *23*(11), 1852–1857. Scopus. https://doi.org/10.1016/S1001-0742(10)60646-8

Zhu, J. K., Liu, J. P., & Xiong, L. M. (1998). Genetic analysis of salt tolerance in Arabidopsis: Evidence for a critical role of potassium nutrition. *Plant Cell*, *10*, 1181–1191.

Zhu, Z., Wei, G., Li, J., Qian, Q., & Yu, J. (2004). Silicon alleviates salt stress and increases antioxidant enzymes activity in leaves of salt-stressed cucumber (*Cucumis sativus* L.). *Plant Science*, *167*(3), 527–533. https://doi.org/10.1016/j.plantsci.2004.04.020

Zrenner, R., Stitt, M., Sonnewald, U., & Boldt, R. (2006). PYRIMIDINE AND PURINE BIOSYNTHESIS AND DEGRADATION IN PLANTS. *Annual Review of Plant Biology*, *57*(Volume 57, 2006), 805–836. https://doi.org/10.1146/annurev.arplant.57.032905.105421

Zulfiqar, F., & Ashraf, M. (2021). Nanoparticles Potentially Mediate Salt Stress Tolerance in Plants. *Plant Physiol. Biochem*, *160*, 257–268. https://doi.org/10.1016/j.plaphy.2021.01.028.

A2: Supplementary materials

The following supporting information can be downloaded at: https://drive.google.com/drive/folders/1S0xGUNGcmE0KjB0FTIZW17kpYfqQ9EpS?usp=drive_link

Supplementary Excel file 1

Table S1-1: Count table of the *de novo* transcript; Table S1-2: Upregulated and downregulated supertranscript genes.

Supplementary Excel file 2

Table S2-1: Upregulated and downregulated contigs_Tomato_control_× _salt stress (T1 × T4); Table S2-2: Upregulated and downregulated contigs_Tomato_control_× _ZnONPs_0.075 g/L (T1 × T2); Table S2-3: Upregulated and downregulated contigs_Tomato_control_× _ZnO-NPs_0.15 g/L (T1 × T3); Table S2-4: Upregulated and downregulated contigs_Tomato_control_× _salt+ZnO-NPs_0.075 g/L (T1 × T5); Table S2-5: Upregulated and downregulated contigs_Tomato_control_× _salt+ZnO-NPs_0.15 g/L (T1 × T6); Table S2-6: Upregulated and downregulated contigs_Tomato_salt_× _salt+ZnO-NPs_0.075 g/L (T4 × T5); Table S2-7: Upregulated and downregulated contigs_Tomato_salt_× _salt+ZnO-NPs_0.15 g/L (T4 × T6).

Supplementary Excel file 3

Table S3-1: Combined pathway analysis using the plant reactome and KEGG databases of blasted, mapped, and annotated upregulated and downregulated contigs_Tomato_control_× _salt stress (T1 × T4); Table S3-2: Combined pathway analysis using the plant reactome and KEGG databases of blasted, mapped, and annotated upregulated and downregulated contigs_Tomato_control_× _ZnONPs_0.075 g/L (T1 × T2); Table S3-3: Combined pathway analysis using the plant reactome and KEGG databases of blasted, mapped, and annotated upregulated and downregulated contigs_Tomato_control_× _ZnONPs_0.15 g/L (T1 × T3); Table S3-4: Combined pathway analysis using the plant reactome and KEGG databases of blasted, mapped, and annotated upregulated and downregulated contigs_Tomato_control_× _salt+ZnO-NPs_0.075 g/L (T1 × T5); Table S3-5: Combined pathway analysis using the plant reactome and KEGG databases of blasted, mapped, and annotated upregulated and downregulated contigs_Tomato_control_× _salt+ZnO-NPs_0.15 g/L (T1 × T6); Table S3-6: Combined pathway analysis using the plant reactome and KEGG databases of blasted, mapped, and annotated upregulated and downregulated contigs_Tomato_salt_× _salt+ZnO-NPs_0.075 g/L (T4 × T5); Table S3-7: Combined pathway analysis using the plant reactome and KEGG databases of blasted, mapped, and annotated upregulated and downregulated contigs_Tomato_salt_× _salt+ZnO-NPs_0.15 g/L (T4 × T6).

Supplementary Excel file 4

Table S4-1: Pairwise analysis of Top 50 upregulated and downregulated blasted, mapped, and annotated contigs_Tomato_control_× _salt stress (T1 × T4); Table S4-2: Pairwise analysis of Top 50 upregulated and downregulated blasted, mapped, and annotated contigs_Tomato_control_× _ZnONPs_0.075 g/L (T1 × T2); Table S4-3: Pairwise analysis of Top 50 upregulated and downregulated blasted, mapped, and annotated contigs_Tomato_control_× _ZnO-NPs_0.15 g/L (T1 × T3); Table S4-4: Pairwise analysis of Top 50 upregulated and downregulated blasted, mapped, and annotated contigs_Tomato_control_× _salt+ZnO-NPs_0.075 g/L (T1 × T5); Table S4-5: Pairwise analysis of Top 50 upregulated and downregulated blasted, mapped, and annotated contigs_Tomato_control_× _salt+ZnO-NPs_0.15 g/L (T1 × T6); Table S4-6: Pairwise analysis of Top 50 upregulated and downregulated blasted, mapped, and annotated contigs_Tomato_salt_× _salt+ZnO-NPs_0.075

g/L (T4 × T5); Table S4-7: Pairwise analysis of Top 50 upregulated and downregulated blasted, mapped, and annotated contigs_Tomato_salt_× _salt+ZnO-NPs_0.15 g/L (T4 × T6).

Supplementary Excel file 5

Table S5-1:Heat map and top 50 DEG contigs_Tomato_control_× _salt stress (T1 × T4); Table S5-2: Heat map and top 50 DEG contigs_Tomato_control_× _ZnONPs_0.075 g/L (T1 × T2); Table S5-3: Heat map and top 50 DEG contigs_Tomato_control_× _ZnO-NPs_0.15 g/L (T1 × T3); Table S5-4: Heat map and top 50 DEG contigs_Tomato_control_× _salt+ZnO-NPs_0.075 g/L (T1 × T5); Table S5-5: Heat map and top 50 DEG contigs_Tomato_control_× _salt+ZnO-NPs_0.15 g/L (T1 × T6); Table S5-6: Heat map and top 50 DEG contigs_Tomato_salt_× _salt+ZnO-NPs_0.075 g/L (T4 × T5); Table S5-7: Heat map and top 50 DEG contigs_Tomato_salt_× _salt+ZnO-NPs_0.15 g/L (T4 × T6).

Supplementary Excel file 6

Table S6-1: Pathways and their sequences linked to *Solanum lycopersicum* L. in the plant reactome database_Tomato_control_× _salt stress (T1 × T4); Table S6-2: Pathways and their sequences linked to *Solanum lycopersicum* L. in the plant reactome database; Table S6-3: Pathways and their sequences linked to *Solanum lycopersicum* L. in the plant reactome database_Tomato_control_× _ZnO-NPs_0.15 g/L (T1 × T3); Table S6-4: Pathways and their sequences linked to *Solanum lycopersicum* L. in the plant reactome database_Tomato_control_× _salt+ZnO-NPs_0.075 g/L (T1 × T5); Table S6-5: Pathways and their sequences linked to *Solanum lycopersicum* L. in the plant reactome database_Tomato_control_× _salt+ZnO-NPs_0.15 g/L (T1 × T6); Table S6-6: Pathways and their sequences linked to *Solanum lycopersicum* L. in the plant reactome database_Tomato_salt_× _salt+ZnO-NPs_0.075 g/L (T4 × T5); Table S6-7: Pathways and their sequences linked to *Solanum lycopersicum* L. in the plant reactome database_Tomato_salt_× _salt+ZnO-NPs_0.15 g/L (T4 × T6).

Supplementary Excel file 7

Table S7-1: Pathways and their sequences linked to KEGG database_Tomato_control_× _salt stress (T1 × T4); Table S7-2: Pathways and their sequences linked to KEGG database; Table S7-3: Pathways and their sequences linked to KEGG database_Tomato_control_× _ZnO-NPs_0.15 g/L (T1 × T3); Table S7-4: Pathways and their sequences linked to KEGG database_Tomato_control_× _salt+ZnO-NPs_0.075 g/L (T1 × T5); Table S7-5: Pathways and their sequences linked to KEGG database_Tomato_control_× _salt+ZnO-NPs_0.15 g/L (T1 × T6); Table S7-6: Pathways and their sequences linked to KEGG database_Tomato_salt_× _salt+ZnO-NPs_0.075 g/L (T4 × T5); Table S7-7: Pathways and their sequences linked to KEGG database_Tomato_salt_× _salt+ZnO-NPs_0.15 g/L (T4 × T6).

Supplementary Excel file 8

Table S8-1: Count table of the *de novo* transcript; Table S8-2: Upregulated and downregulated supertranscript genes.

Supplementary Excel file 9

Table S9-1: Upregulated and downregulated contigs_Maize_control_× _salt stress (M1 × M2); Table S9-2: Upregulated and downregulated contigs_Maize_control_× _salt+ZnO-NPs_2 g/L (M1 × M3); Table S9-3: Upregulated and downregulated contigs_Maize_control_× _ZnO-NPs_2 g/L (M1 × M4); Table S9-4: Upregulated and downregulated contigs_Maize_salt_× _salt+ZnO-NPs_2 g/L (M2 × M3)

Supplementary Excel file 10

Table S10-1: Combined pathway analysis using the plant reactome and KEGG databases of blasted, mapped, and annotated upregulated and downregulated contigs_Maize_control_× _salt stress (M1 × M2); Table S10-2: Combined pathway analysis using the plant reactome and KEGG databases of blasted, mapped, and annotated upregulated and downregulated contigs_Maize_control_× _salt+ZnO-NPs_2 g/L (M1 × M3); Table S10-3: Combined pathway analysis using the plant reactome and KEGG databases of blasted, mapped, and annotated upregulated and downregulated contigs_Maize_control_× _ZnO-NPs_2 g/L (M1 × M4); Table S10-4: Combined pathway analysis using the plant reactome and KEGG databases of blasted, mapped, and annotated upregulated and downregulated contigs_Maize_salt_× _salt+ZnO-NPs_2 g/L (M2 × M3).

Supplementary Excel file 11

Table S11-1: Pairwise analysis of Top 50 upregulated and downregulated blasted, mapped, and annotated contigs_Maize_control_× _salt stress (M1 × M2); Table S11-2: Pairwise analysis of Top 50 upregulated and downregulated blasted, mapped, and annotated contigs_Maize_control_× _salt+ZnO-NPs_2 g/L (M1 × M3); Table S11-3: Pairwise analysis of Top 50 upregulated and downregulated blasted, mapped, and annotated contigs_Maize_control_× _ZnO-NPs_2 g/L (M1 × M4); Table S11-4: Pairwise analysis of Top 50 upregulated and downregulated blasted, mapped, and annotated contigs_Maize_salt_× _salt+ZnO-NPs_2 g/L (M2 × M3).

Supplementary Excel file 12

Table S12-1: Heat map and top 50 DEG contigs_Maize_control_× _salt stress (M1 × M2); Table S12-2: Heat map and top 50 DEG contigs_Maize_control_× _salt+ZnO-NPs_2 g/L (M1 × M3); Table S12-3: Heat map and top 50 DEG contigs_Maize_control_× _ZnO-NPs_2 g/L (M1 × M4); Table S12-4: Heat map and top 50 DEG contigs_Maize_salt_× _salt+ZnO-NPs_2 g/L (M2 × M3).

Supplementary Excel file 13

Table S13-1: Pathways and their upregulated sequences linked to *Zea mays* L. in the plant reactome database_Maize_control_× _salt stress (M1 × M2); Table S13-2: Pathways and their downregulated sequences linked to *Zea mays* L. in the plant reactome database_Maize_control_× _salt stress (M1 × M2); Table S13-3: Pathways and their upregulated sequences linked to *Zea mays* L in the plant reactome database__Maize_control_× _salt+ZnO-NPs_2 g/L (M1 × M3); Table S13-4: Pathways and their downregulated sequences linked to *Zea mays* L. in the plant reactome database__Maize_control_× _salt+ZnO-NPs_2 g/L (M1 × M3); Table S13-5: Pathways and their upregulated sequences linked to *Zea mays* L in the plant reactome database_Maize_control_× _ZnO-NPs_2 g/L (M1 × M4); Table S13-6: Pathways and their downregulated sequences linked to *Zea mays* L. in the plant reactome database_Maize_control_× _ZnO-NPs_2 g/L (M1 × M4); Table S13-7: Pathways and their upregulated sequences linked to *Zea mays* L. in the plant reactome database_Maize_salt_× _salt+ZnO-NPs_2 g/L (M2 × M3); Table S13-8: Pathways and their downregulated sequences linked to *Zea mays* L. in the plant reactome database_Maize_salt_× _salt+ZnO-NPs_2 g/L (M2 × M3).

A3: Data availability

The Bioproject and the SRA-s (RNA-seq reads) for tomato plants are available in National Center for Biotechnology Information (NCBI) database under the accessions: Repository name: Tomato treated with ZnO-nanoparticles against salt stress. Data identification number: PRJNA1141123, and the direct URL to data: https://www.ncbi.nlm.nih.gov/bioproject/PRJNA1141123.

(1) Repository name: Tomato_control. Data identification number: SRR30014447 - SRR30014450. Direct URL to data: https://www.ncbi.nlm.nih.gov/sra/?term=SRR30014447
https://www.ncbi.nlm.nih.gov/sra/?term=SRR30014448
https://www.ncbi.nlm.nih.gov/sra/?term=SRR30014449
https://www.ncbi.nlm.nih.gov/sra/?term=SRR30014450

(2) Repository name: Tomato_salt. Data identification number: SRR30022363 -SRR30022366. Direct URL to data: https://www.ncbi.nlm.nih.gov/sra/?term=SRR30022363
https://www.ncbi.nlm.nih.gov/sra/?term=SRR30022364
https://www.ncbi.nlm.nih.gov/sra/?term=SRR30022365
https://www.ncbi.nlm.nih.gov/sra/?term=SRR30022366

(3) Repository name: Tomato_ZnONP_75mg. Data identification number: SRR30020755 - SRR30020758. Direct URL to data: https://www.ncbi.nlm.nih.gov/sra/?term=SRR30020755
https://www.ncbi.nlm.nih.gov/sra/?term=SRR30020756
https://www.ncbi.nlm.nih.gov/sra/?term=SRR30020757
https://www.ncbi.nlm.nih.gov/sra/?term=SRR30020758

(4) Repository name: Tomato_ZnONP_150 mg. Data identification number: SRR30020776 - SRR30020779. Direct URL to data: https://www.ncbi.nlm.nih.gov/sra/?term=SRR30020776
https://www.ncbi.nlm.nih.gov/sra/?term=SRR30020777
https://www.ncbi.nlm.nih.gov/sra/?term=SRR30020778
https://www.ncbi.nlm.nih.gov/sra/?term=SRR30020779

(5) Repository name: Tomato_salt+ZnONP_75 mg. Data identification number: SRR30035507 - SRR30035510. Direct URL to data:
https://www.ncbi.nlm.nih.gov/sra/?term=SRR30035507
https://www.ncbi.nlm.nih.gov/sra/?term=SRR30035508
https://www.ncbi.nlm.nih.gov/sra/?term=SRR30035509
https://www.ncbi.nlm.nih.gov/sra/?term=SRR30035510

(6) Repository name: Tomato_salt+ZnONP_150 mg. Data identification number: SRR30040799 - SRR30040802. Direct URL to data:
https://www.ncbi.nlm.nih.gov/sra/?term=SRR30040799
https://www.ncbi.nlm.nih.gov/sra/?term=SRR30040800
https://www.ncbi.nlm.nih.gov/sra/?term=SRR30040801
https://www.ncbi.nlm.nih.gov/sra/?term=SRR30040802

The raw reads (SRA's) for maize plants were deposited in the National Center for Biotechnology Information (NCBI) database under accession: PRJNA1141091 and ID: 1141091, and entitled: Maize treated with ZnO-nanoparticles against salt stress. The reads were as follows: (1) Repository name: Maize_control; Data identification number: SRR30013180; Direct URL to data: https://www.ncbi.nlm.nih.gov/sra/?term=SRR30013180 (Registration date: July 28, 2024). (2) Repository name: Maize_salt; Data identification number: SRR30013179; Direct URL to data: https://www.ncbi.nlm.nih.gov/sra/?term=SRR30013179 (Registration date: July 28, 2024). (3) Repository name: Maize_salt+ZnONP; Data identification number: SRR30013178; Direct URL to data: https://www.ncbi.nlm.nih.gov/sra/?term=SRR30013178 (Registration date: July 28, 2024). (4) Repository name: Maize_ZnONP; Data identification number: SRR30013177; Direct URL to data: https://www.ncbi.nlm.nih.gov/sra/?term=SRR30013177 (Registration date: July 28, 2024).

A4: The moisture content and water-holding capacity

A4-1: Determining the moisture content of the potting soil

Air-dried soil (soil + peat moss 1:1), even when thoroughly air-dried, always has moisture, no matter how little. This moisture had to be accounted for when determining the amount of water needed to bring soil to its pot capacity. The first step thus involved the determination of the potting soil's moisture content, i.e., its gravimetric water content.

A4-2: Determining the amount of air-dried soil to place in each pot

Each pot was filled with an amount of soil that would give the required amount of oven-dried soil. Overall, 8445.9 g of oven-dried soil was needed since the air-dried soil had a moisture content of 6.56% (0.0656 g/g). Then, the amount of air-dried soil needed to give a mass of 8445.9 g (8.4459 kg) of oven-dried soil was calculated by determining the amount of water needed to bring a mass of potting soil to pot capacity. The pot capacity (moisture content of the pot) was 67.15%. That value constituted the full amount of water needed to bring the soil to 100% pot capacity. However, a certain mass of air-dried soil was added to each pot, and that air-dried soil was an equivalent mass of oven-dried soil. It was also taken into account that the air-dried soil contained moisture. That amount of moisture needed to be accounted for no matter how small it might seem to be. The moisture needed to bring the soil to pot capacity was 67.15% (0.6715 g/g). This means that each gram of soil would need 0.6715 g of moisture to bring it to pot capacity.

However, the air-dried soil sample already contained 0.0656% moisture. The amount of water needed to bring this soil to pot capacity was as follows: The water needed to bring air-dried soil to 100% pot capacity (PC) = moisture content at PC − moisture content in air-dried soil = 67.15% − 6.56% = 60.59% or (0.6059 g water/g oven-dried soil). The water needed to bring 10 kg oven-dried soil to 100% PC = (0.6059 g of water × 8445.9 g of soil)/1 g = 5117.37 g (5117.37 mL) (5.117 L) (5 L and 117 mL). Since water is much easier to add in volumes than as a weight, the density of water, which is 1 g/cm^3, was recalled. The volume of water needed to be added to the air-dried mass of potting soil of 9 kg to bring it to pot capacity (100%) was already known. The 100% pot capacity would keep plants in pots under well-watered conditions. The equation ($y = 1.0432x + 0.0569$) of the calibration curve of the time domain reflectometer (TDR; FieldScout TDR 300 Soil Moisture Meter, Spectrum Technologies, Inc., Aurora, IL, USA) was used to determine the water requirements every week to irrigate the plants during the whole experiment. The value on the device is substituted in the equation. The result was subtracted from 0.66, which was the moisture of the pot capacity. After the amount of moisture that must be added to make the soils in pots around the pot capacity was calculated, it was multiplied by 8445, which was the weight of completely oven-dried soil. The water requirements were recorded regularly.

DEDICATION

To the one with whom I feel at ease, and with whom the eye finds comfort; the one in whose sanctuary I find security; the one whom the heart has chosen and will choose every time. It was said: "The woman who is right for you will never pass you by. Allah sends her at the right time, ***HIS ALMIGHTY*** *has chosen. She has a written time and a known place. No obstacles will prevent her, no circumstances will hinder her, and she cannot bypass you for someone else. Her destiny and share is you, and you are her destiny and share". To you, the one who completes me. The companion of my journey.*

To the core of my heart and the delight of my eyes: "I swear, a parent's discipline is of no benefit if the Creator's choice for that child has not preceded it. For when ***ALLAH*** *Almighty wills good for someone,* ***HIS ALMIGHTY*** *raises him from childhood, guides him to what is right, directs him to sound judgment, makes him love what is beneficial, grants him righteous companions, makes him detest the opposite, makes base and trivial matters appear ugly to him, protects him from shameful deeds, and takes him by the hand whenever he stumbles. And when* ***ALLAH*** *despises someone,* ***HIS ALMIGHTY*** *leaves him constantly stumbling, floundering in every state, creates in him no ambition to seek lofty things, and occupies him with vices instead of virtues. And if such a person says, 'Why have* ***YOU*** *singled me out with this?' — the response comes, which admits no reply: 'That is for what your own hands have earned.' (Qur'an, Ash-Shūrā: 30)". And indeed, I hope you,* ***Eilaf,*** *will be among those whom ALLAH has enveloped with HIS chosen favor in this world and the hereafter. To you, my sweetie kiddo.*

It is said: 'A mother is a son's first true love, and a son is a mother's last true love.' And it is said: 'A father is the one from whom you ask for two stars, and he returns carrying the sky.' To those who deserve a standing ovation every day of their lives. To my first beloved, and to the one who gifted me the sky.

إِهْدَاء

إِلَى مَنْ أَشْعُرُ مَعَهَا بِالرَّاحَةِ وتَقَرُّ بِهَا العَيْن، مَن أَطْمَئِنُّ فِي رِحَابِهَا، مَنِ اختَارَهَا القَلبُ وسَيَختَارُها في كُلِّ مرَة. قِيلَ: "المرأةُ الْمُنَاسِبُة لَكَ لَنْ تَتَخَطَّاكَ أَبَدًا، يُرْسِلُهَا اللهُ فِي الْوَقْتِ الْمُنَاسِبِ الَّذِي اخْتَارَه، لَهَا زَمَانٌ مَكْتُوب، وَمَكَانٌ مَعْلُوم، لَنْ تَمْنَعَهَا أَسْبَاب، وَلَنْ تَعْتَرِيَهَا ظُرُوف، وَلَا يُمْكِنُ أَنْ تَتَجَاوَزَكَ إِلَى غَيْرِك، قَدَرُهَا وَنَصِيبُهَا أَنْت، وَأَنْتَ قَدَرُهَا وَنَصِيبُها". إِلَيْكِ يَا مَنْ تُكْمِلِينَنِي.. إليكِ رَفِيقَةَ دَربي..

إِلَى مُهْجَةِ القَلْبِ وَرَيْحَانَةِ العَيْنِ، "وَاللهِ، مَا يَنْفَعُ تَأْدِيبُ الْوَالِدِ إِذَا لَمْ يَسْبِقِ اخْتِيَارُ الْخَالِقِ لِذَلِكَ الْوَلَدِ! فَإِنَّهُ سُبْحَانَهُ إِذَا أَرَادَ شَخْصًا رَبَّاهُ مِنْ طُفُولَتِهِ، وَهَدَاهُ إِلَى الصَّوَابِ، وَدَلَّهُ عَلَى الرَّشَادِ، وَحَبَّبَ إِلَيْهِ مَا يَصْلُحُ، وَصَحَّبَهُ مَنْ يَصْلُحُ، وَبَغَّضَ إِلَيْهِ ضِدَّ ذَلِكَ، وَقَبَّحَ عِنْدَهُ سُفْسَافَ الْأُمُورِ، وَعَصَمَهُ مِنَ الْقَبَائِحِ، وَأَخَذَ بِيَدِهِ كُلَّمَا عَثَرَ. وَإِذَا أَبْغَضَ شَخْصًا، تَرَكَهُ دَائِمَ التَّعْثِيرِ، مُتَخَبِّطًا فِي كُلِّ حَالٍ، وَلَمْ يَخْلُقْ لَهُ هِمَّةً لِطَلَبِ الْمَعَالِي، وَشَغَلَهُ بِالرَّذَائِلِ عَنِ الْفَضَائِلِ، وَإِنْ قَالَ: لِمَ خَصَصْتَنِي بِهَذَا؟! قَالَ الْخِطَابَ الَّذِي لَا يُجَابُ: {فَبِمَا كَسَبَتْ أَيْدِيكُمْ} [الشُّورَى: ٣٠]". وَإِنِّي لَأَرْجُو يَا إِيلَافُ أَنْ تَكُونَي مِمَّنْ شَمِلَهُمُ اللَّهُ بِاصْطِفَائِهِ فِي الدُّنْيَا وَالآخِرَةِ. إليكِ حُلوَتي الصغيرة..

يُقَالُ: "الْأُمُّ هِيَ أَوَّلُ حُبٍّ حَقِيقِيٍّ لِابْنِهَا، وَالِابْنُ هُوَ آخِرُ حُبٍّ حَقِيقِيٍّ لِأُمِّهِ"، وَيُقَالُ: "الْأَبُ هُوَ ذَلِكَ الَّذِي تَطْلُبُ مِنْهُ نَجْمَتَيْنِ فَيَعُودُ حَامِلًا السَّمَاءَ". إِلَى أُولَئِكَ الَّذِينَ يَسْتَحِقُّونَ تَصْفِيقًا حَارًّا كُلَّ يَوْمٍ مِنْ حَيَاتِهِمْ. إِلَى أَوَّلِ حَبيبةٍ.. وإلى من أهداني السماء..

ACKNOWLEDGEMENT

All thanks and praise are to God, the all-wise, the all-knowing, the creator of this wonderful world.

I would like to deeply thank ***Dr. ZOLTÁN TÓTH*** *for giving me the opportunity to work on this study. He provided me with direct, helpful supervision and constructive criticism. His valuable advice extended beyond scientific work to other aspects of life. I'm also grateful to* ***Dr. KINCSŐ DECSI*** *for her excellent, sincere supervision and for her continuous support, help, and kindness. She is one of the most amazing characters I have met in my life. Thank you for your priceless efforts - may you always remain a symbol of giving and humbleness.*

I'm especially grateful to all the staff at Georgikon Campus and the members of the departments of Agronomy and Plant Physiology & Ecology at the Hungarian University of Agriculture and Life Sciences, for the continuous care and support I have received since starting my PhD studies. My success in my studies was influenced by the continuous encouragement and motivation from my friends, to whom I'm thankful. Special deep appreciation is given to all international students -especially my brother ***Evan Bassam Dayoub****- their presence made life away from home seem a lot nicer than it really was.*